DISS. ETH NO. 21139

NUMERICAL MODELLING OF CRUSTAL GROWTH IN SUBDUCTION ZONES AND INTRA–CRATONIC SETTINGS

A dissertation submitted to

ETH ZURICH

for the degree of
Doctor of Sciences

presented by

KATHARINA VOGT

M.Sc. in Earth Sciences, Ruhr Universität
Bochum, Germany

born on November 30, 1982

citizen of Germany
and Poland

accepted on the recommendation of

Prof. Dr. Taras V. Gerya, examiner
Prof. Dr. Paul Tackley, co-examiner
Dr. Jeroen van Hunen, co-examiner

2013

Abstract

Crust formation has important implications for the system Earth as a whole. Its growth is generally related to arc magmatism in subduction zones and intra-plate settings, or to the mechanical addition of various crustal units along its active margins. Several of these aspects and related problems are addressed in this thesis, by means of computational geodynamic modelling.

Based on 2-D numerical thermomechanical-petrological models, it is shown that melt production in ocean-continent subduction zones is a strong function of rheological plate coupling and tectonic setting. Partial melting of different lithologies can result in juvenile crust production or crustal recycling, forming a vast variety of different arc magmas. The latter is attributed to partial melting of tectonic rock mélanges at depth, composed of sediment, basalt and hydrated/serpentinized mantle, forming composite diapirs that rise through the mantle prior to emplacement at crustal levels. It is demonstrated that partial melting of such composite diapirs yields granodioritic melt with variable isotopic signatures, typical for many subduction-related intrusions.

Subduction/collision of oceanic plateaus embedded in oceanic lithosphere was investigated numerically in an ocean-continent subduction zone and shown to result in rapid growth of the continental crust. The convergence of oceanic plateaus and a continental margin reveal a wide range of accretion modes, controlled by the rheology of the oceanic plateau and the age of the surrounding lithospheric plate. Oceanic plateaus may block a subduction zone, be scraped off the downgoing slab, or underplate the continental crust. The tectonic responses to terrane accretion might be complex and include, enhanced melt production, surface uplift and compression, slab break off, subduction zone transference, termination of subduction, eduction of crustal material and (U)HP terrane formation. The incorporation of ophiolites into sedimentary sequences is demonstrated to be critically controlled by the existence of a weak subcrustal serpentine horizon that is believed to have evolved in relation to bending related

faulting. Basal detachment of the oceanic crust along this layer, leads to imbrication and emplacement of oceanic crust within accretionary complexes or on land exposure, while the "skinned" slab sinks into the mantle. This process is likely to have implications on arc-magmatism and accretionary tectonics.

Nevertheless, crustal growth is not only attributed to subduction zone settings, but may occur far away from present day plate boundaries'. In a study on Intra-Cratonic deformation it is shown that structural complexity arises in compressed lithosphere with lateral heterogeneities, which is sensitive to lithospheric age and tectonic setting. Crustal reworking of these settings influences localization of deformation, topographic evolution, melt generation, and melt intrusion, revealing a surprisingly large range of instabilities.

Lastly, a brief study is presented on magma rise and emplacement, based on a 3-D thermomechanical model. The preliminary results of this study emphasize that the properties of the overlying crust determine how and where magma is stored.

Kurzfassung

Die Bildung kontinentaler Kruste hat bedeutende Auswirkungen auf das gesamte System Erde. Tragende Mechanismen der Krustenbildung sind Inselbogen- und Intraplatten-Vulkanismus, aber auch die mechanische Anlagerung unterschiedlicher Krusteneinheiten entlang der aktiven Plattengrenzen. Einige dieser Aspekte und die damit verbundenen Probleme werden in dieser Arbeit anhand von numerischer, geodynamischer Modellierung diskutiert.

Basierend auf thermomechanisch - petrologischen 2-D- Modellen wird gezeigt, dass die Produktion von Schmelze in Ozean-Kontinent Subduktionszonen stark von der Rheologie der Platten sowie vom tektonischen Umfeld beeinflusst wird. Das partielle Aufschmelzen unterschiedlicher Gesteine kann zur Bildung neuer Kruste oder zum Recyceln alter Krustenanteile führen, wobei eine grosse Anzahl unterschiedlicher Magmen entstehen kann. Letzteres zeichnet sich aus durch das partielle Aufschmelzen einer tektonischen Gesteins-Mélange, bestehend aus Sediment, Basalt und hydratisiertem/ serpentinisiertem Mantel. In asthenosphärischen Tiefen kann das partielle Aufschmelzen der Mélange Diapire hervorbringen, die durch den Mantel bis auf Krustenniveau aufsteigen. Es wird gezeigt, dass das partielle Aufschmelzen solcher Diapir-Gemische Schmelze mit granodioritischer Zusammensetzung hervorbringt die eine variable Isotopensignatur aufweist, typisch für viele Subduktionsintrusionen.

Die Subduktion und Kollision ozeanischer Plateaus, eingebettet in ozean ischer Lithosphäre, wurde anhand einer Ozean-Kontinent-Subduktionszone numerisch untersucht, und es wird gezeigt, dass dieser Prozess zu einem schnellen Wachstum der kontinentalen Kruste führen kann. Die Kollision ozeanischer Plateaus mit aktiven Kontinentalrändern zeigt eine grosse Bandbreite von Akkretions-Typen auf, die durch die Rheologie der ozeanischen Plateaus und dem Alter der umgebenden Lithosphäre kontrolliert werden. Ozeanische Plateaus können eine Subduktionszone blockieren oder von der abtauchenden Platte geschert werden, sich unter der kontinentalen Kruste anlagern oder in grössere Tiefen subduziert werden. Die

tektonischen Auswirkungen der Akkretion von Terranes können komplex sein. Sie können einhergehen mit verstärkter Schmelzbildung, Kompression und Hebung der Geländeoberfläche, einem Abreissen der subduzierten Platte, einer horizontalen Verlagerung der Subduktionszone, einem Stopp des Subduktionsprozesses, der Obduktion von Krustenmaterial sowie der Bildung von Terranes unter (Ultra-)Hochdruck Bedingungen. Desweiteren wird gezeigt, dass die Eingliederung von Ophioliten in sedimentäre Sequenzen stark von der Existenz eines subkrustalen Serpentinhorizonts abhängt. Es wird angenommen das sich solche Serpentinitlagen im Zuge der Biegung der abtauchenden Platte bilden können. Die Abkoppelung der ozeanischen Kruste entlang dieser Schwächezone führt zur Fragmentierung der Kruste sowie zur Abtrennung und Anlagerung dieser Fragmente innerhalb der Akkretionskomplexe, während die ozeanische Lithosphäre in den Erdmantel subduziert wird. Es wird vermutet, dass ein solcher Prozess Auswirkungen auf den Inselbogenmagmatismus und die Akkretionstektonik hat.

Krustenwachstum ist jedoch nicht nur auf Subduktionszonen beschränkt, sondern kann auch fernab der heutigen Kontinentalränder vorkommen. Es wird gezeigt, dass die Kompression heterogener Kruste in einer Vielfalt struktureller Komplexitäten resultieren kann, abhängig von dem Alter der Platte und dem tektonischen Rahmen. Das Aufarbeiten dieser Gebiete führt zu einer grossen Bandbreite an Instabilitäten. Das hat Einfluss auf die Deformation, topografische Entwicklung, Schmelzbildung sowie die Magmenplatznahme.

Basierend auf thermodynamischen 3-D Modellen, wird abschliessend der Aufstieg von Magma und dessen Platzeinnahme innerhalb der Kruste untersucht. Die vorläufgen Resultate dieser Studie zeigen, dass die Platzeinnahme von Magmen stark durch die rheologischen Eigenschaften der kontinentalen Kruste beeinflusst wird.

Contents

Chapter 1

Introduction

Continental crust formation is a fundamental problem in geology that has important implications for the evolution of the system Earth as a whole (Rudnick and Gao, 2003), but many questions remain open. Has crust formation reached a steady state by crustal recycling after formation in the Archean (Armstrong and Harmon, 1981) or has crust formation been occurring throughout Earth history (Taylor and McLennan, 1985; McCulloch and Wasserburg, 1978)? What are the melt sources and proportions of magma that contribute or have contributed to crustal growth and what are the physical processes that lead to present day crustal growth?

1.1 Structure and chemical composition of the continental crust

The continental crust covers approximately 41 % of the Earth surface and exhibits a vast variety of igneous and metamorphic rocks including some of the oldest rocks ($\sim$ 4 Gyr) found on Earth (Taylor and McLennan, 1995; Rudnick, 1995). It is typically subdivided into two to three distinct layers that in total yield an andesitic bulk composition (e.g. Rudnick, 1995). The upper continental crust is believed to be felsic, while the lower crust is expected to be mafic (Taylor and McLennan, 1995; Wedepohl, 1995; Rudnick and Gao, 2003). Estimates on the structure and composition of the continental crust are based on observations of upper crustal rocks (e.g. Clarke, 1889; Goldschmidt, 1933; Shaw et al., 1976; Taylor and McLennan, 1985) and combined geophysical models of lower crustal rocks (e.g. Taylor and McLennan, 1985; Rudnick and Fountain, 1995; Christensen and Mooney, 1995; Taylor and McLennan, 1995; Rudnick and Gao, 2003; Hacker et al., 2011). The latter are derived from heat flow measurements

and seismic velocity structures that have been compared to natural rocks equilibrated at lower crustal pressures (i.e.: granulites, xenolithes; Rudnick and Fountain, 1995; Rudnick, 1995). However, these are indirect properties and inferring the composition and structure of the continental crust is not straightforward. Recently, it has been argued that the lower continental crust does not need to be mafic, but could be felsic on average (Hacker et al., 2011). The vertical exten of the crust is clearly marked by low seismic wave speeds (Vp $\sim$ 6.45 km/s) and low densities ($\sim$ 2600 - 3000 kg/m^3), which differ from the underlying mantle (Vp $\sim$ 8.09 km/s and $>$ 3300 kg/m^3)(Christensen and Mooney, 1995; Taylor and McLennan, 1995), forming a pronounced discontinuity - the Mohorovičič discontinuity (Mohorovičič, 1909) or Moho. However, the Moho is not a sharp boundary everywhere and may be diffuse or absent locally (Taylor and McLennan, 1995). The thickness of the continental crust is well correlated with tectonic province, with extended continental crust showing an average thickness of 30.5 km and orogens an average of 46.3 km (Christensen and Mooney, 1995). Despite its andesitic bulk composition, the continental crust is enriched in incompatible trace elements (elements that do not fit into the crystal lattice and are therefore concentrated in melts) forming Earth biggest trace element reservoir (e.g. Taylor and McLennan, 1995; Rudnick, 1995). The chemical composition of the continental crust and oceanic crust (Mid-Ocean-Ridge-Basalt: MORB) can be explained by a two-stage model of extracting first continental and then oceanic crust from the initially primitive mantle (Hofmann, 1988). Accordingly, the continental crust is believed to have formed by melting and geochemical fractionation of the mantle (Hofmann, 1988, 1997). In contrast to oceanic crust that is thin, young ($<$ 200 Myr) and relatively homogeneous in composition (basaltic), continental crust is thick (39 km on average), old (2 Gyr on average) and composed of highly diverse lithologies (Rudnick and Gao, 2003).

1.2 Present day crustal growth

1.2.1 Growth rates

Great affort has been put forward in order to decipher the volume, rates and composition of the continental crust. Based on present age distributions of the crust and model age studies (using Sm-Nd isotope systems), it is assumed that 40 % to 100 % of the present mass of the continents may have existed since its initial formation at the end of the Archean (Rudnick,

Location	Volume $[km^3/yr]$	Rate $[km^3/km/Myr]$	Reference
Convergent margins			
Island arcs	–	20 - 95	1 - 5
Continental arcs	–	30 - 90	6
Intraplate magmatism			
Oceanic	0.2	–	1
Continental	0.1	–	1
Incorporation of ophiolites	-	2 - 50	7 - 9
Crustal loss	–	25 - 50	10, 11

Table 1.1: Crustal growth rates related to different tectonic settings after: 1: Reymer and Schubert (1984), 2: Tiara et al. (1998), 3: Holbrook et al. (1999), 4: Larter et al. (2001), 5: Dimalanta et al. (2002), 6: DeCelles et al. (2009), 7: Godfrey and Klemperer (1998), 8: Dimalanta and Yumul (2003) 9: Dimalanta and Yumul Jr (2004), 10: von Huene and Scholl (1991), 11: Scholl and von Huene (2007).

1995; Taylor and McLennan, 1995). Nevertheless, isotope data demonstrate that progressive crustal growth has occurred throughout geological time (Rudnick, 1995). Present day crustal growth (material addition to the continental crust) is ascribed to distinct tectonic settings and takes place by (Reymer and Schubert, 1984):

1. Arc magmatism along convergent margins (oceanic and continental)
2. Intra-plate magmatism (oceanic and intra-continental)
3. Incorporation of ophiolites into sedimentary sequences
4. Underplating in extensional tectonic settings

The respective growths rates obtained in these settings are summarized in Table 1.1.

Arc magmatism along convergent margins

Geological and geophysical estimates on the amount of newly formed crust in ocean-ocean subduction zones indicate that the rates by which new magma is added to the crust may vary on the order of 20 - 95 $km^3/km/Myr$ (Reymer and Schubert, 1984; Tiara et al., 1998; Holbrook et al., 1999; Larter et al., 2001; Dimalanta et al., 2002). Reymer and Schubert (1984)

analysed Mesozoic-Cenozoic crustal addition rates along 17 arcs in the circum Pacific using seismic profiles. Net growth rates of 20 - 40 $km^3/km/Myr$ per arc length led them to conclude that these rates are on average 3 to 4 times smaller than Archean growth rates. More recent estimates of the same region reveal somewhat higher rates of 30 $km^3/km/Myr$ - 95 $km^3/km/Myr$ (Tiara et al., 1998; Holbrook et al., 1999; Dimalanta et al., 2002). In the Atlantic, seismic data from the South Sandwich Island arc exhibit arc growth rates of 60 $km^3/km/Myr$ (Larter et al., 2001), which is comparable to those obtained in the Pacific. Although less data is available for continental margins, where oceanic crust is subducted beneath continental crust, Mesozoic-Cenozoic growth rates are believed to be similar with high flux episodes (30 - 90 $km^3/km/Myr$) separated by magmatic lulls (20 - 30 $km^3/km/Myr$) (DeCelles et al., 2009, and references therein). Numerical modelling studies on crustal growth in ocean-ocean and/or ocean-continent subduction zones are relatively rare, but Nikolaeva et al. (2008) have demonstrated that arc growth in intra-arc subduction zones yields average values of 30 - 50 $km^3/km/Myr$. Similar estimates haven been reported in a subsequent study by Gerya and Meilick (2011) for crust formation along active continental margins (ocean-continent subduction zone).

Intraplate volcanism and terrane accretion

Available geochronology data of crust formation throughout Earth history reveals time periods of fast crust production, alternating with periods of low production (Stein and Ben-Avraham, 2007). Growth rates of the Arabian-Nubian Shield (ANS), Superior Province Canada (SP), Oregon Coastal Range (OR) are 10 times higher than magmatic addition rates obtained during the active lifespan of arcs (Figure 1.1). The rapid growth of these major segments led Reymer and Schubert (1984, 1986) to propose that other large scale mechanisms must have operated during their formation, besides arc-magmatism. This mechanism could involve hot-spot or plume related activity, the formation of oceanic plateaus or volcanic piles, and subsequent accretion onto continental crust (Stein and Ben-Avraham, 2007). Average accretion rates in such accretionary arcs were estimated by Condie (2007) to be 70 - 150 $km^3/km/Myr$ in Phanerozoic orogens and 100 - 200 $km^3/km/Myr$ in Precambrian orogens. Because accretionary orogens are often accompanied by magmatic addition of juvenile crust, Condie (2007) has, moreover, estimated magmatic addition rates related to accretionary orogens, which are believed to be typically 10 % - 30 % lower than the total accretion rate.

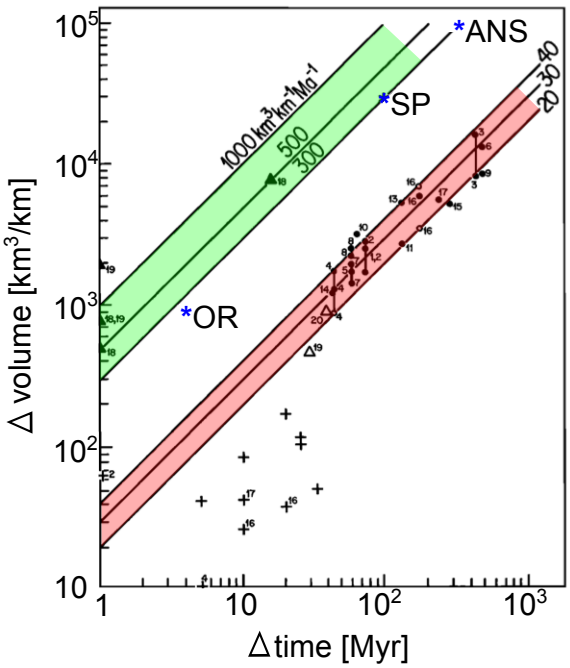

Figure 1.1: Crustal addition rates (volumes) plotted against time after Reymer and Schubert (1984). Straight lines represent constant addition rates $km^3/km/Myr$. Filled circles denote magmatic arc activity, crosses denote volcanic eruption rates. Ocean islands are plotted per hot spot (filled triangles) and per chain (open triangle). The growth of some major segments (ANS, Arabian-Nubian Shield; SP, Superior Province, Canada; OR, Oregon Coastal Range) outgrows the volumes of magmatic addition.

Incorporation of ophiolites

Further contributions to addition come from ophiolites and ophiolitic complexes (obducted fossil oceanic crust) that have either been incorporated into sedimentary sequences of accretionary prisms or obducted onto continental crust (Coleman, 1971; Dewey et al., 1981; Kimura and Ludden, 1995). Large segments of broken oceanic crust have been reported to underplate the continental crust beneath the Pacific and North American subduction zone system (e.g. Singh et al., 2008; Calvert, 2004; Kimura et al., 2010), often related to on land exposures of ancient oceanic crust. However, estimates on ophiolite accretion rates are relatively rare. Dewey et al. (1981) have estimated a global accretion rate of 0.07 km^3/yr, which corresponds approximately to 1.9 $km^3/km/Myr$. Godfrey and Klemperer (1998), on the other hand, derived on ophiolite accretion rate of at least 50 $km^3/km/Myr$ for the Great Valley ophiolite in California, which is comparable to the arc-magmatic addition rate obtained along convergent margins (Table 1.1). Nevertheless, ophiolite accretion rates in the Philippine archipelago yielded somewhat smaller accretion rates of about 2 - 30 $km^3/km/Myr$ (Dimalanta and Yumul, 2003; Dimalanta and Yumul Jr, 2004). Although these rates are significantly smaller compared to arc-magmatic production rates or other accretionary contributions, such as terrane accretion, ophiolite emplacement is a global feature (Vaughan and

Scarrow, 2003) that has been reported to occur episodically (Agard et al., 2009).

Crustal loss

Finally it should be noted, that recent estimates on the net transfer of crustal material on Earth surface suggest that crustal rocks are recycled back into the mantle at a similar rate (25 - 50 $km^3/km/Myr$) that continental crust is formed (Table 1.1; von Huene and Scholl, 1991; Scholl and von Huene, 2007). Crustal material can bypass the accretionary wedge (sediment subduction), as it remains attached to the oceanic crust or be removed from the upper plate in the process of crustal erosion (von Huene and Scholl, 1991; Clift and Vannucchi, 2004; Scholl and von Huene, 2007).

1.2.2 Composition of newly formed crust

It is generally agreed that the continental crust is differentiated from, and recycled to, the mantle (Dewey et al., 1981). However partial melting of the peridotite mantle, produces basaltic magmas that are less evolved (i.e., poorer in silica) than the andesitic bulk composition of the continental crust (Rudnick, 1995; Hawkesworth and Kemp, 2006). To account for this differentiation different mechanisms of crust formation have been proposed, but the extend, balance, timing and rates of these processes remain controversial (Dewey et al., 1981). These processes can be divided into two main groups: (a) models that ascribe juvenile crust formation to partial melting of the mantle and associated secondary processes (e.g. Schmidt and Poli, 1998; Iwamori, 1998; Tatsumi, 2005), such as intracrustal differentiation and lower crustal foundering (Kay and Mahlburg-Kay, 1991) and (b) models of crustal recycling, by which crustal components (oceanic crust, sediment, continental crust) are subducted to mantle depth, to undergo partial melting and chemical reaction with the mantle, prior to emplacement at upper crustal levels (Ringwood and Green, 1966; Ringwood, 1990; Kelemen, 1995; Kelemen et al., 2003; Gerya and Yuen, 2003; Currie et al., 2007; Gerya and Meilick, 2011; Behn et al., 2011; Marschall and Schumacher, 2012), by a process coined "relamination" (Hacker et al., 2011). Other processes that have been considered in the literature include (c) accretion of island arcs and other crustal units onto continental crust, its reworking and subsequent crustal assimilation (e.g. Coney et al., 1980; Ben-Avraham et al., 1981; Jones et al., 1982; Reymer and Schubert, 1986; Condie, 2007) and (d) chemical weathering of surface rocks, transport of soluble elements to the oceans and subsequent alteration of oceanic crust,

which preferentially returns Mg to the mantle (Rudnick, 1995).

"Flux melting"

Maybe the most accepted concept of melt production in island and continental arcs is based on partial melting of the metasomatized mantle (e.g. Stolper and Newman, 1994; Tatsumi and Eggins, 1995; Schmidt and Poli, 1998; Iwamori, 1998). Theoretical considerations and experimental studies have shown that fluids released from the downgoing slab lower the melting temperature of the mantle, causing flux melting (Figure 1.2) and basaltic melt production (e.g. Schmidt and Poli, 1998). Consequently, basaltic liquids are expected to migrate to areas of emplacement, where they undergo various differentiation and assimilation processes, resulting in more silicic rocks typical for the upper continental crust. Differentiation of these rocks is accompanied by the formation of mafic to ultramafic cumulates of high density and its delamination to the mantle (Kay and Mahlburg-Kay, 1991; Kay and Mahlburg Kay, 1993). Tectonic responses to delamination have been reported in some areas and include surface uplift and crustal melting (Kay and Mahlburg-Kay, 1991).

Crustal recycling

Melting of the oceanic crust, on the other hand, is highly debated in the literature, because subducted oceanic crust of most modern subduction zones is believed to be too cold to permit slab melting (Schmidt and Poli, 1998; Peacock et al., 1994) and may hence be restricted to young subduction zones (< 20 Myr) (Kay, 1978; Drummond and Defant, 1990; Defant and Drummond, 1990; Sajona et al., 1993). Nevertheless, it has been argued that hydrous melting of the oceanic crust may result in silicic magmas that rise and react with the peridotite mantle to produce olivine-pyroxene diapirs (Figure 1.3), contaminated with the elements enriched in silicic melts (Ringwood and Green, 1966; Green, 1980; Ringwood, 1990). Migration of such slab derived melts into adjacent regions of depleted or refractory mantle results not only in hybridization with the peridotite mantle, but also in refertilisation of these regions (Ringwood, 1990).

Similar models have been suggested by more recent studies on the density structure of subducted crustal lithologies (Hacker et al., 2011), the geochemistry of metamorphosed sedimentary rocks (Behn et al., 2011) and rock mélanges (Marschall and Schumacher, 2012) and numerical simulations of subduction zone processes (Gerya and Yuen, 2003; Currie et al., 2007; Miller and Behn, 2012). It has been shown that felsic material may

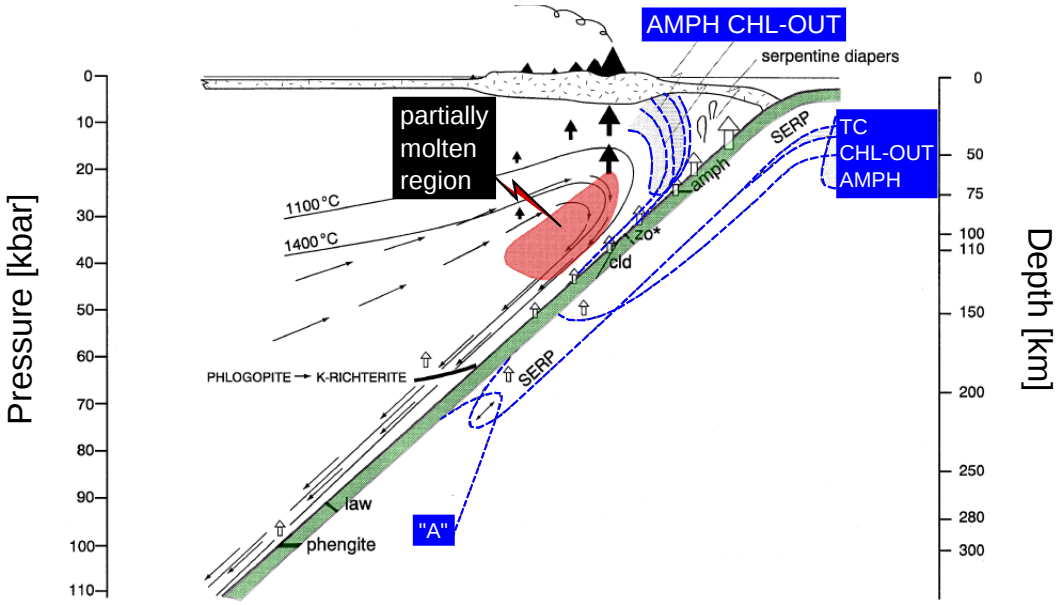

Figure 1.2: Model for the formation of arc magmas after Schmidt and Poli (1998). Dehydration from peridotite and oceanic crust leads to partial melting of the hydrated mantle. The red shaded area denotes a region of high melt fraction. Open arrows indicate fluid ascent, solid arrows denote melt ascent. Long arrows indicate flow in the mantle wedge. Dashed lines outline stability fields of hydrous phases.

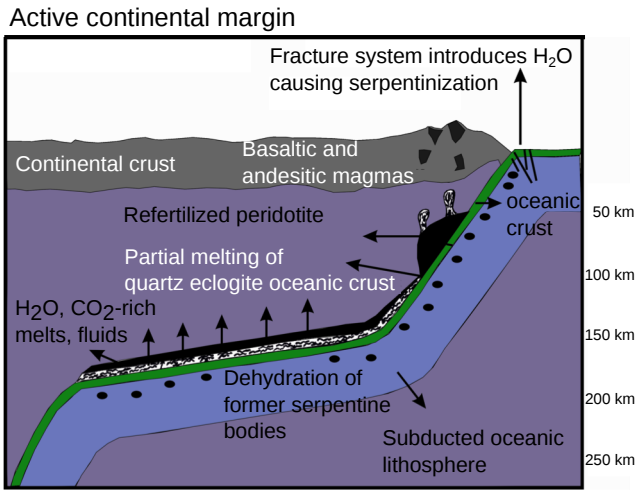

Figure 1.3: Conceptual model of continental arc magmatism after Ringwood (1990). Dehydration of former serpentine bodies induces partial melting of the eclogite crust of the slab. Melt migration results in hybridization with, and refertilisation of, the mantle.

detach from the slab, because of the intrinsic buoyancy of the sediment layer itself (Currie et al., 2007; Behn et al., 2011; Hacker et al., 2011; Miller and Behn, 2012) or due to hydration and partial melting of tectonic rock mélange (composed of sediment, basalt, and hydrated/serpentinized mantle) atop the slab, forming buoyant, composite diapirs (Gerya and Yuen, 2003; Gerya and Meilick, 2011; Marschall and Schumacher, 2012). Either processes are believed to modify the sub arc mantle (Stern, 1991), its geochemistry, the geochemistry of metasomatic agents (hydrous fluids, silicate melts, or miscible supercritical liquids) (King et al., 2006) and consequently arc magmatism.

1.2.3 Transport mechanisms

Lastly, it should be noted that the composition of magma and melt is not only governed by its mineralogy or melting conditions, but also by the physical process controlling its migration and segregation (Jackson et al., 2005). Transport mechanisms that have been proposed in the literature include, propagating fracture zones (Weertman, 1971; Clemens and Mawer, 1992; Petford, 1996; Petford et al., 2000), diapirc ascent (Cruden, 1990; Weinberg and Podladchikov, 1994; Miller and Paterson, 1999; Behn et al., 2011; Gerya and Yuen, 2003), diffusion (Scambelluri and Philippot, 2001), porous flow (McKenzie, 1984; Connolly et al., 1998; Ricard et al., 2001), high permeability channels or low viscosity conduits (Spiegelman and Kenyon, 1992; Kelemen et al., 2003) formed either by melt infiltration (Daines and Kohlstedt, 1994) or stress-driven melt segregation (Stevenson, 1989; Holtzman et al., 2003). Understanding these underlying physical principles will improve our understanding on how continental crust is formed.

1.2.4 Numerical modelling of crustal growth

Different concepts have been elaborated on how continents are formed, but geological observations are often restricted to observations of upper crustal. Given the limitations of field studies, numerical modelling can be used to probe physical concepts of crust formation through time and space, by computing flow fields, deformation patterns and pressure-temperature changes. In this thesis numerical modelling is used as an integrative tool, combining physical processes in the mantle and oceanic/continental lithosphere with surface observations and geological analysis. Two distinct processes are discussed: magmatic and amagmatic contributions to the

continental crust, within the context of present day plate tectonics. The questions asked and analysed in this study are:

1. Origin of different arc magmas in subduction and intra-plate settings
2. Principle melt sources and melting conditions
3. Geochemical variations related to crustal relamination
4. Physical mechanisms of terrane and ophiolite accretion
5. Magmatic and tectonic responses to accretionary tectonics
6. Structural responses to magma emplacement

1.3 Thesis at a glance

The body of the thesis is composed of six chapters, for which I provide an outline below.

Chapter 2 - Numerical procedure

Chapter 2 introduces the reader to the numerical procedure employed throughout this study. This chapter discusses the governing equations, rheological considerations, petrological assumptions, hydration and water migration, partial melting and melt extraction, boundary conditions and the computational strategy.

Chapter 3 - Crustal growth at active continental margins

Chapter 3 seeks physical explanation for the origin of different arc magmas formed in present day subduction zones. What are the melt sources, rates and proportions of magma formed in ocean-continent subduction zones? It is shown that fluid release and melt ascent may significantly influence the tectonic setting and hence melt generation. Three different magma sources are discussed: mantle (wet and dry), oceanic crust (basalt and gabbro) and sediment.
This chapter co-authored by K. Vogt, T. Gerya and A. Castro was published in a slightly modified version in Physics of the Earth and Planetary Interiors, 192 - 193, 1 - 20 (2012).

Chapter 4 - Geochemical variations caused by crustal relamination

Chapter 4 focuses on geochemical consequences in relation to crustal relamination. Can relamination of subducted rock mélanges composed of basalt, sediment and hydrated mantle account for the andesitic bulk composition of the continental crust and what are the geochemical consequences in terms of radiogenic isotopes?
This chapter co-authored by K. Vogt, A. Castro and T. Gerya was published in a slightly modified version in Geochemistry, Geophysics, Geosystems, 14, 470 - 487 (2013).

Chapter 5 - From oceanic plateaus to allochthonous terranes

Chapter 5 discusses how and if crustal accretion in ocean-continent subduction zones can contribute to the rapid growth of some major segments of the continental crust. Influences of crustal rheology upon accretion are investigated and different mechanisms are discussed, including tectonic and magmatic responses to accretion.
This chapter co-authored by K. Vogt and T. Gerya was published in a slightly modified version in Gondwana Research, in press.

Chapter 6 - Deep plate hydration triggers skinning of subducting plates and ophiolite emplacement

Chapter 6 elaborates mechanisms by which dense oceanic crust is obducted and emplaced onto continental crust in ocean-continent subduction zones. It focuses on the dynamics of detachment, migration and emplacement of oceanic crust.
This chapter co-authored by K. Vogt and T. Gerya was submitted in a slightly modified version to Science.

Chapter 7 - Tectonics and melting in intra-cratonic settings

Chapter 7 discusses melt production and magma evolution in intra-cratonic settings. It is shown that reworking of fossil suture zones far away from ambient subduction zones may have profound implications on deformation, topography, melt generation, and melt intrusion.

This chapter co-authored by W. Gorczyk and K. Vogt was submitted in a slightly modified version to Gondwana Research. Both authors have analysed the data and contributed to the manuscript. I have performed the experiments.

Bibliography

Agard, P., Yamato, P., Jolivet, L., Burov, E., 2009. Exhumation of oceanic blueschists and eclogites in subduction zones: timing and mechanisms. Earth-Science Reviews 92 (1), 53–79.

Armstrong, R., Harmon, R., 1981. Radiogenic isotopes: The case for crustal recycling on a near-steady-state no-continental-growth earth [and discussion]. Philosophical Transactions of the Royal Society of London. Series A, Mathematical and Physical Sciences 301 (1461), 443–472.

Behn, M., Kelemen, P., Hirth, G., Hacker, B., Massonne, H., 2011. Diapirs as the source of the sediment signature in arc lavas. Nature Geoscience 4 (9), 641–646.

Ben-Avraham, Z., Nur, A., Jones, D., Cox, A., 1981. Continental accretion: From oceanic plateaus to allochthonous terranes. Science 213, 47–54.

Calvert, A., 2004. Seismic reflection imaging of two megathrust shear zones in the northern cascadia subduction zone. Nature 428 (6979), 163–167.

Christensen, N., Mooney, W., 1995. Seismic velocity structure and composition of the continental crust: A global view. Journal of Geophysical Research 100 (B6), 9761–9788.

Clarke, F. W., 1889. The relative abundance of the chemical elements. Philosophical Society of Washington Bulletin X 1, 131–142.

Clemens, J., Mawer, C., 1992. Granitic magma transport by fracture propagation. Tectonophysics 204 (3), 339–360.

Clift, P., Vannucchi, P., 2004. Controls on tectonic accretion versus erosion in subduction zones: Implications for the origin and recycling of the continental crust. Reviews of Geophysics 42 (2), RG2001.

Coleman, R., 1971. Plate tectonic emplacement of upper mantle peridotites along continental edges. Journal of Geophysical Research 76 (5), 1212–1222.

Condie, K., 2007. Accretionary orogens in space and time. The Geological Society of America Memoir 200, 145–158.

Coney, P., Jones, D., Monger, J., 1980. Cordilleran suspect terranes. Nature 288, 329–333.

Connolly, J., Podladchikov, Y., et al., 1998. Compaction-driven fluid flow in viscoelastic rock. Geodinamica Acta 11 (2-3), 55–84.

Cruden, A. R., 1990. Flow and fabric development during the diapiric rise of magma. The Journal of Geology, 681–698.

Currie, C., Beaumont, C., Huismans, R., 2007. The fate of subducted sediments: A case for backarc intrusion and underplating. Geology 35 (12), 1111–1114.

Daines, M., Kohlstedt, D., 1994. The transition from porous to channelized flow due to melt/rock reaction during melt migration. Geophysical Research Letters 21, 145–145.

DeCelles, P., Ducea, M., Kapp, P., Zandt, G., 2009. Cyclicity in cordilleran orogenic systems. Nature Geoscience 2 (4), 251–257.

Defant, M., Drummond, M., 1990. Derivation of some modern arc magmas by melting of young subducted lithosphere. Nature 347 (6294), 662–665.

Dewey, J., Windley, B., Dewey, J., Windley, B., 1981. Growth and differentiation of the continental crust. Philosophical Transactions of the Royal Society of London. Series A, Mathematical and Physical Sciences 301 (1461), 189–206.

Dimalanta, C., Taira, A., Yumul, G., Tokuyama, H., Mochizuki, K., 2002. New rates of western pacific island arc magmatism from seismic and gravity data. Earth and Planetary Science Letters 202 (1), 105–115.

Dimalanta, C., Yumul, G., 2003. Magmatic and amagmatic contributions to crustal growth of an island-arc system: The philippine example. International Geology Review 45 (10), 922–935.

Dimalanta, C., Yumul Jr, G., 2004. Crustal thickening in an active margin setting (philippines): The whys and the hows. Episodes-Newsmagazine of the International Union of Geological Sciences 27 (4), 260–264.

Drummond, M., Defant, M., 1990. A model for trondhjemite-tonalite-dacite genesis and crustal growth via slab melting: Archean to modern comparisons. Journal of geophysical research 95 (B13), 21503–21.

Gerya, T., Meilick, F., 2011. Geodynamic regimes of subduction under an active margin: effects of rheological weakening by fluids and melts. Journal of metamorphic Petrology 29, 7–31.

Gerya, T., Yuen, D., 2003. Rayleigh–taylor instabilities from hydration and melting propel cold plumes at subduction zones. Earth and Planetary Science Letters 212 (1), 47–62.

Godfrey, N., Klemperer, S., 1998. Ophiolitic basement to a forearc basin and implications for continental growth: The coast range/great valley ophiolite, california. Tectonics 17 (4), 558–570.

Goldschmidt, V., 1933. Grundlagen der quantitativen geochemie. Fortschr. Mineral. Krist. Petrog 17, 112.

Green, T., 1980. Island arc and continent-building magmatisma review of petrogenic models based on experimental petrology and geochemistry. Tectonophysics 63 (1), 367–385.

Hacker, B., Kelemen, P., Behn, M., 2011. Differentiation of the continental crust by relamination. Earth and Planetary Science Letters 307 (3), 501–516.

Hawkesworth, C., Kemp, A., 2006. Evolution of the continental crust. Nature 443 (7113), 811–817.

Hofmann, A., 1988. Chemical differentiation of the earth: the relationship between mantle, continental crust, and oceanic crust. Earth and Planetary Science Letters 90 (3), 297–314.

Hofmann, A., 1997. Mantle geochemistry: the message from oceanic volcanism. Nature 385 (6613), 219–229.

Holbrook, W., Lizarralde, D., McGeary, S., Bangs, N., Diebold, J., 1999. Structure and composition of the aleutian island arc and implications for continental crustal growth. Geology 27 (1), 31–34.

Holtzman, B., Groebner, N., Zimmerman, M., Ginsberg, S., Kohlstedt, D., 2003. Stress-driven melt segregation in partially molten rocks. Geochemistry Geophysics Geosystems 4 (5), 8607.

Iwamori, H., 1998. Transportation of h2o and melting in subduction zones. Earth and Planetary Science Letters 160, 65–80.

Jackson, M., Gallagher, K., Petford, N., Cheadle, M., 2005. Towards a coupled physical and chemical model for tonalite–trondhjemite–granodiorite magma formation. Lithos 79 (1), 43–60.

Jones, D., Cox, A., Coney, P., Beck, M., 1982. The growth of the western north america. Scientific American 247, 70–84.

Kay, R., 1978. Aleutian magnesian andesites: melts from subducted pacific ocean crust. Journal of Volcanology and Geothermal Research 4 (1), 117–132.

Kay, R., Mahlburg-Kay, S., 1991. Creation and destruction of lower continental crust. Geologische Rundschau 80 (2), 259–278.

Kay, R. W., Mahlburg Kay, S., 1993. Delamination and delamination magmatism. Tectonophysics 219 (1), 177–189.

Kelemen, P., 1995. Genesis of high mg# andesites and the continental crust. Contributions to Mineralogy and Petrology 120 (1), 1–19.

Kelemen, P., Yogodzinski, G., Scholl, D., 2003. Along-strike variation in the aleutian island arc: Genesis of high mg# andesite and implications for continental crust. Inside the Subduction Factory, Geophys. Monogr. Ser 138, 223–276.

Kimura, G., Ludden, J., 1995. Peeling oceanic crust in subduction zones. Geology 23 (3), 217–220.

Kimura, H., Takeda, T., Obara, K., Kasahara, K., 2010. Seismic evidence for active underplating below the megathrust earthquake zone in japan. Science 329 (5988), 210–212.

King, R., Bebout, G., Moriguti, T., Nakamura, E., 2006. Elemental mixing systematics and sr–nd isotope geochemistry of mélange formation: obstacles to identification of fluid sources to arc volcanics. Earth and Planetary Science Letters 246 (3), 288–304.

Larter, R., Vanneste, L., Bruguier, N., 2001. Structure, composition and evolution of the south sandwich island arc: Implications for rates of arc magmatic growth and subduction erosion. In: AGU Fall Meeting Abstracts. Vol. 1. p. 10.

Marschall, H., Schumacher, J., 2012. Arc magmas sourced from melange diapirs in subduction zones. Nature Geoscience.

McCulloch, M., Wasserburg, G., 1978. Sm-nd and rb-sr chronology of continental crust formation. Science 200 (4345), 1003–1011.

McKenzie, D., 1984. The generation and compaction of partially molten rock. Journal of Petrology 25 (3), 713–765.

Miller, N., Behn, M., 2012. Timescales for the growth of sediment diapirs in subduction zones. Geophysical Journal International.

Miller, R. B., Paterson, S. R., 1999. In defense of magmatic diapirs. Journal of Structural Geology 21 (8), 1161–1173.

Mohorovičič, A., 1909. Das beben vom 8. oktober 1910. Jahrb. des meteor. Observ. Zagreb für.

Nikolaeva, K., Gerya, T., Connolly, J., 2008. Numerical modelling of crustal growth in intraoceanic volcanic arcs. Physics of the Earth and Planetary Interiors 171, 336–356.

Peacock, S., Rushmer, T., Thompson, A., 1994. Partial melting of subducting oceanic crust. Earth and planetary science letters 121 (1), 227–244.

Petford, N., 1996. Dykes or diapirs? Transactions of the Royal Society of Edinburgh: Earth Sciences 87 (1-2), 105–114.

Petford, N., Cruden, A., McCaffrey, K., Vigneresse, J., et al., 2000. Granite magma formation, transport and emplacement in the earth's crust. Nature 408 (6813), 669–673.

Reymer, A., Schubert, G., 1984. Phanerozoic addition rates to the continental crust and crustal growth. Tectonics 3 (1), 63–77.

Reymer, A., Schubert, G., 1986. Rapid growth of some major segments of continental crust. Geology 14, 299–302.

Ricard, Y., Bercovici, D., Schubert, G., 2001. A two-phase model for compaction and damage. ii- applications to compaction, deformation, and the role of interfacial surface tension. Journal of geophysical research 106 (B5), 8907–8924.

Ringwood, A., 1990. Slab-mantle interactions: 3. petrogenesis of intraplate magmas and structure of the upper mantle. Chemical Geology 82, 187–207.

Ringwood, A., Green, D., 1966. An experimental investigation of the gabbro-eclogite transformation and some geophysical implications. Tectonophysics 3 (5), 383–427.

Rudnick, R., 1995. Making continental crust. Nature 378, 571–577.

Rudnick, R., Gao, S., 2003. Composition of the continental crust. Treatise on geochemistry 3, 1–64.

Rudnick, R. L., Fountain, D. M., 1995. Nature and composition of the continental crust: a lower crustal perspective. Reviews of Geophysics 33, 267–267.

Sajona, F., Maury, R., Bellon, H., Cotten, J., Defant, M., Pubellier, M., 1993. Initiation of subduction and the generation of slab melts in western and eastern mindanao, philippines. Geology 21 (11), 1007–1010.

Scambelluri, M., Philippot, P., 2001. Deep fluids in subduction zones. Lithos 55 (1), 213–227.

Schmidt, M., Poli, S., 1998. Experimentally based water budgets for dehydrating slabs and consequences for arc magma generation. Earth and Planetary Science Letters 163 (1), 361–379.

Scholl, D., von Huene, R., 2007. Crustal recycling at modern subduction zones applied to the pastissues of growth and preservation of continental basement crust, mantle geochemistry, and supercontinent reconstruction. Geological Society of America Memoirs 200, 9–32.

Shaw, D. M., Dostal, J., Keays, R. R., 1976. Additional estimates of continental surface precambrian shield composition in canada. Geochimica et Cosmochimica Acta 40 (1), 73–83.

Singh, S., Carton, H., Tapponnier, P., Hananto, N., Chauhan, A., Hartoyo, D., Bayly, M., Moeljopranoto, S., Bunting, T., Christie, P., et al., 2008. Seismic evidence for broken oceanic crust in the 2004 sumatra earthquake epicentral region. Nature Geoscience 1 (11), 777–781.

Spiegelman, M., Kenyon, P., 1992. The requirements for chemical disequilibrium during magma migration. Earth and Planetary Science Letters 109 (3), 611–620.

Stein, M., Ben-Avraham, Z., 2007. Mechanisms of continental crust growth. Treatise on Geophysics 9, 171195.

Stern, C., 1991. Role of subduction erosion in the generation of andean magmas. Geology 19 (1), 78–81.

Stevenson, D., 1989. Spontaneous small-scale melt segregation in partial melts undergoing deformation. Geophysical Research Letters 16 (9), 1067–1070.

Stolper, E., Newman, S., 1994. The role of water in the petrogenesis of mariana trough magmas. Earth and Planetary Science Letters 121 (3), 293–325.

Tatsumi, Y., 2005. The subduction factory: How it operates in the evolving earth. GSA today 15 (7), 4.

Tatsumi, Y., Eggins, S., 1995. Subduction zone magmatism. Wiley.

Taylor, S., McLennan, S., 1985. The continental crust: its composition and evolution.

Taylor, S. R., McLennan, S. M., 1995. The geochemical evolution of the continental crust. Reviews of Geophysics 33 (2), 241–265.

Tiara, A., Saito, S., Aoike, K., Morita, S., Tokuyama, H., Suyehiro, H., Takahashi, N., Shinohara, M., Kiyokawa, S., Naka, J., Klaus, A., 1998. Nature and growth of the northern izu-bonin (ogasawara) arc crust and their implications to continental crust formation. Island Arc 7, 395–407.

Vaughan, A., Scarrow, J., 2003. Ophiolite obduction pulses as a proxy indicator of superplume events? Earth and Planetary Science Letters 213 (3), 407–416.

von Huene, R., Scholl, D., 1991. Observations at convergent margins concerning sediment subduction, subduction erosion, and the growth of continental crust. Reviews of Geophysics 29 (3), 279–316.

Wedepohl, H. K., 1995. The composition of the continental crust. Geochimica et Cosmochimica Acta 59 (7), 1217–1232.

Weertman, J., 1971. Theory of water-filled crevasses in glaciers applied to vertical magma transport beneath oceanic ridges. Journal of Geophysical Research 76 (5), 1171–1183.

Weinberg, R. F., Podladchikov, Y., 1994. Diapiric ascent of magmas through power law crust and mantle. Journal of Geophysical Research 99 (B5), 9543–9560.

Chapter 2

Method

All numerical experiments are based on the I2VIS code (Gerya and Yuen, 2003). This code uses conservative finite differences and a non-diffusive marker in cell technique to simulate multiphase flow in 2D. It accounts for visco-plastic rheology and petrological phase transitions. The initial geometry and setup used in each study are described in the subsequent chapters. All abbreviations and units used in this chapter are listed in Table 2.1.

Symbol	Meaning	Unit
A	Water percolation constant	
A_D	Material constant	$[MPa^{-n}s^{-1}]$
$A_{peierls}$	Material constant	$[MPa^{-1}s^{-1}]$
C	Composition	$[J/kg/K]$
C_P	Isobaric heat capacity	$[J/kg/K]$
c	Cohesion	$[Pa]$
E_a	Activation energy	$[kJmol^{-1}]$
g	Gravitational acceleration	$[ms^{-1}]$
H_a	Adiabatic heat production	$[Wm^{-1}K^{-1}]$
H_r	Radioactive heat production	$[Wm^{-1}K^{-1}]$
H_s	Shear heat production	$[Wm^{-1}K^{-1}]$
k	Thermal conductivity	$[Wm^{-1}K^{-1}]$
M	Volumetric melt fraction	
n	Stress exponent	
P	Dynamic pressure	$[Pa]$
P_{fluid}, P_{melt}	Pore fluid and melt pressure	$[Pa]$
Q_l	Latent heat	
p	Material constant	
q	Material constant	

q_x, q_z	Horizontal and vertical heat flux components	$[Wm^{-2}]$
R	Gas constant	$[Jmol^{-1}K^{-1}]$
t	Time	$[s]$
T	Temperature	$[K$ or $^oC]$
v_x, v_z	Horizontal and vertical velocity vector	$[ms^{-1}]$
$v_{x_{water}}, v_{z_{water}}$	Horizontal and vertical fluid velocity vector	$[ms^{-1}]$
$v_{percolation}$	Percolation velocity	$[ms^{-1}]$
v_e, v_s	Erosion and sedimentation rate	$[ms^{-1}]$
V_a	Activation volume	$[JMPa^{-1}mol^{-1}]$
X_{H_2O}	Weight percent of pore water	
α	Thermal expansion coefficient	$[K^{-1}]$
β	Thermal compressibility coefficient	$[MPa^{-1}]$
η	Viscosity	$[Pas]$
η_n, η_s	Normal and shear viscosity	$[Pas]$
λ_{fluid}, λ_{melt}	Pore fluid and melt pressure factor	
ρ	Density	$[kgm^{-3}]$
$\dot{\varepsilon}_{ij}$	Strain rate tensor	$[s^{-1}]$
$\dot{\varepsilon}'_{ij}$	Deviatoric strain rate tensor	$[s^{-1}]$
$\dot{\varepsilon}_{II}$	Second strain invariant	$[s^{-1}]$
ϕ	Internal friction angle	$[^o]$
σ_{ij}	Stress tensor	$[Pa]$
σ'_{ij}	Deviatoric stress tensor	$[Pa]$
σ_{II}	Second invariant of the deviatoric stress tensor	$[Pa]$

Table 2.1: Abbreviations used in the text.

2.1 Governing equations

The governing conservation equations of mass, momentum and energy and the constitutive relationships between stress and strain-rate (needed in the creeping flow regime) are solved on an irregularly spaced staggered grid in Eulerian configuration.

Continuity equation

Conservation of mass is described by the Lagrangian continuity equation for a compressible fluid:

$$\frac{\partial v_x}{\partial x} + \frac{\partial v_z}{\partial z} = \frac{-1}{\rho}\frac{D\rho}{Dt}$$

where $\frac{D\rho}{Dt}$ is the substantive density time derivative, which accounts locally for melt extraction.

Momentum equation

The 2D Stokes equation for slow flow (creeping flow) takes the form:

$$\frac{\partial \sigma'_{xx}}{\partial x} + \frac{\partial \sigma_{xz}}{\partial z} = \frac{\partial P}{\partial x}$$

$$\frac{\partial \sigma'_{zz}}{\partial z} + \frac{\partial \sigma_{xz}}{\partial z} = \frac{\partial P}{\partial z} - g\rho(P,T,C)$$

σ'_{xx},σ_{xz},σ'_{zz} are the deviatoric stress tensor components. The density, ρ, depends on P (pressure), T (temperature) and C (composition).

This is followed by the constitutive relationship between deviatoric stress (σ'_{ij}) and strain-rate ($\dot{\varepsilon}'_{ij}$) for a compressible fluid (Gerya and Yuen, 2007). The transport coefficient η represents the viscosity, which depends on the temperature (T), pressure (P), composition (C) and strain-rate:

$$\sigma'_{xx} = 2\eta\dot{\varepsilon}'_{xx}$$

$$\sigma_{xz} = 2\eta\dot{\varepsilon}_{xz}$$

$$\sigma'_{zz} = 2\eta\dot{\varepsilon}'_{zz}$$

$$\dot{\varepsilon}'_{xx} = -\dot{\varepsilon}'_{zz} = \frac{1}{2}\left(\frac{\partial v_x}{\partial x} - \frac{\partial v_z}{\partial z}\right)$$

$$\dot{\varepsilon}_{xz} = \frac{1}{2}\left(\frac{\partial v_x}{\partial z} + \frac{\partial v_z}{\partial x}\right)$$

Energy equation

The temperature equation is solved on a Lagrangian frame for which the extended Boussinesq approximation is used, as follows (Gerya and Yuen, 2003):

$$\rho C_p\left(\frac{DT}{Dt}\right) = -\frac{\partial q_x}{\partial x} - \frac{\partial q_z}{\partial z} + H_r + H_a + H_s$$

$$q_x = -k(P,T,C)\frac{\partial T}{\partial x}$$
$$q_z = -k(P,T,C)\frac{\partial T}{\partial z}$$

where q_x, q_z are the thermal heat flux components, k is the thermal conductivity, which depends on pressure, temperature and composition, H_r, H_a and H_s are the radioactive, adiabatic and shear heat productions.

Radioactive heat production depends on the rock composition and is assumed to be constant (Table 2.3):

$$H_r = constant(C)$$

The adiabatic heat production/consumption is related to pressure changes (compression/decompression):

$$H_a = T\alpha\left(v_x\frac{\partial P}{\partial x} + v_z\frac{\partial P}{\partial z}\right)$$

The shear heat production is related to dissipation of mechanical energy during viscous deformation and depends on the deviatoric stress and deviatoric strain rate:

$$H_s = \sigma'_{xx}\dot{\varepsilon}'_{xx} + 2\sigma_{xz}\dot{\varepsilon}_{xz} + \sigma'_{zz}\dot{\varepsilon}'_{zz}$$

The effect of latent heating/cooling due to equilibrium melting/crystallization is included implicitly by increasing the effective heat capacity ($C_{p_{eff}}$) and the thermal expansion (α_{eff}) of melting/crystallizing rocks:

$$C_{p_{eff}} = C_p + Q_l\left(\frac{\partial M}{\partial T}\right)_{p=const}$$
$$\alpha_{eff} = \alpha + \rho\frac{Q_l}{T}\left(\frac{\partial M}{\partial T}\right)_{p=const}$$

Q_l is the latent heat of melting. For values of ρ, C_p, k, H_r and Q_l see Table 2.3.

2.2 Rheology

The rheologies used in this study are visco-plastic. The viscous creep of rocks is defined in terms of deformation invariants and depends on temperature, pressure and strain rate. The viscosity for dislocation creep is

defined as follows (Ranalli, 1995):

$$\eta_{creep} = \frac{\dot{\varepsilon}_{II}^{\frac{1-n}{n}}}{A_D{}^{\frac{1}{n}}} exp\left(\frac{E_a + PV_a}{nRT}\right)$$

where $\dot{\varepsilon}_{II}$ is the second invariant of the strain rate tensor. A_D (pre-exponential factor), E_a (activation energy), n (creep exponent), V_a (activation volume) are experimentally determined flow law parameters and R is the gas constant.

Plasticity is implemented using the following yield criterion, which limits the creep viscosity, altogether yielding an effective visco-plastic rheology.

$$\eta_{creep} \leq \frac{\sigma_{yield}}{2\dot{\varepsilon}_{II}}$$

$$\sigma_{yield} = c + Psin(\phi_{dry})\lambda_{fluid/melt}$$

The local plastic strength of a rock depends on the mean stress, P (dynamic pressure), ambient brittle/plastic strength c, which is the strength at P = 0, and on the effective internal friction angle, which is calculated from the friction angle of dry rocks ϕ_{dry} and the pore fluid pressure factor $\lambda_{fluid/melt}$. This factor is interpreted as:

$$\lambda_{fluid/melt} = 1 - \frac{P_{fluid/melt}}{P}$$

The pore pressure P_{fluid} and/or melt pressure P_{melt} reduces the yield strength σ_{yield} of fluid or melt containing, porous or fractured rocks. A detailed discussion on fluid and melt related weakening may be found in (Sizova et al., 2010; Gerya and Meilick, 2011).

At high pressure the strength of rocks is limited by the Peierls mechanism (Kameyama et al., 1999; Karato et al., 2001; Katayama and Karato, 2008) which is a temperature-dependent mode of plastic deformation that takes over from the dislocation mechanism at elevated stresses:

$$\eta_{creep} = \frac{1}{2A_{peierls}\sigma_{II}} exp\left(\frac{E_a + PV_a}{nRT}\left(1 - \left(\frac{\sigma_{II}}{\sigma_{peierls}}\right)^p\right)^q\right)$$

The Peierls mechanism is a dominant deformation mechanism of the downgoing slab, where the temperature is low and stress is high (e.g. Karato et al., 2001).

According to our rheological model, plastic deformation of fluid or melt containing rocks is affected by the fluid and melt pressure factor (λ_{fluid}, λ_{melt}), respectively. Because water and melt are also expected to have

an effect on viscous deformation, different flow laws are used for dry and fluid or melt containing rocks (details are given in the respective chapters). As a result, the effective viscosity of rocks at relatively cold temperatures is dominated by weakening effects of fluids and melts. Temperature and stress, on the other hand, are dominant factors, controlling the viscosity of hot rocks. 10^{17} and 10^{25} Pas are the lower and upper cut-off values for viscosity of all types of rocks in our numerical experiments.

2.3 Petrological model

Mineralogical reactions, such as phase transitions, dehydration reactions or melting reactions may significantly affect the physical properties of rocks and hence the geodynamic evolution considered. For this purpose stable phase relations for different lithologies (Table 2.2) were computed as a function of pressure and temperature using the software "perplex" (Connolly, 2005). The thermodynamic database used for the properties of all endmember species and mineral solutions are summarized in Gerya et al. (2006) and Mishin et al. (2008). Examples of the procedure and computational strategy may be found in Kerrick and Connolly (2001) and Connolly (2005). All precomputed properties (e.g. enthalpy, water content and density) were saved on a grid with a resolution of 5 K and 25 MPa, respectively. At every timestep these precomputed properties are updated for all the Lagrangian markers. Figure 2.1 shows an example of the density contrast between the mantle and the metabasalt as a function of pressure and temperature. The water content of various lithologies as a function of pressure and temperature is shown in Figure 2.2. Further examples may be found in Gerya (2010), Gerya and Meilick (2011) and Zhu et al. (2011). Other physical properties used in this study are summarized in Table 2.3.

	Pressure[$kbar$]					
Composition	1-70 [$kbar$]				70-1494 [$kbar$]	
[wt.%]	Sediment	Basalt	Gabbro	Mantle	Basalt	Mantle
SiO_2	61.10	47.62	53.49	45.55	54.54	45.82
Al_2O_3	12.43	14.48	14.07	4.03	13.72	3.61
FeO	5.43	10.41	6.86	7.47	11.25	8.11
MgO	2.59	6.92	12.07	37.42	8.64	38.59
CaO	6.21	13.39	10.73	3.18	11.86	3.87
Na_2o	2.54	2.15	1.22	0.33	–	–
K_2O	2.13	0.58	0.09	0.03	–	–
H_2O	7.6	2.78	1.47	1.98	–	–

Table 2.2: Compositions ($wt.\%$) used for the calculations of stable mineral assemblages by Gibbs free energy minimization (Connolly, 2005) and subsequent thermodynamic properties used in the numerical experiments (e.g. water content). Sediment is the GLOSS average (Plank and Langmuir, 1998); basalt is an average for the upper 500 m of the igneous section of the oceanic crust (Staudigel et al., 1989); gabbro is a synthetic composition for the gabbroic section of the oceanic crust (Behn and Kelemen, 2003) modified to contain up to 1.5 $wt.\%$ water to represent the effects of lower crustal hydrothermal alteration (Carlson, 2003) and peridotite is the LOSIMAG composition (Hart and Zindler, 1986) chosen to represent mantle peridotite. The compositions have been simplified by the omission of minor elements such as Mn, P, Ti, and Cr and the assumption that all Fe is ferrous; additionally CO_2 has been removed from the GLOSS sediment composition. At greater depth the chemical composition reduces to $SiO_2 - Al_2O_3 - FeO - MgO$ (Stixrude and Lithgow-Bertelloni, 2005).

Material	ρ_0 $[kg/m^3]$	k at T_K, P_{MPa} $[W/m/K]$	Q_l $[kJ/kg]$	H_r $[\mu W/m^3]$	C_p $[J/kg/K]$	α $[1/K]$	β $[1/MPa]$
Sediment	2600(solid) 2400(molten)	[0.64+807/(T+77)]× exp(0.00004×P)	300	1.5	1000	3×10^{-5}	1×10^{-11}
Upper continental crust	2700(solid) 2400(molten)	[0.64+807/(T+77)]× exp(0.00004×P)	300	1 1.5	1000	3×10^{-5}	1×10^{-11}
Lower continental crust	2700(solid) 2400(molten)	[0.64+807/(T+77)]× exp(0.00004×P)	380	1 1.5	1000	3×10^{-5}	1×10^{-11}
Upper oceanic crust (basalt)	3000(solid) 2900(molten)	[1.18+474/(T+77)]× exp(0.00004×P)	380	0.25	1000	3×10^{-5}	1×10^{-11}
Lower oceanic crust (gabbro)	3000(solid) 2900(molten)	[1.18+474/(T+77)]× exp(0.00004×P)	400	0.25	1000	3×10^{-5}	1×10^{-11}
Dry mantle	3300(solid) 2900(molten)	[0.73+1293/(T+77)]× exp(1+0.00004×P)	400	0.022	1000	3×10^{-5}	1×10^{-11}
Wet mantle	3300(serp.) 3200(hydrated) 2900(molten)	[0.73+1293/(T+77)]× exp(1+0.00004×P)	400	0.022	1000	3×10^{-5}	1×10^{-11}
Felsic Magmatics	2600(solid)	[0.64+807/(T+77)]× exp(0.00004×P)	300	1.5	1000	3×10^{-5}	1×10^{-11}
Mafic Magmatics	3000(solid)	[1.18+474/(T+77)]× exp(0.00004×P)	380	0.25	1000	3×10^{-5}	1×10^{-11}

Table 2.3: Material properties: ρ = initial density $[kg/m^3]$ (Turcotte and Schubert, 2002; Bittner and Schmeling, 1995), k = thermal conductivity $[W/m/K]$ (Clauser and Huenges, 1995; Hofmeister, 1999), Q_l = latent heat $[kJ/kg]$ (Turcotte and Schubert, 2002; Bittner and Schmeling, 1995), H_r = radioactive heat $[[\mu W/m^3]]$ (Turcotte and Schubert, 2002), C_p = heat capacity $[J/kg/K]$, α = thermal expansion $[1/K]$, β = thermal compressibility $[1/MPa.]$.

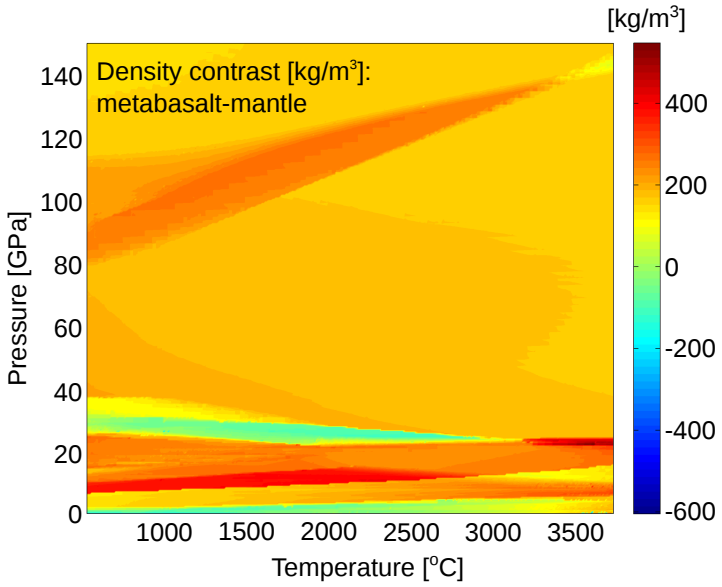

Figure 2.1: Density difference $[kg/m^3]$ between the metamorphosed oceanic crust (metabasalt) and mantle (colour scale indicated by the colour bar to the right) computed from the thermodynamic data used in the numerical experiments. Except for a pressure interval corresponding to the base of the transition zone (Pressure $<$ 40 GPa), metabasalt is predicted to be denser than mantle, with a typical density contrast of 200 - 300 kg/m^3 in the lower mantle.

2.4 Hydration and water migration

Connate water carried into subduction zones is expelled due to compaction and dehydration reactions. Free fluid present in sediment and basalt makes up to 2 $wt.\%$ at the surface and is believed to decrease with depth. To account for compaction it is supposed that this water is released, decreasing from 2 $wt.\%$ to 0 $wt.\%$ at 75 km depth:

$$X_{H_2O(wt.\%)} = (1 - 0.0123\Delta z)X_{H_2O(p0)}$$

where $X_{H_2O(p0)} = 2wt.\%$ is the connate water content at the surface, and Δz is the depth below the surface in km (0 - 75 km). Dehydration reactions and associated water release are computed based on the physicochemical conditions and the assumption of thermodynamic equilibrium (see Petrological model description or Gorczyk et al. (2007). Figure 2.2 shows the

stable water for different rock types (in equilibrium with the mineral assemblage, but without connate water). Expelled water is stored in a newly generated water marker that moves independently. The velocity of the fluid is computed according to pressure gradients (e.g. Faccenda et al., 2009) as:

$$v_{x(water)} = v_x - A\left(\frac{\partial P}{\partial x}\right)$$

$$v_{z(water)} = v_z - A\left(\frac{\partial P}{\partial z} - \rho_{fluid} g\right)$$

$$A = \frac{v_{percolation}}{g(\rho_{mantle} - \rho_{fluid})}$$

where v_x and v_z are the fluid velocities in x and z direction, v_x and v_z indicate the local velocity of the solid mantle, A is a water percolation constant, $v_{percolation} = 10\ cm/yr$, a presumed standard water percolation velocity (Gorczyk et al., 2007; Peacock, 1990), g = 9.81 m/s is the gravitational acceleration, $\rho_{mantle} = 3300\ kg/m^3$ and $\rho_{fluid} = 1000\ kg/m^3$ is the density of the mantle and fluid, respectively.

When a given water marker encounters a lithology capable of absorbing water by hydration or partial melting, the moving water is consumed.

2.5 Partial melting and melt extraction

Melting

In nature variable hydration triggers melting over a range of temperatures. Therefore it is assumed, that the degree of both hydrous and dry melting is a linear function of pressure and temperature (e.g. Gerya and Yuen, 2003). For a given pressure and rock composition the volumetric degree of melting M_0 is:

$$M_0 = \begin{cases} 0, & \text{if } T < T_{solidus} \\ \frac{T - T_{solidus}}{T_{liquidus} - T_{solidus}}, & \text{if } T_{solidus} < T < T_{liquidus} \\ 1, & \text{if } T > T_{liquidus} \end{cases}$$

where $T_{solidus}$ and $T_{liquidus}$ are the solidus and the liquidus temperature at a given pressure and rock composition (Table 2.4). The effective density, ρ_{eff} of partially molten rocks is computed according to the relation:

$$\rho_{eff} = \rho_{solid} - M(\rho_{solid} - \rho_{melt})$$

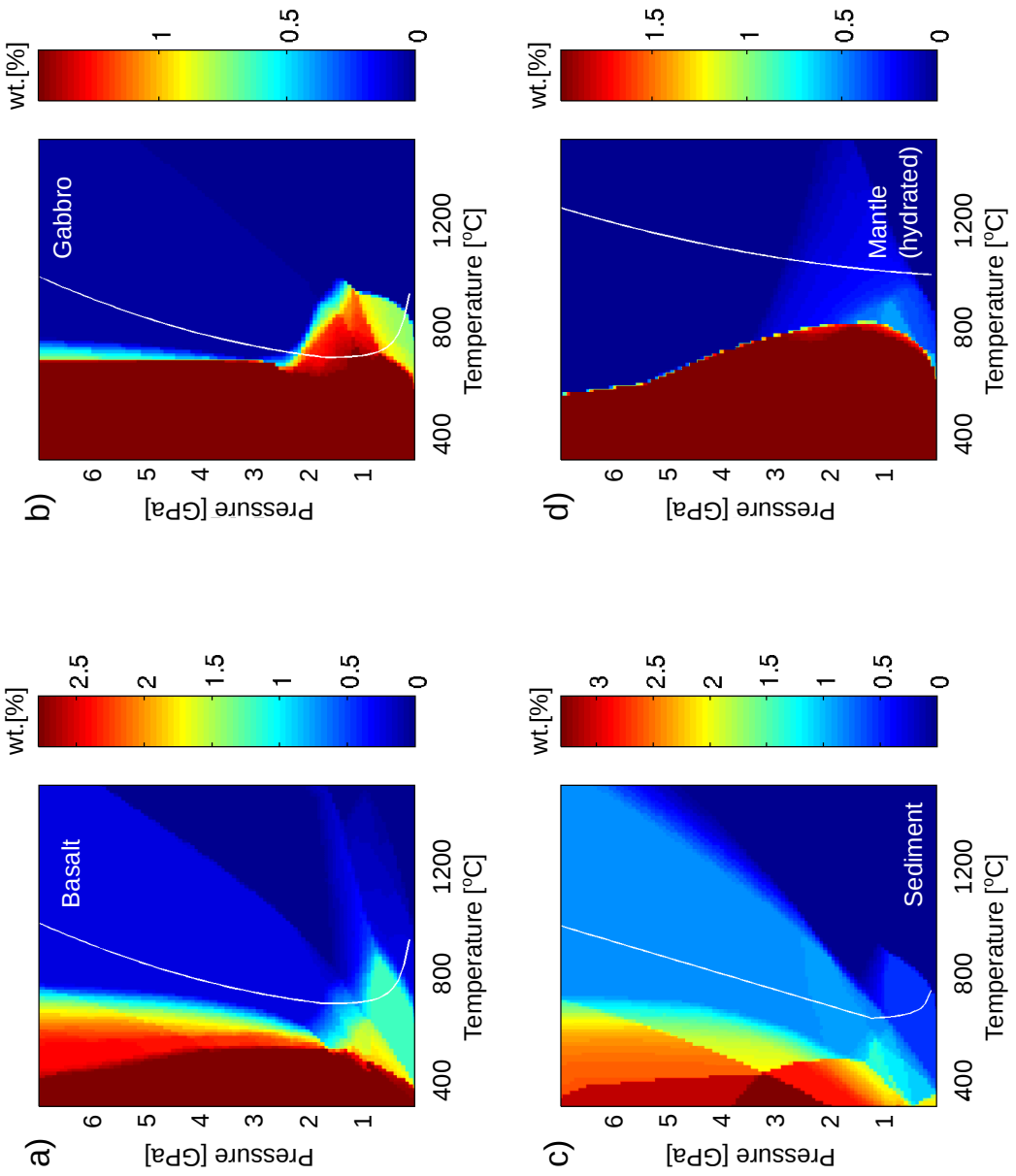

Figure 2.2: Water content in stable mineral assemblages (i.e. without connate water) for a) Basalt b) Gabbro c) Sediment d)Hydrated mantle. Equilibrium mineral assemblages are computed from thermodynamic data and rock compositions (Table 2.2) using Gibbs free energy minimization. White solid lines show the solidus Temperature (Table 2.4). The water content of solid and molten rocks is limited to: basalt = 2.78 wt.% , gabbro = 1.47 wt.%, sediment = 7.60 wt.%, mantle(hydrated) = 1.98 wt.%. For a detailed description of the stable water content see Table 2.2.

where ρ_{solid} and ρ_{melt} are the densities of solid and molten rocks at given pressure P(MPa) and temperature T(K) computed from:

$$\rho_{P,T} = \rho_0(1 - \alpha(T - T_0))(1 + \beta(P - P_0))$$

where α is the thermal expansion coefficient, β is the compressibility coefficient and ρ_0 is the density computed according to the database (Chapter 5 and 7) or the standard density (Chapter 3, 4 and 6) at $P_0 = 0.1$ MPa and $T_0 = 298$ K given in Table 2.3. The effect of latent heat is accounted for by increasing the heat capacity (C_p) and the thermal expansion coefficient (α) as described for the temperature equation. The effective viscosity of partially molten rocks (M > 0.1) is calculated according to (Pinkerton and Stevenson, 1992; Bittner and Schmeling, 1995):

$$\eta_{melt} = \eta_0 exp\left(2.5 + (1 - M)\left(\frac{1 - M}{M}^{0.48}\right)\right)$$

where η_0 is an empirical parameter depending on rock composition, being $\eta_0 = 10^{13}$ Pas for molten mafic rocks (mantle, basalt, gabbro) and $\eta_0 = 5 \times 10^{14}$ Pas for molten felsic rocks (sediment, upper crust, lower crust). Because melt exceeding a predefined melt threshold of 4 % (M > 0.04, see following section) is extracted, the viscosity of partially molten rocks at depth is computed according to experimentally determined flow laws, where the effective creep viscosity is a function of strain rate, pressure and temperature (see Rheology section for details). Intrusive bodies, on the other hand, can contain high melt fractions (M > 0.1) and their viscosity will be affected by the above mentioned formulation.

Material	$T_{solidus}[K]$ at $[MPa]$	condition at $[MPa]$	$T_{liquidus}[K]$ at $[MPa]$
Sediment, upper continental crust, felsic magmatics	$889 + 17900/(P + 54) + 20200/(P + 54)^2$	$P < 1200$	$1262 + 0.09 \times P$
	$831 + 0.06 \times P$	$P > 1200$	
Lower continental crust, oceanic crust (gabbro, basalt), mafic magmatics	$973 - 70400/(P + 354) + 77800000/(P + 354)^2$	$P < 1600$	$1423 + 0.105 \times P$
	$935 + 0.0035 \times P + 0.0000062 \times P^2$	$P > 1600$	
Dry mantle	$1394 + 0.132899 \times P - 0.00000204 \times P^2$	$P < 10000$	$2073 + 0.114 \times P$
	$2212 + 0.030819 \times (P - 10000)$	$P > 10000$	
Wet mantle	$(1240 + 49800)/(P + 323)$	$P < 2400$	$2073 + 0.114 \times P$
	$1266 - 0.0118 \times P + 0.0000035 \times P^2$	$P > 10000$	

Table 2.4: Melting conditions used for the different lithologies after (Schmidt and Poli, 1998; Hess, 1989; Hirschmann, 2000; Johannes, 1985; Poli and Schmidt, 2002). $T_{solidus}$ and $T_{liquidus}$ are the solidus and liquidus Temperature $[K]$ at given Pressure $[MPa]$.

Melt extraction and emplacement

Although melt might accumulate and form large melt reservoirs, it is more likely that melt collects in channels or dykes and leaves the melting zone before reaching high melt fractions (Schmeling, 2006, 2010). Hence, melt exceeding a predefined melt threshold (e.g. Schmeling, 2010) of $M_{max} = 4$ % is extracted and only a non-extractable amount of melt $M_{min} = 2\%$ remains in the source (e.g. Nikolaeva et al., 2008; Sizova et al., 2010; Gerya and Meilick, 2011). Markers track the amount of extracted melt during the evolution of an experiment. The total amount of melt, M, for every marker takes into account the amount of previously extracted melt and is calculated as:

$$M = M_0 - \sum_n M_{ext}$$

where $\sum_n M_{ext}$ is the total melt fraction extracted during the previous n extraction episodes. Rocks are considered refractory when the extracted melt fraction is bigger than the standard one (i.e. when $\sum_n M_{ext} > M_0$). If the total amount of melt exceeds the threshold M_{max}, the melt fraction $M_{ext} = M - M_{min}$ is extracted and $\sum_n M_{ext}$ is updated. Extracted melt is transmitted instantaneously to emplacement areas, as melt migrates faster than rocks deform (Elliott et al., 1997; Hawkesworth et al., 1997).

Although the average and range of intrusive : extrusive (I : E) volume ratios for different petrotectonic settings may differ (ranging from 1 : 1 to 16 : 1), a ratio of 5 : 1 can be viewed as common to most magmatic systems considering the uncertainties (White et al., 2006). Accordingly, intrusive rocks, which comprise 80 % of melt, are emplaced in areas of highest possible intrusion emplacement rate, i.e., highest possible local crustal divergence rate. div_{crust} is evaluated above the melt extraction region by locally computing the ratio of the effective melt overpressure and the effective viscosity of the crust:

$$div_{crust} = [Pz_{melt} - g\rho_{melt}(z_{melt} - z) - Pz]/\eta_z$$

where Pz_{melt} is the pressure at the extraction level z_{melt}, and P_z is the pressure at the current level z, g is the gravitational acceleration in z-direction $[m/s^2]$, ρ_{melt} is the melt density and η_z is the effective local crustal viscosity at the current level z. Extracted melts are thus emplaced at the level z where the computed possible crustal divergence rate div_{crust} is highest. Both the effects of matrix compaction in the melt extraction area and crustal divergence in the melt emplacement area are taken into account in the compressible continuity equation (e.g. Gerya and Yuen, 2007), which provides correct coupling between local and global flow fields.

2.6 Boundary conditions

All mechanical boundary conditions are free slip, only the lower boundary is permeable in vertical direction, satisfying an external free slip boundary condition (Gorczyk et al., 2007). Similar to the usual free slip condition, external free slip allows global conservation of mass in the computational domain. To allow for topographic build up of the lithosphere, the top surface of the lithosphere is treated as an internal free surface (Schmeling et al., 2008) by using a top layer (of 8 to 22 km thickness, depending on the size of the model domain) with low viscosity (10^{18} Pas) and low density (1 kg/m^3 for air, 1000 kg/m^3 for sea water). The large viscosity contrast across this boundary minimizes shear stresses ($< 10^5$ Pa) at the top of the lithosphere, allowing for an efficient free surface (Schmeling et al., 2008).

Surface processes

The topographic evolution accounts for the effects of erosion and sedimentation. The crust/air interface (surface) evolves according to a transport equation, which is solved at each time-step on the Eulerian grid (Gorczyk et al., 2007):

$$\frac{\partial z_{es}}{\partial t} = v_z - v_x \frac{\partial z_{es}}{\partial x} - v_s + v_e$$

where z_{es} is the vertical position of the surface as a function of the horizontal distance x; v_z and v_x are the vertical and horizontal components of the material velocity vector at the surface (z is positive downward, z = 0 at the top of the box); v_s and v_e are the sedimentation and erosion rates, respectively which are defined as follows (Gerya and Meilick, 2011):

$$z < 9km \begin{cases} v_s = & 0.0 \text{ mm/yr} \\ v_e = & 0.3 \text{ mm/yr} \end{cases}$$

$$z > 10km \begin{cases} v_s = & 0.03 \text{ mm/yr} \\ v_e = & 0.0 \text{ mm/yr} \end{cases}$$

In regions with steep surfaces, for example in the trench region, an increased erosion/sedimentation rate (1 mm/yr) is used to account for additional mass transport.

2.7 Computational strategy

The I2VIS code (Gerya and Yuen, 2003, 2007) uses conservative finite differences and a non-diffusive marker in cell technique to simulate mul-

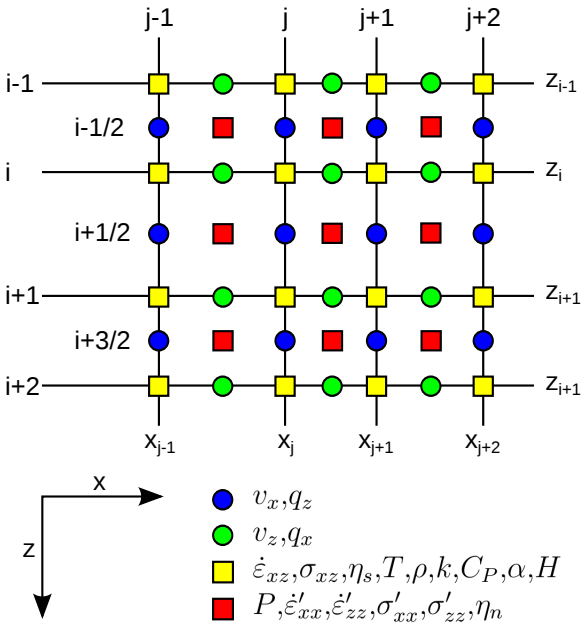

Figure 2.3: Schematic representation of the non-uniform rectangular staggered grid in Eulerian configuration. Different symbols correspond to the nodal points for different scalar properties, vectors and tensors. i, i+1/2 etc. and j, j+1/2 etc. indices represent the staggered grid and denote, the horizontal and vertical position of four different type of nodal points.

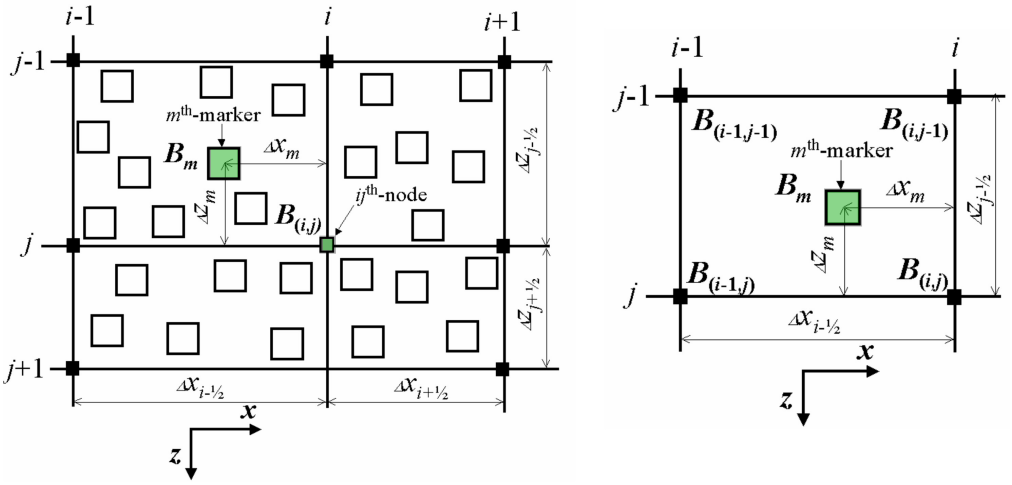

Figure 2.4: Schematic representation of geometrical relations used for the adopted first-order of accuracy interpolation schemes of a parameter B (a) from the markers to Eulerian nodes and (b) from Eulerian nodes back to markers (Gerya and Yuen, 2003). Each marker holds information concerning the temperature, position coordinates, three components of the strain tensor, representing the deformation history and the chemical components C.

tiphase flow. The governing conservation equations of mass, momentum and energy and the constitutive relationships between stress and strain-rate

(needed in the creeping flow regime) are solved using an irregularly-spaced staggered grid in Eulerian configuration (Figure 2.3). Advection of markers is done using a fourth-order in space / first order in time explicit Runge-Kutta interpolation scheme applied to the globally calculated velocity field on the Eulerian grid (Gerya and Yuen, 2003). Physical properties (i.e. water content, melt content, effective density, isobaric heat capacity, thermal expansion, adiabatic heat and latent heat) are transported by Lagrangian markers and move according to the velocity field, which has been interpolated from the Eulerian grid. For interpolation between markers and nodes a distance-dependent bilinear averaging scheme (Gerya and Yuen, 2003) is used, according to which markers located closer to a node have higher statistical weights (Figure 2.4).

Bibliography

Behn, M., Kelemen, P., 2003. Relationship between seismic p- wave velocity and the composition of anhydrous igneous and meta- igneous rocks. Geochemistry Geophysics Geosystems 4, DOI: 10.1029/2002GC000393.

Bittner, D., Schmeling, H., 1995. Numerical modelling of melting processes and induced diapirism in the lower crust. Geophysical Journal International 123 (1), 59–70.

Carlson, R., 2003. Bound water content of the lower oceanic crust estimated from modal analyses and seismic velocities of oceanic diabase and gabbro. Geophysical Research Letters 30, no. 2142.

Clauser, C., Huenges, E., 1995. Thermal conductivity of rocks and minerals. Rock physics and phase relations: a handbook of physical constants 3, 105–126.

Connolly, J., 2005. Computation of phase equilibria by linear programming: A tool for geodynamic modeling and its application to subduction zone decarbonation. Earth and Planetary Science Letters 236, 524541.

Elliott, T., Plank, T., Zindler, A., White, W., Bourdon, B., 1997. Element transport from slab to volcanic front at the mariana arc. Journal of Geophysical Research 102 (B7), 14991–15.

Faccenda, M., Gerya, T., Burlini, L., 2009. Deep slab hydration induced by bending related variations in tectonic pressure. Nature Geoscience 2, 790–793.

Gerya, T., 2010. Introduction to numerical geodynamic modelling. Cambridge University Press.

Gerya, T., Connolly, J., Yuen, D., Gorczyk, W., Capel, A., 2006. Seismic implications of mantle wedge plumes. Physics of the Earth and Planetary Interiors 156 (1), 59–74.

Gerya, T., Meilick, F., 2011. Geodynamic regimes of subduction under an active margin: effects of rheological weakening by fluids and melts. Journal of metamorphic Petrology 29, 7–31.

Gerya, T., Yuen, D., 2003. Characteristics-based marker-in-cell method with conservative nite-differences schemes for modeling geological flows with strongly variable transport properties. Physics of the Earth and Planetary Interiors 140, 293–318.

Gerya, T., Yuen, D., 2007. Robust characteristics method for modelling multiphase visco-elasto plastic thermo-mechanical problems. Physics of the Earth and Planetary Interiors 163, 83–105.

Gorczyk, W., Willner, A., Gerya, T., Connolly, J., Burg, J.-P., 2007. Physical controls of magmatic productivity at pacic-type convergent margins: Numerical modelling. Physics of the Earth and Planetary Interiors 163, 209232.

Hart, S., Zindler, A., 1986. In search of a bulk-earth composition. Chemical Geology 57, 247–267.

Hawkesworth, C. J., Turner, S., McDermott, F., Peate, D., van Calsteren, P., 1997. U-th isotopes in arc magmas: Implications for element transfer from the subducted crust. Science 276, 551–555.

Hess, P., 1989. Origins of Igneous Rocks. Harward University Press.

Hirschmann, M., 2000. Mantle solidus: experimental constraints and the effects of peridotite composition. Geochemistry Geophysics Geosystems 1, doi:10.1029/2000GC000070.

Hofmeister, A., 1999. Mantle values of thermal conductivity and the geotherm from phonon lifetimes. Science 283, 1699 1706.

Johannes, W., 1985. The significance of experimental studies for the formation of migmatites. In: Migmatites. Blackie.

Kameyama, M., Yuen, D., Karato, S.-I., 1999. Thermal-mechanical effects of low temperature plasticity (the peirls mechanism) on the deformation of viscoelastic shear zone. Earth and Planetary Science Letters 168, 159–172.

Karato, S.-I., Riedel, M., Yuen, D., 2001. Rheological structure and deformation of subducted slabs in the mantle transition zone: implications for mantle circulation and deep earthquakes. Physics of the Earth and Planetary Interiors 127, 83–108.

Katayama, I., Karato, S., 2008. Low-temperature, high-stress deformation of olivine under water-saturated conditions. Physics of the Earth and Planetary Interiors 168, 125–133.

Kerrick, D., Connolly, J., 2001. Metamorphic devolatilization of subducted oceanic metabasalts: implications for seismicity, arc magmatism and volatile recycling. Earth and Planetary Science Letters 189, 19–29.

Mishin, Y., Gerya, T., Burg, J.-P., Connolly, J., 2008. Dynamics of double subduction: Numerical modeling. Physics of the Earth and Planetary Interiors 171, 280–295.

Nikolaeva, K., Gerya, T., Connolly, J., 2008. Numerical modelling of crustal growth in intraoceanic volcanic arcs. Physics of the Earth and Planetary Interiors 171, 336–356.

Peacock, S., 1990. Fluid processes in subduction zones. Science 248, 329–337.

Pinkerton, H., Stevenson, R., 1992. Methods of determining the rheological properties of magmas at subliquidus temperatures. Journal of Volcanology and Geothermal Research 53, 47–66.

Plank, T., Langmuir, C., 1998. The chemical composition of subducting sediment and its consequences for the crust and mantle. Chemical Geology 145, 325–394.

Poli, S., Schmidt, M., 2002. Petrology of subducted slabs. Annual Review of Earth and Planetary Sciences 30, 207235.

Ranalli, G., 1995. Rheology of the Earth. Springer.

Schmeling, H., ., 2006. A model of episodic melt extraction for plumes. Journal of Geophysical Research 111, doi:10.1029/2004JB003423.

Schmeling, H., 2010. Dynamic models of continental rifting with melt generation. Tectonophysics 480, 33–47.

Schmeling, H., Babeyko, A., Enns, A., Faccenna, C., Funiciello, F., Gerya, T., Golabek, G., Grigull, S., Kaus, B., Morra, G., van Hunen, J., 2008. A benchmark comparison of spontaneous subduction modelstowards a free surface. Physics of the Earth and Planetary Interiors 171 (1), 198–223.

Schmidt, M., Poli, S., 1998. Experimentally based water budgets for dehydrating slabs and consequences for arc magma generation. Earth and Planetary Science Letters 163 (1), 361–379.

Sizova, E., Gerya, T., Brown, M., Perchuk, L., 2010. Subduction styles in the precambrian: Insight from numerical experiments. Lithos 116, 209–229.

Staudigel, H., Hart, S., Schmincke, H., Smith, B., 1989. Cretaceous ocean crust at dsdp sites 417-418: Carbon uptake from weathering versus loss by magmaticoutgassing. Geochimica et Cosmochimica Acta 53, 30913094.

Stixrude, L., Lithgow-Bertelloni, C., 2005. Mineralogy and elasticity of the oceanic upper mantle: origin of the low-velocity zone. Journal of Geophysical Research 110, no B03204.

Turcotte, D., Schubert, G., 2002. Geodynamics. Cambridge University Press.

White, S. M., Crisp, J. A., Spera, F. J., 2006. Long-term volumetric eruption rates and magma budgets. Geochemistry Geophysics Geosystems 7 (3), Q03010.

Zhu, G., Gerya, T., Honda, S., Tackley, P., Yuen, D., 2011. Influences of the buoyancy of partially molten rock on 3-d plume patterns and melt productivity above retreating slabs. Physics of the Earth and Planetary Interiors 185 (3), 112–121.

Chapter 3

Crustal Growth at Active Continental Margins: Numerical Modelling[1]

3.1 Abstract

The dynamics and melt sources for crustal growth at active continental margins are analysed by using a 2D coupled petrological-thermomechanical numerical model of an ocean-continent subduction zone. This model includes spontaneous slab retreat and bending, dehydration of subducted crust, aqueous fluid transport, partial melting, melt extraction and melt emplacement in form of extrusive volcanics and intrusive plutons. We could identify the following three geodynamic regimes of crustal growth: (i) stable arcs (ii) compressional arcs with diapir formation and (iii) extensional arcs. Crustal growth in a stable subduction setting results in the emplacement of flattened intrusions in the lower crust. At first dacitic melts, extracted from partially molten rocks located atop the slab (gabbro and basalt), intrude into the lower crust followed by mantle-derived (wet peridotite) basaltic melts from the mantle wedge. Thus extending plutons are formed, characterized by a successively increasing mantle component and low magmatic addition rates (10 $km^3/km/Myr$). Compressional arcs are accomplished by the formation and emplacement of hybrid diapirs. In the course of subduction localization and partial melting of basalt and sediment along the slab induces Rayleigh Taylor instabilities. Hence, buoyant diapirs are formed, composed of partially molten sediment and basalt of the oceanic crust. Subsequently, these diapirs ascend, crosscutting the

[1]This chapter co-authored by K. Vogt, T. Gerya and A. Castro was published in a slightly modified version in Physics of the Earth and Planetary Interiors, 192 - 193, 1 - 20 (2012).

lithosphere before they finally crystallize within the upper crust in form of silicic intrusions. Additionally, intrusions are formed in the lower crust derived by partial melting of rocks located atop the slab (basalt, gabbro, wet peridotite) and inside the diapir (basalt and sediment). Magmatic addition rates are somewhat higher compared to stable arcs (40 - 70 $km^3/km/Myr$). Subduction in an extensional arc setting results in decompression melting of dry peridotite. The backward motion of the subduction zone relative to the motion of the plate leads to thinning of the overriding plate. Thus, hot and dry asthenosphere rises into the neck as the slab retreats, triggering decompression melting of dry peridotite. Consequently large volumes of mafic (oceanic) crust are formed in the backarc region with total magmatic addition rates being as high as 90 - 170 $km^3/km/Myr$.

3.2 Introduction

The vast variety of igneous rocks of the continental crust implies that magmatism and crustal growth are closely linked to different geodynamic settings. Present day crustal growth is ascribed to two distinct plate tectonic settings: intraplate and convergent margins (Rudnick, 1995). Here we focus on crustal growth at continental margins, where oceanic crust is subducted beneath the continental lithosphere. The bulk composition of the continental crust is andesitic and cannot be derived directly by partial melting of the mantle (Rudnick, 1995; Hawkesworth and Kemp, 2006). Different mechanisms of crust formation have been proposed by scientists facing this problem (e.g. Taylor, 1966; Taylor and McLennan, 1985; Green, 1980; Ringwood, 1990; Kay and Mahlburg-Kay, 1991; Rudnick, 1995; Tatsumi, 2005). Understanding the dynamics of crustal growth requires identification of melt sources and estimates on the proportions of magmas derived from different sites of production, which add to the growth of the continental crust. Three potential sources of melt production can be identified: the mantle, subducted oceanic crust and continental crust, which experience melting under different physical conditions (Wyllie et al., 1984). It is widely accepted that water released from the subducting plate lowers the melting temperature of the overlying mantle allowing for flux melting of the hydrated mantle (e.g. Stolper and Newman, 1994; Tatsumi and Eggins, 1995; Schmidt and Poli, 1998; Iwamori, 1998). The role of slab derived melts is strongly debated in the literature, because subducted oceanic crust of most modern subduction zones is believed to be too cold to permit slab melting (Schmidt and Poli, 1998; Peacock et al., 1994). Nevertheless, it has been argued, that the formation of slab derived melts is

possible for young subduction zones (Kay, 1978; Drummond and Defant, 1990; Defant and Drummond, 1990; Sajona et al., 1993).

A general problem of crustal production processes within subduction zones is the relation of geodynamics to the composition of newly formed crust. The transition between different geodynamic regimes is closely linked to weakening effects imposed by fluids and melts (Gerya and Meilick, 2011) and has a major influence on arc growth. However, previous crustal growth models (e.g. Nikolaeva et al., 2008; Gerya and Meilick, 2011) neglected possible geodynamic effects of the overriding plate motion (e.g. van Hunen et al., 2000, 2002; Heuret et al., 2007; Sobolev and Babeyko, 2005; Schellart, 2008) and/or intrusion emplacement, which leaves a significant gap in our understanding of crustal growth processes within subduction zones. In order to fill in these gaps and investigate sites of melt production and crustal growth in relation to different geodynamic scenarios we performed a series of 2D numerical experiments by using a coupled petrological-thermomechanical numerical model of an ocean-continent subduction zone. The model includes overriding plate motion, spontaneous slab bending, dehydration of subducted crust, aqueous fluid transport, partial melting, melt extraction and melt emplacement in form of extrusive volcanics and intrusive plutons.

3.3 Numerical model description

Model Setup

The 2D coupled petrological-thermomechanical model simulates forced subduction at an active continental margin. A lithospheric to upper mantle cross-section of a subduction zone is modelled by an area of 4000 km by 200 km within a 50 Myr time span (Figure 3.1). At an imposed convergence rate of 5 cm/yr to 3 cm/yr and varying upper plate velocities, the oceanic plate (2500 km) is pushed toward an either fixed or moving continental plate (1500 km), reproducing subduction. The rectangular grid with 2041 $\times$ 201 nodes is non-uniform, resulting in a high resolution (1 km $\times$ 1 km) area in the centre of the model covering 1500 km horizontally, while the rest of the model remains at a lower resolution (5 $\times$ 1 km). The oceanic crust consists of 2 km of hydrated basalts and 5 km of gabbros. The continental crust is felsic and has a total thickness of 30 km. Both the asthenosphere and the upper mantle are composed of anhydrous peridotite and are defined by the temperature profile. For detailed material properties see Chapter 2. The rheological parameters used in this study are summarized in Table 3.1.

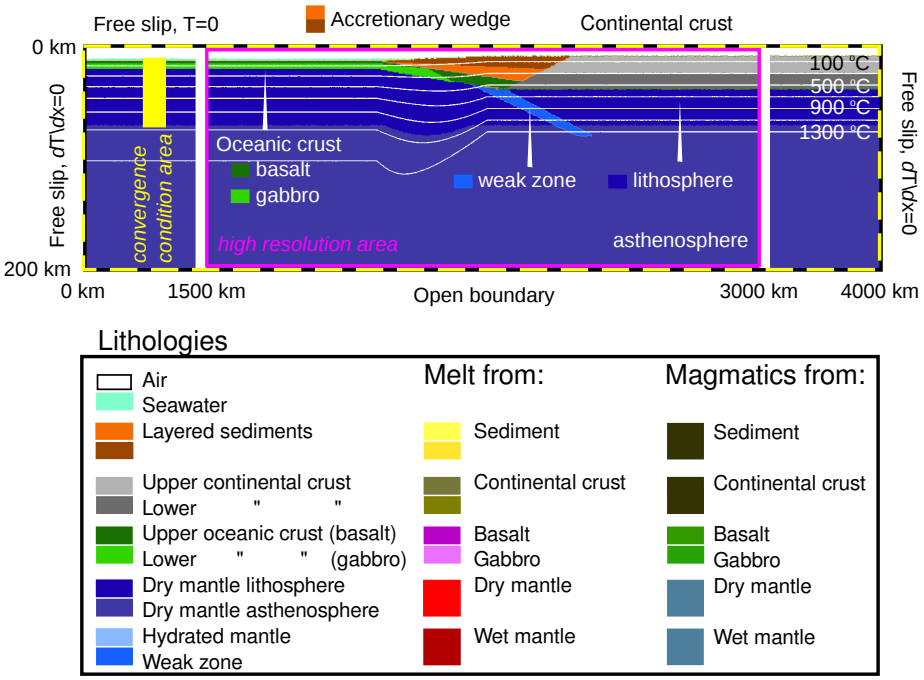

Figure 3.1: Initial setup of the numerical model (see method section for details). Staggered grid resolution is 2041 × 201 nodal points, with more than 10 million randomly distributed markers. Grid step is 1 × 1 km in the subduction zone area (1500 - 3000 km) and 5 × 1 km outside of this area. Isotherms are displayed in white for increments of 200 ^oC, starting from 100 ^oC. Colours indicate materials (i.e. rock type or melt), which appear in subsequent figures. To illustrate deformation, two layers with the same physical properties are distinguished using different colours for sediment, crust (upper and lower crust) and mantle (asthenosphere and lithosphere).

Water release and consumption as a function of pressure and temperature are computed from thermodynamic data by Gibbs free energy minimization (Connolly, 2005; Gerya and Meilick, 2011). The initial temperature field of the oceanic plate is defined by its oceanic geotherm (Turcotte and Schubert, 2002) for a specific lithospheric cooling age of 40 Myr. The initial temperature field of the continental plate increases linearly from 0 $°C$ at the surface to 1367 $°C$ at the lithosphere asthenosphere boundary at 72 km depth. For the asthenospheric mantle ($>$ 72 km) an initial adiabatic like thermal gradient of 0.5 $°C/km$ is used. This is in accordance with recent studies, where sharp lithosphere-asthenosphere boundaries have been imaged at shallow depth ($\sim$ 60 - 90 km), such as for instance beneath the western U.S. (Levander and Miller, 2012). Initialization of subduction is prescribed by a rheologically weak shear zone (wet olivine) with low plastic strength at the bottom of the continental crust. Atop the border of the two plates accretionary sediments are settled. Oceanic plate advance is enabled by an internally prescribed velocity field within the convergence condition region. Bending of the subducting slab is spontaneous (Gorczyk et al., 2007). All mechanical boundary conditions are free slip only the lower boundary being permeable (Gorczyk et al., 2007). The top surface of the lithosphere is treated as an internal free surface by using a top layer (of 8 - 12.5 km thickness) with low viscosity ($10^{18} Pas$) and low density (1 kg/m^3 for air, 1000 kg/m^3 for sea water). The large viscosity contrast across this boundary minimizes shear stresses ($< 10^5 Pa$) at the top of the lithosphere making it an efficient free surface (Schmeling et al., 2008). The topography of the boundary changes due to erosion and sedimentation.

Material	Flow law	$1/A_D\ [Pa^n s]$	n	$E_a\ [J]$	$V_a\ [J/bar]$	$sin(\phi)$	$c\ [Pa]$
Sediment	wet qtz	1.97×10^{17}	2.3	154×10^3	0.8	0.15	1×10^7
Upper crust	wet qtz	1.97×10^{17}	2.3	154×10^3	1.2	0.15	1×10^7
Lower crust	wet qtz	1.97×10^{17}	2.3	154×10^3	1.2	0.15	1×10^7
Basalt	wet qtz	1.97×10^{17}	2.3	154×10^3	0.8	0.10	1×10^7
Gabbro	plag (An75)	4.80×10^{22}	3.2	238×10^3	0.8	0.60	1×10^7
Dry mantle	dry ol	3.98×10^{16}	3.5	532×10^3	0.8	0.60	1×10^7
Wet mantle	wet ol	5.01×10^{20}	4.0	470×10^3	0.8	0.10	1×10^7
Shear zone	wet ol	5.01×10^{20}	4.0	470×10^3	0.8	0.10	1×10^7
Serp. mantle (*)	wet ol	5.01×10^{20}	4.0	470×10^3	0.8	0.00	1×10^7
Magmatics (all)	wet qtz	1.97×10^{17}	2.3	154×10^3	0.8	0.15	1×10^7

Table 3.1: Rheological parameters used in this study: wet qtz = wet quarzite, plag (An75) = anorthite 75 %, wet ol = wet olivine, dry ol = dry olivine after (Ranalli, 1995, and references therein). A_D is the pre-exponential factor, n, is the stress exponent, E_a is the activation energy, V_a is the activation volume, ϕ is the friction angle, and c is the cohesion. * or constant viscosity of $10^{18}\ Pa.s$, see Table 3.2 for details.

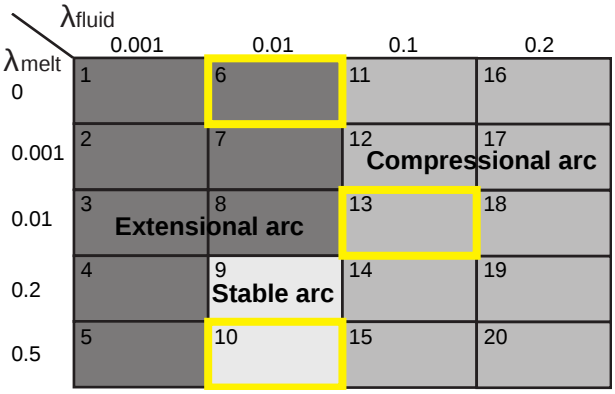

Figure 3.2: Parameter space showing the explored range of variations of fluid- (λ_{fluid}) and melt-related (λ_{melt}) weakening effects. Small values of λ_{fluid} and λ_{melt} correspond to strong weakening. Models are classified into three groups: stable arcs, compressional arcs and extensional arcs. Respective reference models are marked in yellow.

Magma terminology

Along this paper, we use the following terms to refer to the distinct magma types generated in the models. We call dacite to melts generated by partial melting of basalts and gabbros that form part of the subducting oceanic slab. These dacitic magmas can reach the surface in the form of dacitic or adakitic primary magmas or, be emplaced as silicic trondhjemitic and tonalite plutons in the continental crust. Also, these dacitic melts may percolate the mantle wedge contributing to metasomatism and fertilization of peridotite. We call granite to melts generated by partial melting of sediments and granodiorite to melts generated within composite diapirs formed of subduction mélanges. The term basaltic is used for melts generated by partial melting of the wet peridotite. In spite of being widely accepted, we avoid the use of the term adakite to refer to basalt or gabbro partial melts because adakite is a name restricted for dacitic rocks with a particular geochemical signature related to garnet stability (Moyen, 2009) and, thus, to the prevailing pressure - temperature conditions of magma generation. The term dacite is more general and informative about major element composition and source composition with independence of pressure and temperature.

3.4 Results

Here we present a detailed study on crustal growth and evolution of an oceanic-continental subduction process. A key aspect of this study concerns intrusive and extrusive magmatic addition in relation to different

geodynamic settings. In contrast to the previous study by (Gerya and Meilick, 2011) the dynamics of crustal growth have been studied over a range of strong to intermediate fluid and melt related weakening effects (λ= 0.001 - 0.2; λ= 0.0 - 0.5; Table 3.2, Figure 3.2). The results of this study as a function of the parameter space are displayed in Figure 3.3. This range does not include strongly compressional, ablative subduction regimes (Gerya and Meilick, 2011) with an extreme degree of plate coupling, which are not relevant for typical active margins (e.g. Sobolev and Babeyko, 2005). For the sake of simplicity, we also do not discriminate between different compressional arc regimes suggested by Gerya and Meilick (2011) since they produce similar magmatic outputs. Consequently, we have investigated three distinct modes of crustal growth:

(i) Stable arcs characterized by flattened intrusions in the lower crust derived by partial melting of the oceanic crust (basalts, gabbros) and hydrated mantle (wet peridotite)

(ii) Compressional arcs ascribed to partial melting of slab components (basalts, gabbros, sediments) that lead to diapir formation with flattend intrusions in the lower crust and diapir emplacement at upper crustal levels.

(iii) Extensional arcs associated with backarc spreading and ocean floor development.

Applying a wet olivine rheology (Ranalli, 1995) for the mantle reduces the parameter space to only two distinct modes of crustal growth: compressional and extensional arcs (Table 3.2, No.: 21 - 23). Below we describe details of crustal growth processes for these three geodynamic regimes.

No.	λ_{fluid}	λ_{melt}	v_{sub} cm/yr	v_{op} cm/yr	Mantle flow law	Serpentine flow law	Geodynamic Regime
1	0.001	0	5	0	dry ol.	10^{18}	Exten. arc
2	0.001	0.001	5	0	dry ol.	10^{18}	Exten. arc
3	0.001	0.01	5	0	dry ol.	10^{18}	Exten. arc
4	0.001	0.2	5	0	dry ol.	10^{18}	Exten. arc
5	0.001	0.5	5	0	dry ol.	10^{18}	Exten. arc
6	0.01	0	5	0	dry ol.	10^{18}	Exten. arc
7	0.01	0.001	5	0	dry ol.	10^{18}	Exten. arc
8	0.01	0.01	5	0	dry ol.	10^{18}	Exten. arc
9	0.01	0.2	5	0	dry ol.	10^{18}	Stable arc
10	0.01	0.5	5	0	dry ol.	10^{18}	Stable arc
11	0.1	0	5	0	dry ol.	10^{18}	Compr. arc
12	0.1	0.001	5	0	dry ol.	10^{18}	Compr. arc
13	0.1	0.01	5	0	dry ol.	10^{18}	Compr. arc

14	0.1	0.2	5	0	dry ol.	10^{18}	Compr. arc
15	0.1	0.5	5	0	dry ol.	10^{18}	Compr. arc
16	0.2	0	5	0	dry ol.	10^{18}	Compr. arc
17	0.2	0.001	5	0	dry ol.	10^{18}	Compr. arc
18	0.2	0.01	5	0	dry ol.	10^{18}	Compr. arc
19	0.2	0.2	5	0	dry ol.	10^{18}	Compr. arc
20	0.2	0.5	5	0	dry ol.	10^{18}	Compr. arc
21	0.01	0	5	0	wet ol.	10^{18}	Compr. arc
22	0.01	0.5	5	0	wet ol.	10^{18}	Compr. arc
23	0.1	0.01	5	0	wet ol.	10^{18}	Exten. arc
24	0.01	0	5	2	dry ol.	10^{18}	Compr. arc
25	0.01	0.5	5	2	dry ol.	10^{18}	Compr. arc
26	0.1	0.01	5	2	dry ol.	10^{18}	Compr. arc
27	0.01	0	5	4	dry ol.	10^{18}	Compr. arc
28	0.01	0.5	5	4	dry ol.	10^{18}	Compr. arc
29	0.1	0.01	5	4	dry ol.	10^{18}	Compr. arc
30	0.1	0.01	5	0.5	dry ol.	wet ol.	Compr. arc
31	0.1	0.01	5	1	dry ol.	wet ol.	Compr. arc
32	0.1	0.01	5	2	dry ol.	wet ol.	Compr. arc
33	0.1	0.01	6	4	dry ol.	wet ol.	Compr. arc
34	0.001	0.001	3	0	dry ol.	wet ol.	Compr. arc
35	0.001	0.01	3	0	dry ol.	wet ol.	Compr. arc
36	0.001	0.2	3	0	dry ol.	wet ol.	Stable arc
37	0.01	0.001	3	0	dry ol.	wet ol.	Exten. arc
38	0.01	0.01	3	0	dry ol.	wet ol.	Exten. arc
39	0.01	0.2	3	0	dry ol.	wet ol.	Stable arc
40	0.1	0.001	3	0	dry ol.	wet ol.	Compr. arc
41	0.1	0.01	3	0	dry ol.	wet ol.	Compr. arc
42	0.1	0.2	3	0	dry ol.	wet ol.	Compr. arc
43	0.2	0.001	3	0	dry ol.	wet ol.	Compr. arc
44	0.2	0.01	3	0	dry ol.	wet ol.	Compr. arc
45	0.2	0.2	3	0	dry ol.	wet ol.	Compr. arc
46	0.001	0.001	3	0.5	dry ol.	wet ol.	Exten. arc
47	0.001	0.01	3	0.5	dry ol.	wet ol.	Exten. arc
48	0.001	0.2	3	0.5	dry ol.	wet ol.	Stable arc
49	0.01	0.001	3	0.5	dry ol.	wet ol.	Exten. arc
50	0.01	0.01	3	0.5	dry ol.	wet ol.	Exten. arc
51	0.01	0.2	3	0.5	dry ol.	wet ol.	Stable arc
52	0.1	0.001	3	0.5	dry ol.	wet ol.	Compr. arc
53	0.1	0.01	3	0.5	dry ol.	wet ol.	Compr. arc

54	0.1	0.2	3	0.5	dry ol.	wet ol.	Compr. arc
55	0.2	0.001	3	0.5	dry ol.	wet ol.	Compr. arc
56	0.2	0.01	3	0.5	dry ol.	wet ol.	Compr. arc
57	0.2	0.2	3	0.5	dry ol.	wet ol.	Compr. arc
58	0.001	0.001	3	1	dry ol.	wet ol.	Stable arc
59	0.001	0.01	3	1	dry ol.	wet ol.	Stable arc
60	0.001	0.2	3	1	dry ol.	wet ol.	Stable arc
61	0.01	0.001	3	1	dry ol.	wet ol.	Stable arc
62	0.01	0.01	3	1	dry ol.	wet ol.	Stable arc
63	0.01	0.2	3	1	dry ol.	wet ol.	Stable arc
64	0.1	0.001	3	1	dry ol.	wet ol.	Stable arc
65	0.1	0.01	3	1	dry ol.	wet ol.	Stable arc
66	0.1	0.2	3	1	dry ol.	wet ol.	Stable arc
67	0.2	0.001	3	1	dry ol.	wet ol.	Compr. arc
68	0.2	0.01	3	1	dry ol.	wet ol.	Compr. arc
69	0.2	0.2	3	1	dry ol.	wet ol.	Compr. arc
70	0.001	0.001	3	2	dry ol.	wet ol.	Stable arc
71	0.001	0.01	3	2	dry ol.	wet ol.	Stable arc
72	0.001	0.2	3	2	dry ol.	wet ol.	Stable arc
73	0.01	0.001	3	2	dry ol.	wet ol.	Stable arc
74	0.01	0.01	3	2	dry ol.	wet ol.	Stable arc
75	0.01	0.2	3	2	dry ol.	wet ol.	Stable arc
76	0.1	0.001	3	2	dry ol.	wet ol.	Stable arc
77	0.1	0.01	3	2	dry ol.	wet ol.	Compr. arc
78	0.1	0.2	3	2	dry ol.	wet ol.	Stable arc
79	0.2	0.001	3	2	dry ol.	wet ol.	Compr. arc
80	0.2	0.01	3	2	dry ol.	wet ol.	Stable arc
81	0.2	0.2	3	2	dry ol.	wet ol.	Compr. arc

Table 3.2: Summary of all performed experiments. λ_{fluid} = pore fluid pressure factor, λ_{melt} = melt pressure factor, v_{sub} = velocity of the subducting plate [cm/yr], v_{op} = trenchward motion of the overriding plate [cm/yr], dry ol. = dry olivine, wet ol. = wet olivine rheology after (Ranalli, 1995), 10^{18} $[Pas]$ = constant viscosity. Yellow shaded areas mark the reference models described in the text, No.: 1 - 20 see Figure 3.2.

Stable arc settings

Our study reveals stable subduction settings if moderate fluid (λ_{fluid} = 0.01) and melt weakening (λ_{melt} = 0.2 - 0.5; reference model, 3.2, No.:

10) is applied. Shortly after subduction initiation ($< 5\ Myr$) the large thermal contrast between the mantle and the leading edge of the slab induces partial melting in the slab nose (Figure 3.4). This leads to elevated magmatic addition rates of ($35\ km^3/km/Myr$; Figure 3.5). Within the next 20 Myr the thermal contrast between the slab and the mantle remains in a transitional state allowing for partial melting of the oceanic crust, before reaching a thermal equilibrium. Dacitic melts may form and move upwards until they finally form trondhjemites in the lower crust or dacites at the surface (Figure 3.4). Magmatic addition rates decline to typical values of $10\ km^3/km/Myr$ as the thermal contrast is balanced out (Figure 3.5). In the course of subduction, water is expelled due to compaction or as a result of (metamorphic) dehydration reactions. Aqueous fluids percolating from the slab into the mantle wedge may form a serpentinized wedge-like channel at shallow plate interfaces (< 130 km), where subducted sediment and oceanic crust intermix. Hence, a tectonic rock mélange is formed. At asthenospheric depth (> 100 km) progressive hydration of the slab induces partial melting of wet peridotite. Mafic melts are generated and emplacement in form of flattened intrusions in the lower crust and extrusive volcanics (Figure 3.5). Thus volcanic and plutonic rocks are formed, by partial melting of the subducted crustal lithologies (basalts, gabbros, sediments) and mantle components (wet peridotite) with spatial and temporal variations (Figure 3.5). The continental crust grows and newly formed crust is subjected to erosional processes, by which its total volume may decrease (Figure 3.5).

Stable subduction zones are characterized by large growing accretionary wedges, which can be divided into two parts: a plug in the retro-wedge next to the continental margin and a pro-wedge, where material is accreted in form of stacked nappes (Figure 3.5). Most of the incoming sediments are

---

Figure 3.3 *(following page)*: Magmatic compositions (pie charts) and addition rates ($[km^3/km/Myr]$ displayed in circles) after 40 Myr (Table 3.2, No.: 1 - 20). Rates of crust formation are highest for extensional arcs where approximately 75 % of the newly formed crust is formed by decompression melting of dry perdidotite. Most of the crust formed in stable arc settings is derived by partial melting of the oceanic crust and hydrated mantle (flux melting). Magmatic addition rates are low ($10\ km^3/km/Myr$). In compressional arcs, most of the newly formed crust is derived by partial melting of sediments and basalts atop the slab and inside the diapirs (up to 96 %). Partial melting of the hydrous peridotite becomes more important for underplating diapirs (up to 35 %).

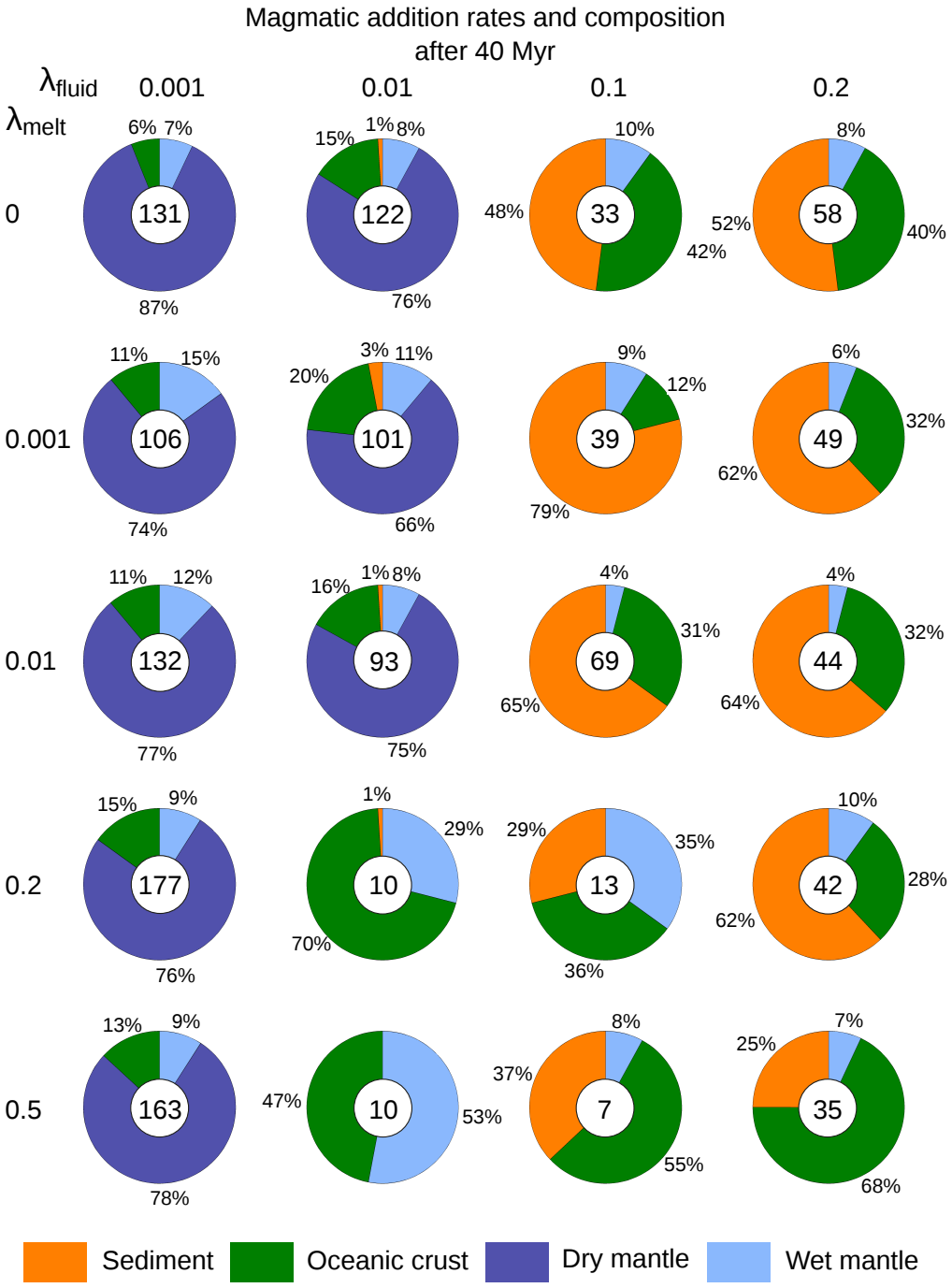
Magmatic addition rates and composition
after 40 Myr
λfluid
λmelt
0.001
0.01
0.1
0.2
0
0.001
0.01
0.2
0.5
6% 7%
131
87%
15% 1% 8%
122
76%
10%
48%
33
42%
8%
52%
58
40%
11% 15%
106
74%
3% 11%
20%
101
66%
9%
12%
39
79%
6%
32%
62%
49
11% 12%
132
77%
16% 1% 8%
93
75%
4%
31%
65%
69
4%
32%
64%
44
15% 9%
177
76%
1%
29%
70%
10
29%
35%
13
36%
10%
28%
62%
42
13% 9%
163
78%
47%
10
53%
8%
37%
7
55%
7%
25%
35
68%
Sediment
Oceanic crust
Dry mantle
Wet mantle

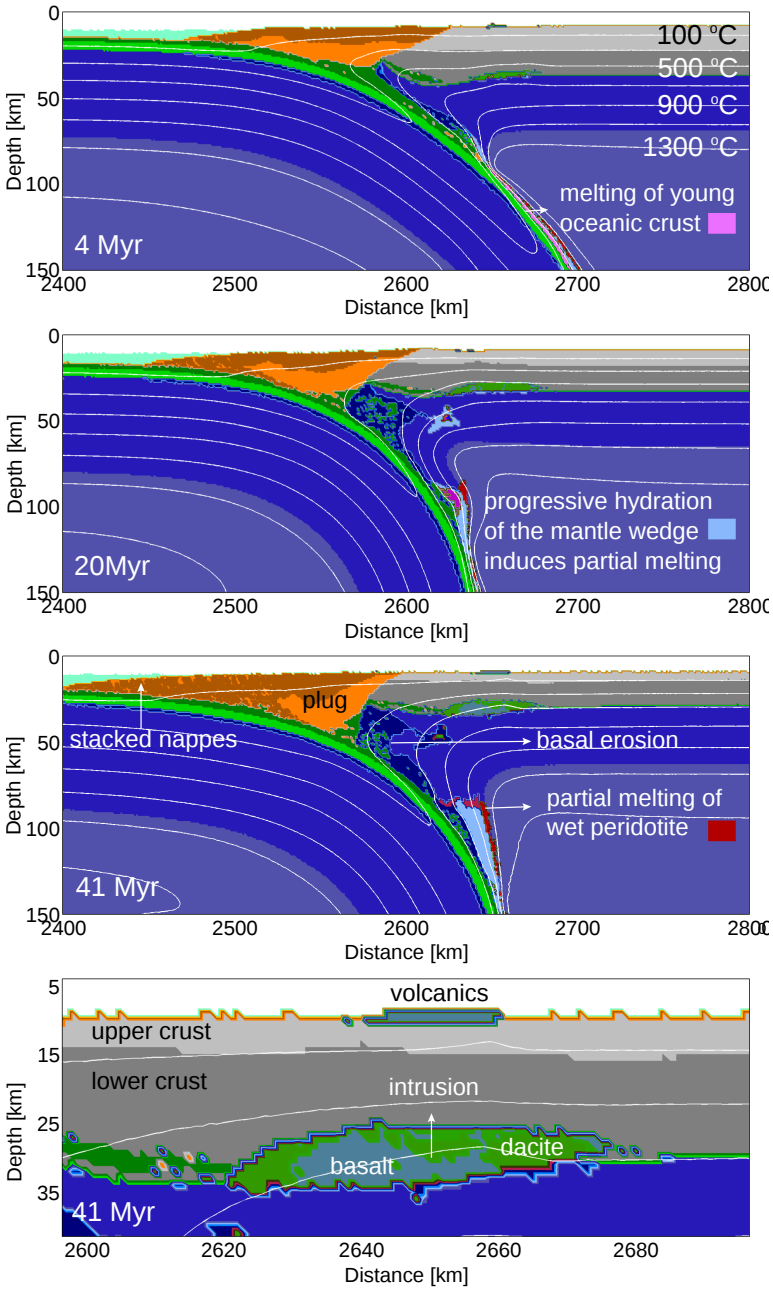

Figure 3.4: Tectonic evolution in a stable arc setting ($\lambda_{fluid} = 0.001$, $\lambda_{melt} = 0.5$; Table 3.2, No.: 10). No backarc spreading is developed and no sedimentary diapirs are formed. Volcanics at the surface and flattened intrusions in the lower crust are formed, due to partial melting of slab and mantle components, resulting in dacitic and basaltic intrusions, respectively. Frontal accretion of incoming sediments forms a laterally growing sedimentary wedge.

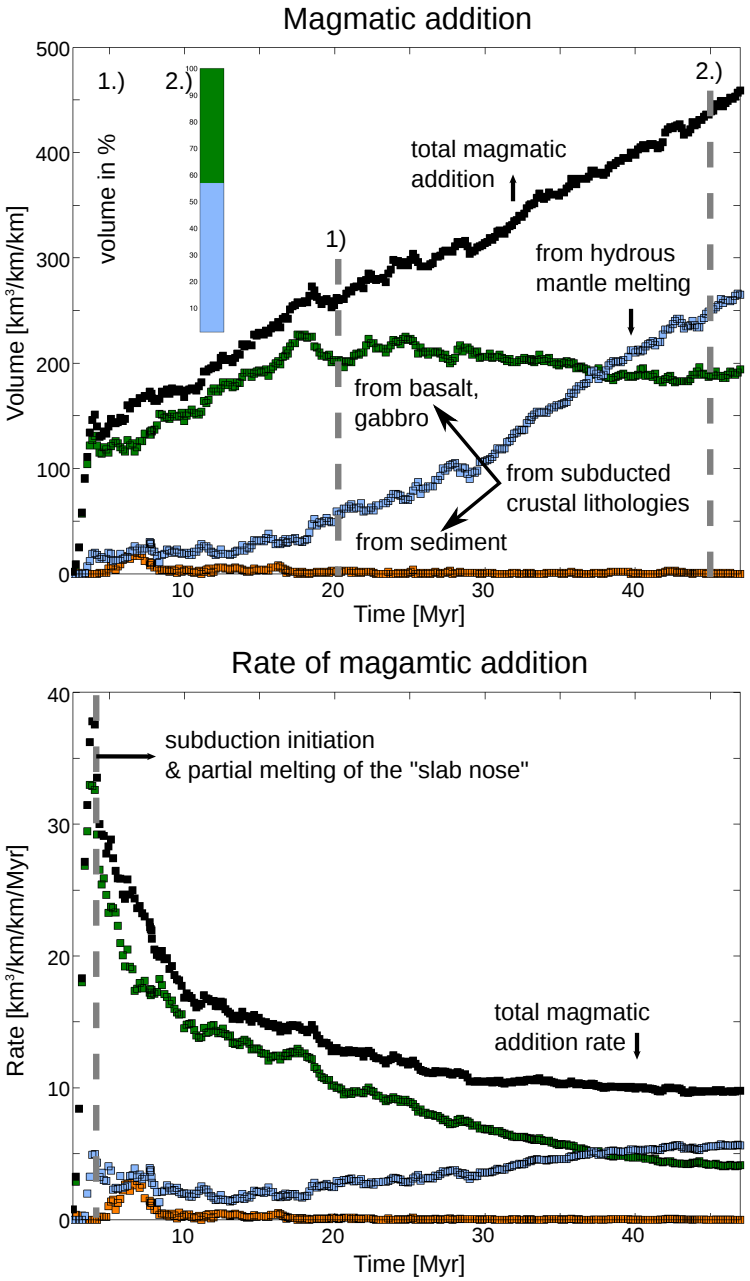

Figure 3.5: Dynamics of crustal growth in stable arc settings (Table 3.2, No.: 10). Lithological structure of newly formed crust (a) and magmatic addition rates of magmas derived from different sites of production (b). At first crustal growth is attributed to partial melting of the young slab. Subsequently hydration of the mantle induces partial melting of wet peridotite. Crustal growth rates are low.

scrapped off in the course of subduction and piled into nappes at the front of the accretion wedge leading to trench retreat (Figure 3.6a). However some of the incoming sediments can also bypass the accretionary wedge as a result of sediment subduction or sediment erosion. Beneath the continental crust, basal erosion is facilitated by sufficiently strong coupling of the plates (Figure 3.4). Serpentinized mantle mixed with basalts, gabbros and sediments from the subducting slab, moves upward and removes crustal material from the upper crust and accretionary prism.

Compressional arcs with diapir development

Compressional arcs associated with diapir development can be observed in experiments with reduced fluid weakening ($\lambda_{fluid} \leq 0.1$; reference model, 3.2, No.:13). At first crust formation is attributed to partial melting of the slab nose, forming dacitic melts. Intrusive trondhjemites and extrusive dacites may form (Figure 3.7), similar to stable arcs. In the course of subduction strong coupling of the plates leads to back-arc compression (Figure 3.6b) and enhances sediment subduction. Localization and partial melting of sediments and basalts atop the slab results in an extended rock mélange formation, thick enough to trigger upwellings followed by diapir development. Favourable conditions for partial melting of slab components are reached at asthenospheric depth, where partial melting of the rock mélange produces thermal-chemical sedimentary diapirs (Figure 3.7). Melts extracted from partially molten rocks (Figure 3.8), which are formed both atop the slab and inside the diapirs, are emplaced in form of extrusive volcanics (dacites, rhyolites) and intrusive plutons (trondhjemites, granites, granodiorites). Once a critical amount of buoyant mass is reached these diapirs ascend from the slab and may intrude into the crust where they finally crystallize as silicic intrusions (batholiths) (Figure 3.7) or underplate the lithosphere (Figure 3.9). Enhanced melt weakening weakens the continental lithosphere and enables diapir emplacement, reduced weakening leads to underplating diapirs (Table 3.2, No.: 14, 15, 19, 20). In cases where diapir emplacement occurs, local extension and slab retreat are observed (Figure 3.6b).

Reduced weakening by fluids strengthens the sediments atop the slab allowing for sediment subduction. Most of the incoming sediments bypass the accretionary wedge and only small to medium sized prisms are formed. Local extension due to diapir emplacement and material uplift next to the continental margin causes a flexure of the continental plate forming a forearc basin (Figure 3.6b and 3.7).

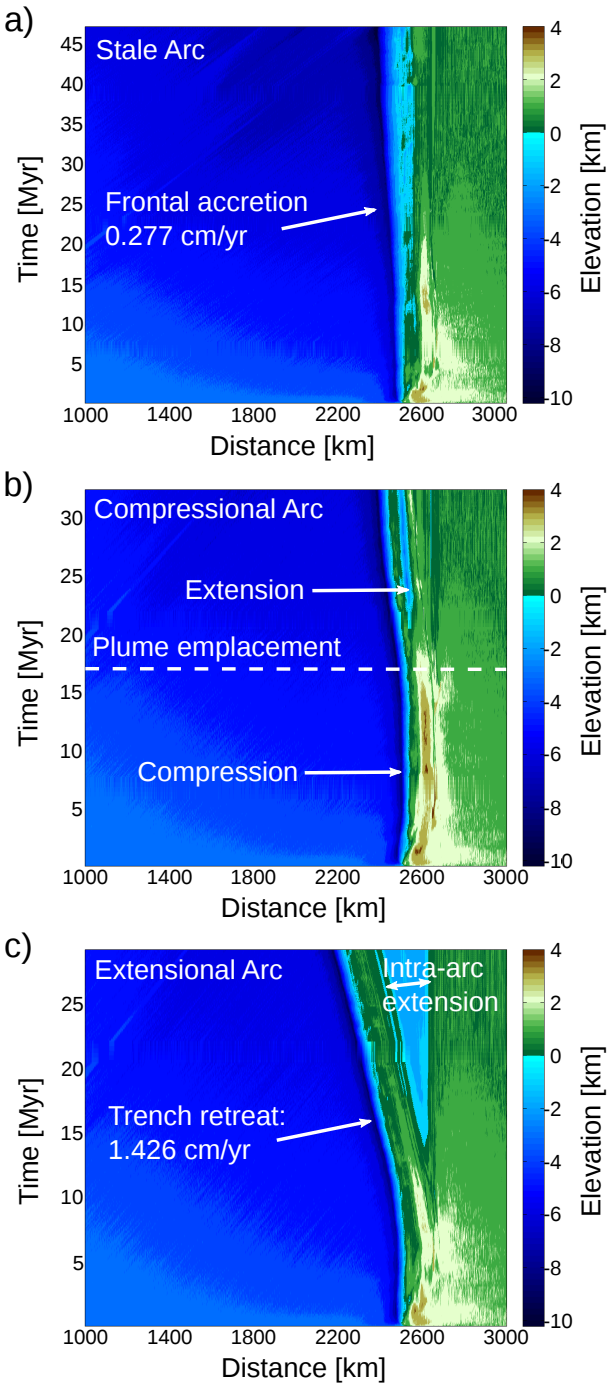

Figure 3.6: Topographic evolution of (a) stable, (b) compressional and (c) extensional arcs. (a) The backward movement of the trench is solely attributed to frontal accretion of sediments, scrapped of the subducting slab. The trench retreats as the sedimentary wedge grows laterally. (b) Strong coupling of the plates promotes compression in the back-arc, followed by local extension due to diapir emplacement. (c) Frontal accretion of sediments and back-arc extension lead to trench retreat. Focused back-arc spreading and intra-arc extension are observed.

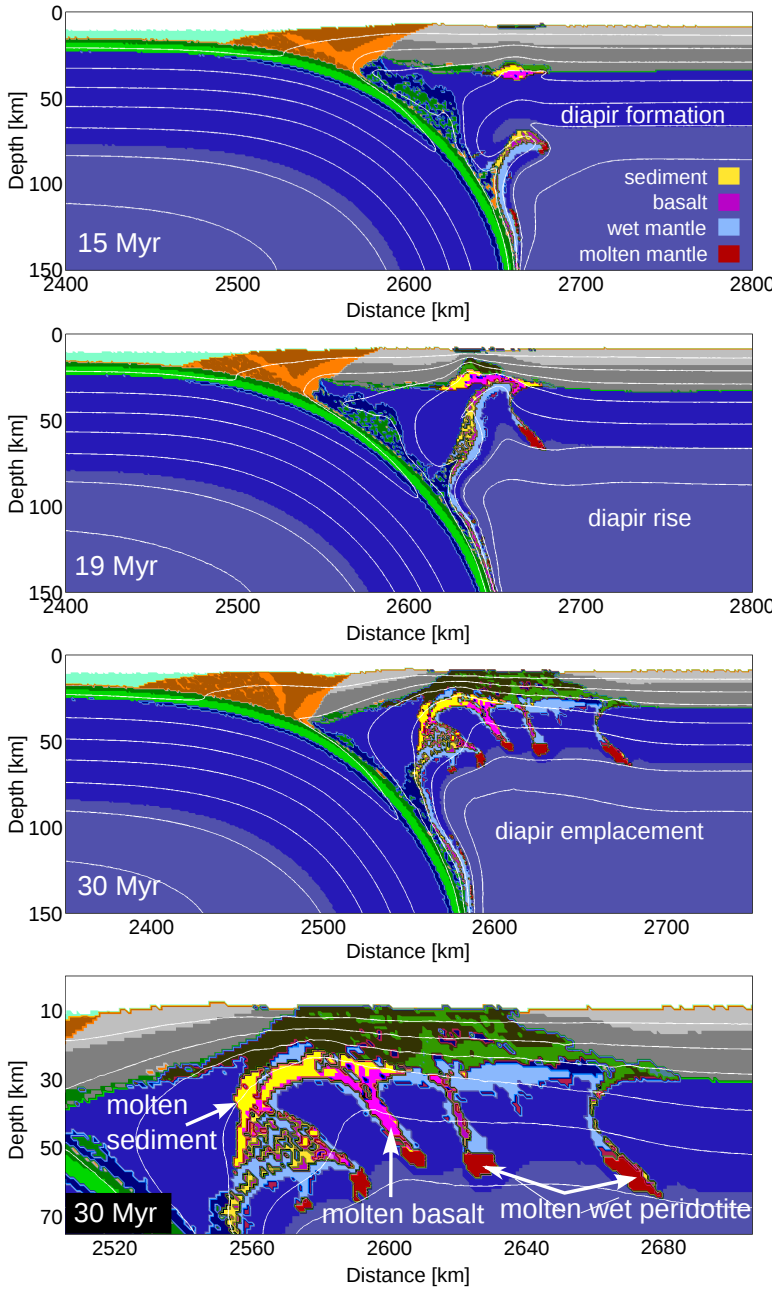

Figure 3.7: Tectonic evolution in compressional arcs ($\lambda_{fluid} = 0.1$, $\lambda_{melt} = 0.001$; Table 3.2, No.: 13). No backarc spreading center develops. Composite diapirs form at asthenospheric depth. Followed by rapid diapir rise and further diapir development. Magmatic addition is ascribed to diapir emplacement and partial melting of mainly slab components located atop the slab, forming flattened intrusions in the lower crust.

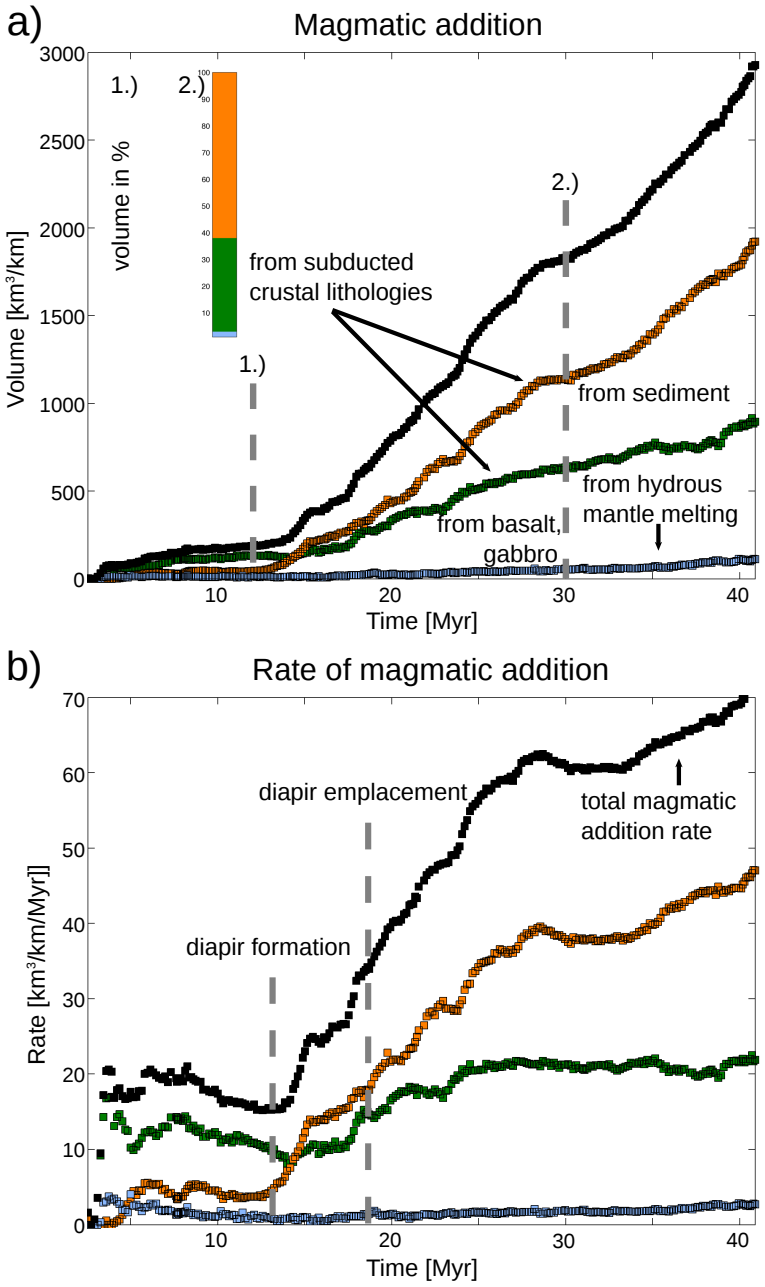

Figure 3.8: Dynamics of crustal growth in compressional arc settings (Table 3.2, No.: 13). Lithological structure of newly formed crust (a) and magmatic addition rates of magmas derived from different sites of production (b). Magmatic addition is mainly attributed to partial melting of sediments and basalts within the diapir and atop the slab. At first magmatic addition rates are low (20 $km^3/km/Myr$) but rise rapidly in the course of diapir formation and emplacement (60 - 70 $km^3/km/Myr$).

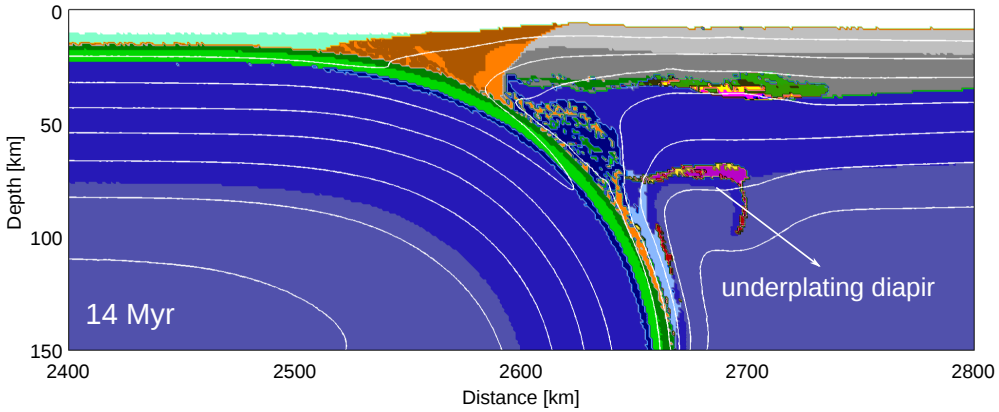

Figure 3.9: Underplating diapir (Table 3.2, No.: 14).

Extensional arcs

Extensional arcs develop in subduction zones with strong fluid related weakening ($\lambda_{fluid} = 0.01$; $\lambda_{fluid} = 0.01$ and $\lambda_{melt} \leq 0.2$; reference model, Table 3.2, No.: 6). Shortly after subduction initiation hydration of the oceanic crust triggers partial melting. Melts derived by partial melting of the slab, move upward forming a magmatic arc at the surface and flattened intrusions in the lower crust until they finally solidify (Figure 3.10). Magmatic addition rates are relatively low, as shown in Figure 3.11. The propagation of melts weakens the lithosphere. In addition, the emplacement of newly produced crust leads to extension within the lithosphere followed by lithospheric necking (Figure 3.10). The backward motion of the subduction zone relative to the motion of the plate leads to thinning of the overriding plate. Thus hot and dry asthenosphere rises into the neck as the slab retreats, triggering decompression melting of dry peridotite. The onset of dry decompression melting associates with an increase in the thermal contrast between the slab and the mantle and partial melting of the subducting oceanic crust. After approximately 15 Myr a backarc spreading center is formed and crustal growth rates rise from about 40 $km^3/km/Myr$ to 80 $km^3/km/Myr$. New MORB (Mod-Ocean-Ridge-Basalt) like crust is produced of mainly basaltic composition (Figure 3.11) at a spreading rate of 0.1 - 0.2 cm/yr (Figure 3.6c). Magmatic addition rates may exceed 100 $km^3/km/Myr$. The thickness of the new MORB-like crust varies from 5 km around the spreading centre to 8 - 10 km toward the edges. After 20 Myr the comparably dense material subsides slightly and the MORB-like crust is flooded (Figure 3.10). Subduction of the oceanic plate leads to frontal accretion of incoming sediments forming stacked nappes in the

pro-wedge and a plug in the retro-wedge with minor sediment subduction, similar to a stable arc setting (Figure 3.6c).

Influences of overriding plate velocity

We have tested the effect of different overriding plate velocities on the tectonic regime (Table 3.2, No.: 24 - 81; Figure 3.12). In agreement with previous studies, we found that the trenchward motion of the upper plate has a major influence on the coupling of the plates (Sobolev and Babeyko, 2005), backarc stresses (Schellart, 2008), slab dip (e.g. van Hunen et al., 2000, 2002) and, consequently on the crustal growth regime. The radius of the slab curvature was calculated using three points measured at 30 km, 70 km and 130 km depth (Figure 3.13). Small radii correspond to strongly curved, steeply dipping slabs, large radii are characteristic for gently bended, shallow dipping slabs. Flattening of the subduction dip with time is a common scenario of all encountered experiments. The degree of this decrease and the radius of the slab curvature at a given time depend on the velocity of the overriding plate and the total convergence rate. Enhanced and reduced velocities result in shallow and steep dipping slabs, respectively. The faster the overriding plate moves (toward the trench), the shallower the angle of subduction, which is in accordance with previous studies (e.g. van Hunen et al., 2000). Variations of the upper plate motion have, moreover, an influence on the geodynamic mode of crustal growth. An enhanced upper plate motion (Figure 3.12) or an elevated convergence rate suppresses extensional arcs that are only achieved for slow (0 - 0.5 cm/yr) upper plate motions.

3.5 Discussion

Magmatic addition rates

Based on our experiments it can be shown that the mode of crustal growth is strongly dependent on the geodynamic regime, namely extension, compression and stable arc settings (Figure 3.3). The lowest rates of crust formation are found in stable arc settings (10 $km^3/km/Myr$, Figure 3.3), where magmatic addition is attributed to partial melting of the downgoing oceanic crust and wet peridotite mantle (Figure 3.5). The result will be a new mafic crust in which basalts are more abundant than felsic magmas of broadly dacitic to andesitic composition. In compressional arcs, the emplacement of hybrid diapirs (basalts plus sediments) and partial melts

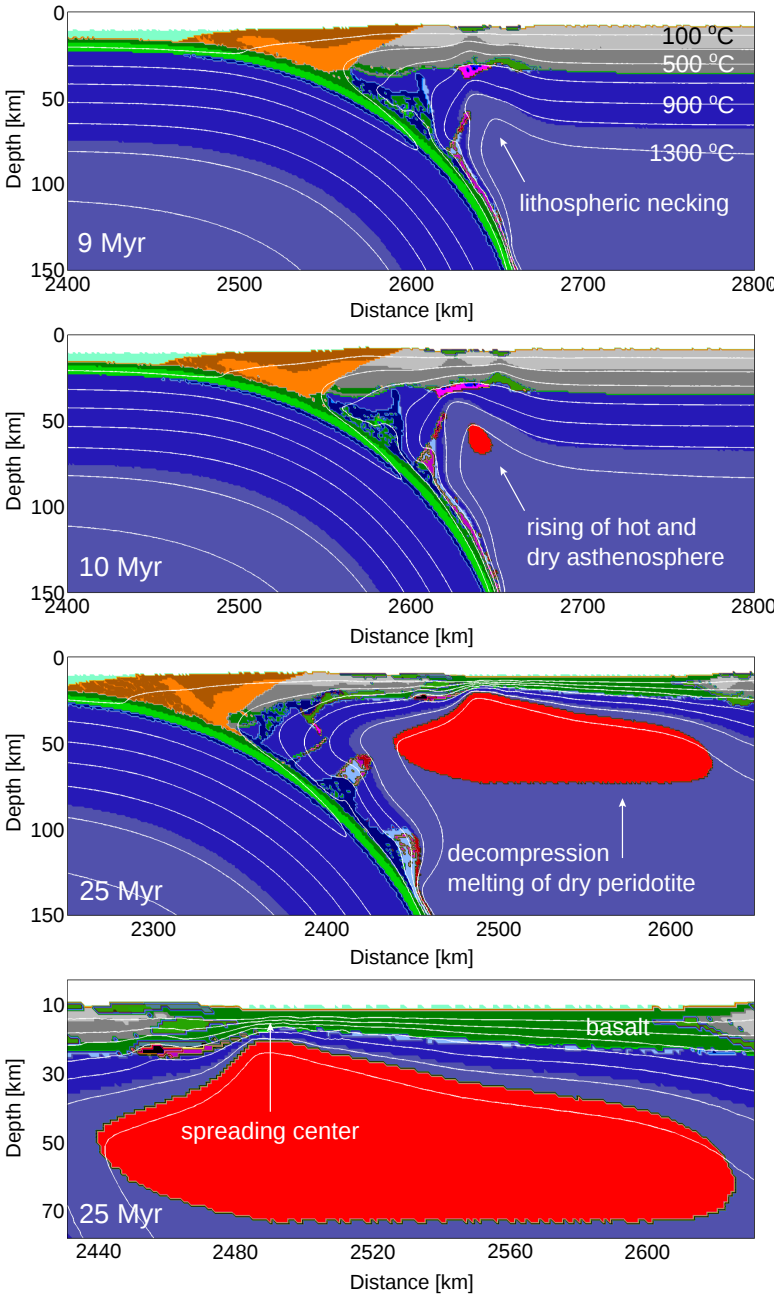

Figure 3.10: Tectonic evolution in extensional arcs (λ_{fluid} = 0.001, λ_{melt} = 0.001; Table 3.2, No.: 6). A focused backarc spreading center develops from intra-arc extension leading to trench retreat. No sedimentary diapirs are observed. Early stage crust formation is attributed to partial melting of the slab, forming trondhjemitic intrusions in the lower crust. Followed by extension in the back-arc, enabling decompression melting of dry peridotite and ocean floor development.

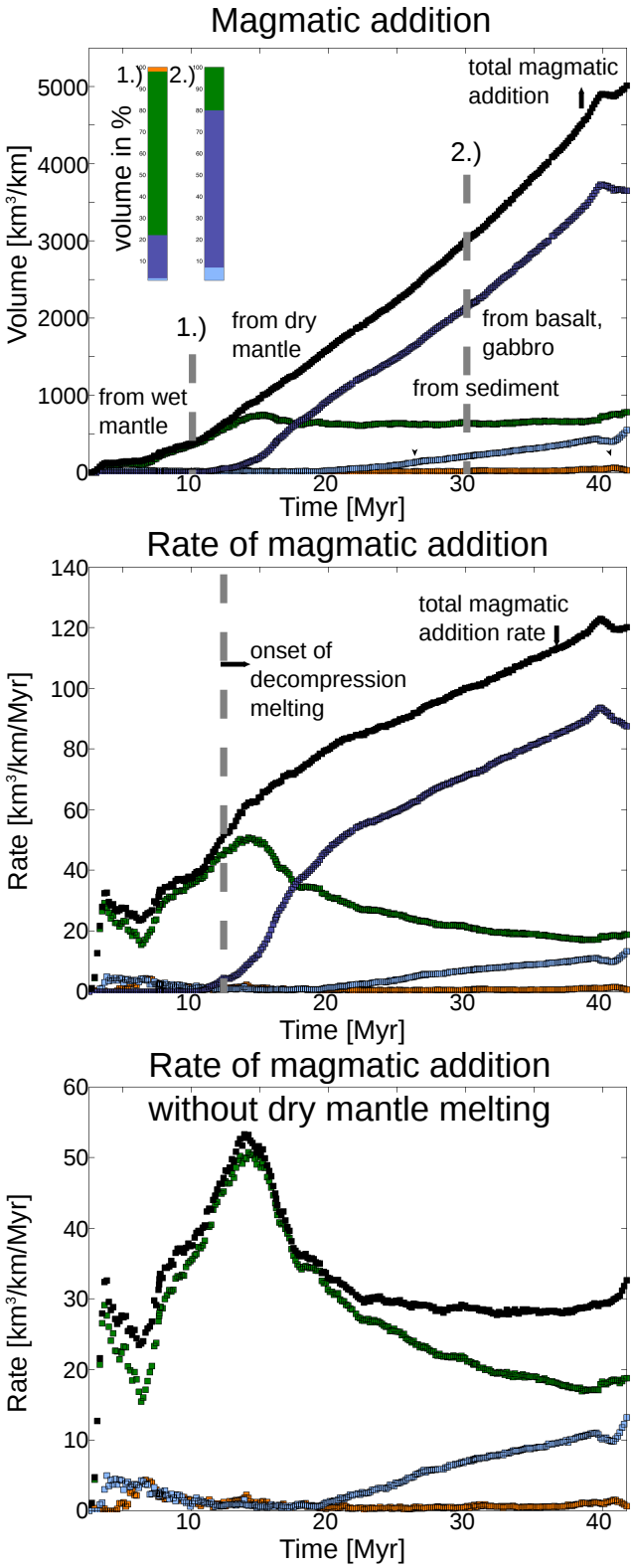

Figure 3.11: Dynamics of crustal growth in extensional arc settings (Table 3.2, No.: 6). Lithological structure of newly formed crust (a) and magmatic addition rates of magmas derived from different sites of production including melts derived by decompression melting (b) and excluding dry mantle melting (c). Back-arc extension leads to extensive decompression melting of dry peridotite. Magmatic addition rates rise to 100 $km^3/km/Myr$ (b). If dry melting is excluded these values drop to 40 - 60 $km^3/km/Myr$ (c).

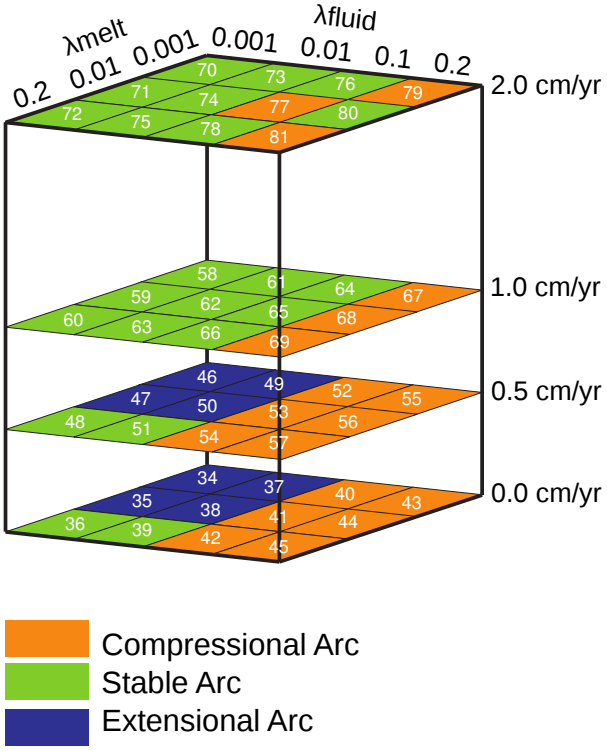

Figure 3.12: Parameter space. Rheological weakening effects induced by fluids and melts were tested against a fixed subducting plate velocity (3 cm/yr) and varying overriding plate velocities ($v_{op} = 0\ cm/yr$, $v_{op} = 0.5\ cm/yr$, $v_{op} = 1\ cm/yr$, $v_{op} = 2\ cm/yr$; Table 3.2: 34 - 81). The trenchward motion of the upper plate has a major influence on the coupling of the plates. Enhanced upper plate velocities lead to strong coupling of the plates, which results in stable or compressional arcs. Extensional arcs do not from for enhanced upper plate velocities.

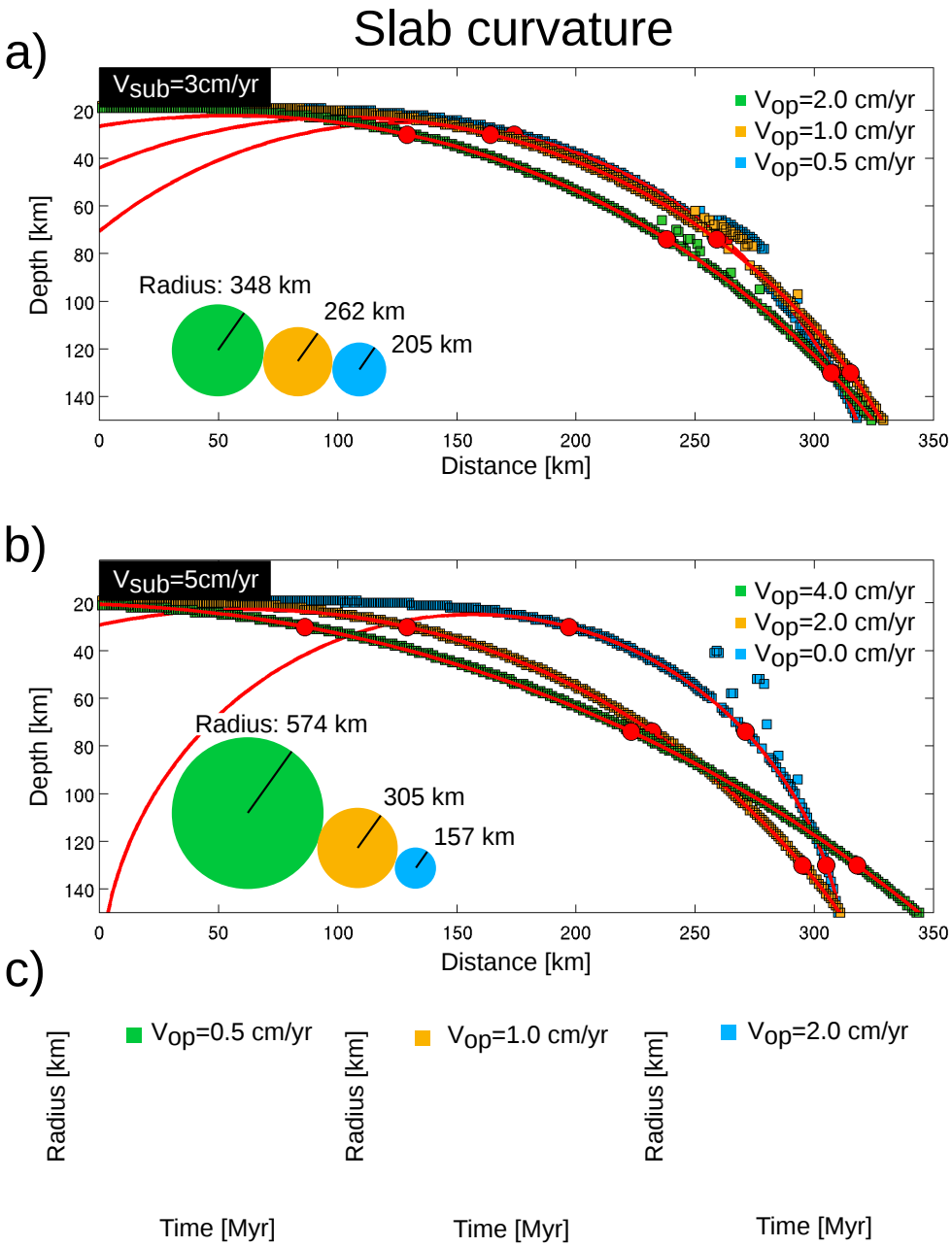

Figure 3.13: Radius of the slab curvature after 12 Myr for a) slow ($v_{sub} = 3$ cm/yr, Table 3.2, No.: 53, 65, 77) and b) fast subducting slabs ($v_{sub} = 5$ cm/yr, Table 3.2, No.: 13, 26, 29). The faster the trenchward motion of the upper plate (the higher the convergence rate) the bigger the radius of the slab curvature (the shallower the slab dip). c) Radius of the slab curvature with time for $v_{sub} = 3$ cm/yr, $v_{op} = 0.5$ cm/yr, v_{op} =1 cm/yr, v_{op} = 2 cm/yr (Table 3.2, No.: 13, 26, 29). The radius of the slab curvature increases with time.

from atop the slab and inside the diapir lead to magmatic addition rates of 40 - 70 $km^3/km/Myr$ (Figure 3.3), three to seven times higher compared to the stable arc setting (Figure 3.8). Extensional arcs associated with new ocean floor development reveal even higher crustal growth rates of up to 180 $km^3/km/Myr$ (Figure 3.3). However, these values are at the upper bound because new oceanic crust is included in the computation (magmatic addition rates of natural arc systems do not typically include new oceanic crust formed by decompression melting around backarc spreading centres) (Figure 3.11). If products of dry melting are excluded values drop down to 30 $km^3/km/Myr$. Thus, magmatic addition rates for the three end-member tectonic models vary between 10 - 70 $km^3/km/Myr$.

Our results are in good agreement with natural observations. Reymer and Schubert (1984) analysed crustal volumes added to 17 arcs during its active lifespan and calculated growth rates of 20 - 40 $km^3/km/Myr$ per arc length. More recent estimates of the same region are somewhat higher. Tiara et al. (1998) estimated the magmatic addition rate of the Izu-Bonin island arc to be 80 $km^3/km/Myr$ and similar values (82 $km^3/km/Myr$) were obtained for the Aleutian island arcs by Holbrook et al. (1999). In the Atlantic, seismic data from the South Sandwich Island arc gave an arc growth rate of 60 $km^3/km/Myr$ (Larter et al., 2001). In the study made by Dimalanta et al. (2002) comparison between different growth rates throughout the western Pacific (Aleutians, Northern and Southern Izu-Boni, Marianas, New Hebrides, Tonga) revealed varying magmatic addition rates of 30 - 95 $km^3/km/Myr$. Less data are available for continental margins, where oceanic crust is subducted beneath continental lithosphere. Estimates on crustal growth rates of Cordilleran orogenic systems exhibit cyclic behaviour with high flux episodes (30 - 90 $km^3/km/Myr$) separated by magmatic lulls (20 - 30 $km^3/km/Myr$) (DeCelles et al., 2009).

Composition

All regimes display an elevated growth rate (of 35 $km^3/km/Myr$) soon after subduction initiation ($<$ 5 Myr) due to partial melting of the slab nose. Because of the large thermal contrast between the mantle and the slab, temperatures at the slab interface may exceed 700 ^oC at depth greater than 80 km, resulting in partial melting. Approximately 20 Myr are needed to balance out the large thermal contrast as shown for stable arcs. Thus partial melting of the subducting slab occurs simultaneously with dehydration reactions, forming dacitic melts. Consistent with our experiments, dacitic magmas with adakitic signatures found in some volcanic arcs associated to subduction of young oceanic crust, are believed to result from

slab melting where temperatures exceed 700 ^oC (Defant and Drummond, 1990; Drummond and Defant, 1990; Sajona et al., 1993; Peacock et al., 1994). For slabs younger than 20 - 30 Myr, Drummond and Defant (1990) envisioned a fertile melting zone at 75 - 85 km depth and 700 - 775 ^oC, where wet partial melting of the subducting slab occurs concurrently with dehydration reactions (dehydration melting). Ringwood (1990) concluded, that slab derived melts, which are formed at depths ranging from 100 - 300 km, may migrate into the adjacent regions of depleted or refractory peridotite, undergoing hybridization and resulting in the refertilisation of these regions, as it was lately confirmed by laboratory experiments (Prouteau et al., 2001). In general, adakites can be subdivided into two groups, high SiO_2 - adakites (HAS; $SiO_2 > 60$ wt. %) and low SiO_2 - adakites (LSA; $SiO_2 < 60$ wt. %) (Martin and Moyen, 2003). The former are considered to represent subducted basaltic-slab melts that have reacted with peridotite during ascent through the mantle wedge, whereas LSA are interpreted to have formed by melting of a peridotitic mantle wedge whose composition has been modified by reaction with felsic melts (Martin et al., 2005). Nevertheless, the composition of these melts may not only be governed by the composition and mineralogy of the source rock, the depth of melting, and the melting reactions, but also by the physical process controlling its migration and segregation (Jackson et al., 2005). After reaching a thermal steady state at the slab interface, crustal growth is attributed to partial melting of the hydrated mantle (Figure 3.5). Water expelled from the subducting plate lowers the melting temperature of the mantle and causes flux melting, which is believed to generate most arc magmas (e.g. Tatsumi, 1989; Tatsumi and Eggins, 1995; Iwamori, 1998). Melt inclusions found in arc lavas containing high water contents (as much as 6 wt. %) (Sisson and Layne, 1993; Sobolev and Chaussidon, 1996) are consistent with fluids, percolating from the subducting slab into the mantle wedge, inducing melting. This process is ubiquitous in all experiments presented here, where basaltic intrusions are derived by partial melting of wet peridotite. In contrast, mid ocean ridge-basalts (MORB) and ocean island basalts (OIB) are believed to have formed by decompression melting of dry mantle (Langmuir et al., 1992; McKenzie and O'nions, 1983), similar to our experiments of extensional arcs associated with ocean floor development. Although there is some evidence for dry melting beneath arcs related to subduction as shown by Sisson and Bronto (1998), it is unlikely that these rocks make a significant material contribution to average continental crust (Hawkesworth and Kemp, 2006).

However, the continental crust has an andesitic bulk composition, which

cannot be produced by the basaltic magmatism that dominates sites of present day crustal growth (Rudnick, 1995). Basaltic intrusions added to the crust might undergo further assimilation and fractional crystallization leading to the formation of felsic rocks (granodiorites, tonalites) as proposed by some workers (Bigazzi et al., 1986; Macera et al., 1985; Taylor, 1980; Thompson et al., 2002). It is expected that mantle derived magmas fractionate and assimilate progressively so that the latest plutons are the most evolved and most radiogenic. This time-compositional evolution is observed in some Cordilleran batholiths of South America (e.g.: the Patagonian batholith Pankhurst et al., 1999) but only for $Sr - Nd$ isotopes and not for major elements, which remain unmodified in the most evolved plutons as it can be expected in an assimilation process. This model is supported by geological observations of mafic rocks associated with granitoids (Blundy and Sparks, 1992; Ulmer et al., 1983). However, this model does not account for the large Cordilleran batholiths generated during Mesozoic times along the American active continental margin from Alaska to Antarctica (Castro et al., 2010). In compressional arcs the emplacement of hybrid diapirs adds additional material to the continental crust. Partially molten rock mélanges accumulate at asthenospheric depth forming diapirs, which rise through the mantle prior to emplacement. These observations are supported by experiments related to the production of silicic plutons from subducted rock mélanges at sublithospheric depths (Castro and Gerya, 2008; Castro et al., 2010). Partial melting of rock mélanges composed of sediments (Bt-rich metagreywacke) and basalts (MORB) produces liquids of granodiorite to tonalite composition (Castro et al., 2010). Hence, following diapir emplacement segregation of liquids and solids may produce granodiorites and tonalites in upper crustal levels and granulites in the lower crust, which is fairly accounting for the layered structure and composition of the continental crust (Rudnick and Gao, 2003; Taylor and McLennan, 1985). Based on dehydration-melting experiments (on pelite, wacke, tonalite and mafic rocks) it was recently shown, that during sediment subduction/erosion, mafic rocks become eclogite and may sink into the mantle, whereas more silicica rich rocks are transformed into felsic gneisses that are positively to neutrally buoyant and can relaminate the base of the upper crust (Hacker et al., 2011). In addition, recycling of older crustal materials is widely supported by isotope geochemistry (McCulloch and Wasserburg, 1978; Allgre and Ben Othman, 1980). The possibility that andesite liquids, generated by reaction between slab melts and the mantle wedge (e.g Kelemen et al., 2003), are fractionated within the continental crust, giving rise to silicic batholiths and mafic granulites, cannot

be discarded. This hypothesis is compatible with the diapir melting model and the melting and melting-reaction experiments of subucted mélanges mentioned above.

Accretionary wedge, sediment subduction, sediment erosion

Crustal growth at continental margins is either accomplished by arc magmatism or the piling up of accretionary masses of sedimentary deposits and fragments of thicker crustal bodies scrapped off the subducting lower plate (von Huene and Scholl, 1991; Pichon et al., 1993). The formation of large accretionary prisms is consistent with our experiments of stable and extensional arcs where most incoming sediments are accreted frontally. Enhanced fluid weakening ($\lambda_{fluid} < 0.1$) weakens the sediments, accumulated atop the slab within the subduction channel. Hence, sediments do not subduct but decouple from the slab and stack up at the surface forming a growing prism. However crustal material can also bypass the accretionary prism as a result of sediment subduction or can be removed from the upper plate by subduction erosion (von Huene and Scholl, 1991). Sediment subduction occurs in two types of convergent margins: margins where little net accretion takes place (all incoming sediments are subducted) and margins where accretionary prisms form (some incoming sediments are scrapped off). Reduced fluid weakening ($\lambda_{fluid} > 0.1$) strengthens the sediments atop the slab, which enhances sediment subduction. von Huene and Scholl (1991) estimated that, where small to medium sized prisms have formed, approximately 20 % of the incoming sediment is accreted and a minimum of 80 % is subducted. This is in good agreement with our results on compressional arcs, where small to medium sized prisms are formed. In contrast to sediment subduction, subduction erosion (Scholl, 1987) requires erosion of rocks, which have been part of the upper crust (von Huene and Scholl, 1991). A combination of reduced fluid ($\lambda_{fluid} > 0.1$) and enhanced melt weakening ($\lambda_{melt} < 0.1$) results in compressional arcs with a weak continental lithosphere. The emplacement of melts within the lower crust enables local extension and facilitates basal erosion, whereby the subcrustal underside of the upper crust is removed. The formation of accretionary prisms is thus mainly controlled by weakening effects imposed by fluids and melts. A major assumption in the present study is that weakening takes place in the bulk of the accretionary wedge that is subjected to aqueous fluid percolation. In nature, such fluid flow is likely to be localized (e.g. Moore and Vrolijk, 1992) and our approach, therefore,

may not necessarily capture all details of the internal accretion wedge structure. Nevertheless, as demonstrated in a previous study (Gerya and Meilick, 2011) general regimes of accretion wedge dynamics that are characteristic for subduction zones (accretionary versus erosional margins) are reproduced by models with different amounts of fluid-related weakening. Further modifications of accretion wedge dynamics may come from spatial and temporal variations of erosion and sedimentation rates (Simpson, 2010) that are also not accounted for in our study.

Mode of subduction

Fluids percolating from the subducting slab into the mantle wedge mainly control the coupling of the plates, whereas melts percolating toward the surface weaken the lithosphere above the arc. Thus two extreme endmembers can be defined: (i) extensional arcs with back-arc extension (Figure 3.10) and (ii) compressional arcs with back-arc compression (Figure 3.7), represented by the Mariana and Peruvian-Chilean arc, respectively. Based on earthquakes studies, Uyeda and Kanamori (1979) argued that there is a significant difference in the mode of plate motion at interplate boundaries between the two types of trench systems. In the Peruvian and Chilean arcs the plate motion is seismic, in the Mariana it is aseismic. Uyeda and Kanamori (1979) attributed these observations to strong mechanical coupling between the upper and lower plate in the Chilean arc and low or no coupling at the Mariana type boundaries. This difference is manifested in our experiments by tectonic features such as volcanic activity, topography and crustal movement. Compressional arcs are accomplished by flattened, sill-like intrusions in the lower crust, diapir development, back-arc compression and trench advance. In contrast, extensional arcs are dominated by decompression melting of dry peridotite, leading to back-arc extension and trench retreat.

Slab geometry and back-arc stresses

We have shown, that the upper plate motion plays an important role on the slab dip, as well as on the geodynamic setting and the mode of crustal growth. All three major subduction settings (stable arcs, compressional arcs and extensional arcs) are realised for slowly moving upper plates (Figure 3.12). When enhanced upper plate velocities are applied ($v_{op} > 0.5$ cm/yr), only stable and compressional arcs are formed, but extensional arcs do not (Figure 3.12; Schellart (2008)). The faster the trenchward motion of the upper plate, the shallower the angle of subduction (e.g. van

Hunen et al., 2000). Thus extensional arcs do not correlate with shallow dipping slabs. Comparison of different parameters along 159 transects of present day subduction zones (Lallemand et al., 2005) revealed similar observation, which where confirmed by laboratory experiments (Heuret et al., 2007), showing that slab dips correlate with the absolute motion of the overriding plate and back arc stresses. Natural examples of shallow dipping slabs associated with back-arc compression are the Peruvian and Chilean arcs. An example of a steep slab and back arc extension is the Mariana subduction zone.

3.6 Conclusions

We have investigated numerically geodynamic regimes of crustal growth at active margins. We conclude that: Magmatic addition in **stable subduction settings** is dominated by flattened intrusions in the lower crust and extrusive volcanics at the surface that are derived by partial melting of slab (basalts, gabbro) and mantle components (wet peridotie). Magmatic addition rates are low (10 $km^3/km/Myr$). In **compressional arcs** magmatic addition is mainly ascribed to partial melting of slab components (basalts, gabbros, sediments) with minor contribution of hydrated mantle. Flattened intrusions are emplaced at lower crustal levels and extrusive volcanics at the surface. In addition, hybrid diapirs are formed at asthenospheric depth that transport subducted crustal material (partially molten sediments and basalts) towards the upper crust, which results in moderate magmatic addition rates ($\sim$ 40 - 70 $km^3/km/Myr$). Crust formation in an **extensional arc setting** is associated with decompression melting of dry peridotite, ocean floor development and elevated magmatic addition rates (>100 $km^3/km/Myr$).

Bibliography

Allgre, C., Ben Othman, D., 1980. Nd-sr isotopic relationship in granitoid rocks and continental crust development: a chemical approach to orogenesis. Nature 286, 335–341.

Bigazzi, G., Moro, A., Macera, P., 1986. A quantitative approach to trace element and sr isotope evolution in the adamello batholith (northern italy). Contributions to Mineralogy and Petrology 94 (1), 46–53.

Blundy, J., Sparks, R., 1992. Petrogenesis of mafic inclusions in granitoids of the adamello massif, italy. Journal of Petrology 33 (5), 1039–1104.

Castro, A., Gerya, T., 2008. Magmatic implications of mantle wedge plumes: experimental study. Lithos 103 (1), 138–148.

Castro, A., Gerya, T., García-Casco, A., Fernández, C., Díaz-Alvarado, J., Moreno-Ventas, I., Löw, I., 2010. Melting relations of morb–sediment mélanges in underplated mantle wedge plumes; implications for the origin of cordilleran-type batholiths. Journal of Petrology 51 (6), 1267–1295.

Connolly, J., 2005. Computation of phase equilibria by linear programming: A tool for geodynamic modeling and its application to subduction zone decarbonation. Earth and Planetary Science Letters 236, 524541.

DeCelles, P., Ducea, M., Kapp, P., Zandt, G., 2009. Cyclicity in cordilleran orogenic systems. Nature Geoscience 2 (4), 251–257.

Defant, M., Drummond, M., 1990. Derivation of some modern arc magmas by melting of young subducted lithosphere. Nature 347 (6294), 662–665.

Dimalanta, C., Taira, A., Yumul, G., Tokuyama, H., Mochizuki, K., 2002. New rates of western pacific island arc magmatism from seismic and gravity data. Earth and Planetary Science Letters 202 (1), 105–115.

Drummond, M., Defant, M., 1990. A model for trondhjemite-tonalite-dacite genesis and crustal growth via slab melting: Archean to modern comparisons. Journal of geophysical research 95 (B13), 21503–21.

Gerya, T., Meilick, F., 2011. Geodynamic regimes of subduction under an active margin: effects of rheological weakening by fluids and melts. Journal of metamorphic Petrology 29, 7–31.

Gorczyk, W., Willner, A., Gerya, T., Connolly, J., Burg, J.-P., 2007. Physical controls of magmatic productivity at pacic-type convergent margins: Numerical modelling. Physics of the Earth and Planetary Interiors 163, 209232.

Green, T., 1980. Island arc and continent-building magmatisma review of petrogenic models based on experimental petrology and geochemistry. Tectonophysics 63 (1), 367–385.

Hacker, B., Kelemen, P., Behn, M., 2011. Differentiation of the continental crust by relamination. Earth and Planetary Science Letters 307 (3), 501–516.

Hawkesworth, C., Kemp, A., 2006. Evolution of the continental crust. Nature 443 (7113), 811–817.

Heuret, A., Funiciello, F., Faccenna, C., Lallemand, S., 2007. Plate kinematics, slab shape and back-arc stress: a comparison between laboratory models and current subduction zones. Earth and Planetary Science Letters 256 (3), 473–483.

Holbrook, W., Lizarralde, D., McGeary, S., Bangs, N., Diebold, J., 1999. Structure and composition of the aleutian island arc and implications for continental crustal growth. Geology 27 (1), 31–34.

Iwamori, H., 1998. Transportation of h2o and melting in subduction zones. Earth and Planetary Science Letters 160, 65–80.

Jackson, M., Gallagher, K., Petford, N., Cheadle, M., 2005. Towards a coupled physical and chemical model for tonalite–trondhjemite–granodiorite magma formation. Lithos 79 (1), 43–60.

Kay, R., 1978. Aleutian magnesian andesites: melts from subducted pacific ocean crust. Journal of Volcanology and Geothermal Research 4 (1), 117–132.

Kay, R., Mahlburg-Kay, S., 1991. Creation and destruction of lower continental crust. Geologische Rundschau 80 (2), 259–278.

Kelemen, P., Yogodzinski, G., Scholl, D., 2003. Along-strike variation in the aleutian island arc: Genesis of high mg# andesite and implications for continental crust. Inside the Subduction Factory, Geophys. Monogr. Ser 138, 223–276.

Lallemand, S., Heuret, A., Boutelier, D., 2005. On the relationships between slab dip, back-arc stress, upper plate absolute motion, and crustal nature in subduction zones. Geochemistry Geophysics Geosystems 6 (9), Q09006.

Langmuir, C., Klein, E., Plank, T., 1992. Petrological systematics of mid-ocean ridge basalts: Constraints on melt generation beneath ocean ridges. Geophysical Monograph Series 71, 183–280.

Larter, R., Vanneste, L., Bruguier, N., 2001. Structure, composition and evolution of the south sandwich island arc: Implications for rates of arc magmatic growth and subduction erosion. In: AGU Fall Meeting Abstracts. Vol. 1. p. 10.

Levander, A., Miller, M. S., 2012. Evolutionary aspects of lithosphere discontinuity structure in the western u.s. Geochemistry Geophysics Geosystems 13, doi:10.1029/2012GC004056.

Macera, P., Ferrara, G., Pescia, A., Callegari, E., 1985. A geochemical study on the acid and basic rocks of the adamello batholith. Mem. Soc. Geol. It 26, 223–259.

Martin, H., Moyen, J., 2003. Secular changes in ttg composition: comparison with modern adakites. In: EGS-AGU-EUG Joint Assembly. Vol. 1. p. 2673.

Martin, H., Smithies, R., Rapp, R., Moyen, J., Champion, D., 2005. An overview of adakite, tonalite–trondhjemite–granodiorite (ttg), and sanukitoid: relationships and some implications for crustal evolution. Lithos 79 (1), 1–24.

McCulloch, M., Wasserburg, G., 1978. Sm-nd and rb-sr chronology of continental crust formation. Science 200 (4345), 1003–1011.

McKenzie, D., O'nions, R., 1983. Mantle reservoirs and ocean island basalts. Nature 301, 229–231.

Moore, J., Vrolijk, P., 1992. Fluids in accretionary prisms. Reviews of Geophysics 30 (2), 113–135.

Moyen, J., 2009. High sr/y and la/yb ratios: the meaning of the adakitic signature. Lithos 112 (3), 556–574.

Nikolaeva, K., Gerya, T., Connolly, J., 2008. Numerical modelling of crustal growth in intraoceanic volcanic arcs. Physics of the Earth and Planetary Interiors 171, 336–356.

Pankhurst, R., Weaver, S., Hervé, F., Larrondo, P., 1999. Mesozoic-cenozoic evolution of the north patagonian batholith in aysén, southern chile. Journal of the Geological Society 156 (4), 673–694.

Peacock, S., Rushmer, T., Thompson, A., 1994. Partial melting of subducting oceanic crust. Earth and planetary science letters 121 (1), 227–244.

Pichon, X., Henry, P., Lallemant, S., 1993. Accretion and erosion in subduction zones: The role of fluids. Annual Review of Earth and Planetary Sciences 21, 307–331.

Prouteau, G., Scaillet, B., Pichavant, M., Maury, R., et al., 2001. Evidence for mantle metasomatism by hydrous silicic melts derived from subducted oceanic crust. Nature 410, 197–200.

Ranalli, G., 1995. Rheology of the Earth. Springer.

Reymer, A., Schubert, G., 1984. Phanerozoic addition rates to the continental crust and crustal growth. Tectonics 3 (1), 63–77.

Ringwood, A., 1990. Slab-mantle interactions: 3. petrogenesis of intraplate magmas and structure of the upper mantle. Chemical Geology 82, 187–207.

Rudnick, R., 1995. Making continental crust. Nature 378, 571–577.

Rudnick, R., Gao, S., 2003. Composition of the continental crust. Treatise on geochemistry 3, 1–64.

Sajona, F., Maury, R., Bellon, H., Cotten, J., Defant, M., Pubellier, M., 1993. Initiation of subduction and the generation of slab melts in western and eastern mindanao, philippines. Geology 21 (11), 1007–1010.

Schellart, W., 2008. Overriding plate shortening and extension above subduction zones: A parametric study to explain formation of the andes mountains. Geological Society of America Bulletin 120 (11-12), 1441–1454.

Schmeling, H., Babeyko, A., Enns, A., Faccenna, C., Funiciello, F., Gerya, T., Golabek, G., Grigull, S., Kaus, B., Morra, G., van Hunen, J., 2008. A benchmark comparison of spontaneous subduction modelstowards a free surface. Physics of the Earth and Planetary Interiors 171 (1), 198–223.

Schmidt, M., Poli, S., 1998. Experimentally based water budgets for dehydrating slabs and consequences for arc magma generation. Earth and Planetary Science Letters 163 (1), 361–379.

Scholl, D., 1987. Plate tectonics the predictor: the history of wonderments about subduction erosion and sediment subduction–a search for the missing. In: Hilde, TWC, and Carlson, RH, Silver anniversary celebration of plate tectonics: Texas A&M University, Geodynamics Research Institute, Geodynamics Symposium. pp. 54–56.

Simpson, G., 2010. Formation of accretionary prisms influenced by sediment subduction and supplied by sediments from adjacent continents. Geology 38 (2), 131–134.

Sisson, T., Bronto, S., 1998. Evidence for pressure-release melting beneath magmatic arcs from basalt at galunggung, indonesia. Nature 391 (6670), 883–886.

Sisson, T., Layne, G., 1993. H_2O in basalt and basaltic andesite glass inclusions from four subduction-related volcanoes. Earth and Planetary Science Letters 117 (3), 619–635.

Sobolev, A., Chaussidon, M., 1996. H_2O concentrations in primary melts from supra-subduction zones and mid-ocean ridges: Implications for H_2O storage and recycling in the mantle. Earth and Planetary Science Letters 137, 45–55.

Sobolev, S., Babeyko, A., 2005. What drives orogeny in the andes? Geology 33 (8), 617–620.

Stolper, E., Newman, S., 1994. The role of water in the petrogenesis of mariana trough magmas. Earth and Planetary Science Letters 121 (3), 293–325.

Tatsumi, Y., 1989. Migration of fluid phases and genesis of basalt magmas in subduction zones. Journal of Geophysical Research 94 (B4), 4697–4707.

Tatsumi, Y., 2005. The subduction factory: How it operates in the evolving earth. GSA today 15 (7), 4.

Tatsumi, Y., Eggins, S., 1995. Subduction zone magmatism. Wiley.

Taylor, H., 1980. The effects of assimilation of country rocks by magmas on¡ sup¿ 18¡/sup¿ o/¡ sup¿ 16¡/sup¿ o and¡ sup¿ 87¡/sup¿ sr/¡ sup¿ 86¡/sup¿ sr systematics in igneous rocks. Earth and Planetary Science Letters 47 (2), 243–254.

Taylor, S., 1966. The origin and growth of continents. Tectonophysics 4, 17–34.

Taylor, S., McLennan, S., 1985. The continental crust: its composition and evolution.

Thompson, A., Matile, L., Ulmer, P., 2002. Some thermal constraints on crustal assimilation during fractionation of hydrous, mantle-derived magmas with examples from central alpine batholiths. Journal of Petrology 43 (3), 403–422.

Tiara, A., Saito, S., Aoike, K., Morita, S., Tokuyama, H., Suyehiro, H., Takahashi, N., Shinohara, M., Kiyokawa, S., Naka, J., Klaus, A., 1998. Nature and growth of the northern izu-bonin (ogasawara) arc crust and their implications to continental crust formation. Island Arc 7, 395–407.

Turcotte, D., Schubert, G., 2002. Geodynamics. Cambridge University Press.

Ulmer, P., Callegari, E., Sonderegger, U., 1983. Genesis of the mafic and ultramafic rocks and their genetical relations to the tonalitic-trondhjemitic granitoids of the southern part of the adamello batholith (northern italy). Memorie della Società Geologica Italiana 26, 171–222.

Uyeda, S., Kanamori, H., 1979. Back-arc opening and the mode of subduction. J. geophys. Res 84 (3), 1049–1061.

van Hunen, J., van den Berg, A., Vlaar, N., 2000. A thermo-mechanical model of horizontal subduction below an overriding plate. Earth and Planetary Science Letters 182 (2), 157–169.

van Hunen, J., van den Berg, A., Vlaar, N., 2002. The impact of the south-american plate motion and the nazca ridge subduction on the flat subduction below south peru. Geophysical research letters 29 (14), 1690.

von Huene, R., Scholl, D., 1991. Observations at convergent margins concerning sediment subduction, subduction erosion, and the growth of continental crust. Reviews of Geophysics 29 (3), 279–316.

Wyllie, P., Osmaston, M., Morrison, M., 1984. Constraints imposed by experimental petrology on possible and impossible magma sources and products [and discussion]. Philosophical Transactions of the Royal Society of London. Series A, Mathematical and Physical Sciences 310 (1514), 439–456.

Chapter 4

Numerical Modelling of Geochemical Variations Caused by Crustal Relamination[1]

4.1 Abstract

Geochemical consequences of composite diapirs formed in subduction zones have been studied using a thermomechanical numerical model of an ocean-continent subduction zone. This model includes dehydration of subducted crust, aqueous fluid transport, partial melting, and melt emplacement. Subduction of crustal material to sublithospheric depth results in the formation of a tectonic rock mélange composed of basalt, sediment and hydrated /serpentinized mantle. At asthenospheric depth, this rock mélange may evolve into partially molten diapirs and rise through the mantle prior to emplacement (relamination) at crustal levels. We have investigated the composition and the geochemical evolution of liquids derived from such composite diapirs by analysing the differing proportions of the crustal end-members in the source, i.e. basalt and sediment. Our results show that the proportions of the components (in the diapiric mélange) are limited to short-range variations within an interval of X_b [=volume fraction of $\frac{basalt}{(basalt+sediment)}$] = 0.4 - 0.8, yielding melt with a relatively stable granodioritic major element composition. Hence, granodioritic melt is transported by rising composite diapirs to crustal levels, contributing to the growth of the continental crust. In addition to this, we have calculated Sr and Nd isotopic initial ratios of the diapiric mélange as a function of time, based

[1]This chapter co-authored by K. Vogt, A. Castro and T. Gerya was published in a slightly modified version in Geochemistry, Geophysics, Geosystems, 14, 470 - 487.

on the fraction of the components in the mélange. Liquids derived from composite diapirs inherit the geochemical characteristics of the composite source and show distinct temporal variations of radiogenic isotopes depending on the changing values of X_b. Partial melting of composite diapirs is therefore expected to produce melt with a constant major element composition, but substantial changes in terms of radiogenic isotopes.

4.2 Introduction

The continental crust is believed to have formed by melting and geochemical fractionation of the mantle (Hofmann, 1988). Although it is unclear if continents have grown with time (Taylor and McLennan, 1985; McCulloch and Wasserburg, 1978) or have reached a steady state by crustal recycling after formation in the Archean (Armstrong and Harmon, 1981), isotopic data demonstrate that continental crust formation has been occurring throughout Earth history (Rudnick, 1995). However, partial melting of the peridotite mantle produces basaltic magmas that are less evolved (i.e., poorer in silica) than the andesitic bulk composition of the crust. Accordingly, different models have been suggested to account for this differentiation: (i) partial melting of the subducted oceanic crust (Drummond and Defant, 1990; Defant and Drummond, 1990), (ii) reaction of slab derived melts with the overlying perioditic mantle (Ringwood and Green, 1966; Kelemen, 1995; Kelemen et al., 2003b; Behn et al., 2011) and (iii) hydration and partial melting of the metasomatized mantle (e.g. Schmidt and Poli, 1998; Iwamori, 1998; Tatsumi, 2005) followed by intracrustal differentiation and lower crustal foundering (Kay and Mahlburg-Kay, 1991). Although foundering is probably an important mechanism in some places (DeBari and Sleep, 1991; Kelemen et al., 2003a), recent studies have shown that felsic material may also detach from the slab because of the intrinsic buoyancy of the sediment layer itself (Currie et al., 2007; Behn et al., 2011; Hacker et al., 2011; Miller and Behn, 2012) and hence modify the sub arc mantle. Alternatively, hydration and partial melting atop the slab may trigger the formation of composite diapirs composed of partially molten basalt, sediment and hydrated/serpentinized mantle (Gerya and Yuen, 2003a; Gerya et al., 2006; Gerya and Meilick, 2011; Zhu et al., 2011a,b; Vogt et al., 2012). Some of these latter studies were examined using laboratory experiments in terms of major element compositions and phase relations (Castro and Gerya, 2008; Castro et al., 2009, 2010, 2012b). The cotectic behaviour of liquid formed by partial melting of subducted rock mélanges at sublithospheric depths (Castro et al., 2010) is a prominent

feature. Cotectic liquids have an almost constant composition, buffered by the solid coexisting assemblage. This phase equilibria experimental study shows, therefore, that composite diapirs are favourable for the production of silicic magmas with minor compositional variations in terms of major elements. This is consistent with the production of large silicic batholiths, composed of rocks of granodiorite to tonalite composition that yield a constant major element composition despite their long lived magmatisim (Castro et al., 2010, and references therein), contributing to the growth of the continental crust (Condie, 1997; Hawkesworth and Kemp, 2006). Geochemical (trace elements) and isotopic variations, on the other hand, are nearly independent of the major element geochemistry and large variations in time and space have been reported for distinct geological settings, where granodioritic intrusions display a constant major element composition. These differences are generally related to (i) changes in crustal thickness with time (Haschke et al., 2002; Mamani et al., 2010) and space (Hildreth and Moorbath, 1988) (ii) involvement of an enriched component i.e. old lithosphere (Rogers and Hawkesworth, 1989) and (iii) source region contamination of the sub arc mantle by sediment subduction, crustal erosion and partial melting of the subducting slab (Stern, 1991). Sediment subduction and crustal subduction erosion are apparent tectonic features of modern plate boundaries (von Huene and Scholl, 1991; von Huene and Lallemand, 1990) and partial melting of these crustal rocks mixed with oceanic crust may account for the geochemical and isotopic variability observed in modern arc magmas. In particular, the source composition of batholiths generated at active continental margins may vary between the two end-members, namely sediment and basaltic oceanic crust (Castro et al., 2010), imposing a wide variability in terms of trace elements and isotopic ratios that has not been explored yet. We have therefore undertaken a detailed study of 2-D petrological-thermomechanical numerical experiments on subduction at continental margins to (i) characterize the variability of geochemical signatures of magmas produced by composite diapirs, and (ii) investigate its implications for batholith formation.

4.3 Numerical model description

Numerical model setup

The numerical model simulates forced subduction of an oceanic plate beneath a continental margin on a lithospheric to upper mantle cross-section (4000 km $\times$ 200 km; Figure 4.1). The rectangular grid with 2041 $\times$ 201

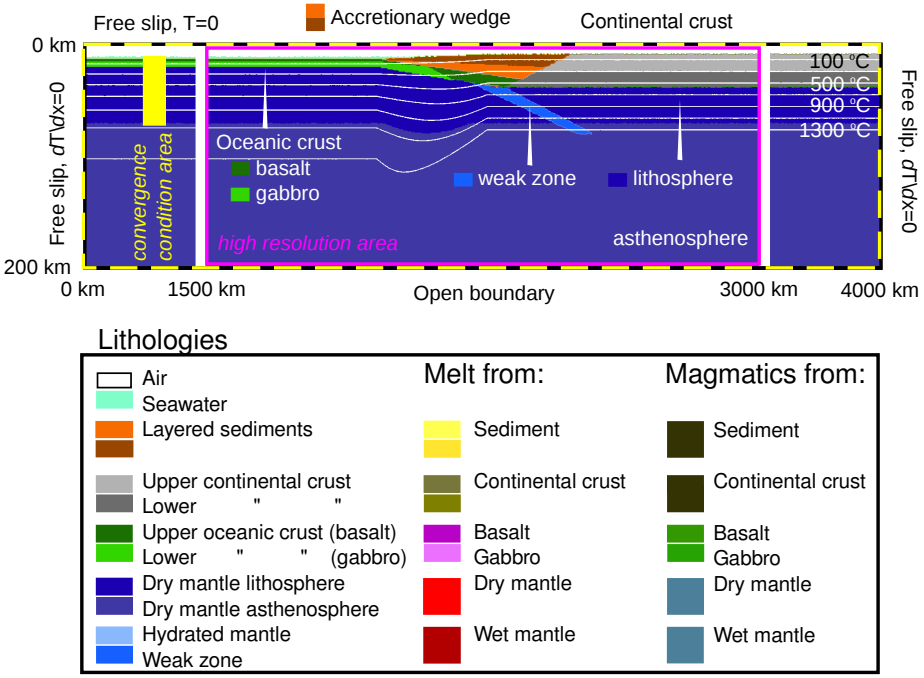

Figure 4.1: Initial setup of the numerical model (see text for details). Staggered grid resolution is 2041 × 201 nodal points, with more than 10 million randomly distributed markers. Grid step is 1 × 1 km in the subduction zone area (1500 - 3000 km) and 5 × 1 km outside of this area. Isotherms are displayed in white for increments of 200 $°C$, starting from 100 $°C$. Colours indicate materials (i.e. rock type or melt), which appear in subsequent figures. To illustrate deformation, two layers with the same physical properties are distinguished using different colours for sediments, crust (upper and lower crust) and mantle (asthenosphere and lithosphere).

nodal points is non-uniform and contains a 1500 km wide high-resolution area of 1 km $\times$ 1 km in the center of the domain while the rest of the model remains at a lower resolution (5 $\times$ 1 km). The oceanic crust (2500 km) is pushed towards a fixed continental crust (1500 km) at an imposed convergence rate of 5 cm/yr. A rheologically weak shear zone at the bottom of the oceanic-continental suture zone prescribes initiation of subduction. The oceanic crust is composed of 2 km of hydrothermally altered basalt, underlain by 5 km of gabbroic rocks that cover 2500 km horizontally. The continental crust is felsic and has a total thickness of 30 km, composed of 15 km upper and 15 km lower crust that extend over 1500 km. The total thickness of the continental crust corresponds to extended continental crust of Western Europe and Western North America (as opposed to orogens) and was adopted according to Christensen and Mooney (1995). Above the trench accretionary sediments are settled separating the continental crust from the downgoing slab. In the course of subduction this layered sediments are exposed to erosion, sedimentation and sediment subduction (Gerya and Meilick, 2011). Both the asthenosphere and the upper mantle are composed of anhydrous peridotite and are defined by the temperature profile. The rheological parameters used for this different lithologies are summarized in Table 4.1. All mechanical boundary conditions are free slip only the lower boundary is permeable satisfying an external free slip boundary condition (Gorczyk et al., 2007; Ueda et al., 2008). To allow for topographic build up of the lithosphere, the top surface of the lithosphere is treated as an internal free surface (Schmeling et al., 2008) by using a top layer (of 8 - 12.5 km thickness) with low viscosity (10^{18} Pas) and low density (1 kg/m^3 for air, 1000 kg/m^3 for sea water). The topography of the upper boundary changes due to erosion and sedimentation (Gorczyk et al., 2007). The initial temperature field of the oceanic plate is defined by its oceanic geotherm (Turcotte and Schubert, 2002) for a specific lithospheric cooling age of 40 Myr. The initial temperature field of the continental plate increases linearly from 0 $°C$ at the surface to 1367 $°C$ at the lithosphere asthenosphere boundary at 72 km depth. For the asthenospheric mantle (>72 km) an initial adiabatic like thermal gradient of 0.5 $°C/km$ is used. This is in accordance with recent studies, where sharp lithosphere-asthenosphere boundaries have been imaged at shallow depth ($\sim$ 60 - 90 km), such as for instance beneath the western U.S. (Levander and Miller, 2012).

Material	Flow law	$1/A_D\ [Pa^n s]$	n	$E_a\ [J]$	$V_a\ [J/bar]$	$sin(\phi)$	$c\ [Pa]$
Sediment	wet qtz	1.97×10^{17}	2.3	154×10^3	0.8	0.15	1×10^7
Upper crust	wet qtz	1.97×10^{17}	2.3	154×10^3	1.2	0.15	1×10^7
Lower crust	wet qtz	1.97×10^{17}	2.3	154×10^3	1.2	0.15	1×10^7
Basalt	wet qtz	1.97×10^{17}	2.3	154×10^3	0.8	0.10	1×10^7
Gabbro	plag (An75)	4.80×10^{22}	3.2	238×10^3	0.8	0.60	1×10^7
Dry mantle	dry ol	3.98×10^{16}	3.5	532×10^3	0.8	0.60	1×10^7
Wet mantle	wet ol	5.01×10^{20}	4.0	470×10^3	0.8	0.10	1×10^7
Shear zone	wet ol	5.01×10^{20}	4.0	470×10^3	0.8	0.10	1×10^7
Serp. mantle	const	10^{18}	1				
Magmatics (all)	wet qtz	1.97×10^{17}	2.3	154×10^3	0.8	0.15	1×10^7

Table 4.1: Rheological parameters used in this study: wet qtz = wet quarzite, plag (An75) = anorthite 75 %, wet ol = wet olivine, dry ol = dry olivine after (Ranalli, 1995). A_D is the pre-exponential factor, n, is the stress exponent, E_a is the activation energy, V_a is the activation volume, ϕ is the friction angle, and c is the cohesion.

	Sediment	MORB	Mantle
$Nd[ppm]$	35	6	–
$Sr[ppm]$	142	94	21
$^{143}Nd/^{144}Nd$	0.5120	0.5128	0.7045
$^{87}Sr/^{86}Sr$	0.72	0.7020	–

Table 4.2: Initial ratios and concentrations of Sr and Nd in sediment (Taylor and McLennan, 1985), basalt (Klein, 2005) and mantle (Sun and McDonough, 1989)

The model is based on the I2VIS code (Gerya and Yuen, 2003a) and uses conservative finite differences and a non-diffusive marker in cell technique to simulate multiphase flow. The governing conservation equations of mass, momentum and energy and the constitutive relationship between stress and strain-rate (needed in the creeping flow regime) are solved on a staggered grid in Eulerian configuration. Conservation of mass is described by the Lagrangian continuity equation for a compressible fluid. The model includes spontaneous slab retreat and bending, dehydration of subducted crust, aqueous fluid transport, partial melting, melt extraction and melt emplacement in form of extrusive volcanics and intrusive plutons. For a detailed description of the governing equations and the numerical procedure employed in this study the reader is referred to Gerya and Yuen (2003a, 2007), and Gerya and Meilick (2011).

Geochemical evaluation of composite diapirs

We have calculated the isotopic initial ratios of Sr and Nd in the mélange (magma source) at any given time during the simulations according to a simple mass balance equation (Faure, 2000):

$$Ri(m) = Ri(b) \times [i]_b \times X_b + Ri(s) \times [i]_s \times (1 - X_b)$$

Ri - isotopic initial ratio of Sr or Nd, i.e.: $[(^{87}Sr/^{86}Sr)_{initial}]$ and $[(^{143}Nd/^{144}Nd)_{initial}]$, calculated at the time of magma generation.

m = mélange; b = basalt; s = sediment

[i] - Concentration in ppm of Sr and Nd

X_b - volume fraction of basalt in the mélange

The isotopic initial ratios of the mélange (Ri(m)) depend on the isotopic ratios of the components (Ri(b), Ri(s)), the element abundances of Sr and Nd in the components (basalt: $[i]_b$, sediment: $[i]_s$ in ppm) and the fraction of the components in the mixture/source (X_b). Our numerical simulations provide the latter parameter (X_b). The initial ratios and concentrations of Sr and Nd in basalt and sediment are summarized in Table 4.2 and were assumed to be constant. In addition to this, we assume: (i) no fractionation of radiogenic isotopes (Sr, Nd) during melting or magma evolution and (ii) isotope homogenization in the source. In natural settings, crustal subduction erosion by which crustal/continental material is scrapped off the upper plate to be subducted and mixed with oceanic crust and sediments from the accretionary prism, will affect the isotopic evolution of the system. However, this process is strongly dependent on the tectonic and chemical setting considered and is therefore difficult to assess. Accordingly, we assume that isotopic ratios of all crustal components (continental crust and sediment) are represented by terrigenous sediment (Table 4.2). Hybridization of the mélange with the surrounding mantle was calculated in a similar manner:

$$Ri(hybrid) = Ri(mantle)\times[i]_{mantle}\times X_{mantle}+Ri(m)\times[i]_{mantle}\times(1-X_{mantle})$$

Ri(hybrid) represents the isotopic ratio of the parental magma (i.e., partially molten diapiric mélange) after reaction with the mantle. X_{mantle} corresponds to the mass fraction of mantle involved in the reaction and was varied from X_{mantle} = 0.8 - 0.95 to ensure equilibrium between melt and mantle. Isotopic ratios and element abundances (Nd and Sr in ppm) of the primordial mantle are summarized in Table 4.2.

The following assumptions have been made concerning the geochemistry of composite diapirs, composed of subducted oceanic crust and sediment. The oceanic crust is relatively homogeneous in major element composition (MORB are among the most homogeneous rocks on Earth in terms of major elements), but differences in trace element compositions are significant between normal, transitional and primitive MORB. We have chosen N-MORB to represent the composition of the oceanic crust because the other two types form oceanic plateaus (T-MORB) and sea mounts (P-MORB and E-MORB), which are less abundant and may not represent the average oceanic crust. Sedimentary material, on the other hand, displays a wide variety of trace element patterns, which makes data selection more difficult. Nevertheless, greywackes are the most abundant terrigenous sediments found in flysch-type synorogenic sedimentary basins (at continental margins) and were chosen to represent the composition of subducted sediment and crustal material (Table 4.2).

Our simplified geochemical assumptions are aimed at evaluating first order influences on the geochemistry of melt derived from partially molten composite diapirs. Compositional changes within the diapir are related to differing proportions of basalt and sediment that will affect the geochemical evolution of melt derived from such sources.

4.4 Results

Dynamics of diapir formation

Because of the large thermal contrast between the leading edge of the subducting slab and the overlying mantle, partial melting of the oceanic crust occurs shortly after subduction initiation (< 5 Myr). Aqueous fluids propagate from the subducting slab into the mantle wedge, hydrating the overlying mantle. Such fluids may either form a serpentinized channel at shallow slab interfaces (< 130 km) within the colder lithospheric portion of the mantle wedge or generate subsolidus metasomatism at greater depth where the mantle is hotter. Where these fluids encounter the wet mantle solidus they induce partial melting of the hydrated mantle, enabling basaltic melt production. In contrast, localization along the slab interface and forced return flow of material within the serpentinized layer, enable the formation of a complex tectonic rock mélange, composed of sediment, basalt and hydrated/serpentinized mantle. The large density contrast (400 - 600 kg/m^3, depending on composition and degree of melting) between this layer and the overlying mantle wedge finally induces Rayleigh-Taylor instabilities atop the slab. Composite diapirs are formed that enable buoyant ascent of crustal material towards shallower levels of the continental lithosphere (Figure 4.2 and 4.3).

Because of the differing proportions of the components in the source (i.e.: basalt and sediment), the composition of these diapiric structures changes with time. Both sediment and basalt are carried into the subduction zone by the downgoing slab and form an inexhaustible source of crustal components. Their relative proportions are a result of the tectonic setting and are not imposed by the model design (Gerya and Meilick, 2011; Vogt et al., 2012). In particular, the relative proportion of sediment and basalt is strongly dependent on the rheological plate coupling. Strong plate coupling promotes compression of the upper plate and enhances sediment subduction, whereas low coupling leads to upper plate extension and sediment accretion, forming large growing accretionary prisms (Gerya and Meilick, 2011). Melt extracted from all molten components (atop the

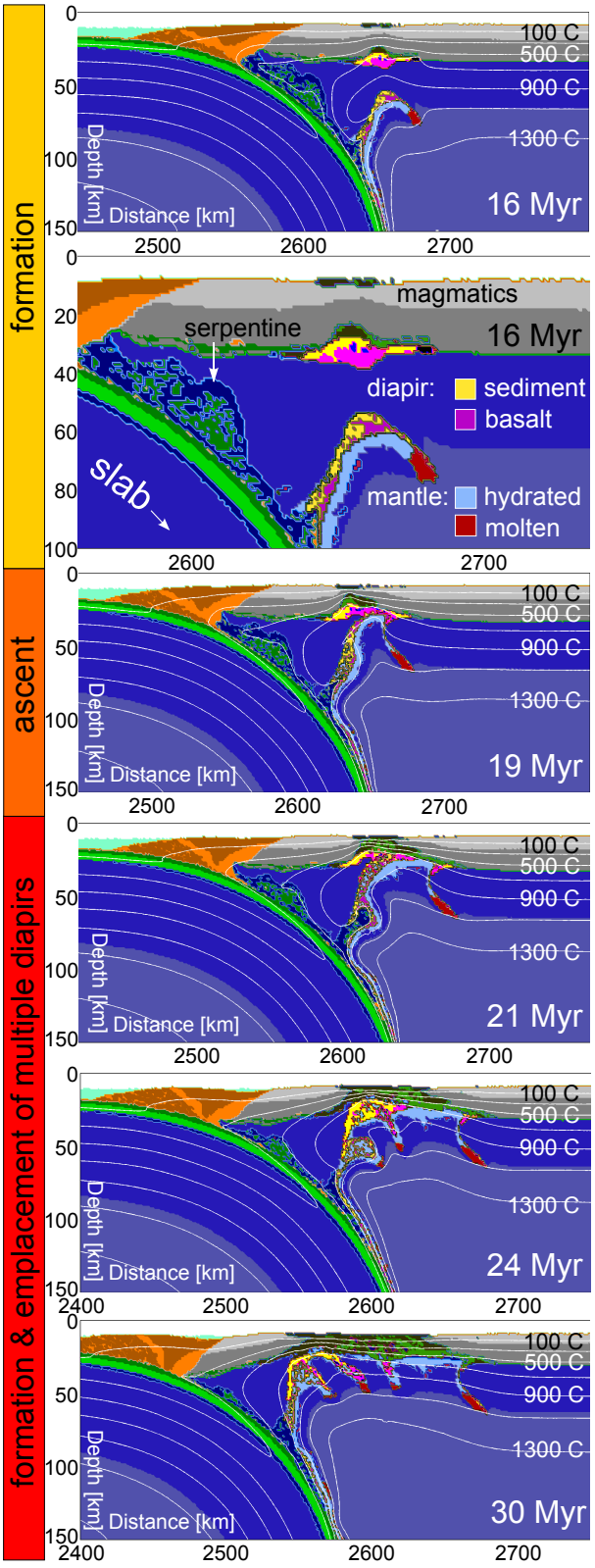

Figure 4.2: Translithospheric diapirs. Localization and partial melting atop the slab triggers Rayleigh-Taylor Instabilities at asthenospheric depths. Hence, composite diapirs are formed composed of sediment, basalt and hydrated/serpentinized mantle. Rapid, buoyant ascent through the mantle is followed by emplacement at crustal levels. Continuous supply of crustal material atop the slab promotes the recurrent formation of composite diapirs.

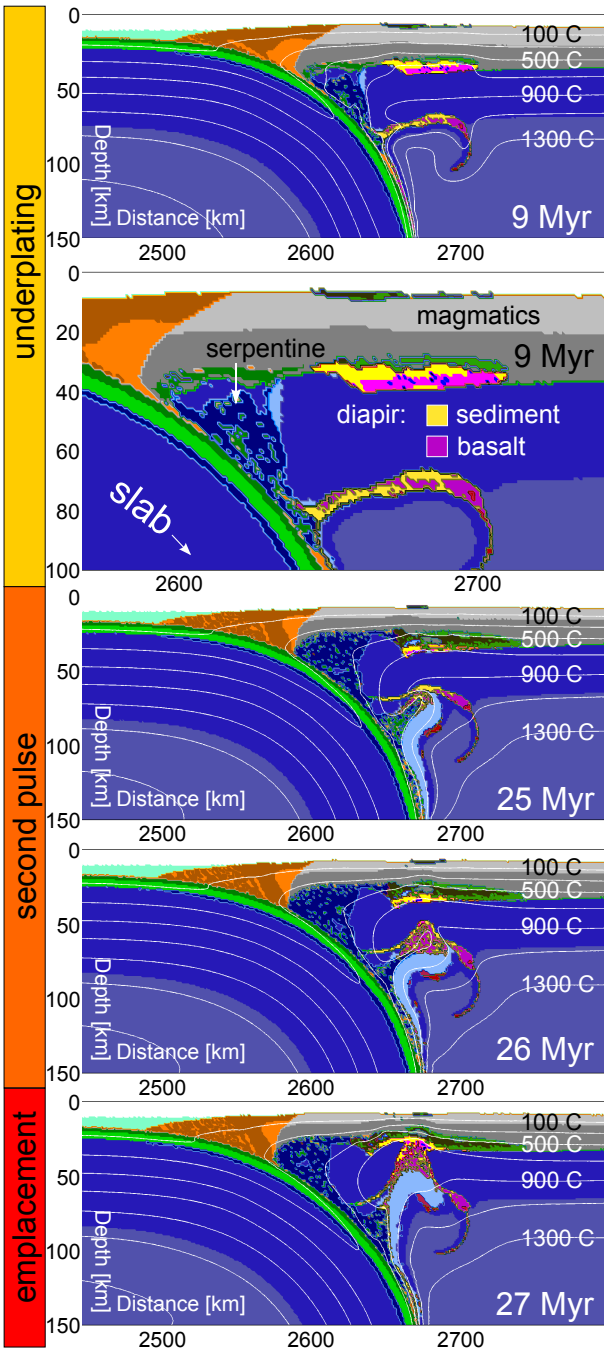

Figure 4.3: Underplating diapirs. Partial melting of crustal material atop the slab enables the formation of composite diapirs at asthenospheric depth. Once a diapir of high volume is formed, it detaches from the slab and no more material is added (for up to 20 Myr). Because of the strong continental lithosphere, diapir ascent is inhibited and the diapir underplates the continental crust for up to 20 Myr until a final upwelling (magma pulse) enables emplacement at crustal levels.

slab and inside the diapir) forms new volcanic crust at the surface and intrusive plutons at deeper crustal levels. Depending on the magnitude of melt weakening effects on the overlying lithosphere, either translithospheric (Figure 4.2) or underplating diapirs (Figure 4.3) will form. Where melt propagation is assumed to weaken the lithosphere (by lowering its plastic strength), rapid translithospheric diapir ascent is feasible (Figure 4.2). If however melt percolation has little effect on the lithospheric strength, diapiric ascent is inhibited and the diapir spreads below the lithosphere (Figure 4.2).

Multiple translithospheric diapirs

The incubation period (0 - 13 Myr) of translithospheric diapirs is characterized by large fluctuations in the basalt fraction ($X_b = \frac{basalt}{basalt+sediment}$) = 1 - 0.3) and an overall decrease in basaltic components (Figure 4.4a). Localization at the slab interface and slab melting at early stages of subduction introduce large amounts of partially molten basalt into the (low viscosity) subduction channel. Progressive sediment subduction and sediment erosion eventually decrease the basalt fraction to a minimum of X_b = 0.3 (Figure 4.4a). Accumulation of sedimentary components enables diapir formation (Figure 4.2), increasing the total volume of partially molten material from 80 km^3/km to 350 km^3/km (Figure 4.4a). Diapiric ascent is triggered and crustal material is transported throughout the hot mantle at speeds of 1.2 cm/yr (13 - 18 Myr). Emplacement of these partially molten structures at crustal levels results in large growing magma chambers at mid to upper crustal levels. In spite of the rapid ascent, lower parts of the diapiric structure (diapir tail) remain attached to the slab, forming a weak zone, composed of partially molten rock and hydrated mantle. This, in turn, enables new material to be added at its base and the total volume of partially molten diapiric material increases to 550 km^3/km (Figure 4.4a). New incoming magma promotes further diapir formation resulting in multiple magma pulses (on a 1 - 5 Myr timescale) and diapir emplacement episodes (Figure 4.2). During this period of time, the basalt fraction is limited to values of X_b = 0.4 - 0.8 and exhibits periodic variations, which reflect the recurrent supply of magma of varying composition (Figure 4.4a). After 28 Myr the magmatic supply from the slab reaches a steady state, the diapir detaches from the slab and no more magma is added to its base for the next 10 Myr at which the basalt ratio remains fixed at $X_b = 0.55$. The volume of the diapir declines from about 600 km^3/km to 400 km^3/km, because of melt extraction. Finally an upwelling is formed ($\sim$ 38 Myr) and additional material (100 km^3/km) is added, but the basalt fraction shows

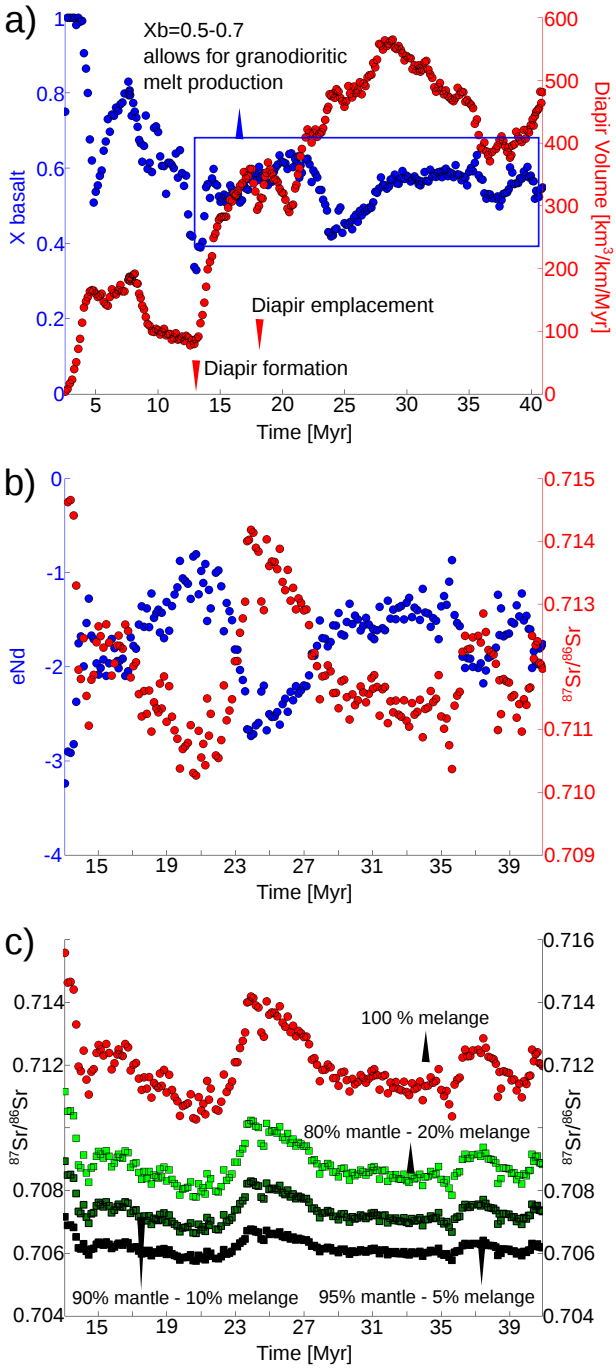

Figure 4.4: Isotopic variations caused by translithospheric diapirs. (a) Compositional variations related to differing material inputs of basalt and sediment (i.e.: volume fraction of basalt and sediment: $X_b = \frac{basalt}{basalt+sediment}$) (blue dots) in relation to diapir growth (red dots). (b) Isotopic variations of liquid/melt derived from composite diapirs, based on the mass fraction of sediment and basalt (i.e. X_b) in the source (diapir). $^{87}Sr/^{86}Sr$ initial ratios are shown in red, ϵNd ratios are displayed in blue. An increase in basaltic components leads to an increase in ϵNd and a decrease in $^{87}Sr/^{86}Sr$. The recurrent supply of magma of varying composition (X_b) leads to periodic variations (c) $^{87}Sr/^{86}Sr$ initial ratios of melt derived from composite diapirs after reactions with the mantle, shown for various melt-mantle fractions.

little variations (Figure 4.4a) in contrast to the large fluctuations at early stages.

Single underplating diapir

The basalt ratio decreases rapidly during the incubation period (0 - 5 Myr) form $X_b = 1$ - 0.5 until a composite diapir of high volume is formed (Figure 4.5a). Shortly after (8 Myr) the volume of the diapir reaches its maximum of $\sim$ 500 km^3/km and no more material is added. The diapir detaches from the slab and underplates the lithosphere for up to 20 Myr, not able to penetrate through the lithosphere (Figure 4.3). During this period (8 Myr - 25 Myr) the basalt ratio remains limited to $X_b = 0.7$ - 0.5, revealing periodic variations on a 10 Myr timescale (Figure 4.5a). Melt extracted from the composite diapir travels through the mantle and forms volcanics at the surface and flattened intrusions in the lower crust. Thus, the volume of the diapir decreases from 300 km^3/km to 200 km^3/km (Figure 4.5a) and percolating melt weakens the lithosphere. Because of the constant supply of sediment and basalt at the slab interface, the diapir finally detaches (24 Myr) after a second upwelling is formed and emplaces at crustal levels shortly after (25 Myr) (Figure 4.3).

4.5 Discussion

Formation of composite diapirs

Observations along active continental margins have revealed that sediments and small crustal bodies can be scrapped off the downgoing slab or form large accretionary prisms (von Huene and Scholl, 1991; Cloos and Shreve, 1988). Crustal material can bypass the accretionary wedge, as it remains attached to the oceanic crust or be removed from the upper plate in the process of crustal erosion (von Huene and Scholl, 1991; Clift and Vannucchi, 2004; Scholl and von Huene, 2007). This is in accordance with our numerical experiments on diapir formation. Strong coupling of the plates promotes sediment subduction and basal erosion of the upper continental crust (Gerya and Meilick, 2011; Vogt et al., 2012). Most of the incoming sediments bypass the accretionary wedge and only small to medium sized prisms are formed. Recent estimates on the net transfer of crustal material on Earth surface suggest that crustal rocks are recycled back into the mantle at the same rate (25 - 50 $km^3/km/Myr$) that continental crust is formed (von Huene and Scholl, 1991; Scholl and von Huene, 2007). Consequently,

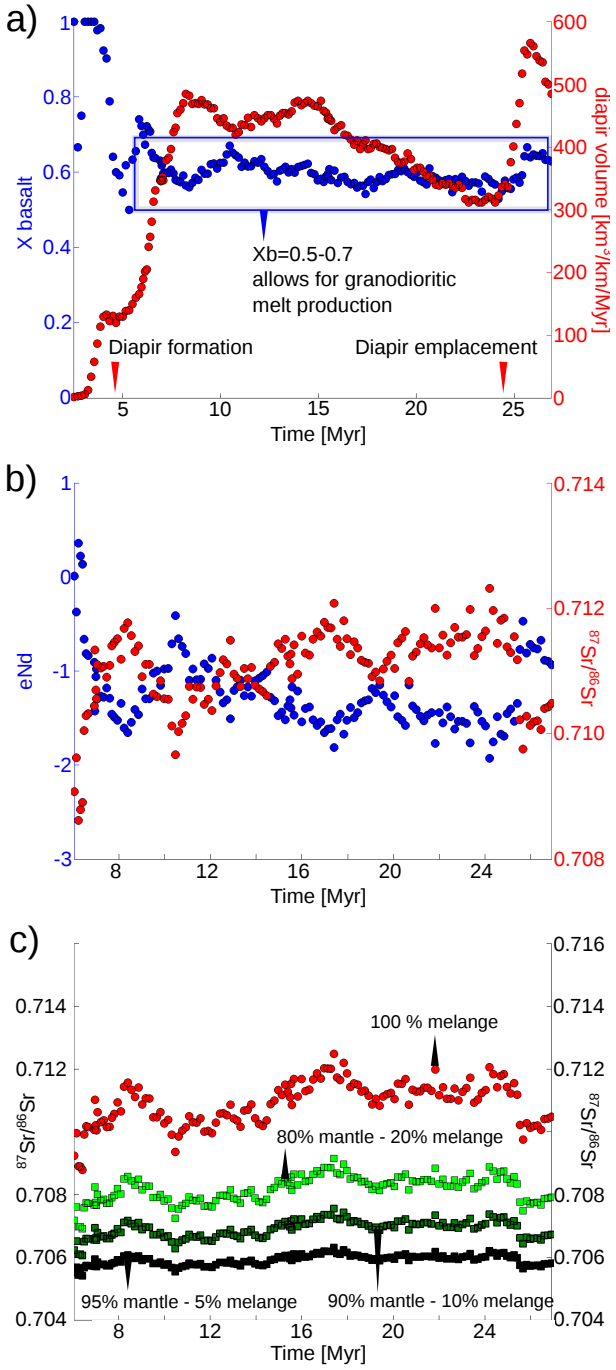

Figure 4.5: Isotopic variations caused by underplating diapirs. (a) Compositional variations related to differing material inputs of basalt and sediment (i.e.: volume fraction of basalt and sediment: $X_b = \frac{basalt}{basalt+sediment}$) (blue dots) in relation to diapir growth (red dots). (b) Isotopic variations of liquid/melt derived from composite diapirs, based on the mass fraction of sediment and basalt (i.e. X_b) in the source (diapir). $^{87}Sr/^{86}Sr$ initial ratios are shown in red, ϵNd ratios are displayed in blue. An increase in basaltic components leads to an increase in ϵNd and a decrease in $^{87}Sr/^{86}Sr$. The limited supply of new magma to the source (diapir) leads to minor, but distinct variations in isotopic ratios (c)$^{87}Sr/^{86}Sr$ initial ratios of melt derived from composite diapirs after reactions with the mantle, shown for various melt-mantle fractions.

sediments sink into the mantle and intermix with the oceanic crust to form a hybrid tectonic rock mélange (Figure 4.2 and 4.3). Natural mélange occurrences comprise highly deformed metasedimentary collages of incipient metamorphism and chaotic hybrid mixtures of peridotite, basalt and sediment produced at blueschist-amphibolite-, or eclogite conditions, formed in forearc to sub-arc regions (King et al., 2006, and references therein). King et al. (2006) have argued that mélange formation is an intrinsic process to all subduction zones and that the geochemistry of mélange will impart the strongest control on the geochemistry of metasomatic agents (hydrous fluids, silicate melts, or miscible supercritical liquids) progressing to arc magmatic source regions in the mantle wedge.

Water released due to dehydration reactions of hydrous phases (e.g Schmidt and Poli, 1998) and compaction of the sedimentary layer and hydrothermally altered oceanic crust (Peacock, 1990) enables partial melting of the tectonic rock mélange. According to our results, buoyant diapirs are formed, composed of partially molten sediment and basalt that detach from the slab, transporting fertile subducted material towards hotter zones of the mantle wedge (Figure 4.2 and 4.3). Early on it was suggested that hydrous partial melting of the oceanic crust (with a quartz eclogite mineralogy at 100 km - 200 km and 700 - 900 $^{\circ}C$) results in silicic magmas that rise and react with the overlying peridotitic mantle to produce olivine-pyroxene diapirs, contaminated with the elements enriched in silicic melts (Ringwood and Green, 1966; Green, 1980; Ringwood, 1990). Later on, phase equilibria and trace element partitioning experiments on pelagic red clay at conditions appropriate to the slab beneath arc volcanoes have demonstrated that sediment melting is required for critical elements (Th and Be) to be transferred to the arc (Plank, 2005; Plank and Langmuir, 1998; Johnson and Plank, 1999). In addition to this, Skora and Blundy (2010) have suggested that serpentine breakdown at sublithospheric depth (100 km, 800 $^{\circ}C$) may enable high degree melting ($\sim$ 54 % melt) of sedimentary rocks (i.e. radiolarian clay) by a process coined flush melting, in contrast to fluid absent melting, which yields negligible melt fraction ($<$ 10%) (Skora and Blundy, 2010). This led Tamura et al. (2011) to propose that such hydrous sediment melt may mix with the overlying mantle to form a crystal-liquid mush (diapir) that is sufficiently buoyant to initiate diapiric ascent, upon which equilibrium between the crystals and the liquid will be maintained over the changing pressure-temperature conditions.

Recent studies on the density structure of subducted sediments demonstrate that during sediment subduction and sediment erosion more silica rich rocks are transformed into felsic gneisses that are less dense than the

peridotite mantle (Behn et al., 2011; Hacker et al., 2011; Miller and Behn, 2012). These felsic gneisses can relaminate to the base of the crust, whereas mafic rocks become eclogite and may sink into the mantle (Hacker et al., 2011). Xenoliths of subducted crustal origin from the Pamir Mountains display natural examples of this process (Ducea et al., 2003; Hacker et al., 2005). The depth and temperature at which sedimentary layers detach from the downgoing slab have repeatedly been reported to vary between 40 - 100 km and 500 - 850 $°C$ (Behn et al., 2011; Hacker et al., 2011; Miller and Behn, 2012), which is in accordance with our study. The timescales over which these instabilities grow depend on the viscosity contrast between the sedimentary layer and overlying mantle, temperature, buoyancy and thickness of the sedimentary layer, but are generally believed to be rapid < 3 Myr (Behn et al., 2011; Miller and Behn, 2012). Analogue studies on diapiric flow at subduction zones have moreover indicated that the interaction between buoyantly upwelling diapirs and subduction induced flow in the mantle creates a network of low density, low viscosity conduits through which flow is rapid (Hall and Kincaid, 2001). Timescales over which such diapiric structures may transverse from the slab (at 70 km depth) to the surface have been estimated to vary between 10^4 to 6×10^6 years (Hall and Kincaid, 2001) and are comparable to our results on translithospheric diapirs ($1 - 5 \times 10^6$ years).

Though there is growing evidence for crustal relamination of subducted material to the base of the continental crust (e.g. Ringwood, 1990; Gerya et al., 2004; Gerya and Meilick, 2011; Hacker et al., 2011; Behn et al., 2011; Tamura et al., 2011), transport mechanisms remain controversial. Kelemen et al. (2003b) suggest andesitic melt percolation along low viscosity conduits, while Behn et al. (2011) assume buoyant ascent of small 3 - 4 km sized diapirs, in contrast to the large (5 - 30 km) diapiric structures proposed by Gerya and Yuen (2003b). The transport of andesitic melt through a network of conduits (Kelemen et al., 2003b) is compatible with our study. However, we argue that hydrous melting of basalt and sediment along the slab interface may give rise to composite diapirs of granodioritic composition that can relaminate the continental crust, having a strong impact on the petrological and geochemical evolution of the continental crust. Some of these consequences are discussed below. However, further studies on the chemical compositon of rock mélange in terms of phase relation and chemical partitioning are necessary to capture its significance in relation to large scale crustal recycling.

Diapir composition and melt generation

Trace-elements that form the sediment melt signature of arc lavas are believed to retain in the sediments until the rocks have experienced temperatures exceeding 1050 $^{\circ}C$ (Behn et al., 2011). Melting experiments on basaltic and sedimentary components at temperatures exceeding 1000 $^{\circ}C$ show that tectonic rock mélanges are favourable for the production of granodioritic liquids (Castro and Gerya, 2008; Castro et al., 2010). However, these temperatures are higher than those at the slab surface (700 - 900 $^{\circ}C$), where according to our studies composite diapirs assemble and form before they finally detach from the slab (Gerya and Meilick, 2011; Vogt et al., 2012). This led Behn et al. (2011) to conclude that although sediment melting may commence at lower temperature, the key elements associated with the sediment melt signature are not released until temperatures exceed 1050 $^{\circ}C$ and proposed that sediments detach from the slab to undergo dehydration melting in the hot mantle wedge. However, our models show that in spite of the intense heat exchange between the ascending diapir and the hot asthenosphere, temperatures inside the diapir rarely exceed 1050 $^{\circ}C$, implying that the rapid ascent outgrows the timescales of thermal diffusion. Alternatively, basaltic melt formed atop the slab at temperatures greater than 1000 $^{\circ}C$ may propagate and interact with the ascending diapir, increasing its temperature and changing its chemical composition. Because of its low viscosity, basaltic melt is expected to move significantly faster than the diapir itself, but further studies on coupled fluid flow are necessary to verify these assumptions. Nevertheless, hybridiaztion of slab-derived melts is strongly supported in terms of experimental phase relations and geochemical mixing line patterns (Carroll and Wyllie, 1989; Johnston and Wyllie, 1989; Rapp et al., 1999; Chauvel et al., 2007). Recent laboratory experiments on MORB-Greywacke and Spinel-lherzolite of Castro et al. (2012b) have demonstrated that reactions between these components produce andesitic melt with magnesium numbers (MgO/MgO/FeO = 0.6), typical for rocks of the continental crust (Kelemen, 1995).

The compositional variations of the parental magma (diapir) shown in this study are limited to X_b = 0.4 - 0.8 (Figure 4.4 and 4.5a), which according to Castro et al. (2010) is favourable for the production of granodioritic melt. Whilst partial melts of the endmembers - sediments and basalts - form granitic and trondhjemitic melts respectively, mixtures of sedimentary and basaltic components are buffered by the coexisting solid assemblage and are likely to produce granodioritic melt, if X_b is limited to 0.25 - 0.75 (Castro et al., 2012b). This melt may hybridize with basaltic

melt, formed by partial melting of the hydrated mantle, reheat and form High-Mg, low-silica andesite magmas. The compositional variations of the parental magma (X_b) are related to material inputs at the slab interface. This results in magmatic pulses that are transferred to crustal levels and may represent different magma batches. Many batholiths formed along the western coast of North and South America show despite their long-lived magmatic activity over tens of millions of years evidence for cyclical growth (DeCelles et al., 2009) by episodically intruded magma pulses (e.g. Pankhurst et al., 1999; Hervé et al., 2007). During emplacement, diapirs may segregate into solid residues and melt, contributing to the generation of granulites in the lower crust and silicic melt at upper crustal levels that may form batholiths and dacitic volcanism (Castro et al., 2012b). Hence, composite diapirs may be an efficient mechanism by which granodioritic melt is produced and transported.

Pressure-Temperature evolution of the melting zone

We have traced the pressure-temperature evolution of 16 different rocks (tracers in the 2D domain) from the translithospheric and underplating diapir shown in Figure 4.2 and 4.3. The red dots in Figure 4.6 represent partially molten rocks within the diapir that have been traced through time. There is a significant difference between the thermal evolution of translithospheric (Figure 4.6a and 4.6b) and underplating diapirs (Figure

Figure 4.6 *(following page)*: Thermodynamic constraints on the melting zone showing pressure-temperature (P-T) conditions of 16 rocks that have been traced during the simulation. The dashed and solid lines represent P-T paths of these rocks/tracers. Partially molten rocks are represented by solid red dots. a) and b) show the Pressure-Temperature and Temperature-time evolution of rocks from different magma batches of the translithospheric diapir. c) and d) show the Pressure-Temperature and Temperature-time evolution of rocks from different magma batches of the underplating diapir.(a) The rapid ascent of crustal material through the mantle results in a broad melting zone. Temperature and pressure vary between 650 - 1000 $°C$ and 2 - 35 kbar, respectively. (b) After reaching peak temperatures of around 800 $°C$ - 1000 $°C$ most rocks undergo rapid cooling.(c) Melting occurs mostly within a region of 800 - 1050 $°C$ and 10 - 25 kbar, which prevails at the base of the lithosphere. (d) Most of the material remains at temperatures of around 1000 $°C$ for up to 20 Myr, prior to emplacement.

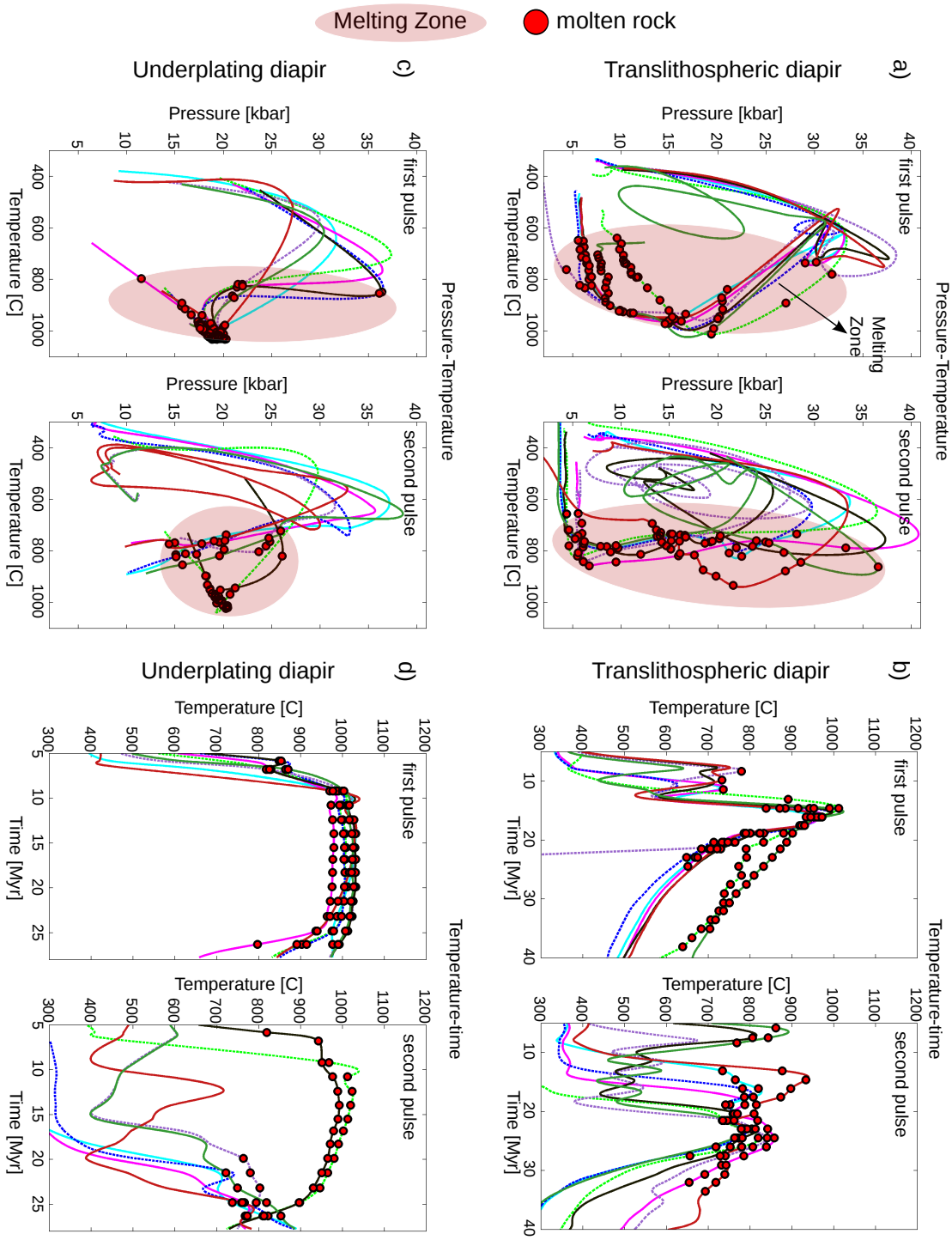
Melting Zone
molten rock
a)
Translithospheric diapir
Underplating diapir
c)
Pressure [kbar]
Temperature [C]
first pulse
second pulse
Melting Zone
Pressure-Temperature
b)
Translithospheric diapir
Underplating diapir
d)
Time [Myr]
Temperature-time

4.6c and 4.6d). While translithospheric diapirs ascend rapidly to cooler regions after reaching peak temperatures of 800 - 1000 $^{\circ}C$ (Figure 4.6a and 4.6b) partial melting of underplating diapirs occurs mainly within the hot region of the mantle (15 - 20 kbar) at temperatures of around 1000 $^{\circ}C$ (Figure 4.6c and 4.6d). Because of the strong continental lithosphere, underplating diapirs cannot penetrate towards shallower levels and spread along the lithospheric base, where they remain for long periods of time (20 Myr). Although melting may commence at lower temperatures ($\sim$ 800 $^{\circ}C$), most of the material melts at temperatures of around 1000 $^{\circ}C$ that prevail at the base of the lithosphere (Figure 4.6d). Translithospheric diapirs, on the other hand, move quickly towards shallower crustal levels and are characterized by the recurrent supply of new magma, forming distinct magma batches. Hence, melting occurs over a broad range of Pressure Temperature conditions (Figure 4.6a) rather than within a focused region. Once peak temperatures of around 800 - 1000 $^{\circ}C$ are reached most of the partially molten material undergoes rapid cooling (Figure 4.6b), because of the rapid ascent of the diapir. These temperatures ($<$ 1000 $^{\circ}C$) are unlikely to produce water-undersaturated granodioritic melt (Castro et al., 2010), but basaltic liquids from the hot mantle wedge may reheat the diapir as they move towards the surface. Partial melting of the hydrated mantle is believed to commence at temperatures exceeding 1000 $^{\circ}C$ (Kushiro, 1974; Green, 1973; Niida and Green, 1999), hence any reaction between ascending hot basaltic melt and the diapir may significantly change its thermal structure. The close spatial association of mantle derived rocks (gabbros) and granodiorite-tonalite intrusions in most Cordilleran (e.g., Sierra Nevada: (Lee et al., 2006; Frost and Mahood, 1987), pre-Cordilleran (e.g.; Famatinan arc: (Castro et al., 2012a) and post collisional batholiths (e.g.; Spanish Central System: (Bea and Montero, 1999); European Caledonides: (Stephens, 1988), suggest a genetic link between mantle derived sources and crustal components.

Geochemical implications

According to experimental data (Castro et al., 2010, 2012b), the major element composition of melt, derived from partially molten diapirs is buffered for sediment to MORB ratios, ranging from 3 : 1 to 1 : 3, producing melt of granodiorite composition. Geochemical and isotopic variations, on the other hand, will be inherited from a composite source, i.e. diapir. During equilibrium melting, the isotopic features of the solid end members, i.e. basalt and sediment will be transferred to the liquid. Although isotopic disequilibrium has been reported with regard to Nd isotopes during

crustal anatexis (e.g. Barbero et al., 1995), the conditions for mélange melting are more favourable for equilibrium melting, because temperatures are expected to be higher and timescales to be larger. Unlike crustal anatexis, where crustal material undergoes rapid cooling after reaching peak temperatures, diapir melting occurs within the hot zone of the mantle, where partially molten crustal material remains hot for several Myr (Figure 4.6).

The compositional variations of the parental magma (Figure 4.4a and 4.5a), produced by material inputs of differing proportions (X_b = 04 - 0.8) are manifested in the geochemical evolution of the liquid (Figure 4.6b and 4.6b). Radiogenic isotopes (Sr, Nd) change with time according to the basalt fraction in the source. For example, an increase in basaltic components (from $X_b = 0.55$ to $X_b = 0.7$) leads to an increase in ϵNd (from -1 to +2) and a decrease in $^{87}Sr/^{86}Sr$ (from 0.707 to 0.705) values. Hence the resulting liquid evolves towards a more primitive (isotopic) composition. In contrast, a decrease in basaltic components results in a more evolved composition with increasing $^{87}Sr/^{86}Sr$ and decreasing ϵNd values (Figure 4.4b and 4.5b). Nevertheless, melt extracted from partially molten diapirs may intermix and react with the overlying mantle as it percolates towards the surface. To account for this behaviour, we have calculated the isotopic signatures that are expected to evolve by chemical interactions of melt derived from composite diapirs and the perioditic mantle (Figure 4.4c and 4.5c). However, hybridization of these liquids with the overlying mantle has little effect on the isotopic characteristics as shown in Figure 4.4c and 4.5c, because the isotopic initial ratios of the hybrid system (diapir+mantle) are related to the element abundances of Sr and Nd in the components (diapir vs. mantle). Crustal diapirs represent strongly fractionated reservoirs, enriched in incompatible elements with Nd and Sr abundances that are an order of magnitude higher compared to the mantle, which is depleted in Sr and Nd (Table 4.2). Therefore any reaction of these liquids with the overlying mantle may produce strong enrichment in Mg, forming High Mg andesites, but insignificant modification in terms of radiogenic isotopes (Sr, Nd) that are mostly controlled by the element abundances of incompatible elements. If magma ascent occurs in a common place this reaction may be even less effective because reaction aureoles may form and prevent further hybridization. Hence any temporal variation of the parental magma in terms of radiogenic isotopes is transferred to the liquids that may react with the peridotite mantle but won't undergo any essential changes in radiogenic isotopes that are imposed by the parental magma. Emplacement of such composite diapirs at crustal levels may finally lead to crustal assimilation, including partial melting, magma

mingling and crustal anatexis that will influence the isotopic evolution of these magmas, but are not considered in this study.

Implications and natural observations

Active continental margins are major sites of magmatism. Silicic magmas of intermediate composition form either plutonic intrusions or extrusive volcanics. The former are assembled in form of large batholiths along active continental margins that contribute to the growth and evolution of continental crust (Condie, 1997; Hawkesworth and Kemp, 2006; Kemp and Hawkesworth, 2005). However, batholiths cannot be derived directly by partial melting of the mantle and their genesis may involve large amounts of recycled crustal material as evidenced by Nd-Sr isotopic ratios (Allgre and Ben Othman, 1980; McCulloch and Wasserburg, 1978). Other characteristic features of calc-alkaline batholiths include (i) the uniformity of major element compositions, (ii) hybrid crust-mantle isotopic signatures and (ii) significant changes in isotopic signatures with time and space. Although generally believed to have formed by fractionation (distillation) of hydrous mantle derived magmas (Hawkesworth and Kemp, 2006; Annen et al., 2006), batholiths may also form by partial melting of crustal components at sublithospheric depth. For example, Takagi (2004) argued based on $^{87}Sr/^{86}Sr$, ϵNd and δO values of granitic plutons in the Japan Arc that the temporal variation of initial $^{87}Sr/^{86}Sr$ isotope ratios is mainly attributed to source contamination, caused by melting of subducted materials in the mantle source region, rather than to the properties of the lower continental crust, which is in accordance with our study on diapir formation. Partial melting of composite diapirs produces homogeneous liquids of granodioritic composition, because compositional variations of the parental magma (diapir) are buffered by the solid residues and are not transferred to the liquids (Castro et al., 2010). In contrast, isotopic and geochemical variations will be inherited from a compositionally heterogenous source, i.e. basalt and sediment (diapir) (Figure 4.4b,c and 4.5b,c). Given the continuous supply of sediment and basalt along the slab, magma supply and melt production may sustain over long periods of time, adding new material of granodioritic composition to the base of the crust with minor changes in major element compositions, but substantial variations in radiogenic isotopes.

Long-time isotopic evolution of batholiths

In some natural geological settings batholiths evolve towards a more primitive composition in terms of initial isotopic ratios (decrease in $^{87}Sr/^{86}Sr$, increase in ϵNd), while their major element composition remains constant over hundreds of Myr (Pankhurst et al., 1999; Hervé et al., 2007). The progressive change from isotopically evolved to isotopically primitive compositions has been explained by the shielding effect of older plutons, resulting in a decrease of crustal contamination of mantle-derived magmas (Bruce et al., 1991) or the simultaneous mixing and melting of more primitive components (Pankhurst et al., 1999). However, if assimilation is the cause of compositional variations, a parallel evolution of major element compositions and isotopic patterns is expected, because assimilation and magma mixing are not selective processes. Isotopically more evolved rocks (increase in $^{87}Sr/^{86}Sr$ ratio and decrease in ϵNd) should have higher silicica and alkali contents, in comparison to more primitive rocks. However, this is not the case. Granites with identical major element compositions plot in both the mantle-like and crustal-like regions in terms of Sr and Nd initial isotopic ratios (see review in Castro et al., 2010). Therefore we argue that differences in isotope ratios are inherited from an already hybrid source (rock mélange composed of basalt and sediment), which does not affect the major element composition of melts derived from it.

Conclusions

Subduction of oceanic crust and sediments results in the formation of tectonic rock mélanges composed of basalt, sediment and hydrated /serpentinized mantle. Our numerical experiments suggest that these rock mélanges may evolve into partially molten crustal diapirs that rise through the mantle prior to emplacement at crustal levels (relamination). The proportions of basaltic and sedimentary components in the mélange are limited to short-range variations within an interval of X_b ($= \frac{basalt}{basalt+sediment}$) = 0.4 - 0.8 and yield granodioritic melt. Melt derived from composite diapirs inherits the geochemical characteristics of the composite source and shows distinct temporal variations of radiogenic isotopes (Sr and Nd) depending on the changing values of X_b in the source. The decoupling between radiogenic isotopes and major elements may explain short-range variations observed in some batholiths along the Andean Cordillera.

Bibliography

Allgre, C., Ben Othman, D., 1980. Nd-sr isotopic relationship in granitoid rocks and continental crust development: a chemical approach to orogenesis. Nature 286, 335–341.

Annen, C., Blundy, J., Sparks, R., 2006. The genesis of intermediate and silicic magmas in deep crustal hot zones. Journal of Petrology 47 (3), 505–539.

Armstrong, R., Harmon, R., 1981. Radiogenic isotopes: The case for crustal recycling on a near-steady-state no-continental-growth earth [and discussion]. Philosophical Transactions of the Royal Society of London. Series A, Mathematical and Physical Sciences 301 (1461), 443–472.

Barbero, L., Villaseca, C., Rogers, G., Brown, P., 1995. Geochemical and isotopic disequilibrium in crustal melting: an insight from the anatectic granitoids from toledo, spain. Journal of Geophysical Research 100 (B8), 15745–15.

Bea, F., Montero, P., 1999. Behavior of accessory phases and redistribution of zr, ree, y, th, and u during metamorphism and partial melting of metapelites in the lower crust: an example from the kinzigite formation of ivrea-verbano, nw italy. Geochimica et Cosmochimica Acta 63 (7), 1133–1153.

Behn, M., Kelemen, P., Hirth, G., Hacker, B., Massonne, H., 2011. Diapirs as the source of the sediment signature in arc lavas. Nature Geoscience 4 (9), 641–646.

Bruce, R., Nelson, E., Weaver, S., Lux, D., 1991. Temporal and spatial variations in the southern patagonian batholith; constraints on magmatic arc development. Andean Magmatism and Its Tectonic Setting (Harmon, RS; Rapela, CW; editors). The Geological Society of America, Special Paper 265, 1–12.

Carroll, M., Wyllie, P., 1989. Experimental phase relations in the system tonalite-peridotite-h2o at 15 kb; implications for assimilation and differentiation processes near the crust-mantle boundary. Journal of Petrology 30 (6), 1351–1382.

Castro, A., Díaz-Alvarado, J., Fernández, C., 2012a. Fractionation and incipient self-granulitization during deep-crust emplacement of lower or-

dovician valle fértil batholith at the gondwana active margin of south america. Gondwana Research.

Castro, A., García-Casco, A., Fernández, C., Corretgé, L., Moreno-Ventas, I., Gerya, T., Löw, I., 2009. Ordovician ferrosilicic magmas: Experimental evidence for ultrahigh temperatures affecting a metagreywacke source. Gondwana Research 16 (3), 622–632.

Castro, A., Gerya, T., 2008. Magmatic implications of mantle wedge plumes: experimental study. Lithos 103 (1), 138–148.

Castro, A., Gerya, T., García-Casco, A., Fernández, C., Díaz-Alvarado, J., Moreno-Ventas, I., Löw, I., 2010. Melting relations of morb–sediment mélanges in underplated mantle wedge plumes; implications for the origin of cordilleran-type batholiths. Journal of Petrology 51 (6), 1267–1295.

Castro, A., Vogt, K., Gerya, T., 2012b. Generation of new continental crust by sublithospheric silicic-magma relamination in arcs: A test of taylor's andesite model. Gondwana Research.

Chauvel, C., Lewin, E., Carpentier, M., Arndt, N., Marini, J., 2007. Role of recycled oceanic basalt and sediment in generating the hf–nd mantle array. Nature geoscience 1 (1), 64–67.

Christensen, N., Mooney, W., 1995. Seismic velocity structure and composition of the continental crust: A global view. Journal of Geophysical Research 100 (B6), 9761–9788.

Clift, P., Vannucchi, P., 2004. Controls on tectonic accretion versus erosion in subduction zones: Implications for the origin and recycling of the continental crust. Reviews of Geophysics 42 (2), RG2001.

Cloos, M., Shreve, R., 1988. Subduction-channel model of prism accretion, melange formation, sediment subduction, and subduction erosion at convergent plate margins: 1. background and description. Pure and Applied Geophysics 128 (3), 455–500.

Condie, K., 1997. Plate Tectonics. Butterworth-Heinemann.

Currie, C., Beaumont, C., Huismans, R., 2007. The fate of subducted sediments: A case for backarc intrusion and underplating. Geology 35 (12), 1111–1114.

DeBari, S., Sleep, N., 1991. High-mg, low-al bulk composition of the talkeetna island arc, alaska: Implications for primary magmas and the nature of arc crust. Geological Society of America Bulletin 103 (1), 37–47.

DeCelles, P., Ducea, M., Kapp, P., Zandt, G., 2009. Cyclicity in cordilleran orogenic systems. Nature Geoscience 2 (4), 251–257.

Defant, M., Drummond, M., 1990. Derivation of some modern arc magmas by melting of young subducted lithosphere. Nature 347 (6294), 662–665.

Drummond, M., Defant, M., 1990. A model for trondhjemite-tonalite-dacite genesis and crustal growth via slab melting: Archean to modern comparisons. Journal of geophysical research 95 (B13), 21503–21.

Ducea, M., Lutkov, V., Minaev, V., Hacker, B., Ratschbacher, L., Luffi, P., Schwab, M., Gehrels, G., McWilliams, M., Vervoort, J., et al., 2003. Building the pamirs: The view from the underside. Geology 31 (10), 849–852.

Faure, G., 2000. Origin of igneous rocks: the isotopic evidence. Springer.

Frost, T., Mahood, G., 1987. Field, chemical, and physical constraints on mafic-felsic magma interaction in the lamarck granodiorite, sierra nevada, california. Geological Society of America Bulletin 99 (2), 272–291.

Gerya, T., Connolly, J., Yuen, D., Gorczyk, W., Capel, A., 2006. Seismic implications of mantle wedge plumes. Physics of the Earth and Planetary Interiors 156 (1), 59–74.

Gerya, T., Meilick, F., 2011. Geodynamic regimes of subduction under an active margin: effects of rheological weakening by fluids and melts. Journal of metamorphic Petrology 29, 7–31.

Gerya, T., Yuen, D., 2003a. Characteristics-based marker-in-cell method with conservative nite-differences schemes for modeling geological flows with strongly variable transport properties. Physics of the Earth and Planetary Interiors 140, 293–318.

Gerya, T., Yuen, D., 2003b. Rayleigh–taylor instabilities from hydration and melting propel cold plumes at subduction zones. Earth and Planetary Science Letters 212 (1), 47–62.

Gerya, T., Yuen, D., 2007. Robust characteristics method for modelling multiphase visco-elasto plastic thermo-mechanical problems. Physics of the Earth and Planetary Interiors 163, 83–105.

Gerya, T., Yuen, D., Maresch, W., 2004. Thermomechanical modeling of slab detachment. Earth and Planetary Science Letters 226, 101–116.

Gorczyk, W., Willner, A., Gerya, T., Connolly, J., Burg, J.-P., 2007. Physical controls of magmatic productivity at pacic-type convergent margins: Numerical modelling. Physics of the Earth and Planetary Interiors 163, 209232.

Green, D., 1973. Experimental melting studies on a model upper mantle composition at high pressure under water-saturated and water-undersaturated conditions. Earth and Planetary Science Letters 19 (1), 37–53.

Green, T., 1980. Island arc and continent-building magmatisma review of petrogenic models based on experimental petrology and geochemistry. Tectonophysics 63 (1), 367–385.

Hacker, B., Kelemen, P., Behn, M., 2011. Differentiation of the continental crust by relamination. Earth and Planetary Science Letters 307 (3), 501–516.

Hacker, B., Luffi, P., Lutkov, V., Minaev, V., Ratschbacher, L., Plank, T., Ducea, M., Patiño-Douce, A., McWilliams, M., Metcalf, J., 2005. Near-ultrahigh pressure processing of continental crust: Miocene crustal xenoliths from the pamir. Journal of Petrology 46 (8), 1661–1687.

Hall, P., Kincaid, C., 2001. Diapiric flow at subduction zones: A recipe for rapid transport. Science 292 (5526), 2472–2475.

Haschke, M., Siebel, W., Günther, A., Scheuber, E., 2002. Repeated crustal thickening and recycling during the andean orogeny in north chile (21–26 s). Journal of Geophysical Research 107 (B1), 2019.

Hawkesworth, C., Kemp, A., 2006. Evolution of the continental crust. Nature 443 (7113), 811–817.

Hervé, F., Pankhurst, R., Fanning, C., Calderón, M., Yaxley, G., 2007. The south patagonian batholith: 150 my of granite magmatism on a plate margin. Lithos 97 (3), 373–394.

Hildreth, W., Moorbath, S., 1988. Crustal contributions to arc magmatism in the andes of central chile. Contributions to Mineralogy and Petrology 98 (4), 455–489.

Hofmann, A., 1988. Chemical differentiation of the earth: the relationship between mantle, continental crust, and oceanic crust. Earth and Planetary Science Letters 90 (3), 297–314.

Iwamori, H., 1998. Transportation of h2o and melting in subduction zones. Earth and Planetary Science Letters 160, 65–80.

Johnson, M., Plank, T., 1999. Dehydration and melting experiments constrain the fate of subducted sediments. Geochemistry Geophysics Geosystems 1 (12), 1007–26.

Johnston, A., Wyllie, P., 1989. The system tonalite-peridotite-h 2 o at 30 kbar, with applications to hybridization in subduction zone magmatism. Contributions to Mineralogy and Petrology 102 (3), 257–264.

Kay, R., Mahlburg-Kay, S., 1991. Creation and destruction of lower continental crust. Geologische Rundschau 80 (2), 259–278.

Kelemen, P., 1995. Genesis of high mg# andesites and the continental crust. Contributions to Mineralogy and Petrology 120 (1), 1–19.

Kelemen, P., Hanghøj, K., Greene, A., 2003a. One view of the geochemistry of subduction-related magmatic arcs, with an emphasis on primitive andesite and lower crust. Treatise on geochemistry 3, 593–659.

Kelemen, P., Yogodzinski, G., Scholl, D., 2003b. Along-strike variation in the aleutian island arc: Genesis of high mg# andesite and implications for continental crust. Inside the Subduction Factory, Geophys. Monogr. Ser 138, 223–276.

Kemp, A., Hawkesworth, C., 2005. Generation and secular evolution of the continental crust. Treatise on Geochemistry: The crust 3, 349.

King, R., Bebout, G., Moriguti, T., Nakamura, E., 2006. Elemental mixing systematics and sr–nd isotope geochemistry of mélange formation: obstacles to identification of fluid sources to arc volcanics. Earth and Planetary Science Letters 246 (3), 288–304.

Klein, E., 2005. Oceanic crust. Treatise on Geochemistry: The Crust 3, 433.

Kushiro, I., 1974. Melting of hydrous upper mantle and possible generation of andesitic magma: an approach from synthetic systems. Earth and Planetary Science Letters 22 (4), 294–299.

Lee, C., Cheng, X., Horodyskyj, U., 2006. The development and refinement of continental arcs by primary basaltic magmatism, garnet pyroxenite accumulation, basaltic recharge and delamination: insights from the sierra nevada, california. Contributions to Mineralogy and Petrology 151 (2), 222–242.

Levander, A., Miller, M. S., 2012. Evolutionary aspects of lithosphere discontinuity structure in the western u.s. Geochemistry Geophysics Geosystems 13, doi:10.1029/2012GC004056.

Mamani, M., Wörner, G., Sempere, T., 2010. Geochemical variations in igneous rocks of the central andean orocline (13 s to 18 s): Tracing crustal thickening and magma generation through time and space. Geological Society of America Bulletin 122 (1-2), 162–182.

McCulloch, M., Wasserburg, G., 1978. Sm-nd and rb-sr chronology of continental crust formation. Science 200 (4345), 1003–1011.

Miller, N., Behn, M., 2012. Timescales for the growth of sediment diapirs in subduction zones. Geophysical Journal International.

Niida, K., Green, D., 1999. Stability and chemical composition of pargasitic amphibole in morb pyrolite under upper mantle conditions. Contributions to Mineralogy and Petrology 135 (1), 18–40.

Pankhurst, R., Weaver, S., Hervé, F., Larrondo, P., 1999. Mesozoic-cenozoic evolution of the north patagonian batholith in aysén, southern chile. Journal of the Geological Society 156 (4), 673–694.

Peacock, S., 1990. Fluid processes in subduction zones. Science 248, 329–337.

Plank, T., 2005. Constraints from thorium/lanthanum on sediment recycling at subduction zones and the evolution of the continents. Journal of Petrology 46 (5), 921–944.

Plank, T., Langmuir, C., 1998. The chemical composition of subducting sediment and its consequences for the crust and mantle. Chemical Geology 145, 325–394.

Ranalli, G., 1995. Rheology of the Earth. Springer.

Rapp, R., Shimizu, N., Norman, M., Applegate, G., 1999. Reaction between slab-derived melts and peridotite in the mantle wedge: experimental constraints at 3.8 gpa. Chemical Geology 160 (4), 335–356.

Ringwood, A., 1990. Slab-mantle interactions: 3. petrogenesis of intraplate magmas and structure of the upper mantle. Chemical Geology 82, 187–207.

Ringwood, A., Green, D., 1966. An experimental investigation of the gabbro-eclogite transformation and some geophysical implications. Tectonophysics 3 (5), 383–427.

Rogers, G., Hawkesworth, C., 1989. A geochemical traverse across the north chilean andes: evidence for crust generation from the mantle wedge. Earth and Planetary Science Letters 91 (3), 271–285.

Rudnick, R., 1995. Making continental crust. Nature 378, 571–577.

Schmeling, H., Babeyko, A., Enns, A., Faccenna, C., Funiciello, F., Gerya, T., Golabek, G., Grigull, S., Kaus, B., Morra, G., van Hunen, J., 2008. A benchmark comparison of spontaneous subduction modelstowards a free surface. Physics of the Earth and Planetary Interiors 171 (1), 198–223.

Schmidt, M., Poli, S., 1998. Experimentally based water budgets for dehydrating slabs and consequences for arc magma generation. Earth and Planetary Science Letters 163 (1), 361–379.

Scholl, D., von Huene, R., 2007. Crustal recycling at modern subduction zones applied to the pastissues of growth and preservation of continental basement crust, mantle geochemistry, and supercontinent reconstruction. Geological Society of America Memoirs 200, 9–32.

Skora, S., Blundy, J., 2010. High-pressure hydrous phase relations of radiolarian clay and implications for the involvement of subducted sediment in arc magmatism. Journal of Petrology 51 (11), 2211–2243.

Stephens, W., 1988. Granitoid plutonism in the caledonian orogen of europe. Geological Society, London, Special Publications 38 (1), 389–403.

Stern, C., 1991. Role of subduction erosion in the generation of andean magmas. Geology 19 (1), 78–81.

Sun, S., McDonough, W., 1989. Chemical and isotopic systematics of oceanic basalts: implications for mantle composition and processes. Geological Society, London, Special Publications 42 (1), 313–345.

Takagi, T., 2004. Origin of magnetite-and ilmenite-series granitic rocks in the japan arc. American Journal of Science 304 (2), 169–202.

Tamura, Y., Ishizuka, O., Stern, R., Shukuno, H., Kawabata, H., Embley, R., Hirahara, Y., Chang, Q., Kimura, J., Tatsumi, Y., et al., 2011. Two primary basalt magma types from northwest rota-1 volcano, mariana arc and its mantle diapir or mantle wedge plume. Journal of Petrology 52 (6), 1143–1183.

Tatsumi, Y., 2005. The subduction factory: How it operates in the evolving earth. GSA today 15 (7), 4.

Taylor, S., McLennan, S., 1985. The continental crust: its composition and evolution.

Turcotte, D., Schubert, G., 2002. Geodynamics. Cambridge University Press.

Ueda, K., Gerya, T., Sobolev, S., 2008. Subduction initiation by thermalchemical plumes. Physics of the Earth and Planetary Interiors 171, 296–312.

Vogt, K., Gerya, T., Castro, A., 2012. Crustal growth at active continental margins: Numerical modeling. Physics of the Earth and Planetary Interiors 192-193, 1–20.

von Huene, R., Lallemand, S., 1990. Tectonic erosion along the japan and peru convergent margins. Geological Society of America Bulletin 102 (6), 704–720.

von Huene, R., Scholl, D., 1991. Observations at convergent margins concerning sediment subduction, subduction erosion, and the growth of continental crust. Reviews of Geophysics 29 (3), 279–316.

Zhu, G., Gerya, T., Honda, S., Tackley, P., Yuen, D., 2011a. Influences of the buoyancy of partially molten rock on 3-d plume patterns and melt productivity above retreating slabs. Physics of the Earth and Planetary Interiors 185 (3), 112–121.

Zhu, G., Gerya, T., Yuen, D., 2011b. Melt evolution above a spontaneously retreating subducting slab in a three-dimensional model. Journal of Earth Science 22 (2), 137–142.

Chapter 5

From Oceanic Plateaus to Allochthonous Terranes[1]

5.1 Abstract

Large segments of the continental crust are known to have formed through the amalgamation of oceanic plateaus and continental fragments. However, mechanisms responsible for terrane accretion remain poorly understood. We have therefore analysed the interactions of oceanic plateaus with the leading edge of the continental margin using a thermomechanical-petrological model of an oceanic-continental subduction zone with spontaneously moving plates. This model includes partial melting of crustal and mantle lithologies and accounts for complex rheological behaviour, including viscous creep and plastic yielding. Our results indicate that oceanic plateaus may either be lost by subduction or accreted onto continental margins. Complete subduction of oceanic plateaus is common in models with old ($>$ 40 Myr) oceanic lithosphere whereas models with younger lithosphere often result in terrane accretion. Three distinct modes of terrane accretion were identified, depending on the rheological structure of the lower crust and oceanic cooling age: frontal plateau accretion, basal plateau accretion and underplating plateaus. Complete plateau subduction is associated with a sharp uplift of the forearc region and the formation of a basin further landward, followed by topographic relaxation. All crustal material is lost by subduction and crustal growth is solely attributed to partial melting of the mantle. Frontal plateau accretion leads to crustal thickening and the formation of thrust and fold belts, since oceanic plateaus are docked onto the continental margin. Strong deformation leads

[1]This chapter co-authored by K. Vogt and T. Gerya was published in a slightly modified version in Gondwana Research, in press.

to slab break off, which eventually terminates subduction, shortly after the collisional stage has been reached. Crustal parts that have been sheared off during detachment melt at depth and thus further modify the composition of the overlying continental crust. Basal plateau accretion scrapes oceanic plateaus off the downgoing slab, enabling the outward migration of the subduction zone. New incoming oceanic crust underthrusts the fractured terrane and forms a new subduction zone behind the accreted terrane. Subsequently, hot asthenosphere rises into the newly formed subduction zone and allows for extensive partial melting of crustal rocks, located at the slab interface, and only minor parts of the former oceanic plateau remain unmodified. Oceanic plateaus may also underplate the continental crust after being subducted to mantle depth. (U)HP terranes are formed with peak metamorphic temperatures of 400 ^oC - 700 ^oC prior to slab break off and subsequent exhumation. Rapid and coherent exhumation through the mantle along the former subduction zone at rates comparable to plate tectonic velocities is followed by somewhat slower rates at crustal levels, accompanied by crustal flow, structural reworking and syndeformational partial melting. Exhumation of these large crustal volumes leads to a sharp surface uplift.

5.2 Introduction

The oceanic crust (which covers 60 % of the Earth surface) is not homogeneous, but contains significantly thicker crust than norm. About 10 % of the present day's ocean floor is covered by anomalous thick crust typified by a high bathymetric relief, low upper crustal velocities, lack of clear magnetic lineations and steep margins (Nur and Ben-Avraham, 1982; Schubert and Sandwell, 1989). Although the origin of these oceanic rises remains controversial most of them are thought to represent extinct arcs or spreading ridges, detached continental fragments, volcanic piles or oceanic swells (Stein and Ben-Avraham, 2007, and references therein). Regardless of their origin, these oceanic features may collide with continental margins to form collisional orogens and accreted terranes in places where oceanic lithosphere is recycled back into the mantle (Taylor, 1966; Taylor and McLennan, 1985; Ben-Avraham et al., 1981; Schubert and Sandwell, 1989). Hence, it has been argued that the rapid growth of some major segments of the continental crust is related to accretionary processes by which new material is added to the continental crust (e.g. Coney et al., 1980; Jones et al., 1982; Stein and Goldstein, 1996; Dobretsov et al., 2004; Reymer and Schubert, 1986). Large areas in western North America (Jones

et al., 1977; Coney et al., 1980; Monger et al., 1982), Alaska (Jones and Silberling, 1986), and the Caribbean (Kerr et al., 1997; Kerr and Tarney, 2005) are believed to have formed through extensive accretion along its active margin. Schubert and Sandwell (1989) have estimated an upper bound to the continental crust addition rate by the accretion of all oceanic plateaus to be 3,7 km^3/yr, which over a time span of 100 Myr would account for 5 % of the total crustal volume of the continental crust. The Ontong-Java Plateau in the south-western Pacific is a present day example of an oceanic plateau that resists subduction and thus modifies subduction between the Pacific and Indian plate (Hughes and Turner, 1977; Mann and Taira, 2004).

In spite of the broad evidence that some plateaus may resist subduction to be accreted in form of collisional terranes others may be lost by subduction (Cloos, 1993), such as in the circum-Pacific where several oceanic plateaus are currently being consumed along with oceanic lithosphere (Rosenbaum and Mo, 2011). Among those are the Nazca (Pilger, 1981) and Juan Fernandez Ridges (Von Huene et al., 1997) that are presently being subducted beneath South America. Geological and geochemical observations (Hilton et al., 1992) as well as analogue (Boutelier et al., 2003; Boutelier and Chemanda, 2011) and numerical experiments (Ranalli et al., 2000; Gerya et al., 2009; van Hunen et al., 2002) have supported the idea of deep subduction of crustal material. Thus significant amounts of continental crust may be recycled back into the mantle or be incorporated into active arcs with geochemical and tectonic implications that still need to be explored (e.g. Hilton et al., 1992; Chopin, 2003; McGeary et al., 1985; Rosenbaum and Mo, 2011).

Despite its implications to crustal growth and/or loss, mechanisms responsible for terrane accretion or its deep subduction remain poorly understood. Previous analytical studies have concentrated on the buoyancy of the oceanic lithosphere and bathymetric rises (Cloos, 1993), while analogue (e.g. Boutelier et al., 2003) and early numerical studies have focused on the rheological strength of these features (Ellis et al., 1999). Ellis et al. (1999) have shown that continental fragments of low crustal strength may be deformed and folded within the subduction channel as they approach the continental margin. However, these models concentrated on the upper crustal section and did not take the sublithospheric mantle into account that will significantly affect the dynamics involved in terrane accretion. Subsequent studies have mainly focused on the consequences of plateau subduction/accretion upon the slab and overriding plate. It has been demonstrated in terms of geodynamic models, that oceanic plateaus

might alter trench behaviour leading to flat subduction, slab break off, trench advance and trench retreat (van Hunen et al., 2002; Gerya et al., 2009; Mason et al., 2010). Three dimensional numerical experiments on the influence of a buoyant oceanic plateau on subduction zones show that oceanic plateaus may spread laterally along the trench during collision, if the plateau itself has a sufficiently low density (Mason et al., 2010). Most recently, Tetreault and Buiter (2012) have presented a detailed numerical study on accretion of various crustal units. Their study emphasizes that lithospheric buoyancy alone does not prevent subduction during constant convergence and that a weak detachment layer is necessary in order to accrete crustal units onto the overriding plate. The depth of this detachment layer controls the amount of accreted crust and may lead to crustal underplating or collisional accretion. However, this recent study has prescribed a constant subduction velocity and has moreover neglected slab dehydration and melting processes. According to recent results on subduction zones of Sizova et al. (2012), a prescribed convergence velocity and the neglect of fluid- and melt-related weakening effects may inhibit the development of several important collisional processes, such as slab breakoff, vertical crustal extrusion, large scale stacking, shallow crustal delamination and relamination, and eduction of the continental plate. Geodynamic models of collisional orogens that have employed spontaneously moving plates demonstrate that crustal delamination and accretion processes are critically controlled by the rheology of the lower crust and age of the subducting slab (Duretz et al., 2011, 2012; Sizova et al., 2012; Ueda et al., 2012). The later parameter has not yet been explored in relation to terrane accretion processes.

In this present work we aim to extend previous terrane accretion models and explore geodynamic regimes with implications to magmatic activity using spontaneously moving plates. We have undertaken a detailed study of 2-D petrological-thermomechanical numerical experiments to (i) characterise the variability of accretion processes, and (ii) investigate the possible effects of melting of subducted crustal units upon magmatic addition rates associated with the terrane accretion. Our parametric study is primary focussed on influences of two major parameters which control crustal accretion in collisional zones: (1) the age of the subducting oceanic plate and (2) the rheology of the lower crust.

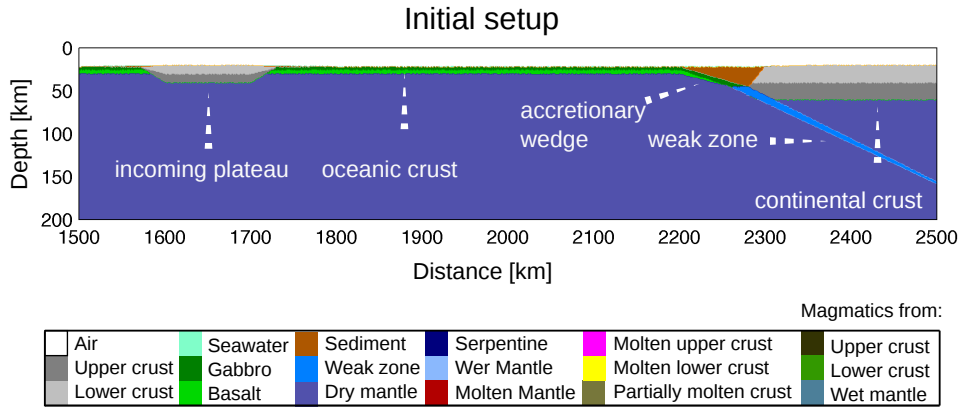

Figure 5.1: Initial setup of the numerical model. Staggered grid resolution is 1361 × 351 nodal points, with more than 10 million randomly distributed markers. The grid resolution is 1 × 1 km in the subduction zone area (1500 - 2500 km) and 10 × 10 km outside of this area. Colours indicate materials (i.e. rock type or melt), which appear in subsequent figures. For rheologies used in the experiments see Table 5.1

5.3 Model Setup

The numerical model simulates forced subduction of an oceanic plate beneath a continental margin on a lithospheric to upper mantle cross-section (4000 km by 1400 km; Figure 5.1). The rectangular grid with 1361 × 351 nodal points is non-uniform and contains a (1000 km wide) high resolution area of 1 km × 1 km in the centre of the domain. The rest of the model remains at a lower resolution (10 × 10 km).

The oceanic crust contains a felsic plateau that moves with the oceanic lithosphere as it migrates towards a fixed continent, fated to collide with the continental margin. The oceanic crust is composed of 2 km of hydrothermally altered basalt, underlain by 5 km of gabbroic rocks that cover 2500 km horizontally. The continental crust is felsic and has a total thickness of 30 km, composed of 15 km upper and 15 km lower crust that extend over 1500 km. The total thickness of the continental crust corresponds to extended continental crust of Western Europe and Western North America and was adopted according to Christensen and Mooney (1995). Since the composition and thickness of oceanic plateaus is not known in detail we have chosen a simplified description and assume the crustal structure to be similar to continental crust (felsic on average). Schubert and Sandwell (1989) have calculated the average crustal thickness of oceanic and continental plateaus, to vary between $\sim$ 10 - 20 km based on global topographic

data analysis. Sandwell and MacKenzie (1989), on the other hand, estimated that continental plateaus with a relief greater than 4.2 km have roots that extend to 25 - 35 km depths, while oceanic plateaus have a lower relief and thus shallower roots (15 - 25 km). For the sake of simplicity, we have chosen a total crustal thickness of 20 km, subdivided into upper and lower crust of 10 km each, which cover 100 km horizontally. Both the asthenosphere and the upper mantle are composed of anhydrous peridotite and are defined by the temperature profile. The rheological parameters used in the experiments are summarized in 5.1. All mechanical boundary conditions are free slip only the lower boundary is permeable satisfying an external free slip boundary condition (Gorczyk et al., 2007; Ueda et al., 2008). To allow for topographic build up of the lithosphere, the top surface of the lithosphere is treated as an internal free surface (Schmeling et al., 2008) by using a top layer (of 20 - 22 km thickness) with low viscosity (10^{18} Pas) and low density (1 kg/m^3 for air, 1000 kg/m^3 for sea water). The initial temperature field of the oceanic plate is defined by its oceanic geotherm (Turcotte and Schubert, 2002) for a specific lithospheric cooling age that was varied from 20 Myr to 80 Myr. Embedded into oceanic crust, the oceanic plateau is assumed to have the same thermal structure as the oceanic lithosphere. The initial temperature field of the continental plate increases linearly from 0 ^oC at the surface to 1344 ^oC at the lithosphere asthenosphere boundary (at 140 km depth). For the asthenospheric mantle ($>$ 140 km) an initial adiabatic like thermal gradient of 0.5 $^oC/km$ is used. An internally prescribed velocity field within the convergence condition region enables spontaneous slab bending of the oceanic crust. During the first 6 Myr the oceanic plate is pushed toward a fixed continental plate with a constant velocity, reproducing an active continental margin. After 6 Myr of forced subduction, subduction and subsequent collision are only driven by the slab pull. A rheologically weak shear zone at the bottom of the oceanic-continental suture zone prescribes initialization of subduction. A detailed description of the governing equations and the numerical procedure employed in this study is given in Chapter 2. The rheological parameters used in this study are summarized in Table 5.1.

Material	Flow law	$1/A_D$ $[Pa^n s]$	n	E_a $[J]$	V_a $[J/bar]$	$sin(\phi)$	c $[Pa]$
Sediment	wet qtz	1.97×10^{17}	2.3	154×10^3	0.8	0.15	1×10^6
Upper crust	wet qtz	1.97×10^{17}	2.3	154×10^3	1.2	0.15	1×10^6
Lower crust (a)	wet qtz	1.97×10^{17}	2.3	154×10^3	0.8	0.15	1×10^6
Lower crust (b)	plag (An75)	4.80×10^{22}	3.2	238×10^3	1.2	0.15	1×10^6
Basalt	wet qtz	1.97×10^{17}	2.3	154×10^3	1.2	0.10	1×10^6
Gabbro	plag (An75)	4.80×10^{22}	3.2	238×10^3	0.8	0.60	1×10^6
Dry mantle	dry ol	3.98×10^{16}	3.5	532×10^3	0.8	0.60	1×10^6
Wet mantle	wet ol	5.01×10^{20}	4.0	470×10^3	0.8	0.60	1×10^6
Shear zone	wet ol	5.01×10^{20}	4.0	470×10^3	0.8	0.00	1×10^6
Serp. mantle	wet ol	5.01×10^{20}	4.0	470×10^3	0.8	0.00	1×10^6
Magmatics (all)	wet qtz	1.97×10^{17}	2.3	154×10^3	0.8	0.15	1×10^6

Table 5.1: Rheological parameters used in this study: wet qtz = wet quarzite, plag (An75) = anorthite 75 %, wet ol = wet olivine, dry ol = dry olivine after (Ranalli, 1995, and references therein). A_D is the pre-exponential factor, n, is the stress exponent, E_a is the activation energy, V_a is the activation volume, ϕ is the friction angle, and c is the cohesion. Parameters used for Peierls mechanism are $A_{peierls}$=107.8×10^{-12}, $\sigma_{peierls} = 2.9$ $[GPa]$ for wet olivine rheology (Katayama and Karato, 2008), and $\sigma_{peierls} = 9.1$ $[GPa]$ for dry olivine rheology (Evans and Goetze, 1979).

5.4 Results

Mechanisms responsible for terrane accretion or its deep subduction have been studied in detail, by varying the cooling age of the downgoing slab (20 Myr, 40 Myr, 60 Myr, 80 Myr) and the rheological structure, of the incoming terrane and overriding plate (Table 5.1). Our results indicate that oceanic plateaus associated with the subduction of old (> 40 Myr) and hence dense oceanic lithosphere, are likely to be lost by subduction. In contrast, oceanic plateaus embedded in young oceanic lithosphere ($\leq$ 40 Myr) are less prone to subduction and may accrete onto continental crust by either (i) frontal or (ii) basal accretion or else may (iii) underplate the continental crust. The results of this study are displayed in Figure 5.2.

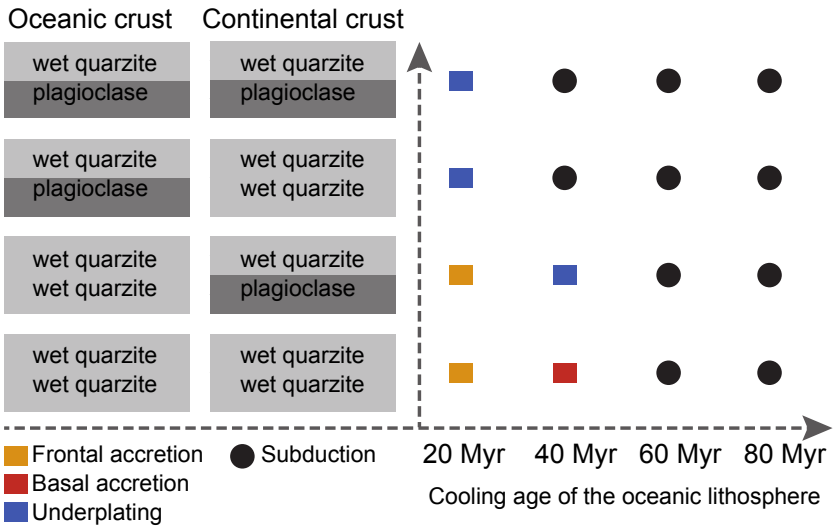

Figure 5.2: Parameter space showing the explored range of cooling ages of the oceanic lithosphere and crustal rheologies of the oceanic plateau and continental crust. Wet quartzite and Plagioclase rheologies are used consistent with experimentally determined flow laws (Ranalli, 1995). Four distinct endmembers are classified: (i) subduction, (ii) frontal plateau accretion (iii) basal plateau accretion and (iv) underplating plateaus.

Complete plateau subduction

Terrane subduction is likely to occur where old (> 40 Myr) oceanic lithosphere is consumed, but oceanic plateaus that have a strong lower crust (plagioclase) will also subduct if embedded in moderately old crust (40 Myr) (Figure 5.2).

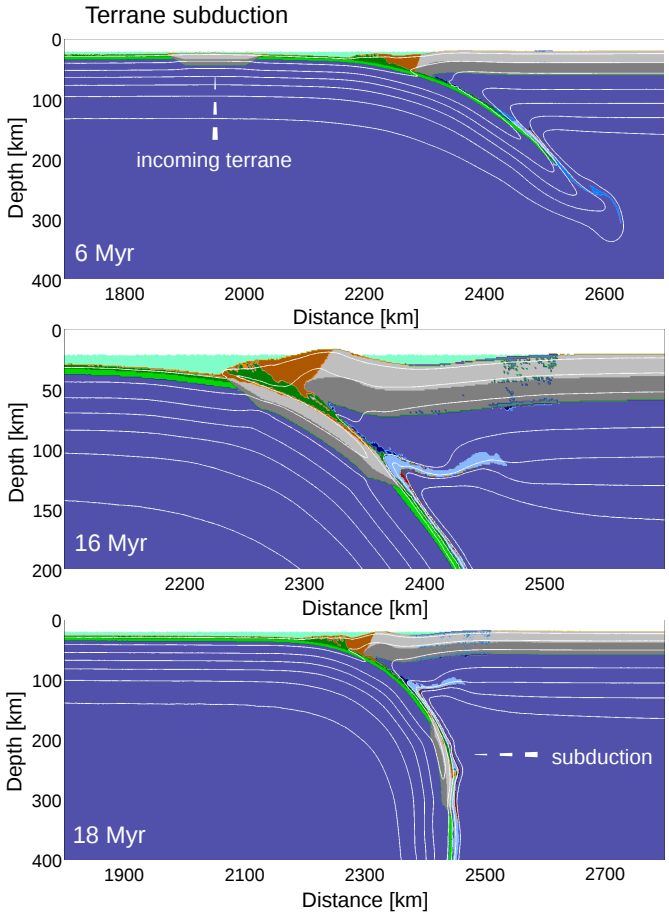

Figure 5.3: Tectonic evolution of subducting plateaus (slab age: 40 Myr; lower crust rheology: oceanic plateau: plagioclase, continental crust: plagioclase). Subduction of oceanic plateaus results in a temporary uplift of the forearc and subsidence further landward, followed by topographic relaxation. Water released from the downgoing slab lowers the melting temperature of the overlying mantle and allows for partial melting of the mantle.

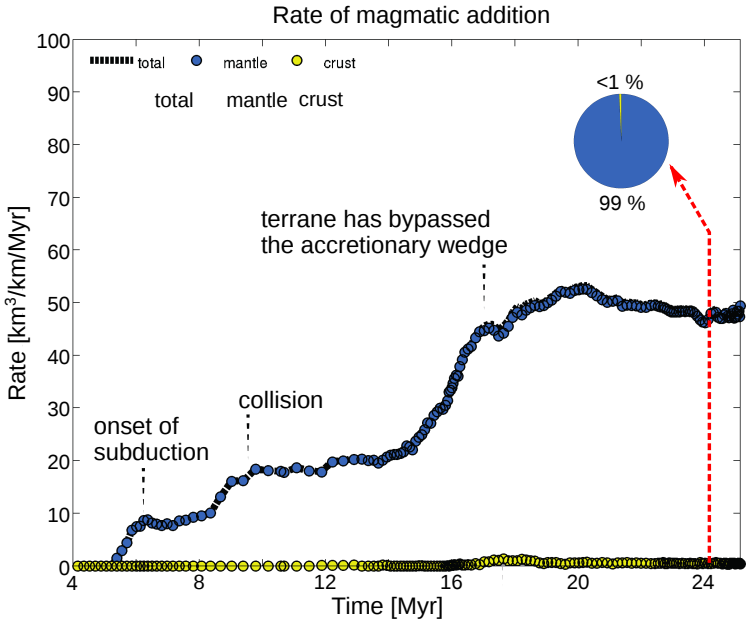

Figure 5.4: Magmatic addition rates in relation to plateau subduction. The inset pie chart illustrates the magmatic composition (crustal (yellow) versus mantle (blue) components) at the time marked by the red dashed line. In the course of collision magmatic addition rates increase from 10 - 20 $km^3/km/Myr$ to typical values of 50 - 60 $km^3/km/Myr$. Water released from the subducting plate lowers the melting temperature of the overlying mantle and crustal growth is solely attributed to partial melting of the mantle.

Shortly after subduction initiation (> 5 Myr), prior to collision, water is released from the downgoing slab due to compaction or mineral dehydration reactions. Fluids percolating from the subducting slab into the overlying mantle may form a serpentinized channel at shallow slab interfaces (<130 km) or generate subsolidus metasomatism at greater depth (Figure 5.3). Where such fluids encounter the wet mantle solidus they induce partial melting, which enables basaltic melt production. In areas where the extent of melting is sufficient to allow for extraction, melts are emplaced at crustal levels forming extrusive volcanics and intrusive plutons. Discrete addition of magmatic products (Figure 5.4) leads to gradual growth of the magmatic crust (20 – 30 $km^3/km/Myr$: see Vogt et al. (2012) for discussion).

The depth at which such igneous bodies accumulate varies between lower and mid crustal levels, according to the rheological structure of the

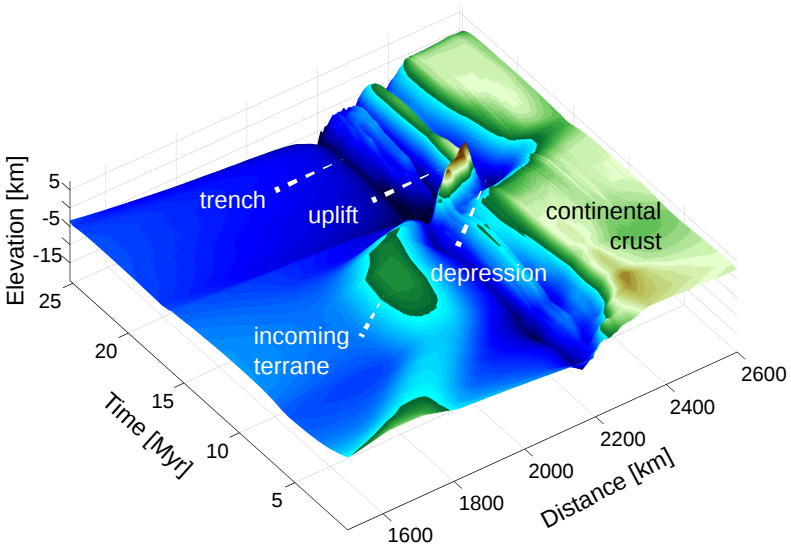

Figure 5.5: Topographic response to terrane subduction. The most dominant tectonic response to the subduction of oceanic plateaus is a sharp uplift of the forearc region and the formation of a basin further landward. Once the oceanic plateau has bypassed the accretionary wedge the topography becomes smoother.

overriding plate. Arrival of anomalously thick oceanic crust at the subduction zone enhances the magmatic productivity (50 - 60 $km^3/km/Myr$), but has no effect on the composition of newly formed crust (Figure 5.4). The continental crust grows simply by the addition of basaltic material, derived from partially molten mantle.

Nevertheless, subduction of high bathymetric reliefs becomes all the more evident in the tectonic response of the overriding plate. While the oceanic plateau is dragged down into the subduction zone, material of the forearc is uplifted and pushed towards the continent to form a thickened topographic high (Figure 5.3 and Figure 5.5). The slab dip steepens significantly and the upper plate is exposed to strong deformation. Localized shear zones of intense plastic deformation are formed that cut through the basement rocks of the overriding plate (Figure 5.6a). Driven by the rapid uplift, farther landward the surface subsides and forms a shallow topographic depression or basin (Figure 5.5a). Subsequently, the oceanic plateau bypasses the overriding plate and sinks into the deep mantle. While the topography becomes smoother with time, localized shear zones remain

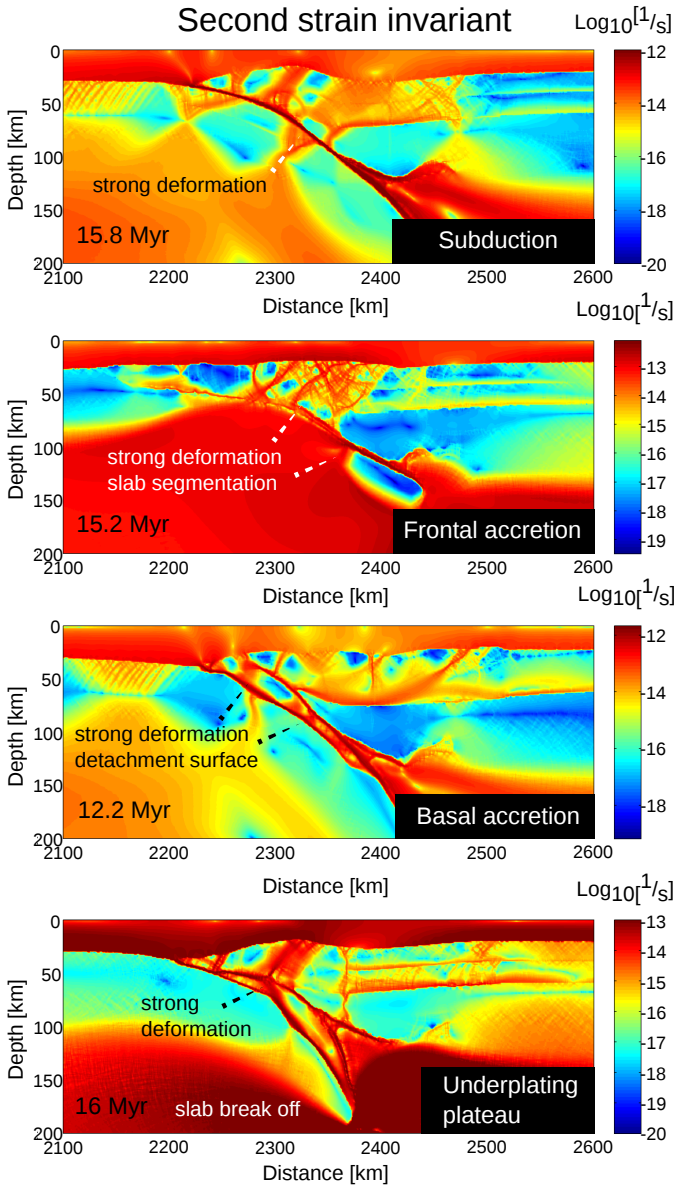

Figure 5.6: Second strain rate invariant ($Log_{10}[1/s]$). a) Plateau subduction b) Frontal plateau accretion c) Basal plateau accretion and d) Underplating plateaus. Collision of oceanic plateaus with the leading edge of the continental margin leads to strong deformation. Localized shear zones are formed, which may cut through the basement rocks of the upper plate. (b,d) Enhanced plastic failure of the downgoing slab leads to break off.

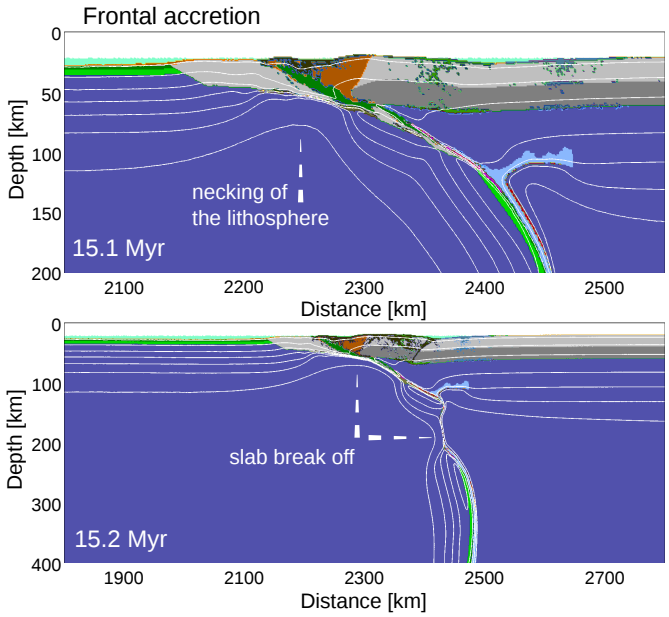

Figure 5.7: Tectonic evolution during frontal plateau accretion (slab age: 20 Myr; lower crust rheology: oceanic plateau: wet quartzite, continental crust: plagioclase). In the course of collision, crustal material is docked onto the continental margin, with minor crustal loss. Rocks that have bypassed the accretionary wedge melt at depth. Shortly after the collisional stage has been reached, strong deformation leads to slab break off and terminates subduction. Hot inflow of asthenospheric material leads to partial melting of crustal lithologies.

visible and may be reactivated during future events.

Frontal plateau accretion

Subduction of young oceanic lithosphere (20 Myr) results in frontal plateau accretion if the oceanic plateau contains a weak lower crust (wet quartzite) (Figure 5.2).

Collision of the oceanic plateau with the leading edge of the continental margin causes strong deformation in the overriding plate and even more so in the downgoing slab (Figure 5.6b). Soon after the collisional stage is reached (1 - 2 Myr), highly localized fracture zones are formed that trigger tear propagation along the slab-plateau interface followed by segmentation of the downgoing slab, which eventually leads to slab break off and terminates subduction (Figure 5.7). The depth at which the oceanic plateau

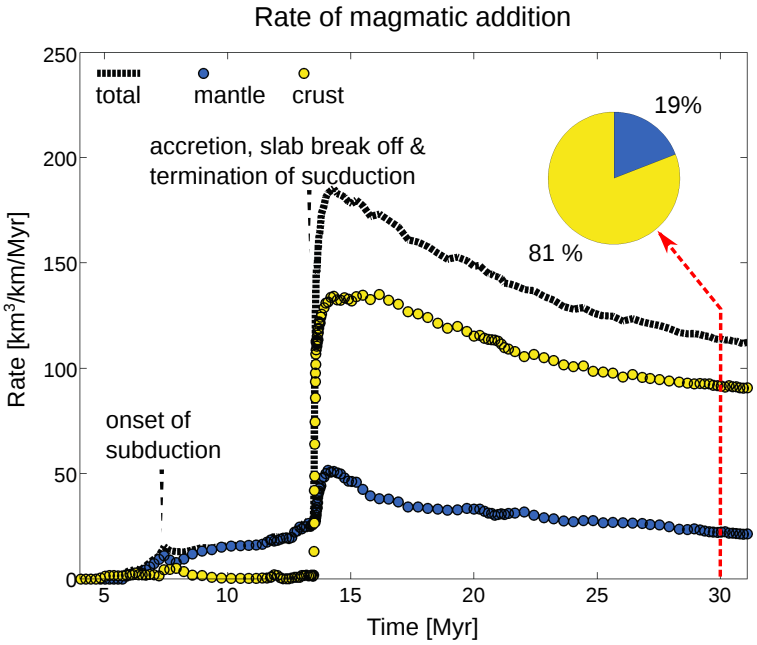

Figure 5.8: Rates of magmatic addition during frontal accretion. Magmatic addition rates rise from 20 - 30 $km^3/km/Myr$ to 200 $km^3/km/Myr$ in the course of collision and subsequent accretion. Asthenospheric inflow of hot material to subcrustal levels leads to partial melting of mainly crustal components with minor contribution of the hydrated mantle.The inset pie chart illustrates the magmatic composition (crustal (yellow) versus mantle (blue) components) at the time marked by the red dashed line

detaches from the downgoing slab may be as shallow as 40 km. While most of the former oceanic plateau is accreted horizontally, minor parts are sheared off and pulled down into the mantle. Following slab detachment, asthenospheric inflow of hot material to subcrustal levels leads to partial melting of mainly crustal components with minor contribution of the hydrated mantle (Figure 5.8). Where such melts exceed the melt extraction threshold they rise to the surface or emplace in predefined fracture zones that have evolved since the onset of collision (Figure 5.7). Melt emplacement weakens the continental lithosphere (according to the adopted pressure factor: $\lambda_{melt} = 0.1$), which in some cases may lead to extension and subsequent decompression melting of dry peridotite.

Tectonic responses to the collision of the oceanic plateau with the continental margin (Figure 5.9) include a slight uplift of the forearc region followed by transpression and transtension in the course of collision. Other characteristics include crustal thickening and the formation of thrust and

fold belts in the back.

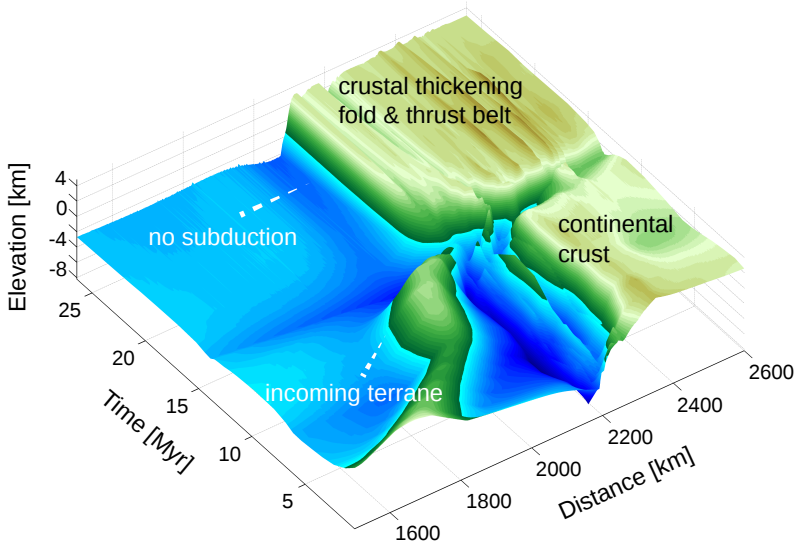

Figure 5.9: Topographic response to frontal plateau accretion. Frontal plateau accretion leads to crustal thickening and the formation of fold and thrust belts in the back-arc region. Subduction ceases, following slab break off.

Basal plateau accretion

Subduction of oceanic lithosphere of moderate age (40 Myr) leads to basal accretion if both the incoming oceanic plateau and the continental crust have a weak lower crust (wet quartzite) (Figure 5.2).

As the incoming plateau approaches the subduction zone it is for the most part scraped of the downgoing plate. Smaller crustal units can bypass the accretionary wedge and be lost by subduction (Figure 5.10). Large stresses that operate during collision lead to strong deformation in the overriding plate and downgoing slab, enabling slab segmentation and slab break off (Figure 5.6). In contrast to frontal accretion, slab break off occurs at somewhat greater depth ($\sim$ 60 km) and does not cease subduction, but allows for the outward migration of the subduction zone (Figure 5.10). New incoming oceanic crust underthrusts the fractured terrane and forms a new subduction zone behind the accreted terrane. Following slab break off, hot asthenosphere rises into the newly formed subduction zone and leads

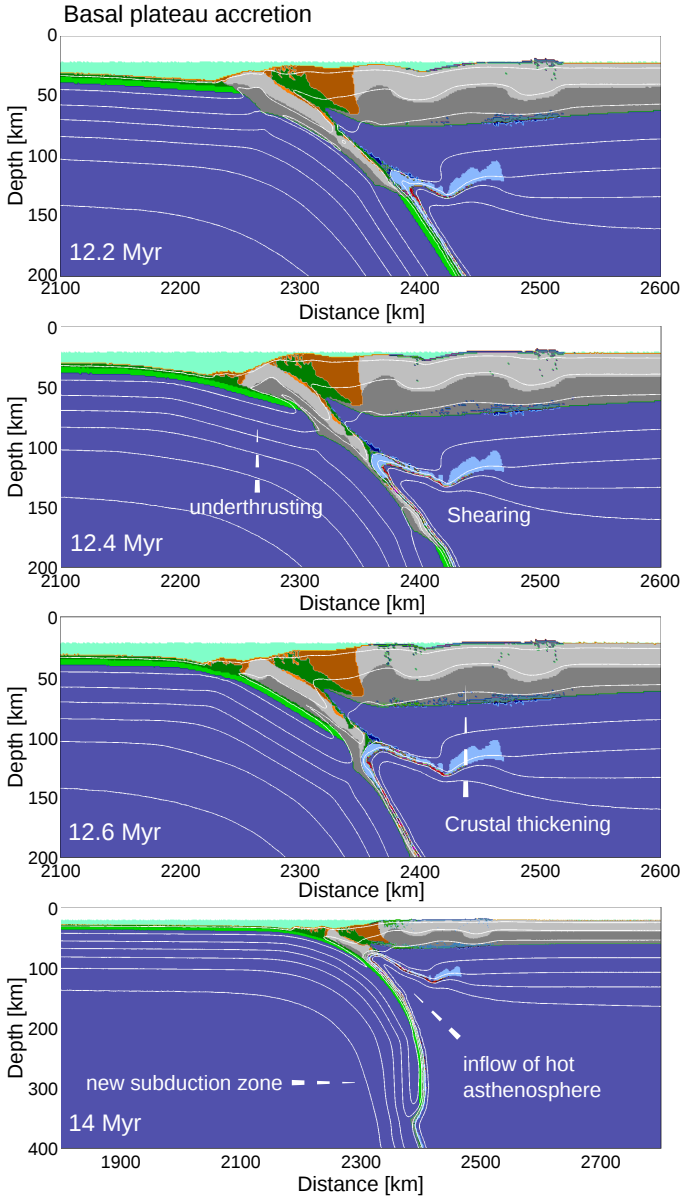

Figure 5.10: Tectonic evolution during basal plateau accretion (slab age: 40 Myr; lower crust rheology: oceanic plateau: wet quartzite, continental crust: wet quartzite). Crustal material of the oceanic plateau is scraped off the downgoing slab and accreted onto the continental margin. Strong deformation leads to slab detachment and the outward migration of the subduction zone. Oceanic crust underthrusts the accreted terrane and forms a new subduction zone (subduction zone jump). Hot asthenosphere rises into the newly formed subduction zone and leads to extensive partial melting of crustal rocks.

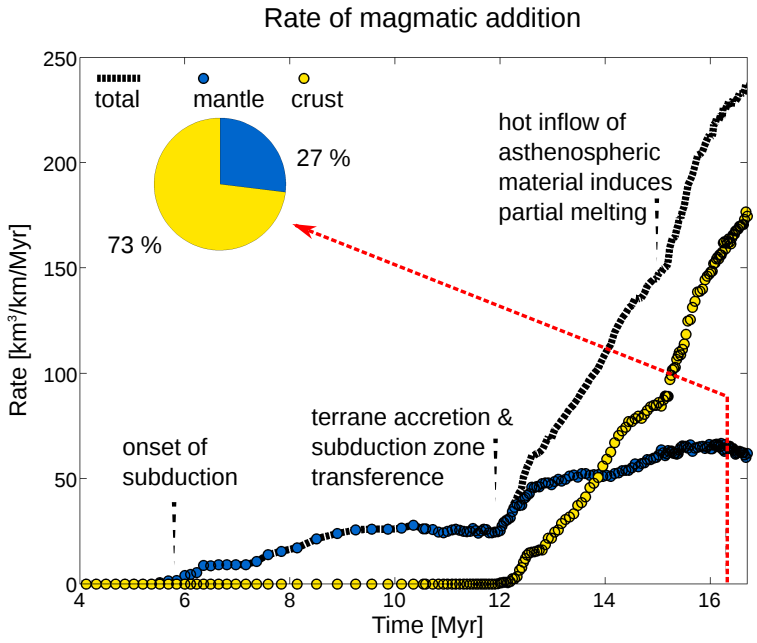

Figure 5.11: Rates of magmatic addition during basal accretion. Magmatic addition rates increase in the course of collision from 20 - 30 $km^3/km/Myr$ to 150 $km^3/km/Myr$ and partial melting of crustal lithologies becomes predominant. The outward migration of the subduction zone at 15 Myr is clearly marked in the magmatic record. The inset pie chart illustrates the magmatic composition (crustal (yellow) versus mantle (blue) components) at the time marked by the red dashed line.

to extensive partial melting of large parts of the former oceanic plateau (Figure 5.11).

Rocks that have remained unmodified are exposed to sedimentation and are fully incorporated into the accretionary wedge.

The topographic response includes crustal thickening and the formation of thrust and fold belts, similar to frontal accretion (Figure 5.12).

Underplating terranes

Underplating plateaus are associated with a strong lower crust (plagioclase) and young oceanic lithosphere (20 Myr). Subduction of slightly older crust (40 Myr) requires oceanic plateaus to have a weak lower crust (wet quartzite) and continental crust to have a strong lower crust (plagioclase) in order to form underpalting plateaus (Figure 5.2).

In the course of subduction the oceanic plateau is dragged down to sub-

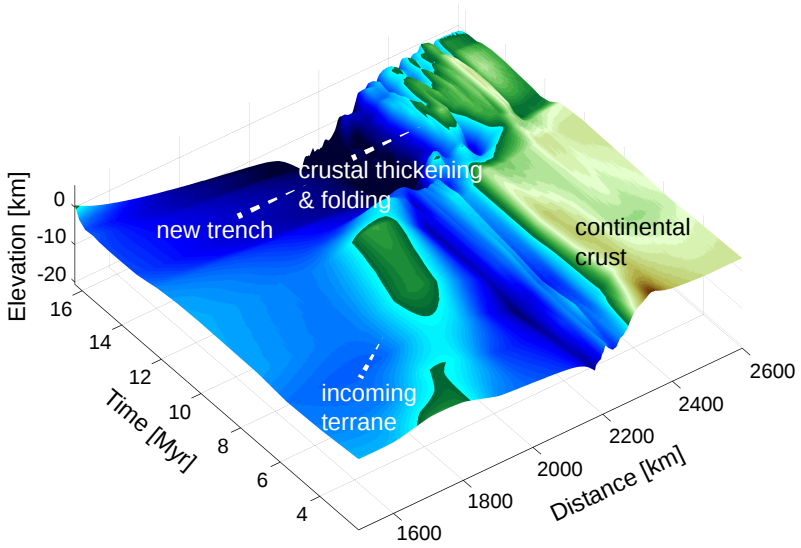

Figure 5.12: Topographic response to basal plateau accretion. Collision of oceanic plateaus with the continental crust leads to crustal thickening and folding of the upper plate. Subduction does not cease, but continues behind the accreted terrane, forming a new subduction zone (subduction zone jump).

lithospheric depths (to up to 160 km depth), where it remains for 1 - 2 Myr (Figure 5.13). Large stresses that operate during collision, lead to strong deformation along the plateau-slab interface (Figure 5.6). This leads to slab break off and subsequent slab eduction along the former subduction zone. In places where the oceanic plateau has encountered greater depth slab eduction is accompanied by the buoyant rise of crustal rocks (from the oceanic plateau) that are less dense than the surrounding mantle (Figure 5.13). While some of these crustal rocks are brought back to the surface or mid crustal levels, others melt during the inflow of hot asthenosphere and only minor parts of the former oceanic plateau are lost to the mantle. The pressure - temperature pathways of rocks that have been traced during collision and subsequent exhumation clearly mark the onset of slab break off by the rapid, nearly isothermal decrease in pressure (Figure 5.14a). Rocks that have been exhumed from mantle depth to subcrustal levels reveal elevated exhumation rates on the order of 6 - 9 cm/yr, followed by somewhat slower rates 0.08 - 0.22 cm/yr that mark the final emplacement at mid to upper crustal levels (Figure 5.14b). Although some of these rocks remain

unmodified, others get incorporated into crustal melting zones and form migmatites or partial melts with complex thermal histories and diverse cooling rates (10 - 173 $^oC/Myr$; Figure 5.14c). Magmatic addition rates (200 $km^3/km/Myr$) are for the most part related to partial melting of crustal components rather than to partial melting of the mantle (Figure 5.15).

The topographic evolution is at first similar to that of subducting plateaus and is characterized by a sharp uplift of the forearc region and the formation of a depression further landward. However, following slab break off, exhumation leads to strong surface uplift rather than topographic relaxation (Figure 5.16).

5.5 Discussion

Mode of collision - subduction versus accretion

The negative buoyancy of the downgoing plate is one of the major driving forces in plate tectonics (e.g. Forsyth and Uyeda, 1975). Its magnitude is strongly dependent on the thermal structure of the oceanic lithosphere and increases with time as the lithosphere cools down (Oxburgh and Parmentier, 1977). Old, dense lithosphere readily sinks, while young, buoyant lithosphere may resist subduction (Stern, 2002). While normal oceanic crust is invariably subductable, anomalously thick crust may form collisional orogens and cease subduction, if sufficiently buoyant material is introduced into the subduction zone.

Our results indicate that the mode of accretion is a strong function of the oceanic plate age, which controls both, the negative buoyancy of the plate (and hence the slab pull) and the rheological strength of the oceanic plateau (and therefore the possibility of its separation from the subducting plate). According to the thermodynamic database used in this study (Chapter 2), an increase in the lithospheric cooling age from 20 Myr to 80 Myr results in an average slab density increase of up to 60 kg/m^3. This strongly enhances slab pull and thus the possibility for plateau subduction. On the other hand, the rheological strength of rocks decreases exponentially with increasing temperature. Crustal rocks embedded in young and hot oceanic lithosphere have therefore a significantly lower strength compared to rocks embedded in old and cold oceanic lithosphere. Delamination and accretion of oceanic plateaus is therefore favoured for young oceanic plates. Figure 5.17 shows the effective crustal strength of the oceanic plateau and underlying mantle for different crustal rheologies and

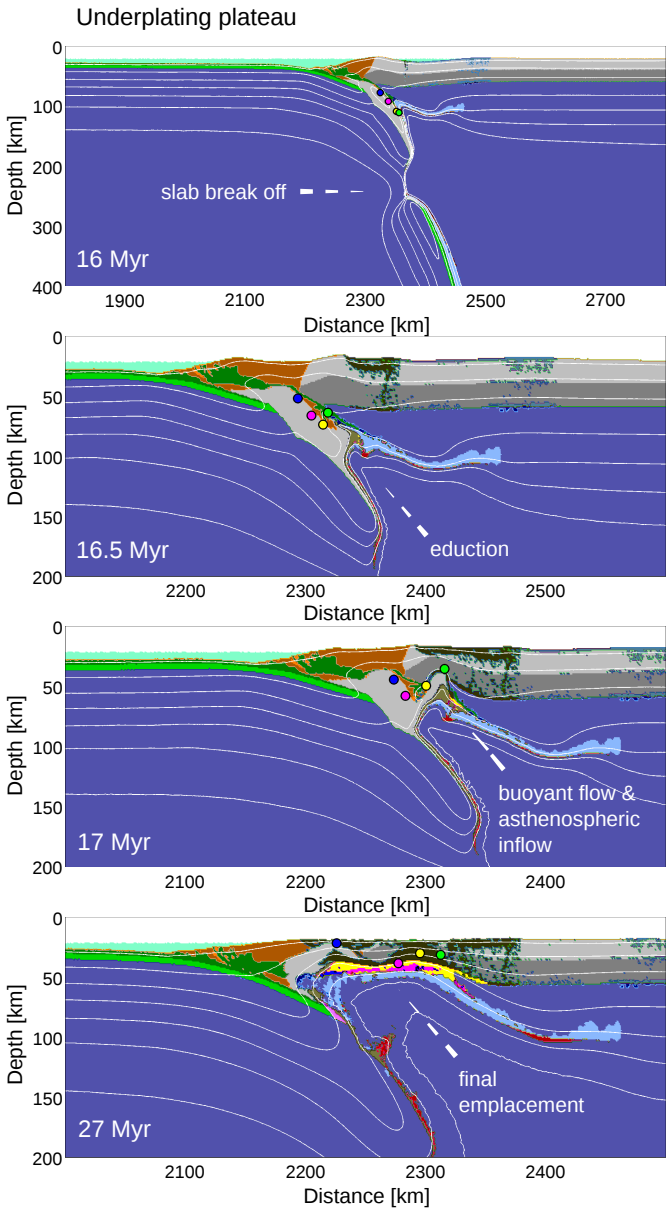

Figure 5.13: Tectonic evolution of underplating plateaus (slab age: 40 Myr; lower crust rheology: oceanic plateau: wet quartzite, continental crust: plagioclase). The oceanic plateau is fully subducted prior to slab break off and subsequent exhumation. The coherent eduction along the former subduction zone is accompanied by buoyant flow of crustal rocks of the former oceanic plateau. Some of these rocks are brought back to the surface (blue coloured dot), while others accumulate at mid-crustal levels (yellow, pink and green coloured dots). The pressure temperature paths, exhumation and cooling rates of these rocks (marked by the coloured dots) are displayed in Figure 5.14

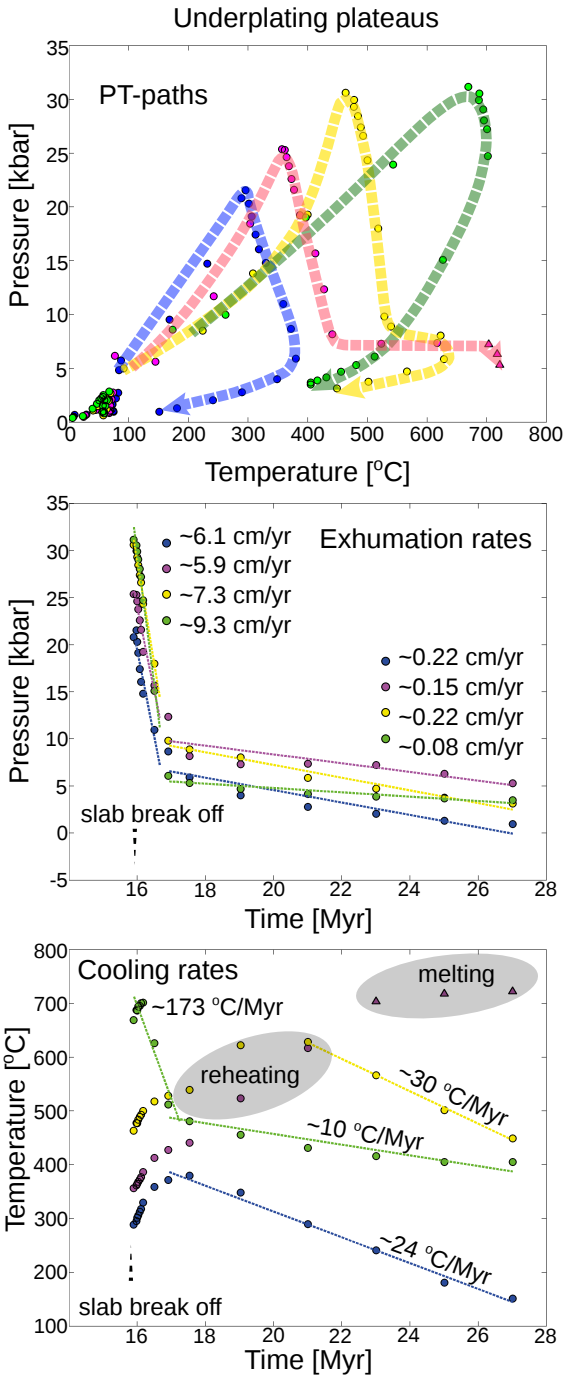

Figure 5.14: Pressure - temperature paths, exhumation and cooling rates of crustal rocks of the underplating plateau shown in Figure 5.13. a) Pressure-Temperature paths of rocks that have been traced during the simulation. Peak metamorphic conditions of 20 - 30 kbar and 300 - 700 ^oC are reached prior to slab break off and subsequent exhumation. Exhumation to subcrustal levels occurs at nearly isothermal conditions. b) Exhumation rates of crustal rocks. Rapid exhumation through the mantle at speeds (6 - 9 cm/yr) comparable to plate tectonic velocities, is followed by slower exhumation at crustal levels (0.08 - 0.22 cm/yr) showing a two stage history of exhumation. c) Cooling rates of exhumed crustal rocks vary in detail according to their thermal history. Rocks that have experienced UHP metamorphism reveal a two-stage history of cooling with rapid cooling followed by significantly slower cooling rates (green coloured dot). Other rocks melt (pink coloured dot) or merge (yellow coloured dot) with magma at mid-crustal levels, which modifies their thermal history. Nevertheless, some rocks reveal a simple cooling history with moderate cooling rates (blue coloured dot).

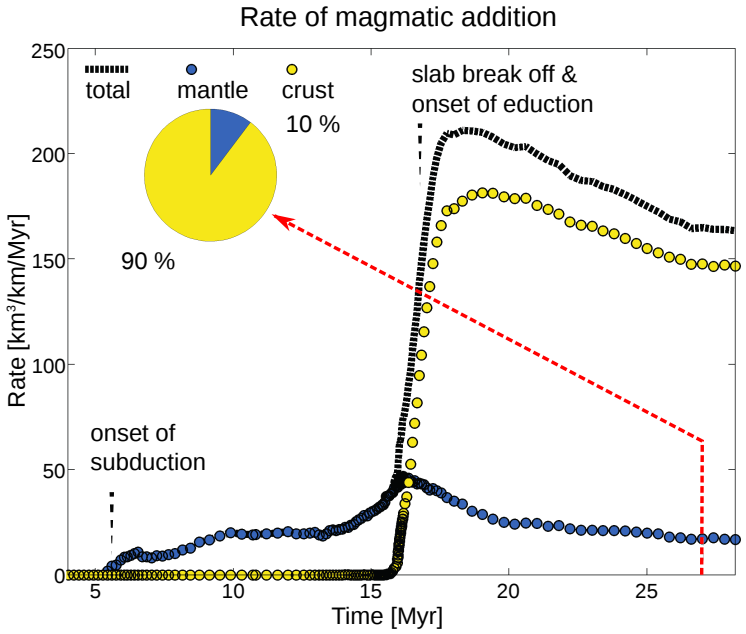

Figure 5.15: Rates of magmatic addition in relation to underplating plateaus. Magmatic addition rates increase from 20 - 30 $km^3/km/Myr$ to more than 200 $km^3/km/Myr$ following accretion. Large parts of the former oceanic plateau melt at depth and partial melting of crustal lithologies outweighs basaltic melt production from partially molten mantle.The inset pie chart illustrates the magmatic composition (crustal (yellow) versus mantle (blue) components) at the time marked by the red dashed line.

slab ages.

Consequently, the general tendency is that oceanic plateaus embedded in old oceanic lithosphere readily sink into the mantle, while oceanic plateaus surrounded by younger oceanic lithosphere may accrete onto the continental crust.

According to our models frontal accretion (Figure 5.7), by which most of the oceanic plateau is accreted laterally to the continental margin without significant crustal loss might be a rare scenario that involves subduction of very young lithosphere ($\leq$ 20 Myr). Basal accretion (Figure 5.10) on the other hand involves detachment of crustal material along the lower surface of the oceanic plateau, whereby some of the material is lost by subduction. This requires a weak lower crust. Based on geological observation of the Caribbean Colombian igneous provinces, Kerr et al. (1997) have postulated that accretion of oceanic plateaus may occur along two detachment

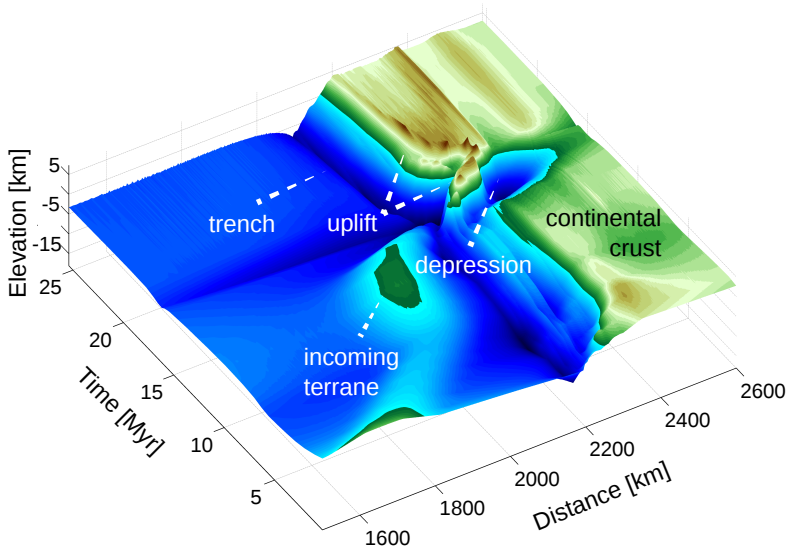

Figure 5.16: Topographic response to underplating plateaus. Tectonic responses to the accretion of underplating plateaus include a sharp uplift of the forearc region and the formation of a depression further landward. Following slab break off, crustal material that underplates the continental crust leads to strong surface uplift.

layers, hydrothermally altered rocks of the upper crust and weak rocks at the base of the Moho. Hydrothermal circulation may form a rheologically weak zone of altered rocks that is underlain by fresh basement rocks, while temperature dependent weakening affects the base of the crust. Similarly, Schubert and Sandwell (1989) have suggested that in places where the crustal thickness exceeds about 15 km, a low viscosity, ductile layer develops above the crust mantle boundary that acts as a weakness for detaching the crust from the mantle. A recent numerical study on subduction, accretion and collision of various crustal units has revealed that a weak ductile layer is of great importance for the ability of an island arc, oceanic plateau or continental fragment to accrete onto continental crust (Tetreault and Buiter, 2012). The depth of this detachment layer crucially controls the amount of accreted crust (Tetreault and Buiter, 2012).

Underplating plateaus (Figure 5.13), on the other hand, continue to subduct as long as the surrounding slab remains denser than the mantle. Deep crustal burial to depth of about 100 - 160 km precedes slab detachment and subsequent exhumation to crustal levels. Natural examples of

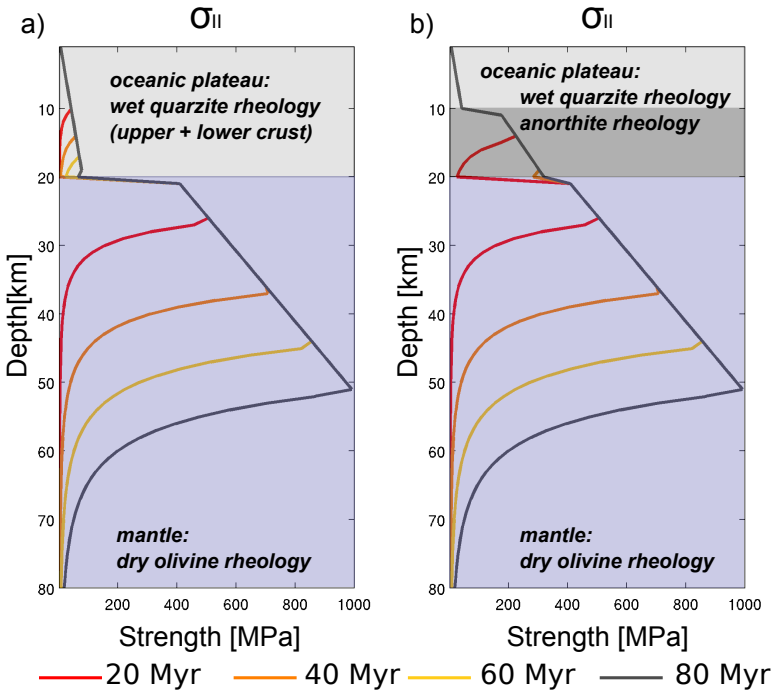

Figure 5.17: Strength profile of the oceanic plateau and underlying (lithospheric) mantle as a function of the oceanic cooling age (20 Myr, 40 Myr, 60 Myr, 80 Myr, after (Turcotte and Schubert, 2002) for a constant strain rate $\dot{\epsilon} = 1 \times 10^{-14}$ $[1/s]$. The ductile strength of the oceanic plateau and underlying mantle increases with increasing cooling age. a) A wet quartzite rheology has been applied to the upper and lower crust of the oceanic plateau. The rheology of the underlying mantle is dry olivine. b) A wet quartzite rheology has been applied to the upper and a plagioclase rheology to the lower crust of the oceanic plateau. The rheology of underlying mantle is dry olivine. For details on the rheological parameters see Table 5.1.

currently underplating plateaus may be found in the forearc region below the North-Western US (Trehu et al., 1994; Gao et al., 2011) and the Bering Sea shelf (McGeary and Ben-Avraham, 1981).

In contrast, oceanic plateaus surrounded by older crust (> 40 Myr) are likely to be lost by subduction (Figure 5.2). Buoyancy analysis, based on the contrasts in lithospheric bulk density of 80 Myr old lithosphere have indicated that only bodies of continental and intra-oceanic arc crust greater than 15 km thick may cause collisional orogens and that oceanic plateaus must have crust greater than 30 km thick to have a similar effect (Cloos, 1993), which is in agreement with our experiments. Mann and Taira (2004) have compiled 11 examples of oceanic plateaus and hotspot tracks presently subducting at the circum-Pacific or circum Caribbean plate boundaries. They have concluded that only one, namely the Ontong Java Plateau is being actively accreting, while the remaining 10 examples are subducting without any significant accretion of the uppermost crust.

One of the main conclusions of our study is that oceanic plateaus embedded in old and cool oceanic lithosphere (> 40 Myr) will be lost by subduction. However, it is difficult to compare these results with natural geological settings, since accreted terranes have distinct, but diverse stratigraphies and complex tectonic histories that in some cases may involve large scale displacement (e.g. Jones et al., 1977). Also, it is evident that increasing the size of the terrane itself or lowering its strength will lead to accretion, even though the terrane is surrounded by older crust. Fluid entry into the base of the imbricating plateau is known to form pegmatites or hydrous melt (Kerr et al., 1997) that could weaken the crust (Crawford and Hollister, 1987). Recent numerical studies confirm that modifications of fluid and melt related weakening (that is taken constant in this study) modifies orogenesis (Faccenda et al., 2009) and hence may significantly affect the dynamics of terrane accretion. In addition, for many present-day oceanic plateaus the age of the surrounding ocean floor is greater than the age of the plateau itself (Schubert and Sandwell, 1989). Crustal accretion can therefore be facilitated, if the oceanic plateau contains some residual formational heat (i.e. in the Caribbean: Kerr and Tarney, 2005). Oceanic plateaus that have a mafic crust, on the other hand, can transform into eclogite, and be prone to subduction. Finally it should be noted, that the third dimension is crucial for evaluating the total effect of buoyant crust on a subduction zone (Stern, 2002). End-on subduction of a linear tract of crust may locally disrupt a subduction zone but not cause it to fail, whereas delivery of similarly buoyant crust parallel to the trench is more likely to lead to subduction zone failure (Stern, 2002). To verify some

of these major controls on accretion dynamics further investigations from both numerical studies and geological observation are necessary.

High pressure and ultrahigh pressure terranes

Where underplating plateaus form, crustal material is dragged down to mantle depth, where it might undergo prograde metamorphism, prior to slab break off and subsequent exhumation. High pressure (HP) - ultra-high pressure (UHP) terranes are formed with peak metamorphic temperatures of 400 - 700 ^oC. Exhumation of such (U)HP terranes occurs by coherent eduction along the former subduction zone or by buoyant flow of crustal rocks, leading to structural reworking and retrograde metamorphism. Geological observations and numerical simulations both support this idea (Duretz et al., 2011; Kylander-Clark et al., 2008; Lexa et al., 2011; Andersen et al., 1991; Little et al., 2011). For example, exhumation of The Western Gneiss region in Western Norway is believed to have been coherent throughout its exhumation history (Kylander-Clark et al., 2008), while crustal flow has been inferred to be a major driving force for the exhumation of high-pressure terranes in the Bohemian Massif (Štípská et al., 2004; Lexa et al., 2011) and in the D'Entrecasteaux islands of Papa New Guinea (Little et al., 2011). The rate by which these U(HP) rocks are brought back to crustal levels, changes with time in our models, suggesting a multi-stage history of transport. Rapid exhumation through the mantle at speeds (6 - 9 cm/yr) comparable to plate tectonic velocities, is followed by slower exhumation at the base of the crust (0.08 - 0.22 cm/yr). This is in accordance with several high-pressure/ultrahigh pressure occurrences worldwide for instance in the Alps (Rubatto and Hermann, 2001) or the Himalaya (Parrish et al., 2006) that are known to have undergone such rapid exhumation, followed by slower exhumation at crustal levels. Our models reveal that during the first stage of exhumation, deformation is mainly localized at the bottom and top of the oceanic plateau. The later stage involves a more complex deformation pattern, which includes localized deformation of rocks of the upper and lower plate. Although some of these rocks reach the surface others melt or merge with magma that has been emplaced at crustal levels, revealing differing thermal histories and cooling rates (10 - 173 $^oC/Myr$). Ultra-high pressure rocks that have reached peak metamorphic temperatures of around 700 ^oC are accompanied by rapid cooling (173 $^oC/Myr$) during the first stage of exhumation ($\sim$ 1 Myr), followed by significantly slower rates at crustal levels 10 $^oC/Myr$. Nevertheless, rocks of the same plateau may also encounter lower peak metamorphic temperatures (400 ^oC) and single stage thermal

histories with moderate cooling rates 24 $^oC/Myr$.

Tectonic responses

Arrival of buoyant material at the subduction zone causes strong surface uplift and considerable structural damage in the upper and lower plate (Figure 5.12, 5.5, 5.9, 5.16 and 5.6). The rheology of the lower continental crust is thereby crucial to the ability to support topography (Clark et al., 2005; Duretz et al., 2011). Significant uplift rates are consistent with a strong lower continental crust (i.e. plagioclase rheology, see Table 5.1 for details), whilst crustal thickening is characteristic for a rheologically weaker crust (wet quartzite rheology). Regardless of the mechanisms that lead to crustal accretion or terrane subduction, large stresses that operate during collision form localized shear zones of intense plastic deformation that in some places may cut through the basement rocks of the overriding plate (Figure 5.6).

Tectonic features that are solely attributed to the accretion of crustal material onto the continental margin include the formation of a suture zone composed of basalts and sediments of the former oceanic crust and accretionary wedge. Such suture zones have been identified in various locations associated with terrane accretion through geological (e.g. Coney et al., 1980; Monger et al., 1982) and geophysical field studies (Brennan et al., 2011). These may contain thick highly deformed sequences of flysch, deformed ophiolite or high-pressure mineral assemblages of the blueschist facies that render a complex structural history. If subjected to post accretionary collision old suture zones may be reactivated throughout intra-plate deformation (Coney et al., 1980) and could play an important role in the assembly and growth of the continental crust (Brennan et al., 2011, and Chapter 7).

Another tectonic feature of accretionary tectonics is strong deformation of the downgoing slab, which eventually leads to slab break off. Slab detachment has been widely discussed in the literature and although mostly related to continental collision settings (e.g. Davies and von Blanckenburg, 1995; Wortel and Spakman, 2000; van Hunen and Allen, 2011) slab detachment has also been reported to be an important mechanism associated with the consumption of oceanic lithosphere (Haschke et al., 2002; Levin et al., 2002; Rogers et al., 2002; Buiter et al., 2002). Consistent with our experiments of frontal and basal plateau accretion, Van Zedde and Wortel (2001) have shown that slab detachment may occur at depth as shallow as 35 km. While slab detachment related to frontal plateau accretion ceases subduction, subduction zone failure associated with basal plateau

accretion allows for the outward migration of the subduction zone. New incoming oceanic crust underthrusts the strongly fractured terrane and forms a new subduction behind the accreted terrane. Both termination of subduction and subduction zone transference/migration have been discussed in the literature as possible consequences to terrane accretion (e.g. Dewey and Bird., 1970; Saunders et al., 1996; Stern, 2004; Cawood et al., 2009). Slab detachment related to underplating plateaus occurs at significantly greater depth. This is in accordance with petrological (Chopin, 1984, 2003, e.g.) and numerical (e.g. Gerya et al., 2004; Duretz et al., 2011; van Hunen and Allen, 2011) considerations that suggest deep crustal burial, but it should be noted that these studies have been conducted in relation to continent-continent collision zones and conditions of terrane accretion might be somewhat different and need to be explored in greater detail. Irrespective of the depth of detachment, slab break off causes significant surface uplift (Figure 5.6). Elasto-plastic (Buiter et al., 2002) and visco-plastic models (Gerya et al., 2004; Andrews and Billen, 2009; Duretz et al., 2011) have been used to obtain surface uplifts on the order of 1 - 6 km.

Natural examples of tectonic responses and consequences to the subduction of high bathymetric relief have recently been reviewed by Rosenbaum and Mo (2011). These include among others thickening and uplift of the forearc region accompanied by thick-skinned deformation and reactivation of basement thrusts, consistent with our observations. Places where surface uplift has been recorded include the Soloman Islands, New Hebrides, Costa Rica and Peru (Rosenbaum and Mo, 2011, and references therein). Subduction of the Nazca Ridge off South America has not only been preserved in the geomorphology and sedimentary facies of the forearc (Hampel, 2002; Clift et al., 2003), but has also been shown to influence far field structure in Amazonian foreland basin, 750 km away from the area of subduction (Espurt et al., 2007). Subduction of aseismic ridges is moreover believed to result in episodic transitions from thin-skinned to thick-skinned deformation and exhumation of basement rocks (Rosenbaum and Mo, 2011), which has been observed in the Andes (Kley et al., 1999).

Although some of these fractures may generate earthquakes, it has been argued that the events tend to be small because the evolving fracture system will limit rupture size (Wang and Bilek, 2011) and act as a seismic barrier to rupture propagation (Wang and Bilek, 2011; Kodaira et al., 2000) consistent with seismic gaps that have been commonly observed in such places (Kelleher and McCann, 1976; McCann et al., 1979; McGeary et al., 1985). Nevertheless it has also been argued that sub-

duction of bathymetric highs enhances seismic coupling at the subduction interface, which causes large magnitude seismicity (Scholz and Small, 1997; Cloos, 1992; Christensen and Lay, 1988). However, it should be noted that subduction of bathymetric highs is not a necessary condition for large subduction earthquakes (Scholz and Campos, 1995) and there are examples of ridge subduction that do not correlate with large earthquakes epicentres (Rosenbaum and Mo, 2011).

Crustal composition

Collision and subsequent accretion of oceanic plateaus are preceded by the subduction of oceanic lithosphere. Water released from the subducting plate lowers the melting temperature of the overlying mantle, allowing for flux melting of the hydrated mantle (e.g. Stolper and Newman, 1994; Tatsumi and Eggins, 1995; Schmidt and Poli, 1998; Iwamori, 1998). Hence, juvenile material of basaltic composition is added to the continental crust by which most arc magmas are believed to have formed. The continental crust, however, has an andesitic bulk composition, which cannot be derived by the basaltic magmatism that dominates present-day crustal growth (Rudnick, 1995). The andesite composition of the continental crust led Taylor to propose that continents may have formed by the accretion of island arcs of andesitic composition (Taylor, 1966; Rudnick, 1995). Later on it has been argued that at least some major segments of the continental crust might have formed through amalgamation of oceanic plateaus and continental fragments (Ben-Avraham et al., 1981; Coney et al., 1980; Jones et al., 1982; Reymer and Schubert, 1986). However, most island arcs and oceanic plateaus are believed to have basaltic rather than andesitic compositions (e.g. Rudnick, 1995; Stein and Hofmann, 1994; Abbott and Mooney, 1955). Nonetheless, it should be noted that the formation of oceanic plateaus is still not fully understood and while some are considered to have formed by plume related magmatism (Stein and Hofmann, 1994; Abbott and Mooney, 1955), others are believed to represent rifted continental fragments of crustal structure (Nur and Ben-Avraham, 1977; Ben-Avraham et al., 1981). Irrespective of their origin, accretion of such structures onto continental crust is of fundamental importance to the growth of continental crust, because even oceanic plateaus of initially basaltic composition may be modified with time to develop a typical upper continental structure (Stein and Ben-Avraham, 2007). Although some of these plateaus have begun to evolve into continental crust before accretion, most terranes probably began this evolution at the time of accretion (Condie, 2001). This is because newly accreted terranes might be

rapidly exposed to subduction zone magmatism, which chemically modifies the newly formed crust (Abbott and Mooney, 1955). On the other hand thick continental crust that is underlain by oceanic plateaus may be hot enough to allow for partial melting or else such melts may mingle and rise with mantle derived basalts along shear zones to form calcalkaline plutons (Crawford and Hollister, 1987; Hollister and Andronicos, 2006). Both scenarios are consistent with our results. In places where oceanic plateaus are sheared off the downgoing plate a new subduction zone is formed following slab break off and basalts derived form partially molten mantle may rise and modify the composition of the accreted terrane. Some rocks of the former oceanic plateau may also bypass the accretionary wedge, melt and further modify the composition of the accreted terrane or otherwise add to the growth of the continental crust. Davies and von Blanckenburg (1995) have argued that slab detachment at shallow slab interfaces (< 50 km) may cause large thermal perturbations that lead to partial melting of the metasomatized overriding plate, producing basaltic magmatism that may form granitic magmatism in the crust. Underpalting plateaus on the other hand are associated with deep crustal burial to depth of about 100 - 160 km. While some of these rocks may be exhumed to form high-pressure terranes on the surface, extensive partial melting of crustal lithologies may significantly affect arc magmatism and therefore the composition of newly produced crust. High-grade metamorphic and granitic welts that are believed to have formed subsequent to collision of large composite terranes (e.g. Monger et al., 1982; Crawford and Hollister, 1987) confirm the above-mentioned observations.

Magmatic addition rates

All our experiments reveal magmatic addition rates on the order of 20 - 30 $km^3/km/Myr$ prior to collision that are solely attributed to partial melting of the mantle. Aqueous fluids that are released from the downgoing slab lower the melting temperature of the overlying mantle allowing for basaltic melt production, which adds to the growth of the continental crust. This is in good agreement with estimates based on natural observations along the cricum Pacific. Here, magmatic addition is known to vary between 20 - 95 $km^3/km/Myr$ among varies locations (Reymer and Schubert, 1984; Tiara et al., 1998; Holbrook et al., 1999; Dimalanta et al., 2002). Less data is available for continental margins, but growth rates that have been measured along the Cordilleren orogenic system are somewhat similar 20 - 90 $km^3/km/Myr$ (DeCelles et al., 2009). Following collision, subduction of bathymetric highs is considered to form volcanic gaps, where volcanic

activity is absent (Nur and Ben-Avraham, 1982; McGeary et al., 1985; Rosenbaum and Mo, 2011). However, we do not observe such behaviour. Although little magmatism is observed in comparison to accretionary margins, magmatism does not cease but increase (50 - 60 $km^3/km/Myr$) as a response to the deep subduction of oceanic plateaus (Figure 5.4). Arrival of buoyant material steepens the slab dip and arc magmas (that are solely attributed to partial melting of the mantle) move closer to the trench.

Accretionary margins on the other hand reveal elevated magmatic addition rates on the order of 150 - 200 $km^3/km/Myr$ that are mostly related to partial melting of crustal material (Figure 5.8, 5.11 and 5.15). Condie (2007) has estimated average accretion rates in accretionary arcs to be 70 - 150 $km^3/km/Myr$ in Phanerozoic orogens and 100 - 200 $km^3/km/Myr$ in Precambrian orogens. Production rates of juvenile crust are believed to be typically 10 - 30 % lower than total accretion rates (Condie, 2007).

5.6 Conclusions

We have analysed the dynamics of terrane accretion or its deep subduction along active continental margins, where oceanic crust is recycled back into the mantle. In addition to terrane subduction three distinct modes of terrane accretion were identified: frontal plateau accretion, basal plateau accretion and underplating plateaus.

Complete plateau subduction: The most dominant tectonic response to the subduction of oceanic plateaus is a temporary uplift of the forearc region and the formation of a depression further landward, followed by subsequent subsidence. Other tectonic features include, steepening of the slab dip and the formation of localized shear zones that in some places may cut through basement rocks of the overriding plate.

Frontal plateau accretion: Oceanic plateaus subjected to frontal plateau accretion are docked onto the continental margin. This leads to crustal thickening. Hence both the downgoing slab and the overriding plate are exposed to intense plastic deformation, which generates deep seated shear zones. Consequently, the slab detaches at shallow depths and ceases subduction shortly after the collisional stage has been reached. Crustal material that has bypassed the accretionary wedge gets incorporated into arcs that have formed above the upper plate.

Basal plateau accretion: During basal accretion, oceanic plateaus are scraped off the downgoing slab to be accreted along the leading edge of the continental margin. Similar to frontal accretion, strong deformation forms localized shear zones of intense plastic failure. However, slab

break off occurs at somewhat greater depth and does not cease subduction, but results in the outward migration of the subduction zone (subduction zone jump/ transference). The large thermal contrast between the newly formed subduction zone and the overlying mantle promotes extensive partial melting of crustal lithologies located at the slab interface.

Underplating plateaus: In contrast to frontal or basal accretion underplating plateaus may be subducted to mantle depth before they underplate the continental crust, following slab break off and subsequent exhumation. The coherent eduction of deep buried material is accompanied by the buoyant flow of crustal rocks, structural reworking and retrograde metamorphism. Rocks that have been brought back to crustal levels form (U)HP terranes or else melt or merge with magma at mid crustal levels. The rate by which these rocks are exhumed changes, whereupon rapid exhumation through the mantle is followed by slower exhumation at crustal levels.

Bibliography

Abbott, D., Mooney, W., 1955. The structural and geochemical evolution of the continental crust: Support for the oceanic plateau model of continental growth. Reviews of Geophys. Suppl., U.S. National report to International Union of Geodesy and Geophysics 1991-1994, 231–242.

Andersen, T., Jamtveit, B., Dewey, J., 1991. Subduction and eduction of continental crust:major mechanisims during continent-continent collision and orogenic extensional collapse, a model based on the south norwegian caledonides. Terra Nova 3, 303–310.

Andrews, E., Billen, M., 2009. Rheological controls on the dynamics of slab detachment. Tectonophysics 464, 60–69.

Ben-Avraham, Z., Nur, A., Jones, D., Cox, A., 1981. Continental accretion: From oceanic plateaus to allochthonous terranes. Science 213, 47–54.

Boutelier, D., Chemanda, A., 2011. Physical modeling of arccontinent collision: A review of 2d, 3d, purely mechanical and thermo-mechanical experimental models. In: Arc-Continent Collision. Springer Verlag.

Boutelier, D., Chemenda, A., Burg, J.-P., 2003. Subduction versus accretion of intra-oceanicvolcanic arcs: insight from thermo-mechanical analogue experiments. Earth and Planetary Science Letters 212, 31–45.

Brennan, P. R., Gilbert, H., Ridgway, K. D., 2011. Crustal structure across the central alaska range: Anatomy of a mesozoic collisional zone. Geochemistry Geophysics Geosystems 12 (4), Q04010.

Buiter, S. J., Govers, R., Wortel, M., 2002. Two-dimensional simulations of surface deformation caused by slab detachment. Tectonophysics 354, 195–210.

Cawood, P. A., Kröner, A., Collins, W. J., Kusky, T. M., Mooney, W. D., Windley, B. F., 2009. Accretionary orogens through earth history. Geological Society, London, Special Publications 318 (1), 1–36.

Chopin, C., 1984. Coesite and pure pyrope in high-grade blueschists of the western alps: a first record and some consequences. Contributions to Mineralogy and Petrology 86, 107–118.

Chopin, C., 2003. Ultrahigh-pressure metamorphism: tracing continental crust into the mantle. Earth and Planetary Science Letters 212, 1–14.

Christensen, D., Lay, T., 1988. Large earthquakes in the tonga region associated withsubduction of the louisville ridge. Journal of Geophysical Research 93, 1336713389.

Christensen, N., Mooney, W., 1995. Seismic velocity structure and composition of the continental crust: A global view. Journal of Geophysical Research 100 (B6), 9761–9788.

Clark, M., Bush, J., Royden, L., 2005. Dynamic topography produced by lower crustal flow against rheological strength heterogeneities bordering the tibetan plateau. Geophysical Journal International 162, 575–590.

Clift, P., Pecher, I., Kukowski, N., Hampel, A., 2003. Tectonic erosion of the peruvian forearc, lima basin, by subduction and nazca ridge collision. Tectonics 22, doi:10.1029/2002TC001386.

Cloos, M., 1992. Thrust-type subduction zone earthquakes and seamount asperities: A physical model for earthquake rupture. Geology 20, 601–604.

Cloos, M., 1993. Lithospheric buoyancy and collisional orogenesis: Subduction of oceanic plateaus, continental margins, island arcs, spreading ridges, and seamounts. Geological Society of America Bulletin 105, 715–137.

Condie, K., 2001. Mantle plumes and continental growth. In: Mantle plumes and their record in earth history. Cambridge University press.

Condie, K., 2007. Accretionary orogens in space and time. The Geological Society of America Memoir 200, 145–158.

Coney, P., Jones, D., Monger, J., 1980. Cordilleran suspect terranes. Nature 288, 329–333.

Crawford, M., Hollister, L., 1987. Crustal deformation and regional metamorphisim across a terrane boundary, coast plutonic complex british columbia. Tectonics 6, 343–361.

Davies, J. H., von Blanckenburg, F., 1995. Slab breakoff: A model of lithosphere detachment and its test in the magmatism and deformation of collisional orogens. Earth and Planetary Science Letters 129, 85–102.

DeCelles, P., Ducea, M., Kapp, P., Zandt, G., 2009. Cyclicity in cordilleran orogenic systems. Nature Geoscience 2 (4), 251–257.

Dewey, J., Bird., J., 1970. Mountain belts and the new global tectonics. Journal of Geophysical Research 75, 2625–2647.

Dimalanta, C., Taira, A., Yumul, G., Tokuyama, H., Mochizuki, K., 2002. New rates of western pacific island arc magmatism from seismic and gravity data. Earth and Planetary Science Letters 202 (1), 105–115.

Dobretsov, N., Buslov, M., Yu, U., 2004. Fragments of oceanic islands in accretion collision areas of gorny altai and salair, southern siberia, russia: early stages of continental crustal growth of the siberian continent in vendian early cambrian time. Journal of Asian Earth Sciences 23, 673690.

Duretz, T., Gerya, T., Kaus, B., Andersen, T., 2012. Thermomechanical modeling of slab eduction. Journal of Geophysical Research - Solid Earth 117, doi:10.1029/2012JB009137.

Duretz, T., Gerya, T., May, D., 2011. Numerical modelling of spontaneous slab breakoff and subsequent topographic response. Tectonophysics 502, 244–256.

Ellis, S., Beaumont, C., Pfiffner, O. A., 1999. Geodynamic models of crustal-scale episodic tectonic accretion and underplating in subduction zones. Journal of Geophysical Research 104, 15169–15190.

Espurt, N. ND Baby, P., Brusset, S., Roddaz, M., Hermoza, W., Regard, V., Antoine, P.-O., Salas-Gismondi, R., Bolanos, R., 2007. How does the nazca ridge subduction influence the modern amazonian foreland basin? Geology 35, 515–518.

Evans, B., Goetze, C., 1979. The temperature variation of hardness of olivine and its implication for polycrystalline yield stress. Journal of Geophysical Research 84, 55055524.

Faccenda, M., Minelli, G., Gerya, T., 2009. Coupled and decoupled regimes of continental collision: Numerical modeling. Earth and Planetary Science Letters 278, 337349.

Forsyth, D., Uyeda, S., 1975. On the relative importance of the driving force of plate motion. Geophys J. R. Astron. Soc. 43, 163–200.

Gao, H., Humphreys, E.D., Yao, H., van der Hilst, R., 2011. Crust and lithosphere structure of the northwestern u.s. with ambient noise tomography: Terrane accretion andcascade arc development. Earth and Planetary Science Letters 304, 202–211.

Gerya, T., Fossati, D., Cantieni, C., Seward, D., 2009. Dynamic effects of aseismic ridge subduction: numerical modelling. European Journal of Mineralogy 21, 649–661.

Gerya, T., Yuen, D., Maresch, W., 2004. Thermomechanical modeling of slab detachment. Earth and Planetary Science Letters 226, 101–116.

Gorczyk, W., Willner, A., Gerya, T., Connolly, J., Burg, J.-P., 2007. Physical controls of magmatic productivity at pacic-type convergent margins: Numerical modelling. Physics of the Earth and Planetary Interiors 163, 209232.

Hampel, A., 2002. The migration history of the nazca ridge along the peruvian active margin: a reevaluation. Earth and Planetary Science Letters 2, 665–679.

Haschke, M., Scheuber, E., Guenther, A., Reutter, K.-J., 2002. Evolutionary cycles during andean orogeny: repeated slab breakoff and flat subduction. Terra Nova 14, 49–55.

Hilton, D., Hoogewerff, J., van Bergen, M., Hammerschmidt, K., 1992. Mapping magma sources in the east sunda-banda arcs, indonesia: constrains from helium isotopes. Geochimica et Cosmochimica Acta 56, 851–859.

Holbrook, W., Lizarralde, D., McGeary, S., Bangs, N., Diebold, J., 1999. Structure and composition of the aleutian island arc and implications for continental crustal growth. Geology 27 (1), 31–34.

Hollister, L., Andronicos, C., 2006. Formation of new continental crust in western british columbia during transpression and transtension. Earth and Planetary Science Letters 249, 29–38.

Hughes, G., Turner, C., 1977. Upraised pacific ocean floor, southern malaita. Geological Society of America Bulletin 88, 412–424.

Iwamori, H., 1998. Transportation of h2o and melting in subduction zones. Earth and Planetary Science Letters 160, 65–80.

Jones, D., Cox, A., Coney, P., Beck, M., 1982. The growth of the western north america. Scientific American 247, 70–84.

Jones, D., Silberling, N., 1986. Collision tectonics in the cordillera of western n america: examples from alaska. Geological Society, London, Sepical Publications 365, 367–387.

Jones, D., Silberling, N., Hillhouse, J., 1977. Wrangellia-a displaced terrane in northwestern north america. Can. J. Earth Sci. 14, 2565–2577.

Katayama, I., Karato, S., 2008. Low-temperature, high-stress deformation of olivine under water-saturated conditions. Physics of the Earth and Planetary Interiors 168, 125–133.

Kelleher, J. A., McCann, W., 1976. Buoyant zones, great earthquakes and unstable boundaries of subduction. Journal of Geophysical Research 81, 4885–4908.

Kerr, A., Tarney, J., 2005. Tectonic evolution of the caribbean and northwestern southamerica: The case for accretion of two late crataceous oceanic plateaus. Geology 33, 269–272.

Kerr, A., Tarney, J., Marriner, G., Nivia, A., Saunder, A., 1997. The caribbean colombian cretaceous igneous province: The internal anatomy of an oceanicplateau. In: Large Igneous Provinces: continental, oceanic, and planetary flood volcanism. American Geophysical Union.

Kley, J., Monaldi, C., Salfity, J., 1999. Along-strike segmentation of the andean foreland: causes and consequences. Tectonophysics 301, 7594.

Kodaira, S., Takahashi, N., Nakanishi, A., Miura, S., Kaneda, Y., 2000. Subducted seamount imaged in the rupture zone of the 1946 nankaido earthquake. Science 289, 104106.

Kylander-Clark, A., Hacker, B., Mattinson, J., 2008. Slow exhumation of uhp terranes: Titanite and rutile ages of the western gneiss region, norwa. Earth and Planetary Science Letters 272, 531–540.

Levin, V., Shapiro, N., Park, J., Ritzwoller, M., 2002. eismic evidence for catastrophic slab loss beneath kamchatka. Nature 418, 763–767.

Lexa, O., Schulmann, K., Janousek, V., tpsk, P., Guy, A., Racek., M., 2011. Heat sources and trigger mechanisms of exhumation of hp granulites in variscan orogenic root. Journal of Metamorphic Geology 29, 79–102.

Little, T., Hacker, B., Gordon, S., Baldwin, S., Fitzgerald, P., Ellis, S., Korchinski, M., 2011. Diapiric exhumation of earth's youngest (uhp) eclogites in the gneiss domes of the d'entrecasteaux islands, papua new guinea. Tectonophysics 510 (1), 39–68.

Mann, P., Taira, A., 2004. Global tectonic significance of the solomon islands and ontong java plateau convergent zone. Tectonophysics 389, 17–190.

Mason, W., Moresi, L., Betts, P., Miller, M., 2010. Three-dimensional numericalmodels of the influence of a buoyant oceanic plateau on subduction zones. Tectonophysics 483, 71–79.

McCann, W., Nishenko, S., Sykes, L., Krause, J., 1979. Seismic gaps and plate tectonics: seismic potential for major boundaries. Pure and Applied Geophysics 117, 1083–1147.

McGeary, S., Ben-Avraham, Z., 1981. Allochthonous terranes in alaska: Implications forthe structure and evolution of the bering sea shelf. Geology 9, 608–614.

McGeary, S., Nur, A., Ben-Avraham, Z., 1985. Spatial gaps and in arc volcanism- the effectof collision or subduction of oceanic plateaus. Tectonophysics 119, 195–221.

Monger, J., Price, R., Tempelman-Kluit, D., 1982. Tectonic accretion and the origin of two major metamorphic and plutonic welts in the canadian cordillera. Geology 10, 70–75.

Nur, A., Ben-Avraham, Z., 1977. The lost pacifica continent. Nature 270, 41–43.

Nur, A., Ben-Avraham, Z., 1982. Oceanic plateaus, the fragments of continents, and mountain building. Journal of Geophysical Research 87, 3644–3661.

Oxburgh, E., Parmentier, E., 1977. Compositional density stratification in the oceanic lithosphere-causes and consequences. Journal of the Geological Society of London 133, 343–355.

Parrish, R., Gough, S., Searle, M., Waters, D., 2006. Plate velocity exhumation of ultrahigh-pressure eclogites in the pakistan himalaya. Geology 34, 989–992.

Pilger, R., 1981. Plate reconstructions, aseismic ridges, and low-angle subduction beneath the andes. Geological Society of America Bulletin 92, 448456.

Ranalli, G., 1995. Rheology of the Earth. Springer.

Ranalli, G., Pellegrini, R., D'Offizi, S., 2000. Time dependence of negative buoyancy and the subduction of continetal lithosphere. Journal of Geophysics 30, 539–555.

Reymer, A., Schubert, G., 1984. Phanerozoic addition rates to the continental crust and crustal growth. Tectonics 3 (1), 63–77.

Reymer, A., Schubert, G., 1986. Rapid growth of some major segments of continental crust. Geology 14, 299–302.

Rogers, R., Karason, H., van der Hilst, R., 2002. Epeirogenic uplift above a detached slab in northern central america. Geology 30, 1031–1034.

Rosenbaum, G., Mo, W., 2011. Tectonic responses to the subduction of high bathymetricrelief. Gondwana Research 19, 571–582.

Rubatto, D., Hermann, J., 2001. Exhumation as fast as subduction. Geology 29, 3–6.

Rudnick, R., 1995. Making continental crust. Nature 378, 571–577.

Sandwell, D., MacKenzie, K., 1989. Geoid height versus topography of oceanic plateaus and swells. Journal of Geophysical Research 94, 7403–7418.

Saunders, A., Tarney, J., Kerr, A., Kent, R., 1996. The formation and fate of large oceanic igneous provinces. Lithos 37, 81–95.

Schmeling, H., Babeyko, A., Enns, A., Faccenna, C., Funiciello, F., Gerya, T., Golabek, G., Grigull, S., Kaus, B., Morra, G., van Hunen, J., 2008. A benchmark comparison of spontaneous subduction modelstowards a free surface. Physics of the Earth and Planetary Interiors 171 (1), 198–223.

Schmidt, M., Poli, S., 1998. Experimentally based water budgets for dehydrating slabs and consequences for arc magma generation. Earth and Planetary Science Letters 163 (1), 361–379.

Scholz, C., Campos, J., 1995. On the mechanism of seismic decoupling and back arc spreading at subduction zones. Journal of Geophysical Research 100, 22103–22115.

Scholz, C., Small, C., 1997. The effect on seamount subduction on seismic coupling. Geology 25, 487–490.

Schubert, G., Sandwell, D., 1989. Crustal volume of the continents and of oceanic and continental submarine plateaus. Earth and Planetary Letters 92, 234–246.

Sizova, E., Gerya, T., Brown, M., 2012. Exhumation mechanisms of melt-bearing ultrahigh pressure crustal rocks during collision of spontaneously moving plates. Journal of Metamorphic Geology.

Stein, M., Ben-Avraham, Z., 2007. Mechanisms of continental crust growth. Treatise on Geophysics 9, 171195.

Stein, M., Goldstein, S., 1996. From plume to continental lithosphere in the arabien-nubianshield. Nature 382, 773–778.

Stein, M., Hofmann, A., 1994. Mantle plumes and episodic crustal growth. Nature 372, 63–68.

Stern, R., 2002. Subduction zones. Reviews of Geophysics 40, doi:10.1029/2001RG000108.

Stern, R., 2004. Subduction initiation: spontaneous and induced. Earth and Planetary Science Letters 226, 275–292.

Stolper, E., Newman, S., 1994. The role of water in the petrogenesis of mariana trough magmas. Earth and Planetary Science Letters 121 (3), 293–325.

Tatsumi, Y., Eggins, S., 1995. Subduction zone magmatism. Wiley.

Taylor, S., 1966. The origin and growth of continents. Tectonophysics 4, 17–34.

Taylor, S., McLennan, S., 1985. The continental crust: its composition and evolution.

Tetreault, J., Buiter, S., 2012. Geodynamic models of terrane accretion: Testing the fate ofisland arcs, oceanic plateaus, and continental fragments in subduction zones. Journal of Geophysical Research 117, doi:10.1029/2012JB009316.

Tiara, A., Saito, S., Aoike, K., Morita, S., Tokuyama, H., Suyehiro, H., Takahashi, N., Shinohara, M., Kiyokawa, S., Naka, J., Klaus, A., 1998. Nature and growth of the northern izu-bonin (ogasawara) arc crust and their implications to continental crust formation. Island Arc 7, 395–407.

Trehu, A., Asuden, I., Brocher, T., Luetgert, J., Mooney, W., Nabelek, J., Nakamura, Y., 1994. Crustal architecture of the cascadia forearc. Science 266, 237–243.

Turcotte, D., Schubert, G., 2002. Geodynamics. Cambridge University Press.

Ueda, K., Gerya, T., Burg, J.-P., 2012. Delamination in collisional orogens: Thermomechanical modeling. Journal of Geophysical Research-Solid Earth 117, doi:10.1029/2012JB009144.

Ueda, K., Gerya, T., Sobolev, S., 2008. Subduction initiation by thermalchemical plumes. Physics of the Earth and Planetary Interiors 171, 296–312.

van Hunen, J., Allen, M., 2011. Continental collision and slab break-off: a comparison of 3d numerical models with observations. Earth and Planetary Science Letters 302, 27–37.

van Hunen, J., van den Berg, A., Vlaar, N., 2002. The impact of the south-american plate motion and the nazca ridge subduction on the flat subduction below south peru. Geophysical research letters 29 (14), 1690.

Van Zedde, D., Wortel, M., 2001. Shallow slab detachment as a transient source of heat at midlithospheric depths. Tectonics 6, 868–882.

Vogt, K., Gerya, T., Castro, A., 2012. Crustal growth at active continental margins: Numerical modeling. Physics of the Earth and Planetary Interiors 192-193, 1–20.

Von Huene, R., Corvaln, J., Flueh, E., Hinz, K., Korstgrad, J., Ranero, C., Weinrebe, W., 1997. Tectonic control on the subducting juan fernandez ridge onthe andean margin near valparaiso, chile. Tectonics 16, 474–488.

Štípská, P., Schulmann, K., Krner, A., 2004. Vertical extrusion and middle crustal spreading of omphacite granulite: a model of syn-convergent exhumation (bohemian massif, czech republic). J. metamorphic Geol. 22, 179198.

Wang, K., Bilek, S., 2011. Do subducting seamounts generate or stop large earthquakes? Geology 39, 819–821.

Wortel, M., Spakman, W., 2000. Subduction and slab detachment in the mediterranean carpathian region. Science 290, 1910–1917.

Chapter 6

Deep plate hydration triggers skinning of subducting plates and ophiolite emplacement[1]

6.1 Abstract

Most of the present day ocean floor is currently being consumed along active convergent margins, but fragments of upper oceanic lithosphere (ophiolites) have also been found on land. Emplacement of such fossil oceanic crust onto continental crust is a fundamental problem, because oceanic lithosphere is significantly denser than crustal rocks of the upper continental crust. Hence, subduction of less dense material beneath future ophiolites (Dewey, 1976; Moores, 1982) trench-ridge interaction or obduction of oceanic thrust slices from the subducting plate (Coleman, 1971) have been proposed as a critical condition for ophiolite emplacement. However, mechanisms for the detachment, migration and emplacement of ophiolitic complexes remain elusive. Here we report that hydrothermal circulation at slow spreading ridges (Johnson and Pruis, 2003) or bending related faulting in the outer trench region (Ranero et al., 2003; Faccenda et al., 2008, 2009; Grevemeyer et al., 2007; Lefeldt et al., 2012) may systematically produce a weak sub-crustal serpentinized horizon along which basal detachment of the entire oceanic crust is feasible. Because of the strong rheological contrast between the oceanic crust and the mechanically weak serpentinized mantle, deformation of this layered lithologies leads to decoupling, imbrication and separation of the oceanic crust from the downgoing slab. Remnants of the former oceanic crust underplate the accretionary wedge

[1]This chapter co-authored by K. Vogt and T. Gerya was submitted in a slightly modified version to Science.

or are emplaced onto continental crust, while the skinned lithospheric part of the slab subducts to greater depth. Our results demonstrate how dense coherent fragments of oceanic crust are detached and emplaced within accretionary complexes to form ophiolitic sequences with major implications to accretionary tectonics and arc magmatism.

6.2 Introduction

Hydration of the oceanic crust and uppermost mantle occurs mainly at mid-ocean ridges (Johnson and Pruis, 2003) and in the outer rise region of subduction zones (Ranero et al., 2003; Faccenda et al., 2008, 2009; Grevemeyer et al., 2007; Lefeldt et al., 2012). Because of the high porosity and permeability caused by lava drainbacks, normal faulting and volume changes, hydrothermal circulation at mid ocean ridges allows seawater to penetrate into the base of the crust, promoting seawater intrusion and mantle serpentinization (Johnson and Pruis, 2003). In the outer rise regions bending related faulting of oceanic crust and upper mantle, promotes deep hydration of the oceanic crust and uppermost mantle (Ranero et al., 2003; Faccenda et al., 2008, 2009; Grevemeyer et al., 2007; Lefeldt et al., 2012). Such fluid-mantle-rock interactions lead to partial serpentinization of the initially dry (peridotitic) mantle lithosphere of subducting slabs (Schmidt and Poli, 1998), altering its chemical and physical properties. Although direct information on the extend and degree of serpentinization below oceanic crust is not available and complete serpentinization of the mantle is unlikely (Schmidt and Poli, 1998), seismic low velocity zones indicate that partial serpentinization (10 - 20 % serpentine) along fracture zones is pervasive down to at least several kilometres depth (Grevemeyer et al., 2007; Lefeldt et al., 2012). The brittle strength of partially serpentinzed mantle rocks (peridotite with 10% - 15% serpentine) has been demonstrated to be as low as those of pure serpentines, because deformation is primarily accommodated by serpentine (the weakest phase), rather than olivine that remains nominally undeformed (Escartin et al., 2001). Likewise, the creep-viscosity (ductile strength) of serpentinized mantle is much lower than that of dry mantle (Hilairet et al., 2007). Consequently, deep slab serpentinization could potentially create a rheologically weak layer below the subducting oceanic crust if sufficient water is supplied. This layer will, in turn, strongly enhance the possibility of slab skinning, by which the oceanic crust is decoupled from the subducting slab and accreted within the accretionary wedge to form ophiolite complexes.

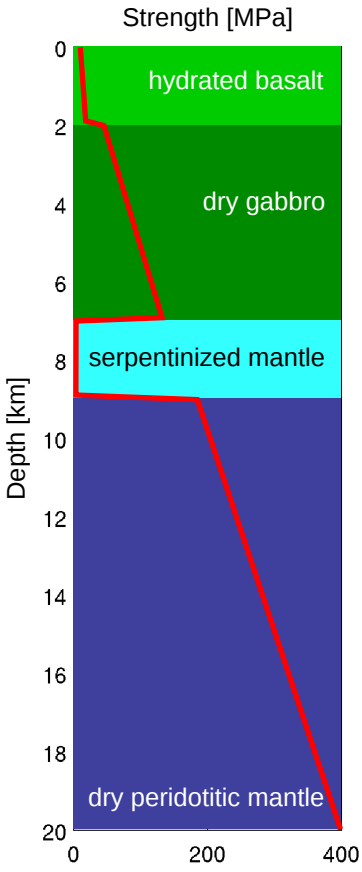

Figure 6.1: Strength profile of the oceanic crust and uppermost mantle for a constant strain rate of $\dot{\varepsilon} = 10^{-13}$ $[1/s]$. Serpentinized mantle provides a mechanically weak subcrustal horizon within which basal detachment of the oceanic crust is feasible. A detailed description of the rheological parameters used in this study, is given in 6.1.

6.3 Results

This work documents results from high-resolution thermo-mechanical numerical experiments of ocean-continental subduction zones to investigate the physical conditions for the decoupling and imbrication of oceanic crust in present day subduction zones. We carried out two-dimensional numerical experiments in which the oceanic plate bends spontaneously under the control of realistic visco-plastic rheologies (Figure 6.1). In this model the subducted oceanic crust is represented by 3 km of hydrothermally altered basalt and 5 km of dry gabbroic rocks. In the outer rise region, $\sim$ 50 km away from the trench, the uppermost mantle of the subducting slab comprises a 3 km thick serpentinized layer, which is assumed to have evolved mainly due to bending related faulting (Ranero et al., 2003; Faccenda et al., 2008, 2009; Grevemeyer et al., 2007; Lefeldt et al., 2012). This is consistent with recent studies, which indicate that most serpentinization occurs at the trench, rather than at mid ocean ridges. Because of this lithological variation and the strong rheological contrast (strength contrast) between the oceanic crust and the weak serpentinized horizon (Figure 6.1), deformation of this layered stratigraphy promotes decoupling, basal sliding and imbrication of the oceanic crust. In the course of subduction, the oceanic crust decouples from the downgoing slab along the weak serpentinized horizon, breaks and thrusts over the accretionary wedge or gets incorporated into the accretionary complex, while the underlying mantle lithosphere remains mainly undeformed and continues to subduct (Figure 6.2). New incoming oceanic crust may underthrust these broken oceanic crustal slices, subduct or break at greater depth. Remnants of the former oceanic crust underplate the accretionary wedge, while the skinned mantle lithospheric part of the slab sinks into the asthenosphere. In subsequent collisional events such stacked slices and broken fragments of oceanic crust can be exposed on land.

At asthenospheric depths, the large thermal contrast between the skinned slab and overlying mantle causes remnant serpentine breakdown and fluid release. Aqueous fluids percolate into the mantle wedge and alter the physical and chemical properties of the overlying mantle by lowering its melting temperature, viscosity and density (Schmidt and Poli, 1998; Escartin et al., 2001; Hilairet et al., 2007). Where such fluids encounter the wet mantle solidus they induce partial melting of the mantle by which most arc magmas are believed to have formed (e.g. Schmidt and Poli, 1998). Dehydration of serpentine at greater depth ($\sim$ 200 km) may have, moreover, profound implication for Earth deep mantle water cycle (Ranero et al., 2003).

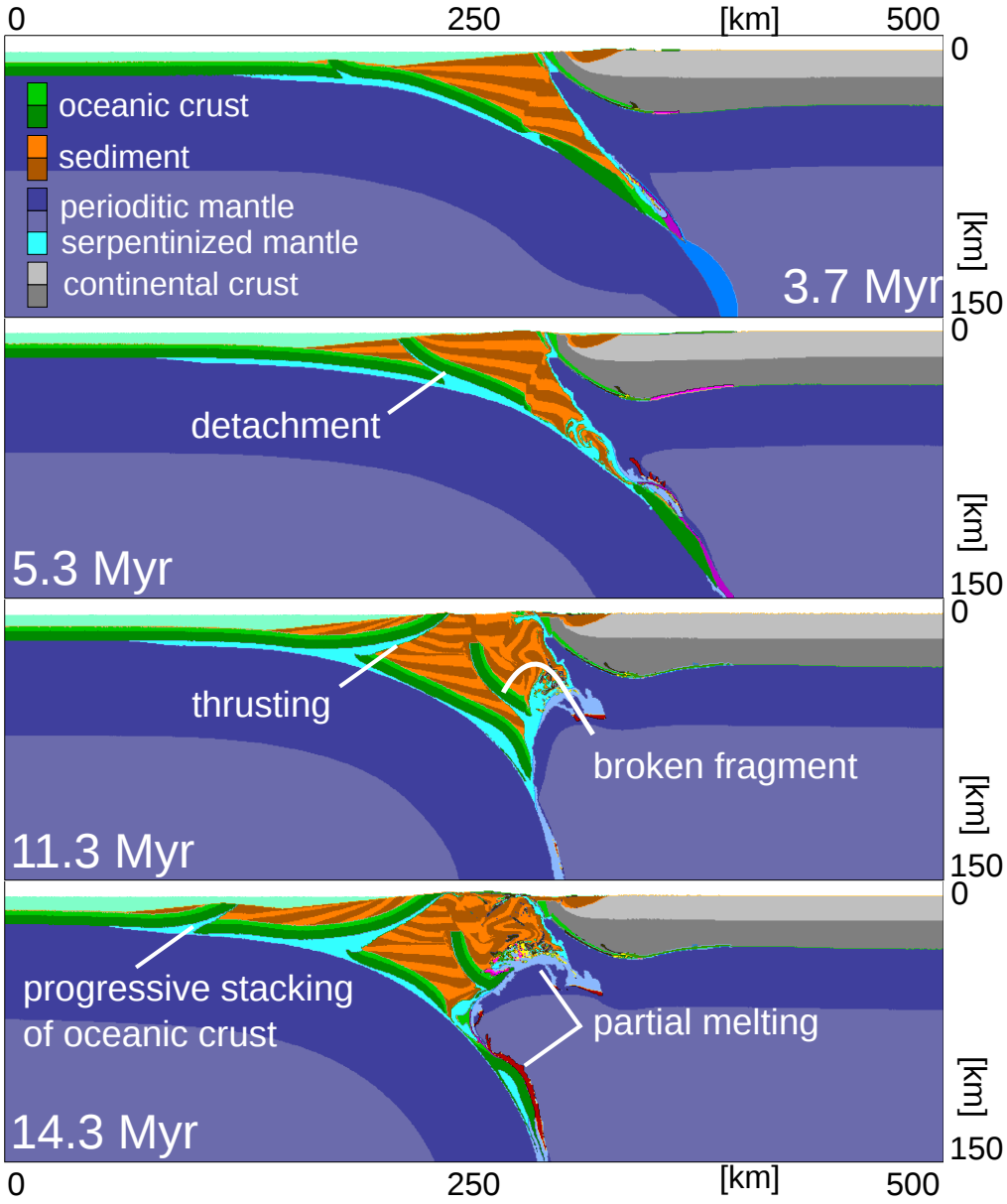

Figure 6.2: Thermomechanical two-dimensional model of mechanical decoupling of oceanic crust from the downgoing slab. Compositional (lithological) map. Oceanic crust detaches along a weak serpentinized horizon, breaks and gets incorporated within the accretionary wedge. Remnants of the oceanic crust underplate the accretionary wedge, while the skinned lithospheric part of the subducting slab sinks into the mantle

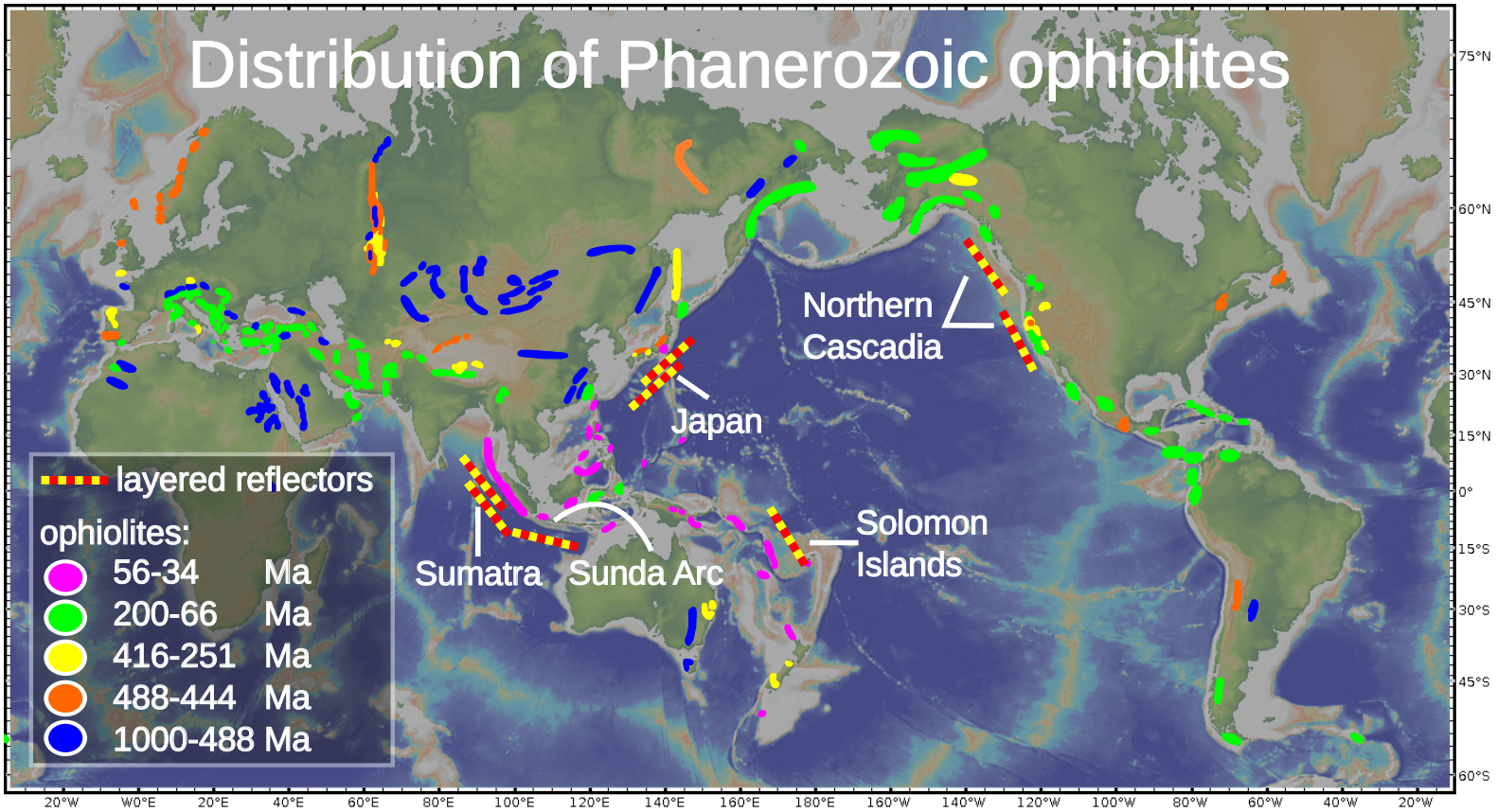

Figure 6.3: Distribution of Phanerozoic ophiolites modified after Vaughan and Scarrow (2003) and layered reflectors at 10 - 30 km depth (Godfrey and Klemperer, 1998; Bernstein-Taylor et al., 1992; Fujiwara et al., 1999; Calvert, 2004; Singh et al., 2008; Kimura et al., 2010; Lüschen et al., 2011; Singh et al., 2012). Such imaged reflection zones indicate, faulted, underplated and/or imbricated oceanic crust below the subsurface.

6.4 Discussion

Ophiolite occurences in modern Earth history

Comparison of ophiolite occurrences throughout modern Earth history (i.e.: Phanerozoic Vaughan and Scarrow, 2003) indicates that ophiolite emplacement has occurred in various tectonic environments, including both ocean-ocean and ocean-continent subduction zones (Figure 6.3). Indeed, oceanic fragments are common features of all modern and ancient accretionary complexes (Kimura and Ludden, 1995) and have been attributed to the progressive stacking of coherent ophiolitic thrust slices against the leading edge of the continental crust (Coleman, 1971) or the off scrapping and underplating of smaller ophiolitic slivers from the upper oceanic crust (Kimura and Ludden, 1995), but examples may also be found in collisional orogens. Exhumed ophiolitic terranes in the Western Alps are believed to represent fossil examples of oceanic crust brecciation under eclogite facies conditions ($\sim$ 23 kbar) and suggest deep burial ($\sim$ 80 km) prior to fluid-assisted fragmentation (imbrication) and subsequent emplacement at crustal levels (Angiboust et al., 2012). Brecciation in the middle part of the oceanic crust has been suggested to invoke intermediate depth earthquakes, consistent with eclogite breccias in ophiolite complexes (Angiboust et al., 2012). The exhumation of oceanic crust and associated mantle is discontinues and short lived, but may occur early with respect to the subduction zone cycle (e.g. Chile, Franciscan, possibly Makran), at the midst of subduction (e.g. Zagros, Himalaya, Andes) or late (e.g. Western Alps, New Caledonia) (Agard et al., 2009). The rate at which oceanic crust is incorporated into accretionary prisms or accreted onto continental crust has been rarely reported in the literature. However, ophiolite accretion rates of at least 50 $km^3/km/Myr$ were derived for the Great Vally ophiolite in California (Godfrey and Klemperer, 1998), while ophiolite accretion rates in the Philippine archipelago yielded somewhat smaller accretion rates of about 2 - 30 $km^3/km/Myr$ (Dimalanta and Yumul, 2003).

Geological observations

The close spatial association of exhumed oceanic fragments with mechanically weak serpentinities in most ophiolitic complexes (Agard et al., 2009) suggest an intimately related tectonic history and emphasizes its physical role in the emplacement mechanism. Unlike other exhumed oceanic crust rocks, serpentines are commonly highly deformed and therefore likely to have governed stress-build up and strain localization (Hilairet et al., 2007).

Structural analyses of fossil accretionary complexes (in various locations) indicate that ophiolitic thrust silvers may either decouple along a weak hydrothermally altered horizon (Kimura and Ludden, 1995) or detach along serpentinized sections at greater depth (Spaggiari et al., 2004). Hence, décollement formation is considered a critical condition for the detachment and emplacement of oceanic fragments by either offscraping or underplating (Kimura and Ludden, 1995).

Geophysical analysis

The subsurface distribution of stacked layers of imbricated oceanic crust, and smaller ophiolitic thrust slivers within modern accretionary complexes of presently active subduction zones, has been detected in terms of combined geophysical methods. Seismic, gravity and magnetic field studies indicate that these oceanic fragments can often be related to on land exposures of ophiolite complexes (Figure 6.3). For example, magnetic structures of the southern Boso Peninsula in Japan indicate fragmented pieces of oceanic plate emplaced at a paleo-boundary at 1 - 3 km depth, consistent with ophiolitic rocks in the Mineoka Belt (Fujiwara et al., 1999). Dissected oceanic crust, fragmented by normal faulting into 5 - 10 km sized blocks, below the forearc of the eastern Sunda Arc has been proposed to account for the ophiolite sheets and nappes of the island arc east of Java (Lüschen et al., 2011). Multichannel reflection seismic data obtained in this region clearly images normal faulting in the outer trench slope and may indicate the onset of detachment. The detected tectonic activity in the study by Lüschen and co-workers (Lüschen et al., 2011) compares well with results of our numerical simulations (Figure 6.4). Large coherent fragments of broken oceanic crust imaged in the Sumatran epicentral region let Singh and co-workers (Singh et al., 2008) to propose that imbrication of the oceanic lithosphere (oceanic crust and uppermost mantle) may invoke earthquakes, by which brittle failure of mantle rocks accounts for Megathrust earthquakes with exceptional magnitudes such as the 2004 Sumatran event. Most recent images of the Sumatran subduction system from the subducting front to the volcanic arc have confirmed that the subducting oceanic plate is fragmented, forming shallow dipping segments of 50 km, separated by 5 - 15 km depth intervals, indicating faulting of the oceanic crust (Singh et al., 2012). Exhumed ophiolites identified on the Mentawai-Andaman island chain have been suggested to represent the long term outcome of such successive episodes of oceanic underplating, based on the high free air gravity anomaly and the seismic reflection image at the south-western part of the accretionary complex (Singh et al., 2012).

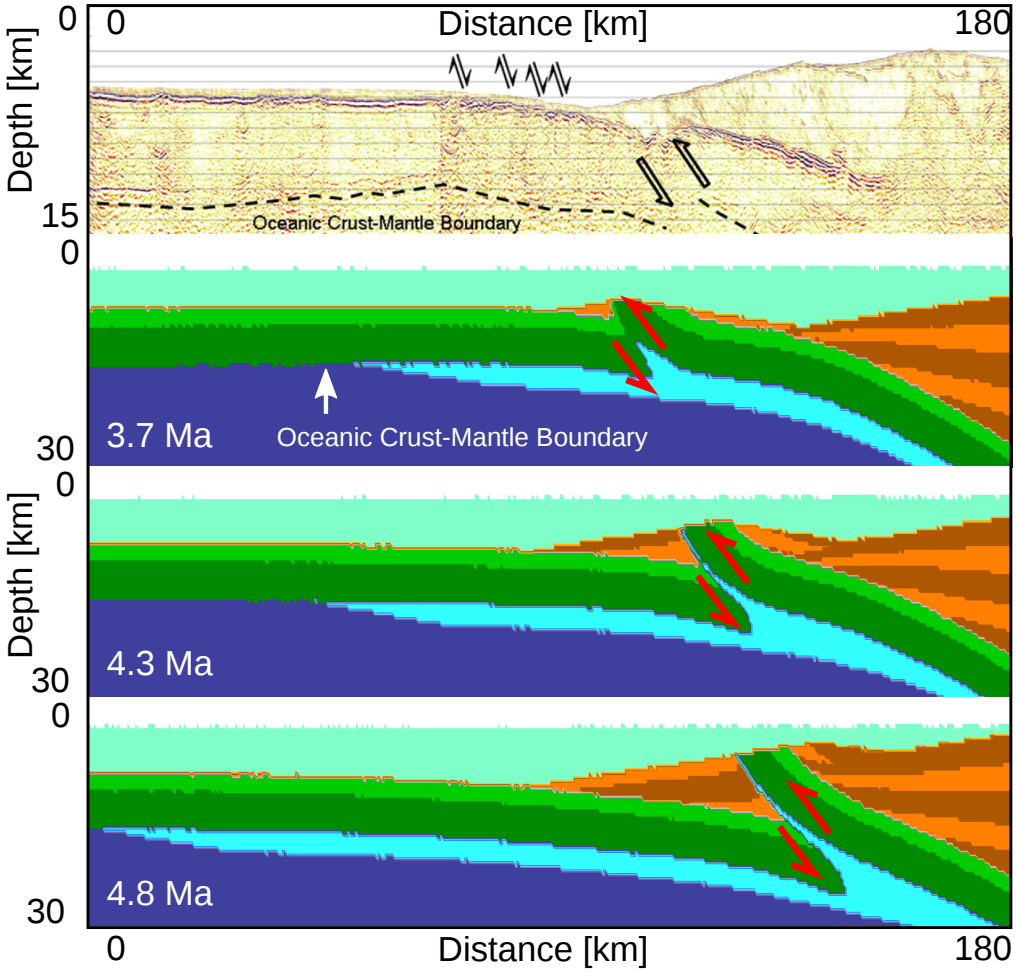

Figure 6.4: Comparison of the seismic reflection data imaged below the forearc of the eastern Sunda Arc (Lüschen et al., 2011) with our numerical simulations. The oceanic crust is faulted at the toe of the accretionary wedge. Arrows mark the relative motion of the imbricated oceanic crust and indicate future detachment as suggested by our numerical simulations.

Other locations where layered reflectors have been identified at 10 - 30 km depth include the Northern Cascadia subduction zone (Calvert, 2004), the central region of Japan (Kimura et al., 2010) and the western Solomon Sea basin (Bernstein-Taylor et al., 1992). Such reflection zones are generally believed to represent crustal scale duplexes associated with underplating or imbricated crustal rocks of the oceanic crust and ophiolitic slivers (Figure 6.3).

Low-Velocity-Zones

Layers of low seismic wave speed (LVZ) associated with subducting slabs in numerous subduction zone settings are commonly interpreted as hydrated oceanic crust that has not transformed into eclogite (Bostock, 2012). However some of these LVZ zones extend to greater depth than the model predicted by basalt-peridotie transformation and have been suggested to represent fluid or hydrous phase minerals rather than the variable metastability of anhydrous gabbro (Abers, 2005). Therefore we propose that such extended LVZ could indicate the skinned, serpentinized lithospheric part of the subducting plate, rather than the hydrated oceanic crust.

Conclusions

Oceanic crust is continuously being consumed in most subduction zones, but large fragments of oceanic crust (ophiolites) have also been recognized on land in various tectonic locations. Here we suggest that bending related faulting in the outer trench region may systematically produce a weak subcrustal hydrated (serpentinized) horizon along which basal detachment of the entire oceanic crust is feasible. Localized deformation of this serpentinized layer may lead to decoupling and separation of the oceanic crust from the downgoing slab. Remnants of the former oceanic crust can underplate the accretionary wedge or be exposed on land, whereas the skinned lithospheric part of the slab subducts into the mantle. The efficiency of this process depends critically on the existence of a continuous (mechanically weak) serpentinized horizon. Water intrusion along interconnected fracture systems is likely to result in extensive serpentinization of the uppermost mantle, but further studies will be needed to capture the global significance of this process.

6.5 Appendix

Model summary

All numerical experiments were performed with the I2VIS code (Gerya and Yuen, 2003). This code is based on conservative finite differences and a marker-in-cell technique. The momentum, continuity and energy equations are solved on an Eulerian frame, and physical properties are transported by Lagrangian markers that move according to the velocity field interpolated from the fix grid. The model uses non-Newtonian visco-plastic rheologies to simulate multiphase flow (Table 6.1). Within a strain interval of 0 - 1, strain weakening is applied (e.g. Lavier et al., 2000; Huismans and Beaumont, 2002; Gerya, 2010) at which the friction angle ($sin(\phi)$) is decreased by a factor of 2 and the cohesion (c) from 10^7 - 10^6 $[Pa]$(Table 6.1). The computational domain is two-dimensional and spans 2000 km $\times$ 200 km (Figure 6.5). It contains a (1000 km wide) high-resolution area of 0.5 km $\times$ 0.5 km in the centre of the domain. The rest of the model remains at a lower resolution. All mechanical boundary conditions are free slip. The oceanic plate is pushed toward a fixed continental plate at an imposed convergence rate of 3.5 cm/year. Both the asthenosphere and the upper mantle are composed of anhydrous peridotite and are defined by the temperature profile. The thermal structure of the oceanic plate was computed from the half space cooling model for a given plate age of 40 Myr (Turcotte and Schubert, 2002). The initial temperature field of the continental plate increases linearly from 0 ^oC at the surface to 1344 ^oC at the base of the continental lithosphere (72 km depth). For the asthenospheric mantle ($>$ 72 km) an initial adiabatic like thermal gradient of 0.5 $^oC/km$ is used.

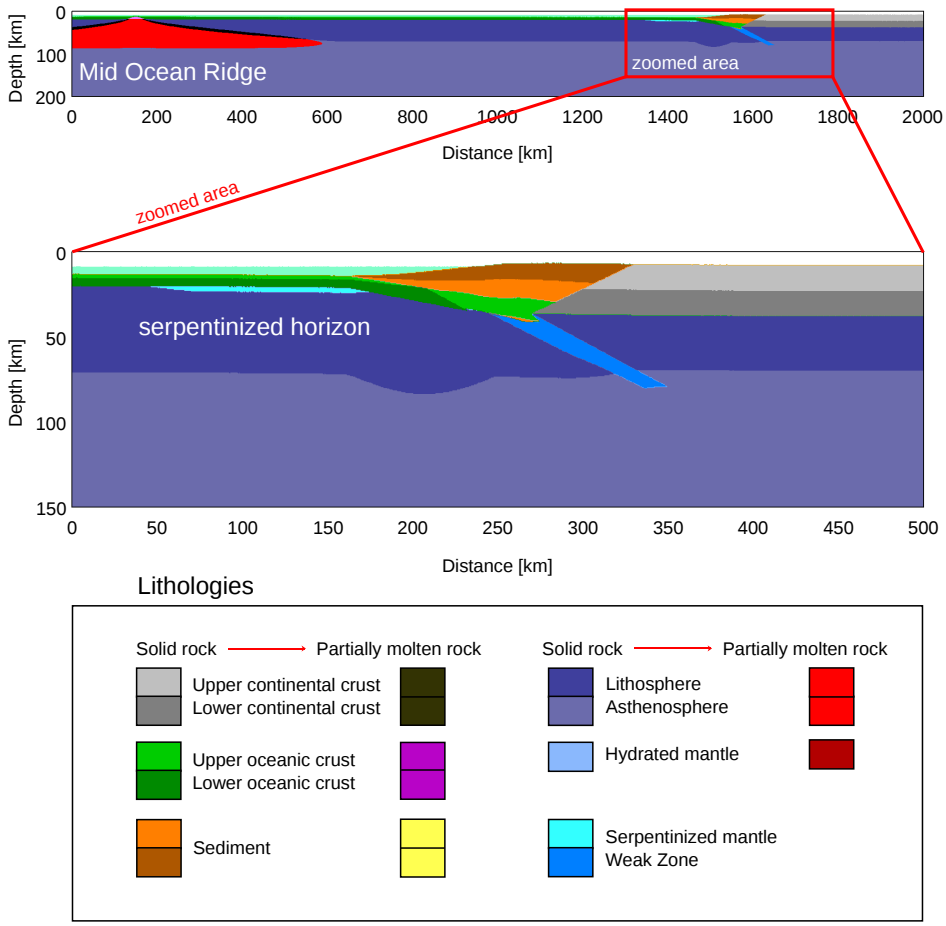

Figure 6.5: Initial setup of the numerical model. Staggered grid resolution is 2131 $\times$ 271 nodal points, with more than 10 million randomly distributed markers. The grid resolution is 0.5 km $\times$ 0.5 km in the ocean spreading region and in the center of the subduction zone area and 2 km outside of this area. Colours indicate materials (i.e. rock type or melt), which appear in subsequent figures.

Material	Flow law	$1/A_D$ $[Pa^n s]$	n	E_a $[J]$	V_a $[J/bar]$	$sin(\phi)$	c $[Pa]$	strain
Sediment	wet qtz	1.97×10^{17}	2.3	154×10^3	0.80	0.15-0.75	$1 \times 10^{7-6}$	1
Upper crust	wet qtz	1.97×10^{17}	2.3	154×10^3	1.20	0.15-0.75	$1 \times 10^{7-6}$	1
Lower crust	plag	4.80×10^{22}	3.2	238×10^3	0.80	0.15-0.75	$1 \times 10^{7-6}$	1
Basalt	wet qtz	1.97×10^{17}	2.3	154×10^3	0.80	0.15-0.75	$1 \times 10^{7-6}$	1
Gabbro	plag	4.80×10^{22}	3.2	238×10^3	0.80	0.60-0.30	$1 \times 10^{7-6}$	1
Dry mantle	dry ol	3.98×10^{16}	3.5	532×10^3	0.80	0.60-0.30	$1 \times 10^{7-6}$	1
Hydrated mantle	wet ol	5.01×10^{20}	4.0	470×10^3	0.80	0.10-0.05	$1 \times 10^{7-6}$	1
Initial shear zone	wet ol	5.01×10^{20}	4.0	470×10^3	0.80	0.10-0.05	$1 \times 10^{7-6}$	1
Serpentinized mantle	serp	3.21×10^{36}	3.8	8.90×10^3	0.32	0.10-0.05	$1 \times 10^{7-6}$	1

Table 6.1: Rheologies used in the experiments. Wet qtz = wet quarzite, plag = plagioclase (anorthite 75%), dry ol = dry olivine, wet ol = wet olivine after (Ranalli, 1995, and references therein) and serp = serpentine after Hilairet et al. (2007). A_D is the pre-exponential factor, n, is the stress exponent, E_a is the activation energy, V_a is the activation volume, ϕ is the friction angle, and c is the cohesion. Strain weakening is applied within a strain interval of 0 - 1, at which the friction angle ($sin(\phi)$) and cohesion (c) are decreased.

Model sensitivity study

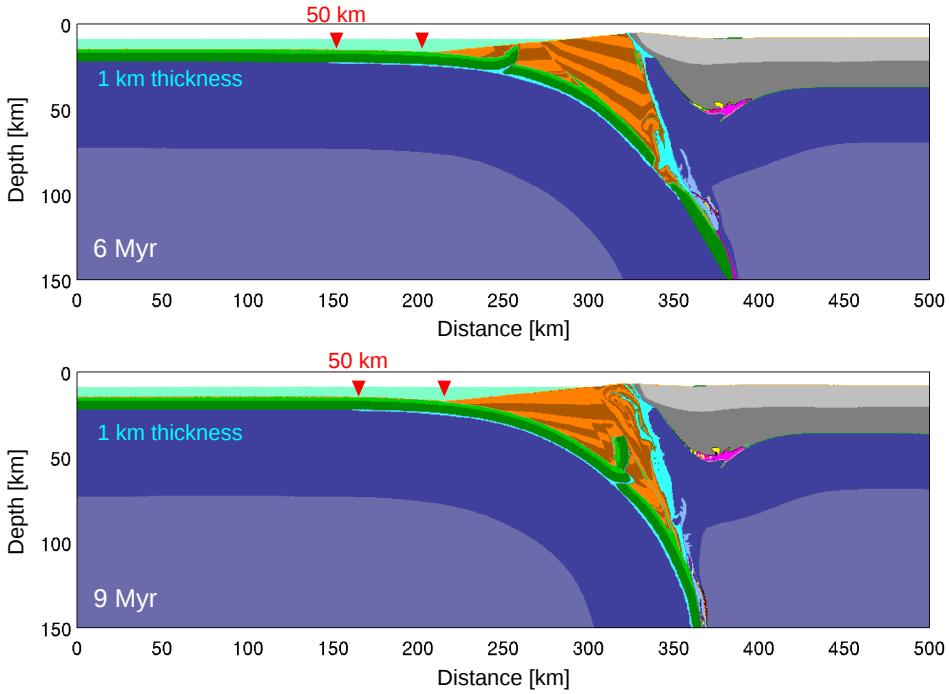

Figure 6.6: Compositional (lithological) map. Tectonic evolution of an ocean - continent subduction zone comprising a 1 km thick serpentine layer, formed approximately 50 km seaward from the trench. Imbrication of the oceanic crust at early stages of subduction is followed by continuous subduction of oceanic crust to greater depth.

The model sensitivity study (Figures 6.6 - 6.8) shows that the efficiency of the ophiolite emplacement process is strongly dependent on the thickness and horizontal extent of the subcrustal serpentinized layer. Figures 6.6 and 6.7 compare the tectonic evolution of an ocean - continent subduction zone, containing a 1 km and 6 km thick serpentine layer, formed at 50 km seaward distance from the trench. Localized deformation as a response to subduction initiation results in imbrication of oceanic crust. Fragments of broken oceanic crust are separated and incorporated into the accretionary wedge. New incoming oceanic crust may either subduct to greater depth (Figure 6.6) or be imbricated and fragmented in subsequent events, depending on the thickness of the serpentine layer. In models where the thickness of the serpentine layer is greater than 1 km successive fragmentation is commonly observed. The horizontal extent of the serpentine

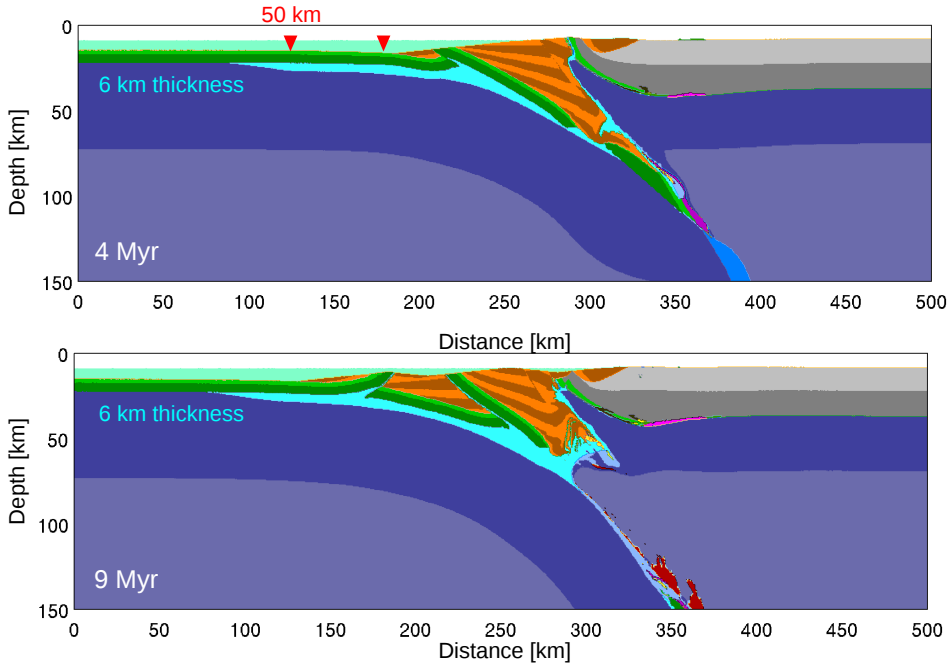

Figure 6.7: Compositional (lithological) map. Tectonic evolution of an ocean - continent subduction zone, comprising a 6 km thick subcrustal serpentine layer. Basal detachment along the serpentine layer leads to decoupling of the oceanic crust from the downgoing slab. The oceanic crust breaks and gets incorporated into the accretionary prism or exposed on land.

layer can likewise notably influence the tectonic evolution (Figures 6.8). In models with a wide serpentine layer formed at 220 km seaward distance from the trench, imbrication can occur already at $\sim$ 70 km seaward from the accretionary wedge (Figure 6.8a), enabling the progressive stacking of the oceanic crust (Figure 6.8b). Hence, our numerical modelling systematically shows that the presence of a continuous wide and thick subcrustal serpentine layer within the subducting plate should typically result in the fragmentation of the oceanic crust and subsequent ophiolite emplacement or incorporation into the accretionary wedge.

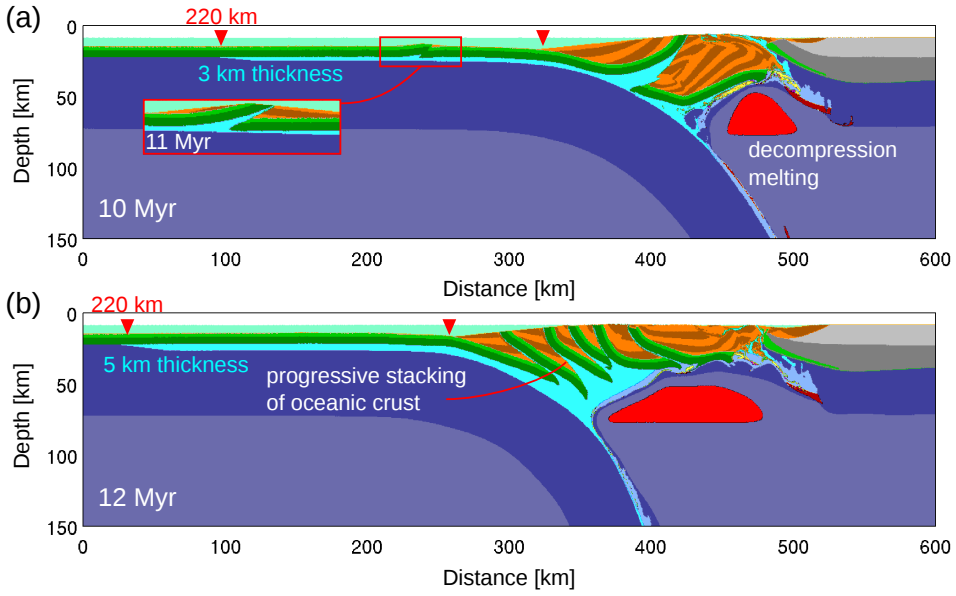

Figure 6.8: Compositional (lithological) map. Tectonic evolution of an ocean - continent subduction zone comprising a 3 km (a) and 5 km (b) thick subcrustal serpentine layer, formed approximately 220 km seaward from the trench. Imbrication of the oceanic crust may occur at 70 km seaward distance from the trench (a) and be followed by progressive stacking of oceanic crust.

Bibliography

Abers, G., 2005. Seismic low-velocity layer at the top of subducting slabs: observations, predictions, and systematics. Physics of the Earth and Planetary Interiors 149 (1), 7–29.

Agard, P., Yamato, P., Jolivet, L., Burov, E., 2009. Exhumation of oceanic blueschists and eclogites in subduction zones: timing and mechanisms. Earth-Science Reviews 92 (1), 53–79.

Angiboust, S., Agard, P., Yamato, P., Raimbourg, H., 2012. Eclogite breccias in a subducted ophiolite: A record of intermediate-depth earthquakes? Geology 40 (8), 707–710.

Bernstein-Taylor, B., Kirchoff-Stein, K., Silver, E., Reed, D., Mackay, M., 1992. Large-scale duplexes within the new britain accretionary wedge: a possible example of accreted ophiolitic slivers. Tectonics 11 (4), 732–752.

Bostock, M., 2012. The moho in subduction zones. Tectonophysics.

Calvert, A., 2004. Seismic reflection imaging of two megathrust shear zones in the northern cascadia subduction zone. Nature 428 (6979), 163–167.

Coleman, R., 1971. Plate tectonic emplacement of upper mantle peridotites along continental edges. Journal of Geophysical Research 76 (5), 1212–1222.

Dewey, J., 1976. Ophiolite obduction. Tectonophysics 31 (1), 93–120.

Dimalanta, C., Yumul, G., 2003. Magmatic and amagmatic contributions to crustal growth of an island-arc system: The philippine example. International Geology Review 45 (10), 922–935.

Escartin, J., Hirth, G., Evans, B., 2001. Strength of slightly serpentinized peridotites: Implications for the tectonics of oceanic lithosphere. Geology 29 (11), 1023–1026.

Faccenda, M., Burlini, L., Gerya, T., Mainprice, D., 2008. Fault-induced seismic anisotropy by hydration in subducting oceanic plates. Nature 455 (7216), 1097–1100.

Faccenda, M., Gerya, T., Burlini, L., 2009. Deep slab hydration induced by bending related variations in tectonic pressure. Nature Geoscience 2, 790–793.

Fujiwara, T., Kinoshita, H., Morijiri, R., 1999. Magnetic structure of the southern boso peninsula, honshu, japan, and its implications for the formation of the mineoka ophiolite belt. Earth Planets and Space 51 (6), 413–424.

Gerya, T., 2010. Dynamical instability produces transform faults at mid-ocean ridges. Science 329 (5995), 1047–1050.

Gerya, T., Yuen, D., 2003. Characteristics-based marker-in-cell method with conservative nite-differences schemes for modeling geological flows with strongly variable transport properties. Physics of the Earth and Planetary Interiors 140, 293–318.

Godfrey, N., Klemperer, S., 1998. Ophiolitic basement to a forearc basin and implications for continental growth: The coast range/great valley ophiolite, california. Tectonics 17 (4), 558–570.

Grevemeyer, I., Ranero, C., Flueh, E., Kläschen, D., Bialas, J., 2007. Passive and active seismological study of bending-related faulting and mantle serpentinization at the middle america trench. Earth and Planetary Science Letters 258 (3), 528–542.

Hilairet, N., Reynard, B., Wang, Y., Daniel, I., Merkel, S., Nishiyama, N., Petitgirard, S., 2007. High-pressure creep of serpentine, interseismic deformation, and initiation of subduction. Science 318 (5858), 1910–1913.

Huismans, R. S., Beaumont, C., 2002. Asymmetric lithospheric extension: The role of frictional plastic strain softening inferred from numerical experiments. Geology 30 (3), 211–214.

Johnson, H., Pruis, M., 2003. Fluxes of fluid and heat from the oceanic crustal reservoir. Earth and Planetary Science Letters 216 (4), 565–574.

Kimura, G., Ludden, J., 1995. Peeling oceanic crust in subduction zones. Geology 23 (3), 217–220.

Kimura, H., Takeda, T., Obara, K., Kasahara, K., 2010. Seismic evidence for active underplating below the megathrust earthquake zone in japan. Science 329 (5988), 210–212.

Lavier, L. L., Buck, W. R., Poliakov, A. N., 2000. Factors controlling normal fault offset in an ideal brittle layer. J. geophys. Res 105 (23), 431–23.

Lefeldt, M., Ranero, C., Grevemeyer, I., 2012. Seismic evidence of tectonic control on the depth of water influx into incoming oceanic plates at subduction trenches. Geochemistry Geophysics Geosystems 13 (null), Q05013.

Lüschen, E., Müller, C., Kopp, H., Engels, M., Lutz, R., Planert, L., Shulgin, A., Djajadihardja, Y., 2011. Structure, evolution and tectonic activity of the eastern sunda forearc, indonesia, from marine seismic investigations. Tectonophysics 508 (1), 6–21.

Moores, E., 1982. Origin and emplacement of ophiolites. Reviews of Geophysics 20 (4), 735–760.

Ranalli, G., 1995. Rheology of the Earth. Springer.

Ranero, C., Morgan, J., McIntosh, K., Reichert, C., 2003. Bending-related faulting and mantle serpentinization at the middle america trench. Nature 425 (6956), 367–373.

Schmidt, M., Poli, S., 1998. Experimentally based water budgets for dehydrating slabs and consequences for arc magma generation. Earth and Planetary Science Letters 163 (1), 361–379.

Singh, S., Carton, H., Tapponnier, P., Hananto, N., Chauhan, A., Hartoyo, D., Bayly, M., Moeljopranoto, S., Bunting, T., Christie, P., et al., 2008. Seismic evidence for broken oceanic crust in the 2004 sumatra earthquake epicentral region. Nature Geoscience 1 (11), 777–781.

Singh, S., Chauhan, A., Calvert, A., Hananto, N., Ghosal, D., Rai, A., Carton, H., 2012. Seismic evidence of bending and unbending of subducting oceanic crust and the presence of mantle megathrust in the 2004 great sumatra earthquake rupture zone. Earth and Planetary Science Letters 321, 166–176.

Spaggiari, C., Gray, D., Foster, D., 2004. Ophiolite accretion in the lachlan orogen, southeastern australia. Journal of structural geology 26 (1), 87–112.

Turcotte, D., Schubert, G., 2002. Geodynamics. Cambridge University Press.

Vaughan, A., Scarrow, J., 2003. Ophiolite obduction pulses as a proxy indicator of superplume events? Earth and Planetary Science Letters 213 (3), 407–416.

Chapter 7

Tectonics and Melting in Intra-Cratonic Settings[1]

7.1 Abstract

Most geodynamic theories of deformation as well as metamorphism and melting of continental lithosphere are focussed on plate boundaries and are dominated by the effects of subduction upon deformation of the margins of continental lithospheric blocks. However, it is becoming increasingly apparent that suture zones, or so-called mobile belts, presumably representing fossil subduction zones, but occurring far from active continent boundaries, play a key role in intra-cratonic deformation. In such zones, the crust is strongly sheared and the mantle lithosphere is metasomatized. Reworking of such settings reveals a surprisingly large range of instabilities that develop in compressed lithosphere with lateral heterogeneities inherited from fossil subduction/amalgamation settings. Structural complexity arises, which is sensitive to lithospheric age and tectonic setting. This complexity influences localization of deformation, topographic evolution, melt generation, and melt intrusion. In this paper, various tectonic responses are correlated with magmatic events in intra-continental settings and are compared to observed intra-cratonic orogenies and magmatic events.

7.2 Introduction

Since the 1960s, many studies have invoked strong thermal anomalies as the main cause of both oceanic and continental intra-plate magmatism

[1]This chapter co-authored by W. Gorczyk and K. Vogt was submitted to Gondwana Research. I have performed the experiments. Both authors have analysed the data and contributed to the manuscript.

associated with the existence of deep thermal anomalies such as mantle plumes, whose origins have been placed near the core-mantle boundary ($\sim$ 2900 km, i.e.: Begg et al., 2010; Condie, 2001; Davies, 1988; Dobretsov et al., 2010; Morgan, 1971; Sobolev et al., 2011; White and McKenzie, 1989; Wilson, 1963), or upper-lower mantle transition zone (410 - 660 km discontinuity, i.e.: Allégre and Turcotte, 1985; Hofmann, 1997; McKenzie and O'nions, 1983). In many continental flood basalt provinces (mostly on boundaries of two cratonic blocks), the active role of mantle plumes has been invoked to explain the high melt productivity (Begg et al., 2010; Faccenna and Becker, 2010). Furthermore, it has been shown that the removal of the mantle lithosphere (i.e.: the sub-crustal portion of the lithosphere) can occur by (1) Rayleigh-Taylor instabilities (i.e.: Elkins-Tanton, 2007; Gorczyk et al., 2011; Harig et al., 2010; Houseman et al., 1981; Houseman and Molnar, 2007) or by (2) delamination [peeling off] (i.e.: Bird, 1979; Göğüş and Pysklywec, 2008; Kay and Mahlburg Kay, 1993) of the base of the mantle lithosphere. These processes can introduce high thermal anomalies at the base of the Moho. Chemical heterogeneity in the shallow mantle may explain features of oceanic and continental magmatism (Meibom et al., 2003). The internal parts of continental crust are not homogeneous, but rather contain major tectonic boundaries and discontinuities that may significantly weaken the continental lithosphere. Some of these weak zones (mobile belts, i.e.: Lenardic et al., 2000, 2003; Yoshida, 2010, 2012) may have formed by the amalgamation of micro-continents and oceanic plateaus while others remain enigmatic. These regions are mobile because the lithosphere is sufficiently weak and may be deformed by the forces that developed at plate boundaries. Regardless of their origin these discontinuities may significantly affect the tectonic evolution of intra-plate settings (Cruden et al., 2006; Sokoutis and Willingshofer, 2011). Recent numerical (Gorczyk et al., 2011) and experimental (Bajolet et al., 2012) studies suggest that these weak zones may be responsible for the removal of large portions of the mantle lithosphere by either the sinking of gravitationally unstable mantle and lower crust by Rayleigh-Taylor instabilities or by delamination, where the coherent mantle lithosphere is peeled away. However, the magmatic consequences of either process remain elusive and little is known about how the tectonic evolution of such orogens will affect melt production and melt emplacement.

In this paper we present a systematic study of tectonic and magmatic responses for shortening of laterally heterogeneous continental lithosphere containing a rheologically weak mobile belt. Based on systematic numerical experiments we analyse influences of two major physical character-

istics of the intra-continental collision: (1) lithosphere thermal thickness (variable age of the continental lithosphere) (2) rate of intra-continental convergence.

7.3 Model Setup

All experiments have been performed in a spatial coordinate frame of 2000 km × 400 km that represents a continental to upper mantle cross-section (Figure 7.1). The rectangular grid with 781 × 201 nodal points is non-uniform and contains a (600 km wide) high-resolution (1 km × 2 km) in the center of the domain while the rest of the model remains at a lower resolution (10 × 2 km). The continental crust is composed of 15 km upper and 15 km lower felsic crust. The subjacent asthenosphere and the upper mantle are composed of anhydrous peridotite and are defined by the given temperature profile. The continental lithosphere contains a 100 km wide discontinuity of lowered plastic strength (with respect to the surrounding rocks) that separates the continental crust and underlying mantle into two adjacent blocks (Figure 7.1). Such discontinuities (mobile belts) have been widely discussed in the literature and are believed to have formed by for example the amalgamation of micro-continents and oceanic plateaus (Lenardic et al., 2000, 2003; Yoshida, 2010, 2012). All mechanical boundary conditions are free slip only the lower boundary is permeable satisfying an external free slip boundary condition (Gorczyk et al., 2007). Similar to the usual free slip condition, external free slip allows global conservation of mass in the computational domain. The initial temperature field of the continental plate increases linearly from 0 ^oC at the surface to 1344 ^oC at the lithosphere asthenosphere boundary. An initial adiabatic like thermal gradient of 0.5 $^oC/km$ is used for the asthenospheric mantle. An internally prescribed velocity field within the convergence condition region ensures horizontal compression between the two continental blocks. The convergence rate is symmetric; each side is pushed with the same constant velocity for 6 Myr. After 6 Myr convergence rate is set to zero and deformation is purely self-driven.

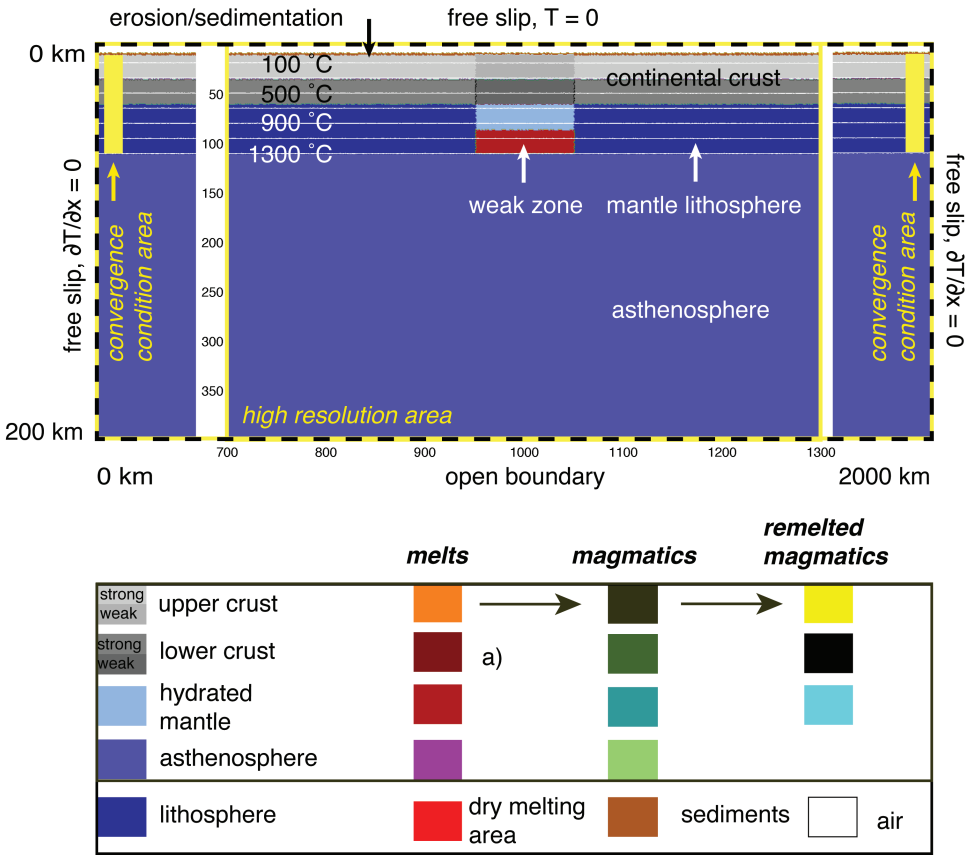

Figure 7.1: Model setup and boundary conditions. Initial setup of the numerical model (see text for details). Staggered grid resolution is 781 × 201 nodal points, with more than 10 million randomly distributed markers. The grid resolution is 1 × 2 km in the subduction zone area (700 - 1300 km) and 10 × 2 km outside of this area. Isotherms are displayed in white for increments of 200 ^oC, starting from 100 ^oC. Colours indicate materials, i.e. rock type or melt, which appear in subsequent figures. For rheologies used in the experiments, see Table 7.1. All boundary conditions are free slip. The top surface of the lithosphere is treated as an internal free surface and accounts for sedimentation and erosion.

Material	Flow law	$1/A_D\ [Pa^n s]$	n	$E_a\ [J]$	$V_a\ [J/bar]$	$sin(\phi)$	$c\ [Pa]$
Sediment	wet qtz	1.97×10^{17}	2.3	154×10^3	0.8	0.15	1×10^7
Wet upper crust	wet qtz	1.97×10^{17}	2.3	154×10^3	0.0	0.05	1×10^6
Dry upper crust	wet qtz	1.97×10^{17}	2.3	154×10^3	0.0	0.15	1×10^6
Lower crust	plag (An75)	1.13×10^{21}	4.2	445×10^3	0.0	0.40	1×10^7
Dry mantle	dry ol	3.98×10^{16}	3.5	532×10^3	0.8	0.60	1×10^7
Wet mantle	wet ol	5.01×10^{20}	4.0	470×10^3	0.8	0.60	1×10^7
Magmatics (all)	wet qtz	1.97×10^{17}	2.3	154×10^3	0.8	0.15	1×10^7

Table 7.1: Rheological parameters used in this study: wet qtz = wet quarzite, plag (An75) = anorthite 75 %, wet ol = wet olivine, dry ol = dry olivine after (Ranalli, 1995, and references therein). A_D is the pre-exponential factor, n, is the stress exponent, E_a is the activation energy, V_a is the activation volume, ϕ is the friction angle, and c is the cohesion.

7.4 Results

Lithospheric discontinuities subjected to intra-continental deformation control the tectonic evolution of the continental lithosphere and underlying mantle. The thickness of the continental lithosphere (lithospheric age) and the convergence rate are found to be crucial parameters controlling the tectonic response of intra-plate deformation. Three distinct modes of deformation have been observed: (1) mechanical removal of part of the lithosphere by: (a) plastic instabilities that arise from processes induced by forces normal to the surface between two media (b) gravitational instabilities, (c) and delamination, a wholesale peeling away of a coherent block of mantle lithosphere, (2) intra-continental subduction and (3) long term wedging of the Moho. The results of this study are summarized in Figure 7.2.

Mechanical removal of part of the lithosphere

Mechanical removal of the lithosphere can exhibit itself in three ways: (a) plastic delamination, (b) Rayleigh Taylor instabilities and (c) lithospheric delamination. (a) Plastic delamination arises due to differences in yield strength between two media (Piriz et al., 2005; Robinson and Swegle, 1989; Swegle and Robinson, 1989). To induce such delamination, a small wavelength of perturbation is required. Therefore, this type of delamination occurs at the initial stage of most experiments (Figure 7.3a, time-slice = 14.9 Myr). (b) Classical Rayleigh-Taylor instabilities (Houseman and McKenzie, 1982; Houseman et al., 1981; Houseman and Molnar, 2007) arise due to density variations between a perturbed contact of two materials (Figure 7.3). This type of instability occurs in all runs marked with grey colour in Figure 7.2. It also preludes the third type of delamination (convergence 2 cm/yr - 60, 80, 100 km lithospheric thickness): (c) lithospheric delamination (Figure 7.5), where the cold and dense part of the lithosphere peels away as a coherent slice from overlying material (Bird, 1978, 1979).

Plastic instabilities - Model I - 100km - mantle lithosphere depth, 0.5 cm/yr compression rate

Plastic delamination occurs within the first few million years of compression and is a common feature to all experiments. However, it is mostly pronounced in runs with a low convergence rate (0.5 - 1 cm/yr), where the partially molten (hydrated) mantle lithosphere sinks into the astheno-

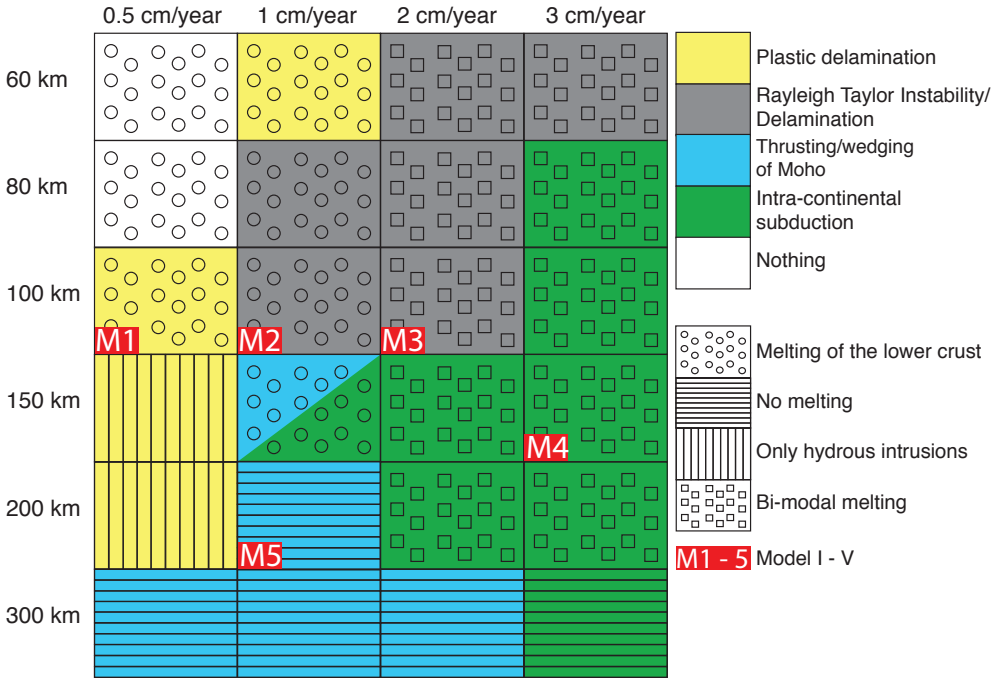

Figure 7.2: Graphical representation of results (block diagram). Parameter space showing the explored range of lithospheric cooling ages (lithospheric thickness) and convergence rates, which control the tectonic response and melt evolution of intra-continental deformation. Three distinct modes of deformation have been observed: (1) mechanical removal of part of the lithosphere by: (a) plastic instabilities (b) gravitational instabilities, (c) and delamination (2) intra-continental subduction and (3) long-term wedging of the Moho.

sphere due to difference in plastic strengths of the rocks, not the density variation (detailed description of the process can be found in Gorczyk, 2012, accepted to GR). In the top frame of Figure 7.3b, it can be seen that the lowermost part of the weak zone has a lower density than the surrounding mantle material. Nevertheless, the lowermost part of the partially molten mantle lithosphere drips down, as indicated in Figure 7.3a (time frame 14.9 Myr). This delamination does not affect melting processes in a significant way, but it may lead to melting of the lower crust in the weak zone when the lithosphere recovers thermally after the compressive episode. It is also important to note that plastic delamination alone does not leave any imprints on the surface topography (Figure 7.3c). All high elevations observed at the initial stage of the runs result from compression. Due to the ease of initiation of this process, and lack of visible imprints of it, it may be quite common in nature and could be responsible for fertilizing the asthenosphere.

Gravitational instability - Model II - 100km - mantle lithosphere depth, 1 cm/yr compression rate

Figure 7.3 represents the tectonic evolution of Model II, where at first plastic delamination is followed by gravitational delamination. At the beginning of an experiment, horizontal compression leads to mechanical thickening of the lithosphere and enables immediate strain localization and deformation within the weak zone. Where the hydrated mantle encounters the wet mantle solidus, basaltic melt production is triggered, followed by melt emplacement in mid to upper crustal levels. This, in turn, leads to partial melting of the upper continental crust (Figure 7.3a). As the crustal material thickens, the base of the Moho reaches the eclogite stability field and part of the lower crust is exposed to eclogitization; here, the density increases by 100 kg/m^3 to 180 kg/m^3. Because of the density variation between the eclogitizised lower crust and surrounding mantle, a gravitational instability develops and detached dense material sinks into the deep mantle (Figure 7.3b). The timing and depth at which this occurs varies according to the convergence rate and thickness of the lithosphere. For young lithosphere and high compression rates, delamination occurs early. Parts of the lower crust melt as the crust encounters greater temperatures ($> 700\,^oC$) due to crustal thickening. Thus, the main melting episode takes place after the detachment of the drip (Figure 4a). Subsequently, thermal equilibration takes place, which leads to fast temperature increase at the base of the crust above the delaminated material. Such thermal anomalies lead to partial melting of the lower continental crust at temperatures rang-

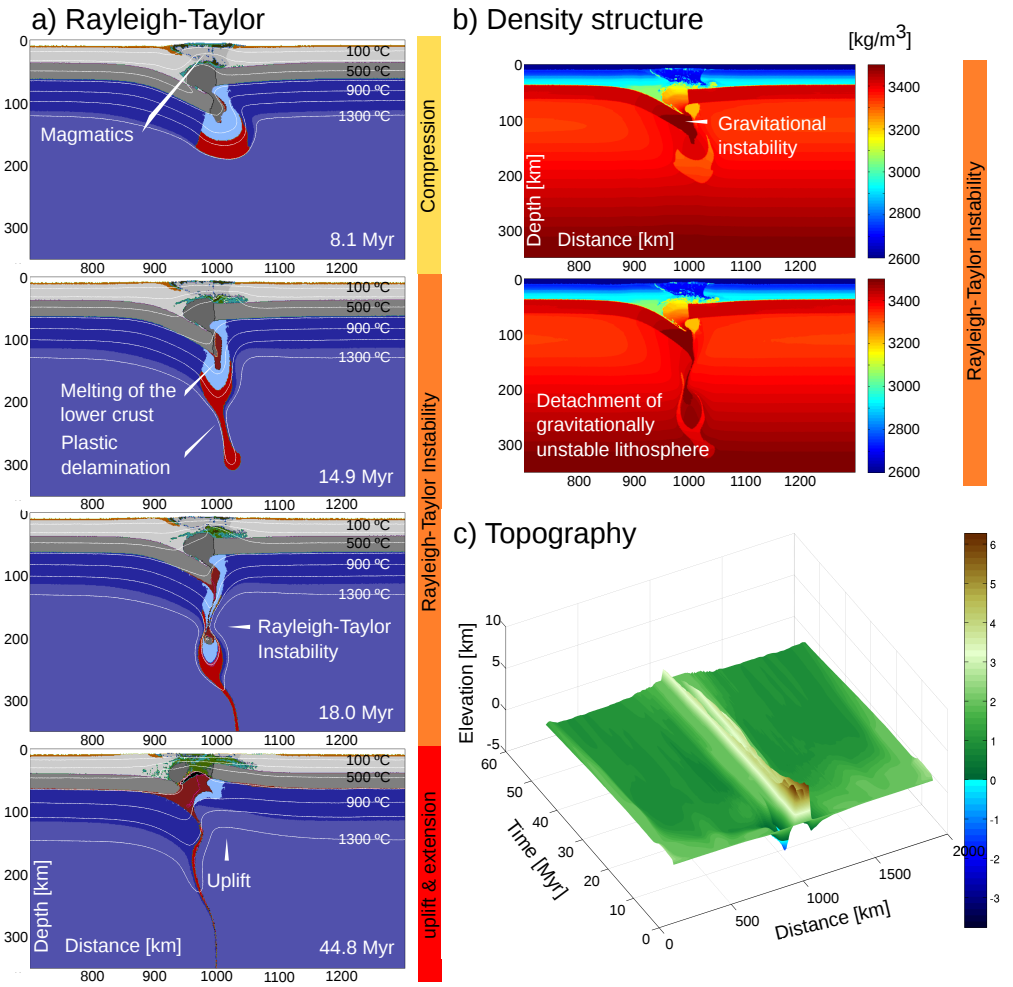

Figure 7.3: Rayleigh-Taylor instabilities. a) Dynamic evolution of the lithosphere and underlying mantle after 6 Myr of compression at a rate of 1 cm/yr and a lithospheric thickness of 100 km. Compression leads to crustal thickening at which the lower crust becomes eclogitized. The density of the lower crust increases and a gravitational instability develops, followed by detachment of dense crustal material that sinks into the mantle. b) Density structure of the modelled domain. c) Dynamic evolution of the topography over time. Strong surface uplift during the compressional stage is followed by topographic relaxation at later stages.

ing from 700 ^oC to 900 ^oC, forming large felsic batholiths (of up to 200 km in length) at mid to upper crustal levels that may reach the surface in subsequent tectonic events, such as crustal rebounds. The detached part of the lower crust melts and as before predicted by Elkins-Tanton (2007), melts are extracted and volatiles are released, perhaps contributing to the composition and geochemical evolution of the batholiths formed in the upper crust. Other tectonic features include a sharp surface uplift during the initial stage of convergence (as a result of mechanical thickening), followed by topographic relaxation that can be correlated with thermal equilibration after the detachment.

Delamination and detachment, Model III - 100km - mantle lithosphere depth, 2 cm/yr compression rate

Visual representation of Model III is presented in Figure 7.5. In this model initial gravitational instability is followed by asymmetric delamination of part of the mantle lithosphere. After the first episode of detachment, when gravitation develops an asymmetric geometry, hot asthenopsheric material can intrude into the lithosphere (Figure 7.5a, 5.4 Myr). As a consequence, decompression melting of the dry perioditic mantle and horizontal melt intrusion at crustal levels occurs (Figure 7.5a, 9.1 Myr). A portion of the lower crust and underlying mantle lithosphere decouples from the upper part, then peels away, and finally detaches as the density of the subducting part increases during eclogitization of the sinking material. Extension in the remaining upper crust enables additional asthenospheric inflow of hot mantle material to shallow depths; this results with ultra-high temperatures at very shallow levels (Figure 7.5, a, 10.4 Myr, 11.3 Myr, b temperatures over 1000 ^oC are recorded at depths of 30 km). Occurrence of such elevated temperatures (exceeding 1000 ^oC) promotes melting of different kinds of rocks. Due to localized input of hot material, rocks experience melting under different thermal conditions - from the center of the heat influx to its flanks. A large growing magma chamber forms, where magma mixing and mingling accounts for multiple melting events that strongly affect the petrological and geochemical evolution of these rocks. For example, more than 30 % of all magmatic rocks are remelted after decompression melting is triggered, despite the continued supply of new volcanic and plutonic rocks. The main melting event (Figure 7.4b) onsets after 9 Myr and lasts for 12 Myr, when decompression melting is introduced and fertile crustal material melts for the first time. Since high temperatures remain for over 10 Myr, rocks are exposed to periodic remelting and freezing episodes. Crystallized rocks may sink into partially molten melt reservoirs

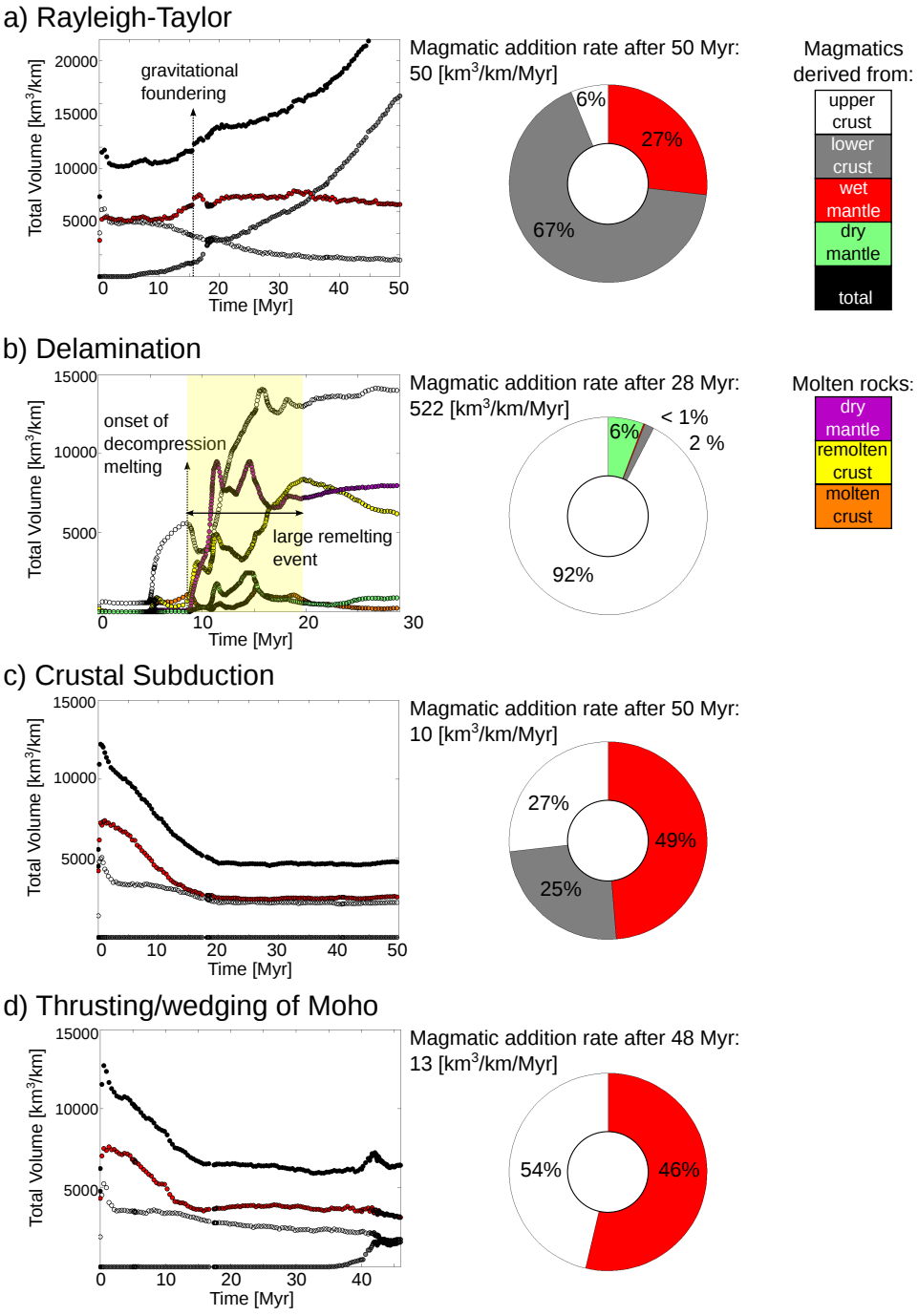

Figure 7.4: Magmatic consequences to intra-continental deformation in terms of magmatic addition $[km^3/km]$ for: a) Rayleigh Taylor instabilities (see Figure 7.3 for details) b) Crustal delamination (see Figure 7.5 for details) c) Crustal subduction (see Figure 7.6 for details) and c) Long-term crustal wedging (see Figure 7.7 for details). The subsequent pie charts illustrate the magmatic composition and total magmatic addition rate $[km^3/km/Myr]$ at the end of each simulation.

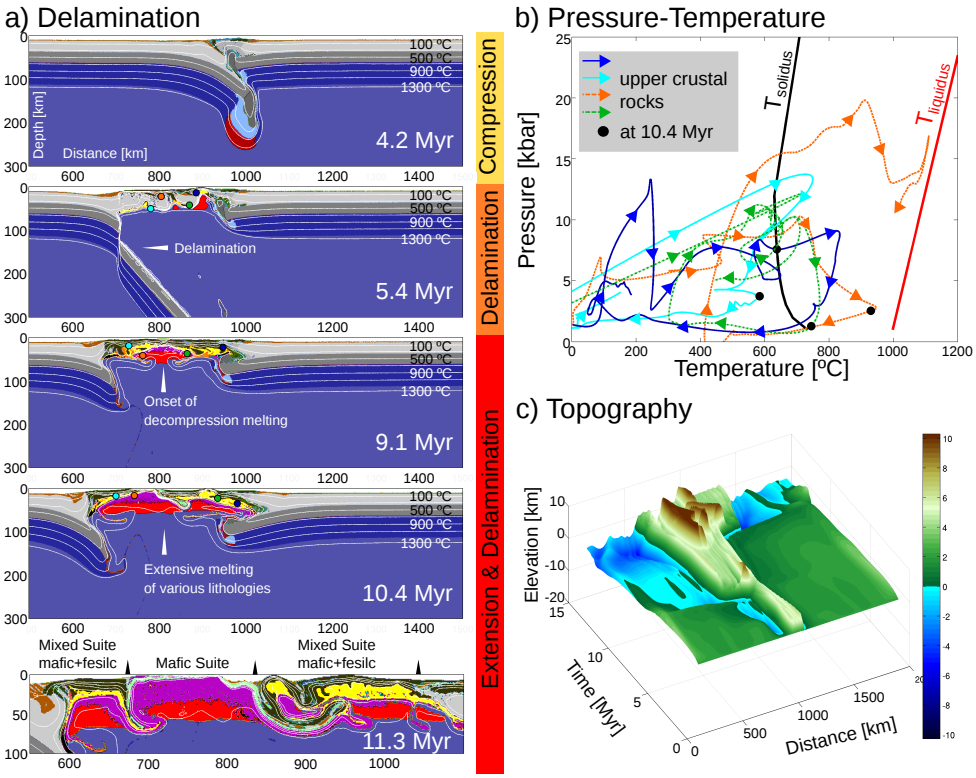

Figure 7.5: Delamination - mechanical removal/peeling away of the lithosphere. a) Dynamic evolution of the lithosphere after 6 Myr of convergence at a rate of 2 cm/yr and a lithospheric thickness of 100 km. Detachment of dense lithosphere develops an asymmetric geometry and allows for hot inflow of asthenospheric material. Hence, decompression melting is triggered and results in ultra-high temperatures at shallow levels and multiple melting and remelting events of crustal and mantle derived rocks. The temperature-pressure evolution of upper crustal rocks is shown in b). c) Topographic evolution with time. The initial uplift caused by compression is overprinted by a strong topographic response above the melt zone. Areas distant form the major melting event are characterized by the development of deep intra-continental basins.

and mobile melt may rise to upper levels where it solidifies before reaching densities high enough for foundering. However, after 20 Myr, decompression melting ceases and the fertile source becomes depleted. All subsequent melting events are related to remelting processes, as temperatures remain high enough to allow for crustal anatexis. The spatial distribution of rocks related to delamination and detachment is related to its tectonic evolution. Melting onsets from a central point with the highest temperatures and extension, which leads to continental breakup, and is dominated by mafic melts originating from the mantle. Farther to the sides of the initiation zone, the addition of the crustal material is observed and strong mixing and mingling of mafic and felsic material takes place. The melting zone is rimmed by a zone of thermally metamorphosed crustal rocks.

Strong topographic response is observed in the major melt zone, which overprints the initial topographic uplift resulting from compression. Areas distal from the major melting event are characterized by the development of deep intra-continental basins. This type of behaviour occurs for runs with 2 cm/yr convergence rate and lithospheric thickness of 60, 80 and 100 km (Figure 7.2).

Intra-continental subduction Model IV - 150km - mantle lithosphere depth, 3 cm/yr compression rate

Figure 7.6 represents the evolution of an experiment in which intra-continental subduction develops. In this case, crustal material underthrusts the weak zone, forming a major thrust boundary (crustal subduction zone, Figure 7.6a). Although partial melting of mantle and upper crustal rocks located at the crust mantle interface may commence in the course of compression, the amount of intrusive and extrusive rocks is negligible and melting only occurs at early stages (Figure 7.4c). This is in contrast to delamination or gravitational foundering, where the main melting event occurs at a later stage. Motion along this thrust boundary accounts for most of the shortening and deformation, which leads to a complex overall geometry involving surface subsidence and uplift (Figure 7.6b). In response to these thrust-related tectonics, large quantities of crustal material (upper and lower continental crust) may enter depths greater than 100 km but remain unaffected by melting because of the relatively cool thermal environment. After 10 Myr melting activity nearly diminishes (Figure 7.4c). Instead, rocks of the upper crust are subjected to strong structural reworking. Return flow in a subduction channel records low temperature (< 700 ^oC) and moderate pressure (< 50 kbar). The surface responds with high topographic relief above the subduction slab with a deep basin on one side.

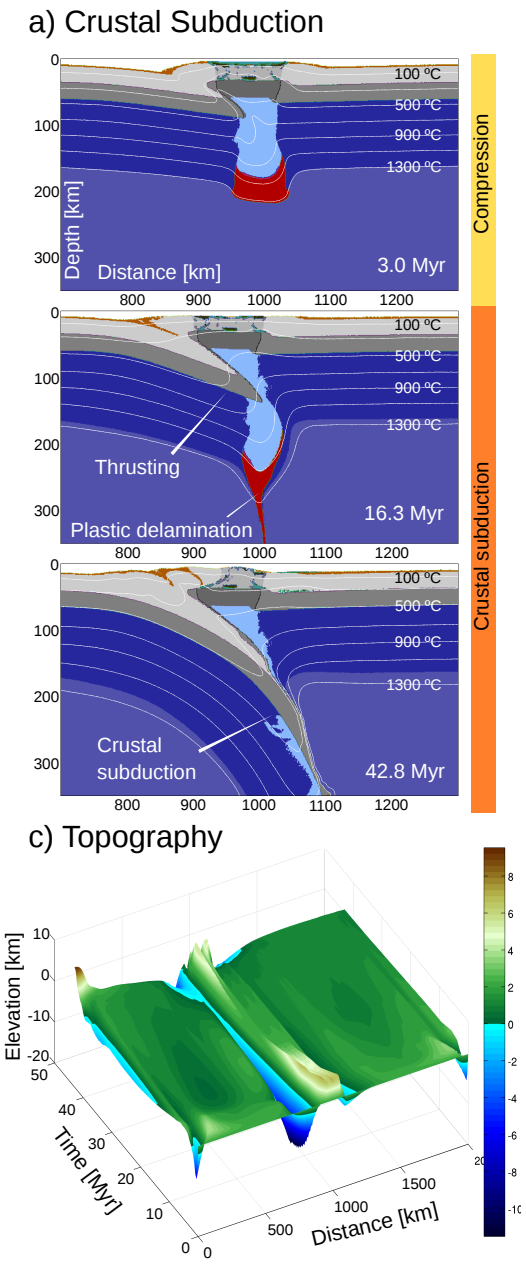

Figure 7.6: Intra-continental subduction. Dynamic evolution of the lithosphere after 6 Myr of convergence at a rate of 1 cm/yr and a lithospheric thickness of 150 km. a) Crustal material underthrusts the weak zone, forming a major thrust boundary, which accounts for most of the shortening/deformation. b) Topographic response with time. The surface expression related to the motion along the major thrust boundary includes surface subsidence and uplift, forming a deep-seated basin.

This configuration corresponds to the trench and mountains characteristic of conventional subduction settings. Intra-plate continental subduction typically forms where intermediate to thick continental lithosphere (Figure 7.2) is subjected to convergence rates greater than 1 cm/yr. This is similar to settings where pure gravitational instabilities are formed.

Long term wedging of the Moho. Model V - 200 km - mantle lithosphere depth, 1 cm/yr compression rate

Model V represents failed intra-plate subduction (Figure 7.7). The subducted material does not reach the eclogite stability field, thus does not reach the potential for the down-pull after far field compression is released. The dragged crustal material remains stagnant for an extended period of time $>$ 80 Myr, even after thermal equilibration; this can be described by a double Moho. The magmatic productivity is low and only attributes to partial melting of the mantle and upper continental crust at the onset of compression (Figure 7.4c). Trench-like basins develop, as initially the lithospheric material is subducted, which shallows with time as thermal equilibration takes place. As in the case of subduction, no melting events are observed due to low temperature of the environment. This type of behavior is characteristic for extra cold/old continental lithosphere (Figure 7.2).

7.5 Discussion

Mechanical removal of part of the lithosphere and melt production

There is a number of documented examples in nature indicating various ways of delamination of the lower part of the lithosphere that leads to extensive deformation, melt production, and topographic response. Some examples are: the Carpathian-Pannonian system of Eastern and Central Europe (Ren et al., 2012), the Proterozoic Nampula Complex, northern Mozambique (Ueda et al., 2012), lithospheric delamination beneath the Alboran Sea and Rif-Betic mountains (Seber et al., 1996), lithospheric delamination in the core of Pangea (Gutiérrez-Alonso et al., 2011), the Great Basin Drip in Nevada (West et al., 2009) and lithospheric deformation in the South Island of New Zealand (Pysklywec et al., 2002). It is important to note that in a number of areas the geodynamic interpretation is being now re-evaluated. One of the most exciting events is the Musgrave orogeny

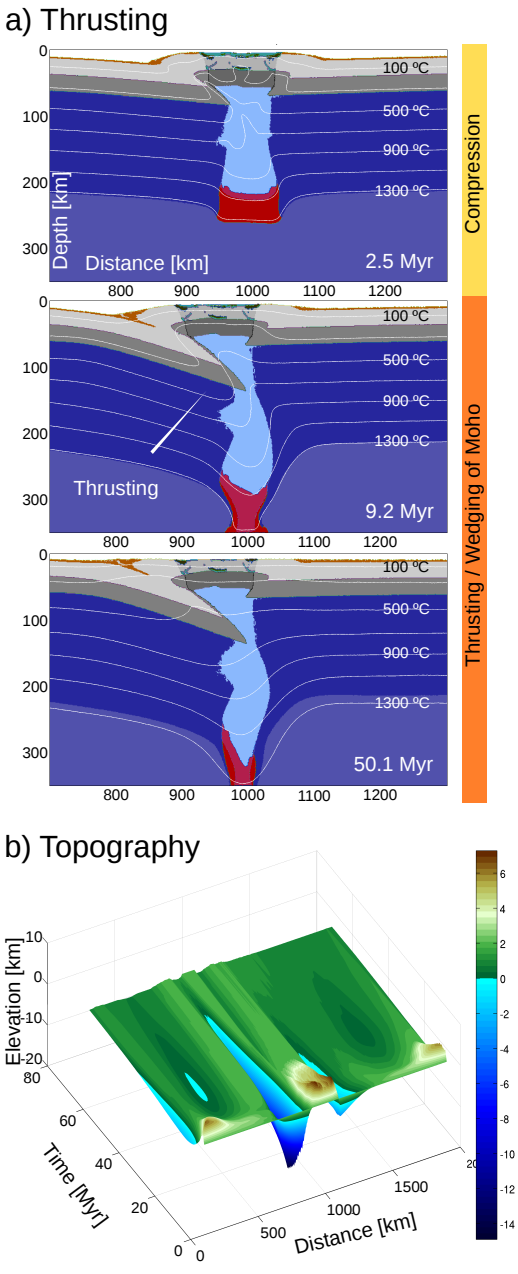

Figure 7.7: Long-term crustal wedging. Dynamic evolution of the lithosphere after 6 Myr of convergence at a rate of 1 cm/yr and a lithospheric thickness of 200 km. a) Similar to crustal subduction (Figure 7.6), crustal material underthrusts the weak zone, but does not subduct to greater depth, which results in long-term wedging of the Moho. b) Topographic evolution with time. Wedging of the Moho results in a trench-like basin.

in central Australia. This orogeny is interpreted as an intra-continental and dominantly extensional event in which ultrahigh-temperature (UHT) conditions persisted from c. 1220 to c. 1120 Ma (Smithies et al., 2011). The duration of UHT conditions is inconsistent with a mantle plume and reflects an intracontinental lithospheric architecture where the Musgrave Province was rigidly fixed at the nexus of three thick cratonic masses. This tectonic scenario could have lead to focusing of asthenospheric upwelling beneath this province, providing a constant supply of both heat and mantle-derived magma. The onset of UHT conditions is heralded by a change from low-Yb granites to voluminous Yb enriched granites, reflecting a rapid decrease in crustal thickness. The Pitjantjatjara granites are ferroan, calc-alkalic to alkali-calcic rocks, and include charnockites with an orthopyroxene bearing primary mineralogy. Such a scenario could be explained by mechanical delamination of part of the weakened lithosphere that is at the junction of three major cratonic bodies, similar to the scenarios presented in Figure 7.5. Although the time span of the Musgrave orogeny is a few times longer than the one shown in this set of numerical models, the process of delamination seems to be a best fit for this particular geological scenario, especially when the supply of hot material from asthenosphere and remelting of the crustal material is consistent with available geochemical data.

The eastern North China Craton (NCC) west of the Pacific Ocean has a long history of rifting from Early Cretaceous to the end of Paleogene when the craton experienced destruction and significant thinning of the lithosphere. The cause and geotectonic environment for this destruction remain controversial. The main processes proposed in previous studies are delamination (Gao et al., 2009), thermal-chemical erosion (Menzies et al., 1993; Menzies and Xu, 1998; Xu, 2001) and deformation/destruction in an extensional back arc tectonic setting (Xu et al., 2012). The latest work on pyroxenitic xenoliths entrained by Early Cretaous Flaxian basalts reveals that the ancient peridotitic lithospheric mantle was modified to form pyroxenitic mantle via a reaction between peridotite and melt derived from recycled continental crust. It also implies that the formation of pyroxenitic mantle was induced by delamination (Xu et al., 2012). Gao et al. (2009) indicated delamination as the key process for fertilization of depleted Archean mantle and introduction of felsic melts which were exposed to multiple-melting events. As in case of Musgrave orogeny the timing of the delamination presented in Figure 7.5 is inconsistent with geological records, but the bulk characteristic of the geological and geochemical data (i.e.: adakitic magmas, high-Mg diorite) are consistent with

the delamination model proposed in this paper.

Adakites are considered by many to be associated with subduction zones. However, the origins of some adakitic rocks have also been attributed to several alternative mechanisms, such as partial melting of thickened lower crust or delaminated mafic lower crust, and to assimilation and fractional crystallization (AFC) processes acting on mantle-derived mafic magmas (i.e.: Castillo et al., 1999; Kay and Mahlburg Kay, 1993; Smithies, 2000). As an example we address here felsic adakites in the Yangtze Block and the Dabie Orogen, eastern China (Wang et al., 2007). Field relations, isotope systematics, and plate tectonic reconstructions clearly indicate that they were not derived from a subducting slab. They are thought to originate from deep melting of the lower crust, and can occur after delamination of gravitational instability, as a result of thermal equilibration of the system and fast temperature increase at the base of the Moho. See the numerical results in Figure 7.3.

Several anorthosite provinces coincide with structural weakness in the lithosphere, which appear to have controlled and favoured the emplacement of the diapirs. Indeed, the Nain anorthosite province straddles the limit between the Nain and Churchill (Rae) Provinces (Emslie et al., 1994; Wiebe, 1992); the Lac St Jean and Havre-St. Pierre anorthosite complexes and are associated with long lineaments (van Breemen and Higgins, 1993; Higgins and van Breemen, 1992); in the Laramie anorthosite complex two generations of anorthosites are linked to a terrane boundary (Scoates and Chamberlain, 1997); Suwalki anorthosite was emplaced in the Svecofennian platform along an EW lineament (Wiszniewska et al., 1999). Duchesne et al. (1999) present a tongue melting model that is consistent with the gravitational instability model presented in Figure 7.3 for the origin of some anorthosites, and account for the crustal origin of anorthosite parent magmas. Duchesne et al. (1999) conceptual model indicates the importance of deep lithospheric tectonic structures in producing a variety of magmas, from granitic to high alumina basaltic, and in controlling their emplacement.

A number of post-collisional granites in Sveconorvegian Province are related to major terrane boundaries (Andersson et al., 1996).

The origin of voluminous anorthosite, mangerite, charnockite, granite, and related granitoids (AMCG complexes: Emslie, 1978) in the Mesoproterozoic Grenville province is a matter of considerable debate (Corrigan and Hanmer, 1997). The association of crustal thickening, emplacement of mafic dikes and voluminous mantle-derived melts, sedimentation within an intraplate setting, and syncollisional extension can be best explained by re-

placement of the continental mantle lithosphere by asthenosphere during crustal shortening. Replacement of lithosphere by asthenosphere is predicted by convective thinning models, providing a viable mechanism for such a process during convergent tectonism, and does not necessitate the postulation of a mantle plume beneath a supercontinent (i.e.: Hofmann, 1997) nor postcollisional extension (i.e. Windley, 1991). With respect to the Grenvillian orogeny, the convective thinning model provides a plausible way to explain the episodic nature of AMCG-type magmatism synchronous with contractional tectonics. In addition, it provides a mechanism to explain the important contribution of mantle-derived heat that is necessary for the formation of anorthosite (Emslie, 1978) which is also implied from the generally high ambient grade of metamorphism accompanying AMCG-type magmatism (Corrigan and Hanmer, 1997).

Intra-continental subduction

The Dabie-Sulu ultra-high pressure metamorphic (UHPM) belt in eastern China is one of the type UHPM terranes known on Earth, which is explained by intracontinental subduction of Yangtze craton underneath the North China craton (Zhao et al., 2011). This intra-continetal subduction is taking place in relatively thick continental lithosphere, what is consistent with results presented in Figure 7.6.

Long term wedging of the Moho

Perhaps the most interesting aspect of the Petermann orogeny (Central Australia) architecture is the emplacement of a wedge of lithospheric mantle within the lower crust, and its preservation for more than 500 million years despite local isostatic disequilibrium and a number of major tectonic events elsewhere in the continent. The preservation of the crust-mantle boundary offset implies that this block of lithosphere is sufficiently strong to resist tectonic and isostatic forces (Aitken et al., 2009). Such a behaviour one can observe in numerical results in Figure 7.7.

7.6 Summary and Conclusions

Over last few decades it has been shown that continents, are composed of various lithospheric domains with different ages and tectonic histories (i.e.: Begg et al., 2009; O'Reilly and Griffin, 1996). They have been agglomerated through orogenic processes that generated a pervasive tectonic

fabric within the colliding continents. Even in the absence of orogenesis, continents are subjected to intraplate processes (i.e., rifting, thrusting, buckling) that may produce local thermal/rheological perturbations. A more realistic model for continental lithosphere would be one that is mechanically heterogeneous and anisotropic. In this work we have raised the question of the influence of pre-existing rheological heterogeneities and mechanical anisotropy on the deformation of continents. The systematic numerical studies have not only indicated that preexisting zones of weakness are crucial in localization of deformation and melting, as recently presented by Gorczyk et al. (2011) and (Bajolet et al., 2012), but also show that additional factors play a key role in tectonic and magmatic response in the area of deformation. Diagram in Figure 7.2 illustrates that the thickness of the lithosphere and initial compression rate (in this study initial 6 Myr) strongly influence the tectonic and magmatic processes in the weak/deformation zone.

- (1) Young, relatively thin continental lithosphere (60 - 100 km) is mostly subjected to delamination processes. As the lowermost part of the weakened lithosphere delaminates it can trigger further responses. The subsequent reactions of the lithosphere are dependent on the rate of compression. As the convergence increases the delamination/deformation is more pronounced. For the compression rates 1 cm/yr, the lithosphere delaminates in plastic or gravitational manner. The related magmatism is more pronounced for 100 km thickness and 1 cm/yr, thus it is still only limited to the lower crust. Extremely hot lithospheres are too flexible to for very low compression rates to deform. Higher compression rates 2 cm/yr, trigger stronger asymmetric deformation/delamination, which leads to introduction of hot asthenospheric material to shallow levels. Consequently, the vast amounts of melts (crustal and mantle) are produced (Figure 7.4b, magmatic addition rate after 28 Myr exceeds 500 $km^3/km/Myr$), and rejuvenation of the lithosphere is observed. At 3 cm/yr compression rate, the lithosphere can continue subducting after it is liberated from far filed stress.

- (2) Old continental lithosphere (150 - 300 km), due to its rigidity, exhibits on one-hand, a strong tectonic deformation and on the other very limited melt production. The deformation rate increases with compression rate. Very thick continental lithosphere (300 km) thrusts and may exhibit wedging of the Moho (double Moho) for extended periods of time 80 Myr. In younger lithosphere intracontinental subduction is observed. This case is characterized by

metamorphism of the upper crustal material, which is trapped and transported in a subduction channel that develops along the thrust.

Continental suture zones (weak zones) exposed to compression can respond in 4 types of tectonic deformation: (1) gravitational instability with melting of the lower crust, (2) peeling of part of the lithosphere with bi-modal magmatics, (3) intra-continental subduction and (4) wedging of the Moho exhibiting very little magmatic activity.

Bibliography

Aitken, A. R., Betts, P. G., Ailleres, L., 2009. The architecture, kinematics, and lithospheric processes of a compressional intraplate orogen occurring under gondwana assembly: The petermann orogeny, central australia. Lithosphere 1 (6), 343–357.

Allégre, C. J., Turcotte, D. L., 1985. Geodynamic mixing in the mesosphere boundary layer and the origin of oceanic islands. Geophysical Research Letters 12 (4), 207–210.
URL http://dx.doi.org/10.1029/GL012i004p00207

Andersson, M., Lie, J., Husebye, E., 1996. Tectonic setting of post-orogenic granites within sw fennoscandia based on deep seismic and gravity data. Terra Nova 8 (6), 558–566.

Bajolet, F., Galeano, J., Funiciello, F., Moroni, M., Negredo, A.-M., Faccenna, C., 2012. Continental delamination: Insights from laboratory models. Geochemistry Geophysics Geosystems 13 (null), Q02009.

Begg, G., Griffin, W., Natapov, L., O'Reilly, S. Y., Grand, S., O'Neill, C., Hronsky, J., Djomani, Y. P., Swain, C., Deen, T., et al., 2009. The lithospheric architecture of africa: Seismic tomography, mantle petrology, and tectonic evolution. Geosphere 5 (1), 23–50.

Begg, G. C., Hronsky, J. A., Arndt, N. T., Griffin, W. L., OReilly, S. Y., Hayward, N., 2010. Lithospheric, cratonic, and geodynamic setting of ni-cu-pge sulfide deposits. Economic Geology 105 (6), 1057–1070.

Bird, P., 1978. Initiation of intracontinental subduction in the himalaya. Journal of Geophysical Research 83 (B10), 4975–4987.

Bird, P., 1979. Continental delamination and the colorado plateau. Journal of Geophysical Research 84 (B13), 7561–7571.

Castillo, P. R., Janney, P. E., Solidum, R. U., 1999. Petrology and geochemistry of camiguin island, southern philippines: insights to the source of adakites and other lavas in a complex arc setting. Contributions to Mineralogy and Petrology 134 (1), 33–51.

Condie, K., 2001. Mantle plumes and continental growth. In: Mantle plumes and their record in earth history. Cambridge University press.

Corrigan, D., Hanmer, S., 1997. Anorthosites and related granitoids in the grenville orogen: A product of convective thinning of the lithosphere? Geology 25 (1), 61–64.

Cruden, A., Nasseri, M., Pysklywec, R., 2006. Surface topography and internal strain variation in wide hot orogens from three-dimensional analogue and two-dimensional numerical vice models. Geological Society, London, Special Publications 253, 79–104.

Davies, G. F., 1988. Ocean bathymetry and mantle convection 1. large-scale flow and hotspots. Journal of Geophysical Research 93 (B9), 10467–10.

Dobretsov, N., Borisenko, A., Izokh, A., Zhmodik, S., 2010. A thermochemical model of eurasian permo-triassic mantle plumes as a basis for prediction and exploration for cu-ni-pge and rare-metal ore deposits. Russian geology and geophysics 51 (9), 903–924.

Duchesne, J.-C., Liégeois, J.-P., Vander Auwera, J., Longhi, J., 1999. The crustal tongue melting model and the origin of massive anorthosites. Terra Nova 11 (2-3), 100–105.

Elkins-Tanton, L. T., 2007. Continental magmatism, volatile recycling, and a heterogeneous mantle caused by lithospheric gravitational instabilities. Journal of Geophysical Research 112 (B3), B03405.

Emslie, R., 1978. Anorthosite massifs, rapakivi granites, and late proterozoic rifting of north america. Precambrian Research 7 (1), 61–98.

Emslie, R., Hamilton, M., Theriault, R., 1994. Petrogenesis of a mid-proterozoic anorthosite-mangerite-charnockite-granite (amcg) complex: Isotopic and chemical evidence from the nain plutonic suite. The Journal of Geology, 539–558.

Faccenna, C., Becker, T. W., 2010. Shaping mobile belts by small-scale convection. Nature 465 (7298), 602–605.

Gao, S., Zhang, J., Xu, W., Liu, Y., 2009. Delamination and destruction of the north china craton. Chinese Science Bulletin 54 (19), 3367–3378.

Göğüş, O. H., Pysklywec, R. N., 2008. Near-surface diagnostics of dripping or delaminating lithosphere. Journal of Geophysical Research 113 (B11), B11404.

Gorczyk, W., Guillot, S., Gerya, T. V., Hattori, K., 2007. Asthenospheric upwelling, oceanic slab retreat, and exhumation of uhp mantle rocks: Insights from greater antilles. Geophysical Research Letters 34 (21), L21309.

Gorczyk, W., Hobbs, B., Gerya, T., 2011. Initiation of rayleigh-taylor instabilities in intra-cratonic settings. Tectonophysics.

Gutiérrez-Alonso, G., Murphy, J. B., Fernández-Suárez, J., Weil, A. B., Franco, M. P., Gonzalo, J. C., 2011. Lithospheric delamination in the core of pangea: Sm-nd insights from the iberian mantle. Geology 39 (2), 155–158.

Harig, C., Molnar, P., Houseman, G. A., 2010. Lithospheric thinning and localization of deformation during rayleigh-taylor instability with nonlinear rheology and implications for intracontinental magmatism. Journal of Geophysical Research 115 (B2), B02205.

Higgins, M. D., van Breemen, O., 1992. The age of the lac-saint-jean anorthosite complex and associated mafic rocks, grenville province, canada. Canadian Journal of Earth Sciences 29 (7), 1412–1423.

Hofmann, A., 1997. Mantle geochemistry: the message from oceanic volcanism. Nature 385 (6613), 219–229.

Houseman, G., McKenzie, D. P., 1982. Numerical experiments on the onset of convective instability in the earth's mantle. Geophysical Journal of the Royal Astronomical Society 68 (1), 133–164.

Houseman, G. A., McKenzie, D. P., Molnar, P., 1981. Convective instability of a thickened boundary layer and its relevance for the thermal evolution of continental convergent belts. Journal of Geophysical Research: Solid Earth 86 (B7), 6115–6132.
URL `http://dx.doi.org/10.1029/JB086iB07p06115`

Houseman, G. A., Molnar, P., 2007. Gravitational (rayleigh-taylor) instability of a layer with non-linear viscosity and convective thinning of

continental lithosphere. Geophysical Journal International 128 (1), 125–150.

Kay, R. W., Mahlburg Kay, S., 1993. Delamination and delamination magmatism. Tectonophysics 219 (1), 177–189.

Lenardic, A., Moresi, L., Miihlhaus, H., 2000. The role of mobile belts for the longevity of deep. Geophysical research letters 27 (8), 1235–1238.

Lenardic, A., Moresi, L.-N., Mühlhaus, H., 2003. Longevity and stability of cratonic lithosphere: insights from numerical simulations of coupled mantle convection and continental tectonics. Journal of Geophysical Research 108 (B6), 2303.

McKenzie, D., O'nions, R., 1983. Mantle reservoirs and ocean island basalts. Nature 301, 229–231.

Meibom, A., Anderson, D. L., Sleep, N. H., Frei, R., Chamberlain, C. P., Hren, M. T., Wooden, J. L., 2003. Are high $^3He/^4He$ ratios in oceanic basalts an indicator of deep-mantle plume components? Earth and Planetary Science Letters 208 (3), 197–204.

Menzies, M. A., Fan, W., Zhang, M., 1993. Palaeozoic and cenozoic lithoprobes and the loss of¿ 120 km of archaean lithosphere, sino-korean craton, china. Geological Society, London, Special Publications 76 (1), 71–81.

Menzies, M. A., Xu, Y., 1998. Geodynamics of the north china craton. Geodynamics Series 27, 155–165.

Morgan, W. J., 1971. Convection plumes in the lower mantle.

O'Reilly, S., Griffin, W., 1996. 4-d lithosphere mapping: methodology and examples. Tectonophysics 262 (1), 3–18.

Piriz, A., Cela, J. L., Cortazar, O., Tahir, N., Hoffmann, D., 2005. Rayleigh-taylor instability in elastic solids. Physical Review E 72 (5), 056313.

Pysklywec, R. N., Beaumont, C., Fullsack, P., 2002. Lithospheric deformation during the early stages of continental collision: Numerical experiments and comparison with south island, new zealand. Journal of geophysical research 107 (B7), 2133.

Ranalli, G., 1995. Rheology of the Earth. Springer.

Ren, Y., Stuart, G., Houseman, G., Dando, B., Ionescu, C., Hegedüs, E., Radovanović, S., Shen, Y., 2012. Upper mantle structures beneath the carpathian–pannonian region: Implications for the geodynamics of continental collision. Earth and Planetary Science Letters 349, 139–152.

Robinson, A. C., Swegle, J., 1989. Acceleration instability in elastic-plastic solids. ii. analytical techniques. Journal of Applied Physics 66 (7), 2859–2872.

Scoates, J. S., Chamberlain, K. R., 1997. Orogenic to post-orogenic origin for the 1.76 ga horse creek anorthosite complex, wyoming, usa. The Journal of Geology 105 (3), 331–344.

Seber, D., Barazangi, M., Ibenbrahim, A., Demnati, A., 1996. Geophysical evidence for lithospheric delamination beneath the alboran sea and rif–betic mountains.

Smithies, R., 2000. The archaean tonalite–trondhjemite–granodiorite (ttg) series is not an analogue of cenozoic adakite. Earth and Planetary Science Letters 182 (1), 115–125.

Smithies, R., Howard, H. M., Evins, P., Kirkland, C., Kelsey, D. E., Hand, M., Wingate, M., Collins, A. S., Belousova, E., 2011. High-temperature granite magmatism, crust–mantle interaction and the mesoproterozoic intracontinental evolution of the musgrave province, central australia. Journal of Petrology 52 (5), 931–958.

Sobolev, S. V., Sobolev, A. V., Kuzmin, D. V., Krivolutskaya, N. A., Petrunin, A. G., Arndt, N. T., Radko, V. A., Vasiliev, Y. R., 2011. Linking mantle plumes, large igneous provinces and environmental catastrophes. Nature 477 (7364), 312–316.

Sokoutis, D., Willingshofer, E., 2011. Decoupling during continental collision and intra-plate deformation. Earth and Planetary Science Letters 305 (3), 435–444.

Swegle, J., Robinson, A. C., 1989. Acceleration instability in elastic-plastic solids. i. numerical simulations of plate acceleration. Journal of Applied Physics 66 (7), 2838–2858.

Ueda, K., Gerya, T., Burg, J.-P., 2012. Delamination in collisional orogens: Thermomechanical modeling. Journal of Geophysical Research-Solid Earth 117, doi:10.1029/2012JB009144.

van Breemen, O., Higgins, M. D., 1993. U-pb zircon age of the southwest lobe of the havre-saint-pierre anorthosite complex, grenville province, canada. Canadian Journal of Earth Sciences 30 (7), 1453–1457.

Wang, Q., Wyman, D. A., Xu, J.-F., Zhao, Z.-H., Jian, P., Zi, F., 2007. Partial melting of thickened or delaminated lower crust in the middle of eastern china: Implications for cu-au mineralization. The Journal of geology 115 (2), 149–161.

West, J. D., Fouch, M. J., Roth, J. B., Elkins-Tanton, L. T., 2009. Vertical mantle flow associated with a lithospheric drip beneath the great basin. Nature Geoscience 2 (6), 439–444.

White, R., McKenzie, D., 1989. Magmatism at rift zones: The generation of volcanic continental margins and flood basalts. Journal of Geophysical Research: Solid Earth 94 (B6), 7685–7729.
URL http://dx.doi.org/10.1029/JB094iB06p07685

Wiebe, R., 1992. Proterozoic anorthosite complexes. Developments in Precambrian Geology 10, 215–261.

Wilson, J. T., 1963. A possible origin of the hawaiian islands. Canadian Journal of Physics 41 (6), 863–870.

Windley, B. F., 1991. Early proterozoic collision tectonics, and rapakivi granites as intrusions in an extensional thrust-thickened crust: the ketilidian orogen, south greenland. Tectonophysics 195 (1), 1–10.

Wiszniewska, J., Duchesne, J., Claesson, S., Stein, H., Morgan, J., 1999. Geochemical constraints on the origin of the suwalki anorthosite massif and related fe-ti-v ores, ne poland (abstract presented at eug 10). J. Conf. Abstr. 4, 686.

Xu, W.-L., Zhou, Q.-J., Pei, F.-P., Yang, D.-B., Gao, S., Li, Q.-L., Yang, Y.-H., 2012. Destruction of the north china craton: Delamination or thermal/chemical erosion? mineral chemistry and oxygen isotope insights from websterite xenoliths. Gondwana Research.

Xu, Y.-G., 2001. Thermo-tectonic destruction of the archaean lithospheric keel beneath the sino-korean craton in china: Evidence, timing and mechanism. Physics and Chemistry of the Earth, Part A: Solid Earth and Geodesy 26 (9), 747–757.

Yoshida, M., 2010. Preliminary three-dimensional model of mantle convection with deformable, mobile continental lithosphere. Earth and Planetary Science Letters 295 (1), 205–218.

Yoshida, M., 2012. Dynamic role of the rheological contrast between cratonic and oceanic lithospheres in the longevity of cratonic lithosphere: A three-dimensional numerical study. Tectonophysics.

Zhao, Z., Niu, Y., Christensen, N., Zhou, W., Hou, Q., Zhang, Z., Xie, H., Zhang, Z., Liu, J., 2011. Delamination and ultra-deep subduction of continental crust: constraints from elastic wave velocity and density measurement in ultrahigh-pressure metamorphic rocks. Journal of Metamorphic Geology 29 (7), 781–801.

Chapter 8

Outlook

8.1 Thesis Summary

The continental crust grows by the magmatic and amagmatic contribution to its base and along its margins. Partial melting in subduction zones and intra-plate settings leads to juvenile crust production, forming spectacular magma eruptions in near-surface regions or large growing magma bodies at subcrustal levels. Mechanical addition of crustal units along active continental margins can result in terrane accretion or amalgamation, forming large and rapid growing segments, all of which has magmatic, structural and metamorphic implications. More importantly, these processes can be closely related to each other, as magmatism may lead to rifting and accretion can induce melting.

Chapter 3

Chapter 3 discusses how fluid ascent and melt percolation may influence the tectonic setting and hence melt production. Three distinct settings are discussed: stable arcs, compressional arcs and extensional arcs. Melt production in "stable arcs" is mainly attributed to partial melting of the oceanic crust at early stages and hydrated mantle at later stages, resulting in "flux melting" of the metasomatized mantle. In contrast, partial melting of slab components (i.e.: sediment, basalt), is a common feature of "compressional arcs". Tectonic rock mélanges, composed of sediment, basalt and hydrated/serpentinized mantle, melt at asthenospheric depth, enabling the formation of composite diapirs. Such diapirs rise through the mantle transporting crustal material (i.e. sediment, basalt) through the hot mantle wedge prior to emplacement at upper crustal levels. Crust formation in "extensional arcs" is associated with extensive decompression

melting of dry peridotite and ocean floor development.

Chapter 4

Chapter 4 evaluates the petrological and geochemical consequences of crustal relamination. Composite diapirs formed in "compressional arcs" transport crustal components of varying proportions (i.e.: sediment and basalt) throughout the mantle. Based on mass balance considerations and previous experimental studies it is shown that partial melting of theses components, yields granodioritic melt with a relatively stable major element composition, but substantial changes in terms of radiogenic isotopes. These changes are related to the differing proportions of the endmenbers (i.e.: sediment, basalt) in the source. It is concluded that crustal relamination accounts for the bulk composition of the continental crust and may be an important process by which crustal material is recycled.

Chapter 5

Chapter 5 explores different tectonic modes of, and tectonic responses to, terrane accretion or its deep subduction along active continental margins. The age of the subducting plate is shown to be a crucial parameter controlling if and how oceanic plateaus are accreted onto continental crust. While oceanic plateaus embedded in young oceanic lithosphere are likely to be accreted onto continental crust, oceanic plateaus surrounded by older lithosphere will be lost by subduction. Tectonic responses to plateau accretion include, surface uplift and subsidence, crustal thickening, juvenile melt production and crustal reworking, slab break off and slab transference. Hence it is concluded that terrane accretion may not only result in rapid growth of the continental crust, but may also modify the subduction zone system.

Chapter 6

Chapter 6 investigates tectonic responses to subduction of serpentinized slabs along active continental margins. Because progressive hydration related to bending related faulting in the outer trench region may result in extensive serpentinization of the uppermost mantle, a mechanically weak horizon is expected to develop (below the oceanic crust). The strong rheological contrast between this layer (mechanically weak serpentine) and the oceanic crust (strong) is shown to enable, decoupling, imbrication and separation of the oceanic crust from the downgoing slab. While the skinned

lithospheric part of the slab sinks into the mantle, remnants of the former oceanic crust underplate the accretionary wedge or form ophiolitic complexes at upper crustal levels. The tectonic consequences of such a behaviour have implications to accretionary tectonics and arc magmatism.

Chapter 7

Chapter 7 demonstrates how suture zones, so-called mobile belts, can influence intra-cratonic deformation and melt production. If subjected to compressional forces such suture zones are shown to result in crustal reworking and structural complexity, which is sensitive to lithospheric age and tectonic setting (i.e. convergence rate). A wide range of instabilities may develop (Rayleigh-Taylor instabilities, crustal delamination, crustal subduction, wedging of Moho), which influences localization of deformation, topographic evolution, melt generation and melt intrusion. Hence, it is concluded that crustal growth in intra-cratonic settings could be strongly controlled by lateral lithospheric heterogeneities inherited from fossil subduction/amalgamation settings.

8.2 Magma emplacement in 3D

Introduction

Magma generation and emplacement is an important material and geochemical transfer process (e.g. Petford et al., 2000) that shapes much of Earth continental crust (Menand, 2011). Molten material formed in deeper crustal levels or below the lithosphere contributes to the growth of the continental crust (Anderson, 1994; Tatsumi and Eggins, 1995; Schmidt and Poli, 1998), forming magma eruptions in near-surface regions or large growing magma bodies at subcrustal levels. Understanding the physical processes involved in magma generation and its emplacement requires knowledge about the geochemical and physical properties of melt (e.g. Dingwell and Webb, 1989, 1990; Webb and Dingwell, 1990; Giordano et al., 2008), magma (melt plus crystals) (e.g. Pinkerton and Sparks, 1978; Dingwell et al., 1993; Petford, 2003; Caricchi et al., 2007) and host lithologies (Parsons et al., 1992; Menand, 2008; Ferré et al., 2012; Gerya and Burg, 2007). Different magma sources, melting conditions and differentiation processes have been discussed in the literature to account for the basaltic and andesitic magmatism that operates on Earth surface (e.g. Rudnick, 1995; Schmidt and Poli, 1998; Tatsumi, 2005; Annen et al., 2006; Hacker et al., 2011; Behn et al., 2011; Richards et al., 1989). However,

it is becoming increasingly apparent that magma evolution is intrinsically related to its transport mechanism, controlling emplacement depths, structures and petrogenesis. Transport mechanisms that have been proposed in the past can be divided into two main groups, processes that consider diapiric-like emplacement (Cruden, 1990; Weinberg and Podladchikov, 1994; Miller and Paterson, 1999) and those that favour magma ascent in dikes (Clemens and Mawer, 1992; Petford, 1996; Petford et al., 2000). However, Weinberg (1996) argued that magma ascent is probably a combination of both processes, which may simultaneously or sequentially control ascent and emplacement. On the other hand, crustal heterogeneities, rheological anisotropies and local and far field stresses are likely to play a key role in magma emplacement (e.g. Vigneresse et al., 1999; Galland et al., 2006; Kavanagh et al., 2006; Menand, 2008, 2011; Ferré et al., 2012). Feedbacks between these processes are crucial for our understanding of how and where magma is stored (Menand, 2011).

Despite the fast growing volume of geological, geophysical and experimental data on magma rheology, chemistry, structure and emplacement, numerical simulations on the dynamics of magma ascent and emplacement are comparably rare. Because numerical studies devoted to magmatism have mainly focused on the internal dynamics of magma chambers (e.g. Bergantz, 2000; Longo et al., 2006; Dufek and Bachmann, 2010), little is known about the visco-brittle/plastic interplay between magma and crust. In one of the few studies on magma rise and emplacement, Gerya and Burg (2007) have demonstrated the importance of host rock rheology upon emplacement in a two dimensional setting. However, emplacement dynamics are intrinsically three dimensional phenomena and two dimensional studies lack to resolve the different shapes of magma, such as cone shaped, saucer shaped, funnel shaped and tabular intrusions. In spite of this, there is a long standing debate of how and if magma emplacement is controlled by preexisting shear zones and fractures (e.g. Hutton et al., 1990; Brown and Solar, 1998; Paterson and Schmidt, 1999; Weinberg et al., 2004; Ferré et al., 2012) that needs to be resolved by means of numerical modelling.

Numerical model

Computational strategy

The numerical model is based on the I3VIS code (Gerya, 2012) and resolves magma ascent and emplacement on a lithospheric to upper mantle cross-section in three dimensions. It combines a conservative finite differences method employed on a uniformly spaced staggered grid in Eulerian config-

uration and a non diffusive marker in cell technique with a multigrid solver (Gerya and Yuen, 2003, 2007; Gerya, 2010, 2012). The computational domain is 98 km long, 98 km wide, and 151 km deep, with a corresponding resolution of 197 × 197 × 309 nodes in x, z, y direction, which corresponds to an effective resolution of 0.5 km in each direction. The mass, momentum and energy equation are solved on the Eulerian grid, while transport properties are advected with Lagrangian markers (e.g. Zhu et al., 2009).

Governing equations

Continuity equation

The incompressible continuity equation takes the form:

$$\frac{\partial v_x}{\partial x} + \frac{\partial v_y}{\partial y} + \frac{\partial v_z}{\partial z} = 0$$

Momentum equation

The Stokes equation for slow flow is computed from:

$$\frac{\partial \sigma'_{xx}}{\partial x} + \frac{\partial \sigma_{xy}}{\partial y} + \frac{\partial \sigma_{xz}}{\partial z} = \frac{\partial P}{\partial x}$$

$$\frac{\partial \sigma_{xy}}{\partial x} + \frac{\partial \sigma'_{yy}}{\partial y} + \frac{\partial \sigma_{yz}}{\partial z} = \frac{\partial P}{\partial y}$$

$$\frac{\partial \sigma_{xz}}{\partial x} + \frac{\partial \sigma_{yz}}{\partial y} + \frac{\partial \sigma'_{zz}}{\partial z} = \frac{\partial P}{\partial z} - \rho(P,T,C)g_z$$

where σ'_{xx}, σ_{xy}, σ_{xz}, σ'_{yy}, σ_{yz}, σ'_{zz} are the deviatoric stress tensor components, P is pressure and ρ is the density, which depends on pressure (P), temperature (T) and composition (C).

This is followed by the constitutive relationship between deviatoric stress (σ'_{ij}) and strain-rate ($\dot{\varepsilon}$) for an incompressible fluid:

$$\sigma'_{xx} = 2\eta\dot{\varepsilon}_{xx}, \sigma'_{yy} = 2\eta\dot{\varepsilon}_{yy}, \sigma'_{zz} = 2\eta\dot{\varepsilon}_{zz}$$

$$\sigma_{xy} = 2\eta\dot{\varepsilon}_{xy}, \sigma_{xz} = 2\eta\dot{\varepsilon}_{xz}, \sigma_{yz} = 2\eta\dot{\varepsilon}_{yz}$$

where, η represents the viscosity, which depends on pressure (P), temperature (T), composition (C) and strain rate($\dot{\varepsilon}$):

$$\dot{\varepsilon}_{xx} = \frac{\partial v_x}{\partial_x}, \dot{\varepsilon}_{yy} = \frac{\partial v_y}{\partial_y}, \dot{\varepsilon}_{zz} = \frac{\partial v_z}{\partial_z}$$

$$\dot{\varepsilon}_{xy} = \frac{1}{2}\left(\frac{\partial v_x}{\partial_y} + \frac{\partial v_y}{\partial_x}\right), \dot{\varepsilon}_{xz} = \frac{1}{2}\left(\frac{\partial v_x}{\partial_z} + \frac{\partial v_z}{\partial_x}\right), \dot{\varepsilon}_{yz} = \frac{1}{2}\left(\frac{\partial v_y}{\partial_z} + \frac{\partial v_z}{\partial_y}\right)$$

Energy equation

The heat conservation equation takes the form:

$$\rho C_p \left(\frac{DT}{Dt}\right) = -\frac{\partial q_x}{\partial x} - \frac{\partial q_y}{\partial y} - \frac{\partial q_z}{\partial z} + H_r + H_a + H_s$$

$$q_x = -k(P,T,C)\frac{\partial T}{\partial x}$$
$$q_y = -k(P,T,C)\frac{\partial T}{\partial y}$$
$$q_z = -k(P,T,C)\frac{\partial T}{\partial z}$$

where q_x, q_y, q_z are the thermal heat flux components, k is the thermal conductivity, which depends on pressure, temperature and composition H_r, H_a, H_s, are the radioactive, adiabatic and shear heat productions, respectively. Radioactive heat production depends on the rock composition and is assumed to be constant (Table 2.3):

$$H_r = constant(C)$$

The adiabatic heat production/consumption is related to pressure changes (compression/decompression):

$$H_a = T\alpha\left(v_x\frac{\partial P}{\partial x} + v_y\frac{\partial P}{\partial y} + v_z\frac{\partial P}{\partial z}\right)$$

The shear heat production is related to dissipation of the mechanical energy during viscous deformation and depends on the deviatoric stress and strain rate:

$$H_s = \sigma'_{xx}\dot{\varepsilon}_{xx} + \sigma'_{yy}\dot{\varepsilon}_{yy} + \sigma'_{zz}\dot{\varepsilon}_{zz} + 2(\sigma_{xy}\dot{\varepsilon}_{xy} + \sigma_{xz}\dot{\varepsilon}_{xz} + \sigma_{yz}\dot{\varepsilon}_{yz})$$

The effect of latent heating/cooling (H_l) due to equilibrium melting/crystallization is included implicitly by increasing the effective heat capacity ($C_{p_{eff}}$) and the thermal expansion (α_{eff}) of melting/crystallizing rocks:

$$C_{p_{eff}} = C_p + Q_l\left(\frac{\partial M}{\partial T}\right)_{p=const}$$

$$\alpha_{eff} = \alpha + \rho \frac{Q_l}{T} \left(\frac{\partial M}{\partial T} \right)_{p=const}$$

Q_l is the latent heat of melting . For values of ρ, C_p, k, H_r and Q_l see Table 2.3.

Melting

The volumetric degree of mantle melting M is computed as a function of pressure and temperature, according to the parameterized batch melting model of Katz et al. (2003). Melting of other components is computed as described in Chapter 2 (Table 2.3).

The effective density, ρ_{eff} of partially molten rocks is computed according to the relation:

$$\rho_{eff} = \rho_{solid} - M(\rho_{solid} - \rho_{melt})$$

where ρ_{solid} and ρ_{melt} are the densities of solid and molten rocks at given pressure P(MPa) and temperature T(K) computed according to:

$$\rho_{P,T} = \rho_0(1 - \alpha(T - T_0))(1 + \beta(P - P_0))$$

Here α and β are the thermal expansion and compressibility coefficients and ρ_0 is the standard density at $P_0 = 0.1$ MPa and $T_0 = 298$ K given in Table 2.3.

Rheology

The rheologies employed in this study are visco-plastic. The viscosity of partially molten rocks is assumed to be constant (10^{18}). The viscous creep of solid rocks is defined in terms of deformation invariants (Ranalli, 1995):

$$\eta_{creep} = \frac{\dot{\varepsilon}_{II}^{\frac{1-n}{n}}}{A_D{}^{\frac{1}{n}}} exp\left(\frac{E_a + PV_a}{nRT} \right)$$

where $\dot{\varepsilon}_{II}$ is the second invariant of the strain rate tensor. A_D (pre-exponential factor), E_a (activation energy), n (creep exponent), V_a (activation volume) are experimentally determined flow law parameters and R is the gas constant. 10^{18} and 10^{24} are the lower and upper cut off values for all kinds of rocks. Plasticity is implemented using the following yield criterion, which assumes fracture-related strain weakening (e.g.: Lavier et al., 2000; Huismans and Beaumont, 2002; Gerya, 2010, 2012).

$$\sigma_{II} \leq C + \phi(P - P_{fluid})$$

$$C = \begin{cases} C_a + (C_b - C_a) \times \frac{\gamma}{\gamma_{cr}}, & \text{if } \gamma \leq \gamma_{cr} \\ C_b, & \text{if } \gamma > \gamma_{cr} \end{cases}$$

when $P \geq P_{fluid}$ (confined fracture):

$$\phi = \begin{cases} \phi_a + (\phi_b - \phi_a) \times \frac{\gamma}{\gamma_{cr}}, & \text{if } \gamma \leq \gamma_{cr} \\ \phi_b, & \text{if } \gamma > \gamma_{cr} \end{cases}$$

when $P < P_{fluid}$ (tensile fracture): $\phi = 1$.

$$\gamma = \int \sqrt{\frac{1}{2}(\dot{\varepsilon}_{ij})^2 dt}$$

where σ_{II} is the second stress invariant, P is the dynamic pressure, P_{fluid} is the fluid pressure, γ is the integrated plastic strain and γ_{cr} is the upper strain limit for fracture related weakening. C and ϕ are the strength values (cohesion and friction angle) that depend on the plastic strain. C_a and ϕ_a are the initial and C_a and ϕ_b are final strength values, respectively. Because fluids released from the magmatic source are expected to follow predefined fracture zones, the plastic strength of these fractured rocks may be significantly lowered as a result of the high pore fluid pressure.

Model setup

The model contains a 35 km thick continental crust, underlain by lithospheric/asthenospheric mantle material. The continental crust is subdivided into 15 km upper and 20 km lower crust. The mantle is composed of anhydrous peridotite. In the center of the domain a 3 km wide gabbroic channel is prescribed, which connects the underlying sublithospheric magmatic source region (SMSR) at the bottom of the box with the continental crust. In nature such magmatic channels may evolve at early stages of magmatism as a result of the rapid ascent of hot magmatic fluids/melts and may represent differentiation products derived from the underlying magmatic source region (SMSR). The SMSR is composed of hydrated/partially molten peridotite and has a radius of 20 km. It corresponds to a chemically distinct region and does not represent a fully molten magma chamber at depth. The initial model setup is represented in Figure 8.1. The rheologies used in this study are summarized in Table 8.1.

The initial temperature field (geotherm) of the domain decreases linearly from 0 ^oC at the surface to 400 ^oC to 800 ^oC at Moho depth and

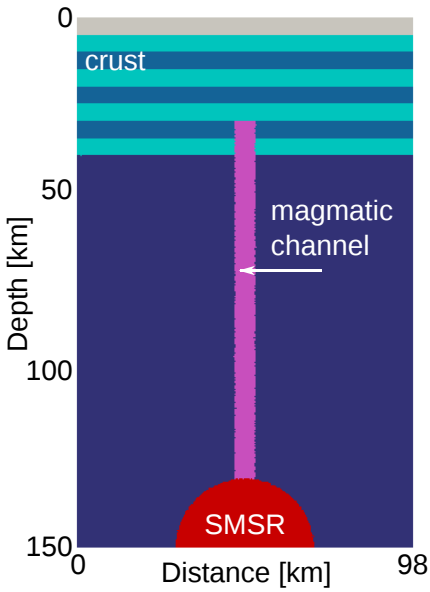

Figure 8.1: Initial setup of the numerical model, showing a crosssection in x and y direction. Staggered grid resolution is 197 × 197 × 309 nodal points. Grid step is 0.5 km × 0.5 km × 0.5 km. Colours indicate material properties (i.e. rock type), which appear in subsequent figures. To illustrate deformation, two layers with the same physical properties are chosen to represent the crust. SMSR stands for sublithospheric magmatic source region

1300 ^oC at the bottom of the box. The SMSR and the connecting channel are assumed to have a uniform temperature of 1400 ^oC.

Material	Flow law	$1/A_D$ $[Pa^n s]$	n	E_a $[J]$	V_a $[J/bar]$	$sin(\phi)$	C $[Pa]$	γ_{cr}
Upper crust (a)	wet qtz	1.97×10^{17}	2.3	154×10^3	0	0.1-0.0	$1 \times 10^{7-6}$	0.1
Upper crust (b)	wet qtz	1.97×10^{17}	2.3	154×10^3	0	0.1-0.0	$1 \times 10^{7-6}$	0.1
Lower crust	plag	4.80×10^{22}	3.2	238×10^3	0	0.1-0.0	$1 \times 10^{7-6}$	0.1
Mantle	dry ol	3.98×10^{16}	3.5	532×10^3	1.6	0.60	1×10^7	–
SMSR, channel	const.					0.0	$3 * 10^6$	–

Table 8.1: Rheologies used in subsequent experiments. Wet qtz = wet quarzite, plag = plagioclase (anorthite 75%), dry ol = dry olivine after Ranalli (1995) and references therein. A_D is the pre-exponential factor, n, is the stress exponent, E_a is the activation energy, V_a is the activation volume, ϕ is the friction angle, C is the cohesion and γ_{cr} is the strain limit for fracture related weakening. Both the magmatic channel and SMSR have a constant viscosity of 10^{18} $[Pas]$. Different rheologies (a-b) have been used to represent the upper crust.

Magma ascent and model shortcomings

In nature melt and magma (melt plus solids) transport might be a complex process, involving small-scale movement of melt (e.g. melt segregation on a decimetre scale) and large scale ascent from the source region through the continental crust to the site of final emplacement (Petford et al., 2000). The physical transport mechanisms that lead to emplacement are diverse and include, propagating fracture zones (Weertman, 1971; Clemens and Mawer, 1992), diffusion (Scambelluri and Philippot, 2001), porous flow (McKenzie, 1984; Connolly and Podladchikov, 1998; Ricard et al., 2001) and high permeability channels (Spiegelman and Kenyon, 1992) formed either by melt infiltration (Daines and Kohlstedt, 1994) or stress-driven melt segregation (Stevenson, 1989; Holtzman et al., 2003). This study focuses on the large scale ascent of magma from a sublithospheric source region along a magmatic channel and is not able to resolve these open questions, but is meant to give first order estimates on intrusion geometries and related feedbacks between intruding magma and host lithologies. Magma ascent in these models develops spontaneously and is controlled by magma rheology and density (Gerya and Burg, 2007). Partially molten material has a much lower viscosity than the surrounding dry mantle or the continental crust (Pinkerton and Stevenson, 1992) and can move along the magmatic channel as a crystal/melt mixture (Gerya and Burg, 2007). The viscosity contrast between melt/magma (i.e. 10^{4-14} Pas: Pinkerton and Stevenson, 1992; Petford et al., 2000; Caricchi et al., 2007), and continental crust (i.e.: $10^{22-26}Pas$) in natural settings is too high to be resolved numerically at the current stage. Therefore we assume partially molten material to be represented by a constant viscosity of 10^{18} Pas. Because magma flow in a magmatic channel (Poisson flow), depends on the magma viscosity and channel width, our elevated magma viscosity should be regarded as a scaled viscosity in relation to the channel width (3 km), which is likewise too high in comparison to natural settings (30 - 300 m). Finally it should be noted that the rheology employed in this study is visco-plastic and neglects the elastic response of rocks. Elasticity may affect the stress distribution and lead to energy release, which may alter the tectonic response related to intrusion emplacement. Future studies on magma flow and emplacement should employ a visco-elasto-plastic rheology (Gerya and Burg, 2007) and fully coupled two-phase formulations.

Preliminary results

Magma emplacement is strongly related to the physical properties of the continental crust. Depending on the rheological properties and thermal structure of the crust, incoming magma may either pool along the crust-mantle boundary or form ring structures and rise to upper crustal levels. The transition between these emplacement modes is related to the viscous and brittle/plastic response of the crust. Ductile deformation of a hot and weak lower crust (Moho-temperature $\geq 600\ ^oC$) enables inflation of magma at the crust-mantle boundary (ballooning), forming big magma chambers at low crustal levels (Figure 8.2). Deformation in a cooler systems (Moho-temperature $< 600\ ^oC$) is characterized by plastic deformation. The incoming magma disturbs the stress field of the crust and can form complex ring structures and fracture zones, facilitating magma ascent and emplacement (Figure 8.3). In models where regional heterogeneities are present such as fracture or shear zones, magma will follow these predefined zones of weakness (Figure 8.4). However, these preliminary results need to be resolved in a more detailed study, employing different rheological parameters (e.g. $\phi_{a,b}$, $C_{a,b}$, γ_{cr}) and host lithologies to better understand the feedbacks between magma ascent and melt intrusion.

Brief discussion

Ring complexes

Because subvolcanic ring complexes (circular intrusive complexes in map view, i.e.: cone sheets and ring dikes) preserve instantaneous magmatic events, they are believed to represent a rich source of information on magma transport and emplacement (Johnson et al., 2002). Such ring complexes have been identified in a number of locations, for example in Scottland (Magee et al., 2012), Nothern Ireland (Anderson, 1937), on the Canary Islands (Schirnick et al., 1999; Ancochea et al., 2003), in Baja California, Mexico (Johnson et al., 1999, 2002) and North (Clemens-Knott and Saleeby, 1999) and South America (Bussell, 1988).

Cone sheets can have mafic to felsic compositions, gently to steeply inward dipping contacts ($30\ ^o$ - $70\ ^o$), with a typical sheet thickness of up to tens of meters (e.g. Anderson, 1937; Phillips, 1974; Schirnick et al., 1999; Johnson et al., 2002). Ring dikes, on the other hand, are typically felsic in composition (Johnson et al., 2002), have nearly vertical or steeply outward dipping contacts and can reach up to several kilometres in thickness (Anderson, 1937; Johnson et al., 2002). These ring structures are generally underlain by a central intrusion at depth and are related to its magmatic

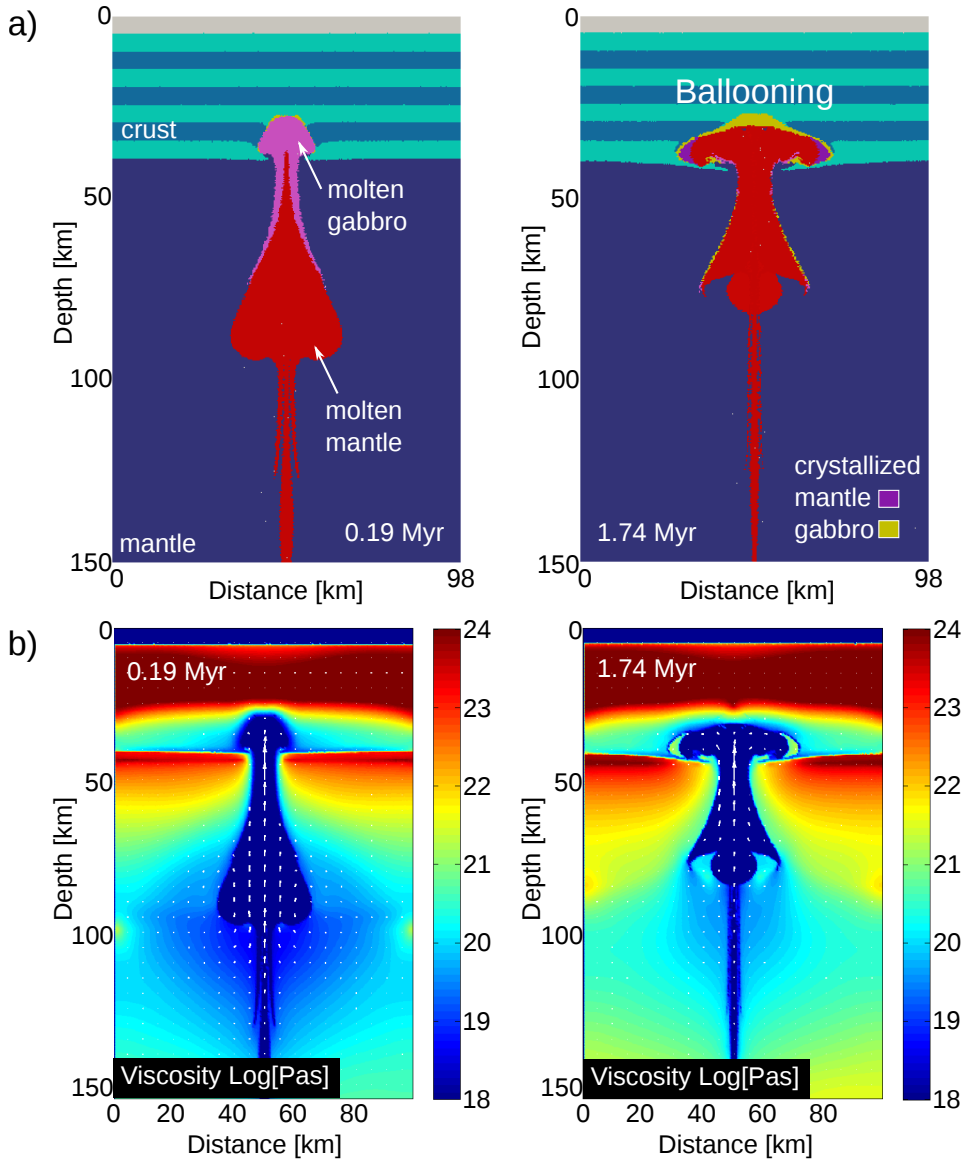

Figure 8.2: Incoming magma pools along the crust-mantle boundary, forming large intrusions at deep levels. a) Compositional (lithological) map. b) Viscosity field ($Log[Pas]$). White arrows denote the flow field in x - y direction. Physical parameters: Moho temperature = 800 ^oC, $\gamma_{cr} = 0.1$, $C = 10^{7-6}$, $\phi = 0.1$-0.

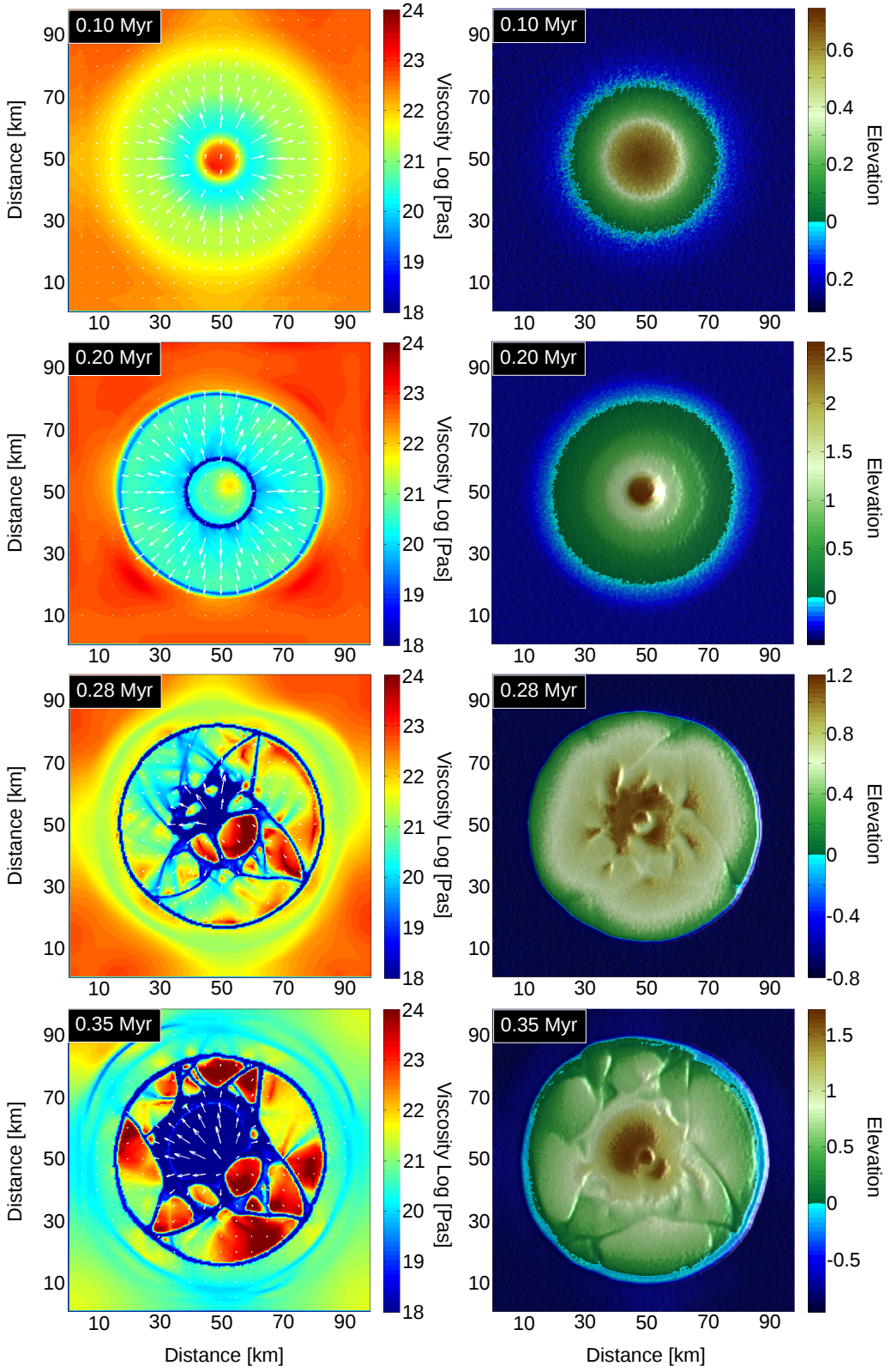

Figure 8.3: Formation of ring structures. Top view, showing changes in the viscosity field (5 km below the surface) with time and related topographic responses. White arrows denote the flow field in x - z direction. Physical parameters: Moho temperature = 600 ^oC, $\gamma_{cr} = 0.1$, $C = 10^{7-6}$, $\phi = 0$.

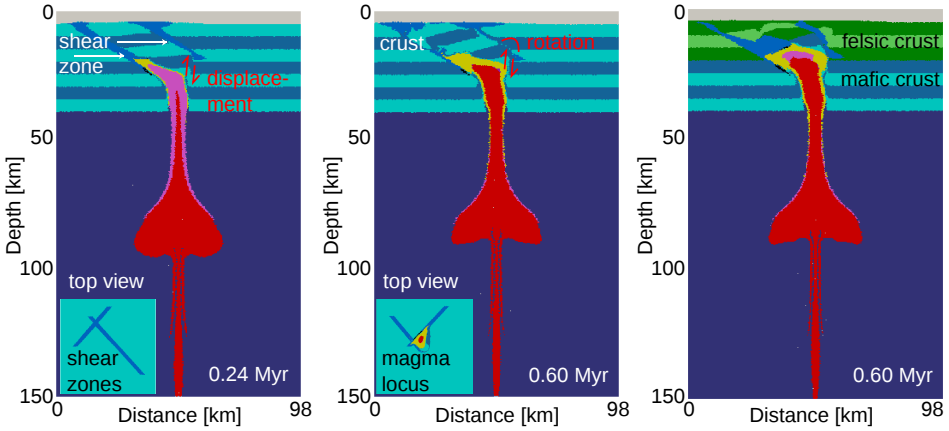

Figure 8.4: Magma ascent along predefined fracture zones. Compositional (lithological) map. White arrows denote the flow field in x - y direction. Physical parameters: Moho temperature = 600 ^oC, $\gamma_{cr} = 0.1$, $C = 10^{7-6}$, $\phi = 0.1$-0.

evolution. Cone sheets are believed to have evolved as a result of magma overpressure that imparts a local stress field on the overlying country rock, forming conical fracture zones (e.g. Anderson, 1937; Phillips, 1974), which is in good agreement with our results. Intrusion of magma along these fractures is rapid and often associated with quenched margins (Johnson et al., 2002). Recurrent supply of new magma along a common conduit may result in complex cone sheet geometries, forming a simple stack of cones with concentric age progression between center and rim or complex age relations as a result of lateral expansion, contraction and subsidence of the central intrusion (Schirnick et al., 1999). However, the results presented in this study demonstrate that even a single intrusion event may form multiple ring structures (Figure 8.3), at which steep dipping inner faults are followed by more gently dipping outer faults.

In contrast, caldera or caldron collapse at a later magmatic stage, may lead to the formation of nearly vertical to outward dipping faults (Acocella et al., 2000; Troll et al., 2002), providing conduits for the ascent of relatively felsic material that form ring dikes (e.g. Johnson et al., 2002). Depending on the vertical extend of these fracture zones, such faults may evolve into deep kinematic zones (Johnson et al., 2002) and change their dip.

Spatial and temporal relation between shear zones and magma emplacement

Magma emplacement mechanisms can be divided in two main groups: forceful emplacement, by the body forces of the intruding magma pushing the crust aside and passive emplacement by replacive or transfer mechanisms, whereby melt flows into fractures and openings formed by regional stresses (e.g. Hutton, 1988; Paterson and Fowler, 1993). Direct tectonic consequences of these processes are for instance doming, ballooning (e.g. Bateman, 1985; Ramsay, 1989), stoping (e.g. Fowler and Paterson, 1997; Clarke et al., 1998; Yoshinobu et al., 2003) and cauldron subsidence, but space for magma is likely to be generated by a combination of the above mentioned processes in accordance with this study.

Because of the common spatial and temporal relationship between intrusive bodies and crustal scale shear zones it was suggested that there is a genetic link between the two (Weinberg et al., 2004), whereby shear zones facilitate magma transport and emplacement (Hutton et al., 1990; Brown and Solar, 1998; Weinberg et al., 2004) or magma emplacement triggers shear zone nucleation (Neves et al., 1996). Based on various field (e.g. Hutton et al., 1990; Weinberg et al., 2004) and analogue studies (Ferré et al., 2012) on intrusion emplacement it has been demonstrated that magma can rise along predefined fracture or thrust zones, highlighting the geometrical control of magma pathways in the final intrusion shape. In contrast, Neves et al. (1996) have argued that intrusion emplacement introduces rheological heterogeneities, induces strain localization and favours shear zone nucleation, stating that shear zones are a consequence, rather than a cause of pluton emplacement. Both mechanisms are in accordance with the preliminary results presented in this study. Magma coming from depth may localize deformation causing fracture zone propagation and structural damage, but where preexisting fracture/shear zones exist magma is likely to follow those paths of weakness. The intersection of two major fault zones is moreover shown to be a likely loci for magma intrusions.

Nevertheless it should be noted that based on statistical evaluations Paterson and Schmidt (1999), have argued that there is no close spatial relationship between faults and intrusions in the Armorican Massif (France) and Alleghanian plutons (southern Appalachians, USA), indicating that plutons have a tendency to occur away from faults.

8.3 Future directions

Arc magmatism

Recent advances in computational geology allow us to study complex relations between magma production and its emplacement (at crustal levels) in three dimensions. Some of these processes have been questioned and analysed by Zhu et al. (2009, 2011a,b), but detailed studies on the geometry of intrusive bodies, related cooling histories and tectonic responses are still dispute.

However, maybe the most pending issue related to numerical studies on arc magmatism, is the incorporation of intra-crustal differentiation and crustal assimilation processes. Physical formulations or efficient parameterizations are needed to fully understand the physical and geochemical evolution of arc magmas, verifying the long standing debate of how continental crust is formed. Tracing the geochemical evolution of different rock types could give additional insights into crust formation processes (Nikolaeva, 2011), but future studies on this topic are closely related to how fluid and melt flow will be treated in future. Other mechanisms that could have a great impact on crustal growth are surface processes, such as erosion, sedimentation and climate changes, which have been partly neglected or incorporated in a simplified manner. Burov and Toussaint (2007) have demonstrated how surface processes can influence the tectonic evolution of continental collision, but feedbacks between processes in the deep mantle, the surface, deep magma production, its evolution and emplacement need to be explored in greater detail.

Accretionary tectonics

The third dimension is crucial for evaluating topographic and structural responses of accretionary tectonics. Tear propagation, slab detachment (van Hunen and Allen, 2011), subduction zone transference and ophiolite emplacement are intrinsically three dimensional features and future studies should take this into account. For example, end-on subduction of a linear tract of crust may locally disrupt a subduction zone but not cause it to fail, whereas delivery of similarly buoyant crust parallel to the trench is more likely to lead to subduction zone failure (Stern, 2002). Although, three-dimensional numerical experiments evaluating the total effect of buoyant crust on a subduction zone exist (Mason et al., 2010), feedbacks between different rheologies and tectonic responses are still missing. Likewise, ophiolite emplacement processes proposed in this study, could be affected by

the 3-D geometry of the subducting slab.

Bibliography

Acocella, V., Cifelli, F., Funiciello, R., 2000. Analogue models of collapse calderas and resurgent domes. Journal of Volcanology and Geothermal Research 104 (1), 81–96.

Ancochea, E., Brändle, J., Huertas, M., Cubas, C., Hernán, F., 2003. The felsic dikes of la gomera (canary islands): identification of cone sheet and radial dike swarms. Journal of volcanology and geothermal research 120 (3), 197–206.

Anderson, D. L., 1994. The sublithospheric mantle as the source of continental flood basalts; the case against the continental lithosphere and plume head reservoirs. Earth and Planetary Science Letters 123 (1), 269–280.

Anderson, E., 1937. Cone-sheets and ring-dykes: the dynamical explanation. Bulletin of Volcanology 1 (1), 35–40.

Annen, C., Blundy, J., Sparks, R., 2006. The genesis of intermediate and silicic magmas in deep crustal hot zones. Journal of Petrology 47 (3), 505–539.

Bateman, R., 1985. Aureole deformation by flattening around a diapir during in situ ballooning: The cannibal creek granite. The Journal of Geology 93 (3), 293–310.

Behn, M., Kelemen, P., Hirth, G., Hacker, B., Massonne, H., 2011. Diapirs as the source of the sediment signature in arc lavas. Nature Geoscience 4 (9), 641–646.

Bergantz, G. W., 2000. On the dynamics of magma mixing by reintrusion: implications for pluton assembly processes. Journal of Structural Geology 22 (9), 1297–1309.

Brown, M., Solar, G. S., 1998. Shear-zone systems and melts: feedback relations and self-organization in orogenic belts. Journal of Structural Geology 20 (2), 211–227.

Burov, E., Toussaint, G., 2007. Surface processes and tectonics: forcing of continental subduction and deep processes. Global and Planetary Change 58 (1), 141–164.

Bussell, M. A., 1988. Structure and petrogenesis of a mixed-magma ring dyke in the peruvian coastal batholith: eruptions from a zoned magma chamber. Transactions of the Royal Society of Edinburgh: Earth Sciences 79 (2-3), 87–104.

Caricchi, L., Burlini, L., Ulmer, P., Gerya, T., Vassalli, M., Papale, P., 2007. Non-newtonian rheology of crystal-bearing magmas and implications for magma ascent dynamics. Earth and Planetary Science Letters 264 (3), 402–419.

Clarke, D. B., Henry, A. S., White, M. A., 1998. Exploding xenoliths and the absence of elephants graveyards in granite batholiths. Journal of Structural Geology 20 (9), 1325–1343.

Clemens, J., Mawer, C., 1992. Granitic magma transport by fracture propagation. Tectonophysics 204 (3), 339–360.

Clemens-Knott, D., Saleeby, J. B., 1999. Impinging ring dike complexes in the sierra nevada batholith, california: Roots of the early cretaceous volcanic arc. Geological Society of America Bulletin 111 (4), 484–496.

Connolly, J., Podladchikov, Y., 1998. Compaction-driven fluid flow in viscoelastic rock. Geodinamica Acta 11 (2-3), 55–84.

Cruden, A. R., 1990. Flow and fabric development during the diapiric rise of magma. The Journal of Geology, 681–698.

Daines, M., Kohlstedt, D., 1994. The transition from porous to channelized flow due to melt/rock reaction during melt migration. Geophysical Research Letters 21, 145–145.

Dingwell, D. B., Bagdassarov, N., Bussod, G., Webb, S. L., 1993. Magma rheology.

Dingwell, D. B., Webb, S. L., 1989. Structural relaxation in silicate melts and non-newtonian melt rheology in geologic processes. Physics and Chemistry of Minerals 16 (5), 508–516.

Dingwell, D. B., Webb, S. L., 1990. Relaxation in silicate melts. European Journal of Mineralogy (4), 427–449.

Dufek, J., Bachmann, O., 2010. Quantum magmatism: Magmatic compositional gaps generated by melt-crystal dynamics. Geology 38 (8), 687–690.

Ferré, E. C., Galland, O., Montanari, D., Kalakay, T. J., 2012. Granite magma migration and emplacement along thrusts. International Journal of Earth Sciences, 1–16.

Fowler, T. K., Paterson, S. R., 1997. Timing and nature of magmatic fabrics from structural relations around stoped blocks. Journal of Structural Geology 19 (2), 209–224.

Galland, O., Cobbold, P. R., Hallot, E., de Bremond D'Ars, J., Delavaud, G., 2006. Use of vegetable oil and silica powder for scale modelling of magmatic intrusion in a deforming brittle crust. Earth and Planetary Science Letters 243 (3), 786–804.

Gerya, T., 2010. Dynamical instability produces transform faults at mid-ocean ridges. Science 329 (5995), 1047–1050.

Gerya, T., Yuen, D., 2003. Characteristics-based marker-in-cell method with conservative nite-differences schemes for modeling geological flows with strongly variable transport properties. Physics of the Earth and Planetary Interiors 140, 293–318.

Gerya, T., Yuen, D., 2007. Robust characteristics method for modelling multiphase visco-elasto plastic thermo-mechanical problems. Physics of the Earth and Planetary Interiors 163, 83–105.

Gerya, T. V., 2012. Three-dimensional thermomechanical modeling of oceanic spreading initiation and evolution. Physics of the Earth and Planetary Interiors.

Gerya, T. V., Burg, J.-P., 2007. Intrusion of ultramafic magmatic bodies into the continental crust: Numerical simulation. Physics of the Earth and Planetary Interiors 160 (2), 124–142.

Giordano, D., Russell, J. K., Dingwell, D. B., 2008. Viscosity of magmatic liquids: A model. Earth and Planetary Science Letters 271 (1), 123–134.

Hacker, B., Kelemen, P., Behn, M., 2011. Differentiation of the continental crust by relamination. Earth and Planetary Science Letters 307 (3), 501–516.

Holtzman, B., Groebner, N., Zimmerman, M., Ginsberg, S., Kohlstedt, D., 2003. Stress-driven melt segregation in partially molten rocks. Geochemistry Geophysics Geosystems 4 (5), 8607.

Huismans, R. S., Beaumont, C., 2002. Asymmetric lithospheric extension: The role of frictional plastic strain softening inferred from numerical experiments. Geology 30 (3), 211–214.

Hutton, D., Dempster, T., Brown, P., Becker, S., 1990. A new mechanism of granite emplacement: intrusion in active extensional shear zones.

Hutton, D. H., 1988. Granite emplacement mechanisms and tectonic controls: inferences from deformation studies. Transactions of the Royal Society of Edinburgh: Earth Sciences 79 (2-3), 245–255.

Johnson, S., Paterson, S., Tate, M., 1999. Structure and emplacement history of a multiple-center, cone-sheet–bearing ring complex: The zarza intrusive complex, baja california, mexico. Geological Society of America Bulletin 111 (4), 607–619.

Johnson, S., Schmidt, K., Tate, M., 2002. Ring complexes in the peninsular ranges batholith, mexico and the usa: magma plumbing systems in the middle and upper crust. Lithos 61 (3), 187–208.

Katz, R. F., Spiegelman, M., Langmuir, C. H., 2003. A new parameterization of hydrous mantle melting. Geochemistry Geophysics Geosystems 4 (9), 1073.

Kavanagh, J. L., Menand, T., Sparks, R. S. J., 2006. An experimental investigation of sill formation and propagation in layered elastic media. Earth and Planetary Science Letters 245 (3), 799–813.

Lavier, L. L., Buck, W. R., Poliakov, A. N., 2000. Factors controlling normal fault offset in an ideal brittle layer. J. geophys. Res 105 (23), 431–23.

Longo, A., Vassalli, M., Papale, P., Barsanti, M., 2006. Numerical simulation of convection and mixing in magma chambers replenished with co2-rich magma. Geophysical research letters 33 (21), L21305.

Magee, C., Stevenson, C., ODriscoll, B., Schofield, N., McDermott, K., 2012. An alternative emplacement model for the classic ardnamurchan cone sheet swarm, nw scotland, involving lateral magma supply via regional dykes. Journal of Structural Geology.

Mason, W., Moresi, L., Betts, P., Miller, M., 2010. Three-dimensional numericalmodels of the influence of a buoyant oceanic plateau on subduction zones. Tectonophysics 483, 71–79.

McKenzie, D., 1984. The generation and compaction of partially molten rock. Journal of Petrology 25 (3), 713–765.

Menand, T., 2008. The mechanics and dynamics of sills in layered elastic rocks and their implications for the growth of laccoliths and other igneous complexes. Earth and Planetary Science Letters 267 (1), 93–99.

Menand, T., 2011. Physical controls and depth of emplacement of igneous bodies: A review. Tectonophysics 500 (1), 11–19.

Miller, R. B., Paterson, S. R., 1999. In defense of magmatic diapirs. Journal of Structural Geology 21 (8), 1161–1173.

Neves, S., Vauchez, A., Archanjo, C., 1996. Shear zone-controlled magma emplacement or magma-assisted nucleation of shear zones? insights from northeast brazil. Tectonophysics 262 (1), 349–364.

Nikolaeva, K., 2011. Coupled geochemical-petrological-geodynamical modelling of subduction zones. Ph.D. thesis, Diss., Eidgenössische Technische Hochschule ETH Zürich, nr. 19425, 2011.

Parsons, T., Sleep, N. H., Thompson, G. A., 1992. Host rock rheology controls on the emplacement of tabular intrusions: Implications for underplating of extending crust. Tectonics 11 (6), 1348–1356.

Paterson, S., Schmidt, K., 1999. Is there a close spatial relationship between faults and plutons? Journal of Structural Geology 21 (8), 1131–1142.

Paterson, S. R., Fowler, T. K., 1993. Re-examining pluton emplacement processes. Journal of Structural Geology 15 (2), 191–206.

Petford, N., 1996. Dykes or diapirs? Transactions of the Royal Society of Edinburgh: Earth Sciences 87 (1-2), 105–114.

Petford, N., 2003. Rheology of granitic magmas during ascent and emplacement. Annual Review of Earth and Planetary Sciences 31 (1), 399–427.

Petford, N., Cruden, A., McCaffrey, K., Vigneresse, J., et al., 2000. Granite magma formation, transport and emplacement in the earth's crust. Nature 408 (6813), 669–673.

Phillips, W., 1974. The dynamic emplacement of cone sheets. Tectonophysics 24 (1), 69–84.

Pinkerton, H., Sparks, R., 1978. Field measurements of the rheology of lava.

Pinkerton, H., Stevenson, R., 1992. Methods of determining the rheological properties of magmas at subliquidus temperatures. Journal of Volcanology and Geothermal Research 53, 47–66.

Ramsay, J. G., 1989. Emplacement kinematics of a granite diapir: the chindamora batholith, zimbabwe. Journal of Structural Geology 11 (1), 191–209.

Ranalli, G., 1995. Rheology of the Earth. Springer.

Ricard, Y., Bercovici, D., Schubert, G., 2001. A two-phase model for compaction and damage. ii- applications to compaction, deformation, and the role of interfacial surface tension. Journal of geophysical research 106 (B5), 8907–8924.

Richards, M. A., Duncan, R. A., Courtillot, V. E., 1989. Flood basalts and hot-spot tracks: plume heads and tails. Science 246 (4926), 103–107.

Rudnick, R., 1995. Making continental crust. Nature 378, 571–577.

Scambelluri, M., Philippot, P., 2001. Deep fluids in subduction zones. Lithos 55 (1), 213–227.

Schirnick, C., van den Bogaard, P., Schmincke, H.-U., 1999. Cone sheet formation and intrusive growth of an oceanic islandthe miocene tejeda complex on gran canaria (canary islands). Geology 27 (3), 207–210.

Schmidt, M., Poli, S., 1998. Experimentally based water budgets for dehydrating slabs and consequences for arc magma generation. Earth and Planetary Science Letters 163 (1), 361–379.

Spiegelman, M., Kenyon, P., 1992. The requirements for chemical disequilibrium during magma migration. Earth and Planetary Science Letters 109 (3), 611–620.

Stern, R., 2002. Subduction zones. Reviews of Geophysics 40, doi:10.1029/2001RG000108.

Stevenson, D., 1989. Spontaneous small-scale melt segregation in partial melts undergoing deformation. Geophysical Research Letters 16 (9), 1067–1070.

Tatsumi, Y., 2005. The subduction factory: How it operates in the evolving earth. GSA today 15 (7), 4.

Tatsumi, Y., Eggins, S., 1995. Subduction zone magmatism. Wiley.

Troll, V., Walter, T. R., Schmincke, H.-U., 2002. Cyclic caldera collapse: piston or piecemeal subsidence? field and experimental evidence. Geology 30 (2), 135–138.

van Hunen, J., Allen, M., 2011. Continental collision and slab break-off: a comparison of 3d numerical models with observations. Earth and Planetary Science Letters 302, 27–37.

Vigneresse, J.-L., Tikoff, B., Améglio, L., 1999. Modification of the regional stress field by magma intrusion and formation of tabular granitic plutons. Tectonophysics 302 (3), 203–224.

Webb, S. L., Dingwell, D. B., 1990. Non-newtonian rheology of igneous melts at high stresses and strain rates: experimental results for rhyolite, andesite, basalt, and nephelinite. Journal of Geophysical Research (B10), 15695–15701.

Weertman, J., 1971. Theory of water-filled crevasses in glaciers applied to vertical magma transport beneath oceanic ridges. Journal of Geophysical Research 76 (5), 1171–1183.

Weinberg, R., Sial, A., Mariano, G., 2004. Close spatial relationship between plutons and shear zones. Geology 32 (5), 377–380.

Weinberg, R. F., 1996. Ascent mechanism of felsic magmas: news and views. Transactions of the Royal Society of Edinburgh: Earth Sciences 87 (1-2), 95–103.

Weinberg, R. F., Podladchikov, Y., 1994. Diapiric ascent of magmas through power law crust and mantle. Journal of Geophysical Research 99 (B5), 9543–9560.

Yoshinobu, A. S., Fowler Jr, T. K., Paterson, S. R., Llambias, E., Tickyj, H., Sato, A. M., 2003. A view from the roof: magmatic stoping in the shallow crust, chita pluton, argentina. Journal of structural geology 25 (7), 1037–1048.

Zhu, G., Gerya, T., Honda, S., Tackley, P., Yuen, D., 2011a. Influences of the buoyancy of partially molten rock on 3-d plume patterns and melt

productivity above retreating slabs. Physics of the Earth and Planetary Interiors 185 (3), 112–121.

Zhu, G., Gerya, T., Yuen, D., 2011b. Melt evolution above a spontaneously retreating subducting slab in a three-dimensional model. Journal of Earth Science 22 (2), 137–142.

Zhu, G., Gerya, T., Yuen, D., Honda, S., Yoshida, T., Connolly, J., 2009. Three-dimensional dynamics of hydrous thermal-chemical plumes in oceanic subduction zones. Geochemistry Geophysics Geosystems 10 (11), Q11006.

Acknowledgements

First and foremost i would like to thank Taras for all the scientific support and freedom at the same time. I would also like to thank Jeroen van Hunen and Paul Tackley for accepting to examine my work.

- Chapter 3 has benefited from reviews of Dave Stegman. Chapter 4 has been improved by comments from Brad Hacker and Vlad Manea. Chapter 5 has benefited from suggestions by Jeroen van Hunen and Susanne Buiter. Results presented in Chapter 7 have been conducted in close and fruitful cooperation with Weronika Gorczyk and have benefited from comments by Taras.
- Many thanks to the Adamello kids (Alex, Cindy, Sylvia, David, Nik(laus), Roel, Rohit, Tobi K.) for lowering my pain tolerance, a great time in the field and in the city. It has been a great time.
- Many thanks to all my present and past office mates of whom i had many: Sanja, Jess, Diana, Tobi, Thibault, Andre, Gang, Daniel, Christoph and the Lin(s). I enjoyed the chaos, noise and rough atmosphere a lot.
- I whish all the best to all GFD (Guizhi, Diana, Bettina, Ria, Tobi $\times$ 2, Jie, Yang, Diogo, Marcel, Fabio, Dave, Gregor and Giovanni) and EPM (too many to list..) group members. Go brittle dynamos! In particular I would like to thank Guizhi and Jie for all those discussions and Dave for last minute support.
- I thank Naveen, Franzi, Laura and all those people who lived in Vinzenz for an outstanding first year and Rita, Diana, Jenneke and Jess for chats, drinks, trips and a great time in Zurich!
- Lastly, I thank my parents and Christian for the constant support throughout these years.